Sheffield Hallam University

Enhancing the tribological properties of CrN/NbN nanoscale multilayer PVD coatings.

SAVISALO, Tuukka S.

Available from Sheffield Hallam University Research Archive (SHURA) at:

http://shura.shu.ac.uk/20329/

This document is the author deposited version. You are advised to consult the publisher's version if you wish to cite from it.

Published version

SAVISALO, Tuukka S. (2008). Enhancing the tribological properties of CrN/NbN nanoscale multilayer PVD coatings. Doctoral, Sheffield Hallam University (United Kingdom)..

Copyright and re-use policy

See http://shura.shu.ac.uk/information.html

Sheffield Hallam University Research Archive
http://shura.shu.ac.uk

AAu&cus venire vuy vampus
Sheffield S1 1WB

101 923 059 2

IIIIIIIH I

, GheS:o,^ i safiam university
| Learning and IT Services
i Adsetts Centre City Campus
\ Sheffield SI 1WB

2-60 GO

REFERENCE

ProQuest Number: 10700975

All rights reserved

INFORMATION TO ALL USERS
The quality of this reproduction is dependent upon the quality of the copy submitted.

In the unlikely event that the author did not send a complete manuscript
and there are missing pages, these will be noted. Also, if material had to be removed,
a note will indicate the deletion.

uest

ProQuest 10700975

Published by ProQuest LLC(2017). Copyright of the Dissertation is held by the Author.

All rights reserved.
This work is protected against unauthorized copying under Title 17, United States Code
Microform Edition © ProQuest LLC.

ProQuest LLC.
789 East Eisenhower Parkway
P.O. Box 1346
Ann Arbor, MI 48106- 1346

Enhancing the Tribological Properties of CrN/NbN Nanoscale Multilayer PVD Coatings

Tuukka Savisalo

A thesis submitted for partial fulfillment of the requirements of Sheffield Hallam University for the degree of Doctor of Philosophy

2008

ABSTRACT

This work is based on a large body of previous research work done in Sheffield Hallam University and other research institutes and private companies under the support of European Union Framework program. This research developed a CrN/NbN coating with promising properties for tribological applications where corrosion plays a big role. Building on this knowledge base a novel approach to the surface treatment was selected, in which multiple layers, each chosen for a specific purpose, were optimised to combine the best properties of each. In this approach a careful consideration of macro- and microstructure of each layer is required in order to extract the good properties of each layer while eliminating the negative ones. It was shown in the work that, if such consideration is neglected, a catastrophic failure may follow. For example poor adhesion may cause a total failure of the coating. As the number of layers and interfaces increase a good understanding on the structure and the properties of each layer becomes very important as the number of parameters and possible combinations increase many times.

In this whole work the intention was to take a very practical approach to the coating. The objective was to combine different approaches, such as duplex treatments and multi layering and investigate the specific interactions that are not otherwise apparent.

The results of this work show that such an approach is viable and should lead to excellent results as long as the wear mechanisms of the coating are understood and the coating is correctly engineered for the application.

ACKNOWLEDGEMENTS

I would like to thank many people for the help and support I have received during this endeavour. First and foremost I would like to thank my family who pushed me forward when I was losing my faith. Without your love and persistence I would not have finished this.

Second I would like to thank my supervisors Papken Hovesepian and Wolf-Dieter Münz for the inspiration, guidance and encouragement during this work. I would also like to express gratitude to all my co-workers and researchers at Surface Engineering Group, and Materials Engineering Research Institute.

I wish to express my gratitude to the team in University of Illinois, especially Ivan Petrov. I had a chance to learn a lot form all the expert staff and to use your splendid laboratory.

I need to also thank Savcor for the opportunity to do this work and for the financial support and the flexibility that enabled me to finish this thesis. I want to express special thanks to Kaj Pischow for your expert opinions and guidance.

I want to also express my warmest thanks to my dear friend Maria Romero. You really helped me a lot when I was going through rough time in my life. And of course also for all the fun times I had under your endless hospitality. I shall not forget you either Mirkka. You are also a true friend. And thanks to all the other friends and people who made my time in Sheffield absolutely fabulous. I also want to thank you, Elina. You gave me motivation to finish this work.

List of PUBLICATIONS

T. Savisalo, D. B. Lewis, P. Eh. Hovsepian and W. -D. Münz, *Influence of ion bombardment on the properties and microstructure of unbalanced magnetron deposited niobium coatings,* Thin Solid Films, 460 (2004) 94-100

T. Savisalo, D.B. Lewis, P.Eh. Hovsepian, *Microstructure and properties of novel wear and corrosion resistant CrON/NbON nano-scale multilayer coatings*, Surface & Coatings Technology 200 (2006) 2731– 2737

T. Savisalo, D. B. Lewis, Q. Luo, M. Bolton, P. Hovsepian, *Structure of Duplex CrN/NbN Coatings and their Performance Against Corrosion and Wear,* Surface & Coatings Technology 202 (2008) 1661-1667

Advanced Studies (Courses, Presentations at conferences including ABS days)

2001 Seventh International ABS Days, Sheffield

2002 1st Mikkeli International Industrial Coating Seminar (MIICS), Mikkeli, Finland

2002 The International Conference for Metallurgical Coatings and Thin Films (ICMCTF), San Diego, CA, USA

2002 Eighth International ABS Days, Sheffield

2002 International Conference on Plasma Surface Engineering (PSE), Garmisch-Partenkirchen, Germany

2003 The International Conference for Metallurgical Coatings and Thin Films (ICMCTF), San Diego, CA, USA

2003 Ninth International ABS Days, Sheffield

2004 First ABS/HIPIMS Days, Sheffield

2004 2nd Mikkeli International Industrial Coating Seminar (MIICS), Mikkeli, Finland

2006 3rd Mikkeli International Industrial Coating Seminar (MIICS), Mikkeli, Finland

2007 The International Conference for Metallurgical Coatings and Thin Films (ICMCTF), San Diego, CA, USA

2007 Nanotech Exhibition and Conference, Tokyo, Japan

2007 Fourth Sheffield HIPIMS Days

Table of Contents

1 Introduction

The first PVD processes were identified in the 1800s, but due to lack of suitable vacuum systems they were not used routinely until the 1930's. [1] Bunsen and Grove first documented the deposition of thin metal films in 1852 sputtering silver in an experimental vacuum tube [1a]. Shortly after this Faraday reported vacuum deposition using an exploding wire [1b]. In 1877 Wright devised an apparatus to form metallic thin films and to study their properties [1c] and in 1887 Nahrwold developed a thermal evaporation method with which it was feasible to produce thin film coatings [1d]. T.A. Edison was one of the first to use sputtering in a commercial process, using sputtering to deposit a seed layer for electro-deposition for his wax phonograph masters [1e]. The first truly commercial uses of PVD coating appeared in early 1930's when the use of thin films for optical coatings, such as mirrors, began. The reactive PVD process was first reported in 1933, though the term reactive sputtering was first used by Veszi in 1953 [1f]. Magnetron sputtering was developed simultaneously by several groups in the late 1960s [1g].

From the 1950's silicon processes have led the new developments in PVD technology, being the fundamental enabling technology in the manufacture of high density microprocessors with complex designs. Thin film coatings are currently used in numerous applications in manufacture of integrated circuits ranging from metal for conduits to diffusion barrier films.

The rapid increase in the number of industrial applications led to intense research in the field of thin films and thus the discovery of the key factors affecting PVD processes between 1950 and 1980 [2]. The research has further advanced since then, yet the understanding of the growth and the behaviour of the films is still incomplete.

In the early 1980's PVD technologies were introduced for tool coating. Initially coatings were relatively simple TiN coatings used for tools, such as drills and milling bits, but as the knowledge of the tribology of the hard PVD coatings grew, more complicated processes have been developed for cutting or milling of different

materials under lubricated or non-lubricated conditions [2-5]. Currently most commercial coating providers have 20-30 standard coatings that have different properties. Though detailed information on commercial coatings is scarce, most state-of-the-art coatings utilise multilayer structures and advanced pre-treatments.

Tribological coatings were initially developed for space applications, where they acted as dry film lubricants. Further development and the availability of industrial coating machines and processes have brought these coatings into our day to day lives. The reduced tolerances and increased wear and lubrication requirements has increased the demand for tribological coatings in engines and drive trains as the higher operating pressures and temperatures in modern engines require new methods for sealing and lubrication that can only be provided by thin film coatings. The commercial tribological coatings that currently focus on reducing friction and wear are not suitable for use in corrosive environments. Prolonged exposure to corrosive environments often lead to pitting corrosion of the substrate or in the worst case delamination of the coating due to the large electrochemical potential difference that exists between the coating and the substrate.

PVD coatings that can withstand simultaneous mechanical and chemical attack [6], have become feasible in more and more applications as the coating facilities have become more economical and readily available. New environmental and safety legislation also forces industry to find new alternatives to traditional surface treatments that use hazardous and environmentally unfriendly chemicals and processes, such as is the case with electrochemical hard chrome. Sheffield Hallam University participated in an European Commission funded BRITE-ERAM Newcrome [6a] project with an objective to find environmentally friendly alternatives to hard chrome. The approach chosen by the Sheffield Hallam University research group to accomplish this goal was to study multilayered PVD coatings of chromium and niobium and their nitrides as these materials are electrochemically stable. Good wear results were quickly reached, but initially the corrosion resistance of the electroplated coating remained superior. The CrN/NbN nanoscale multilayer coatings were the result of this development work. Later, a pre-treatment with niobium metal ion etching using the patented Arc Bond Sputtering (ABS) process was found to improve the corrosion resistance further [7]. In the conclusion of the research report

the developed PVD coatings were found to be superior to hard chrome in performance and also economically viable.

Further development of this coating has focused in surpassing the performance of hard chrome in all performance aspects. The enhancement of the performance comes from adding layers with specific function. For example, one can have an adhesion layer of gradient hardness to reduce the shear stress at the interface, a barrier layer to provide good corrosion resistance or a low friction topcoat. As the resulting family of coatings are complex systems with numbers of layers and interfaces it was regarded vital to be able to understand and optimise the parameters in each process step to meet the specific demands of each application. This work comprises detailed microstructural analysis of the coating after altering the key parameters of each layer of the coating. The resulting changes in the microstructure of the coating are then reflected in the coating performance in laboratory tests. When the interactions between the layers and key parameters are understood it is possible to lay down the best possible coatings for the requirements of the future.

The performance of a PVD coating should be regarded as a combination of the properties of the substrate, the interfaces and the coating. A failure in any of these will be seen as a failure of the coating. One can also combine PVD coating with other types of coating, such as sol-gel or plasma enhanced chemical vapour deposition (PE-CVD) coatings or other surface treatments, such as nitriding, creating a duplex coating. It is however very important to understand the interactions of these different layers/coatings as a chain is as only as strong as its weakest link. For coatings this means that incompatible or poorly designed layers or treatments can cause catastrophic failure of the coating and consequently the system relying on the coated part.

The thin coatings do not have load bearing capacity and thus rely on the substrate to provide the mechanical rigidity required to handle the mechanical loads to which the coated part is subjected.. If the substrate deformation is larger than the coating can tolerate then the coating will break and/or delaminate. The hard, wear resistant coatings with high internal stresses are often brittle and thus cannot generally tolerate large deformations and therefore require a hard substrate to function properly. This

issue can be alleviated by enhancing the surface hardness of the substrate using surface hardening methods, such as nitriding. Generally these processes affect the substrate deep enough (hundreds of microns compared with a few microns thickness of the PVD coatings) to give good support to the coating while still retaining the desired properties at the core, such as ductility, impact resistance and machinability. The substrate material also affects the corrosion resistance. This is critical at the defect locations where the solution can penetrate the coating and cause corrosion of the substrate. In this work the use of commercial low-pressure pulse plasma nitriding as the substrate treatment in a duplex coating was studied in order to enhance the tribological performance of the CrN/NbN coatings on soft steel substrates. When using two separate processes special care must be taken to eliminate deposits or scale that may reduce the adhesion of the PVD coating. In this work the treated test pieces were mechanically polished. The resulting duplex coatings performed very well in the mechanical and corrosion testing. The optimal microstructure of the nitrided layer, and thus the process, was found to depend on the application.

The substrate-coating interface is critical to a number of aspects in a coatings performance. Mainly it affects the adhesion of the coating, which has been directly related to the performance of a cutting tool [7]. Further, any impurities, voids or droplets at the interface can alter the local growth pattern of the coating. This leads to formation of pinholes or growth defects in the coatings that degrade the overall performance of the coating. Metal ion etching provides a tool to enhance the performance of the coating by controlled interface engineering. As the interface region is very thin (less than 100 nm) the identification of the microstructure is a technical challenge. The latest transmission electron microscopes with sensitive analysis tools can provide accurate information of the interface region. Niobium metal etching has been shown to have a positive effect on the corrosion performance of the CrN/NbN superlattice coating. The detailed investigation of the microstructure of the interface, combined with its effects on the performance of the coating was done to gain information on how to optimise the ion etching process for tribological coatings. It was found that the optimal etching rate of the Nb-ions is rather limited below -1000V bias voltage, yet a nanostructured Nb layer that deposits at the interface improves the corrosion resistance. Thus a two-step approach was developed, where a

high bias voltage step provided the etching and a short lower voltage step created a deposition layer.

Multi-layering has been shown to have a beneficial effect on the corrosion performance of the coatings [8]. An additional layer of highly corrosion-resistant material (Nb) was added to enhance the corrosion behaviour of the coating. The effects of deposition parameters on the corrosion behaviour was studied in detail. A thin Nb barrier enhanced the corrosion resistance, yet a thicker layer reduced the corrosion to a fraction compared to the thinner one. However the mechanical performance of the thinner layer was superior.

Finally, a topcoat to reduce the sliding friction was studied. Thin oxynitride topcoats have been successfully applied to cutting tools, where the topcoat reduces friction and enhances oxidation resistance [9]. Similar treatments were investigated for CrN/NbN coatings along with the effects on the tribological properties of CrN/NbN superlattice multilayer coatings. The friction was not significantly affected, but a significant reduction of a counter-body wear was observed.

2 LITERATURE REVIEW

2. 1 Physical Vapou

PVD (Physical Vapour Deposition) processes are atomistic deposition processes in which material is vaporised from a solid or liquid source in form of atoms or molecules through vacuum of low pressure gaseous (or plasma) atmosphere to the substrates, where it condenses [6]. Typically PVD deposited films are thin, with a thickness from few nanometres to several micrometres. PVD processes can be used to deposit elements and alloys as well as compounds using reactive processes.

The vaporisation of the coating material can occur in number of ways. Generally it is achieved by either heating the material beyond boiling point (with induction heating, hot filament, electron beam, arc discharge, etc.) or by momentum transfer from impacting ions (sputtering) [2-5].

In plasma processes the type of discharge can be determined from the voltage-current relation as shown in Figure 1. Initially, as the voltage is increased an almost linear increase in current is observed, yet the current remains very low. This region is called the Townsend discharge region. After a certain threshold voltage is reached the current increases significantly as the discharge is self-sustained by ionisation avalanches. As a consequence the plasma discharge increases to cover the entire surface of the cathode and the voltage drops as the normal glow is obtained. After the cathode surface has been covered any subsequent increase of voltage will result in a much larger increase of current. This region, called the abnormal glow, is the plasma in most commercial plasma processes. Further increase in the current leads to the occurrence of an arc discharge that causes a dramatic drop in the voltage [2-4],

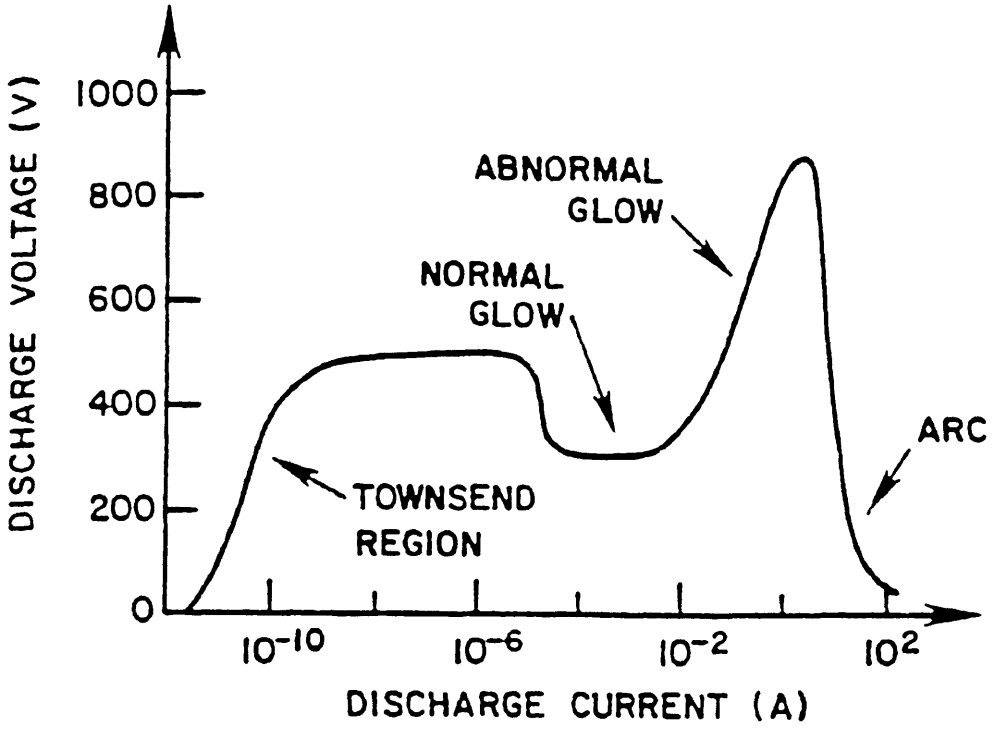

Figure 1Voltage-current dependence of different plasma discharge regions

The transport of the coating material takes place through vacuum, gas or plasma. The environment can be adjusted to allow a controlled chemical reaction thus producing the desired compounds. The path of the atoms is more or less direct (line of sight) depending on the initial kinetic energy and the pressure in the process chamber, as collisions with other atoms will cause atoms to alter direction. If the vaporised material is ions/ionised, electric and magnetic fields can be used to control the transport.

Film formation depends on the vaporised and substrate materials, surface conditions, available energy (temperature and ion bombardment) and atmosphere (chemical reactions, i.e. reactive deposition). The basic principles of film formation are explained in section 2.2

2.1.1 Sputtering and Unbalanced Magnetron Sputtering

In the sputtering process coating material is ejected from a solid surface (target) due to momentum transfer from bombarding ions. Typically sputtering uses a glow discharge or an ion beam to generate a flux of ions incident on the target surface [10]. In a simple glow discharge (dc sputtering, Figure 2) the positively charged ions are accelerated towards the target by applying negative voltage to the target material (cathode). Under the right conditions, with adequate voltage and appropriate gas pressure, the gas will break down to form a plasma discharge. In this plasma the potential is fairly uniform and close to the anode potential. Near the cathode is a dark space with a large electrical field in which the positively charged ions are accelerated toward the cathode. The impact of the ions on the cathode will cause sputtering if the energy of the impacting ions is high enough [11]. In commercial systems the gas in the system is generally argon, although other gases can also be used.

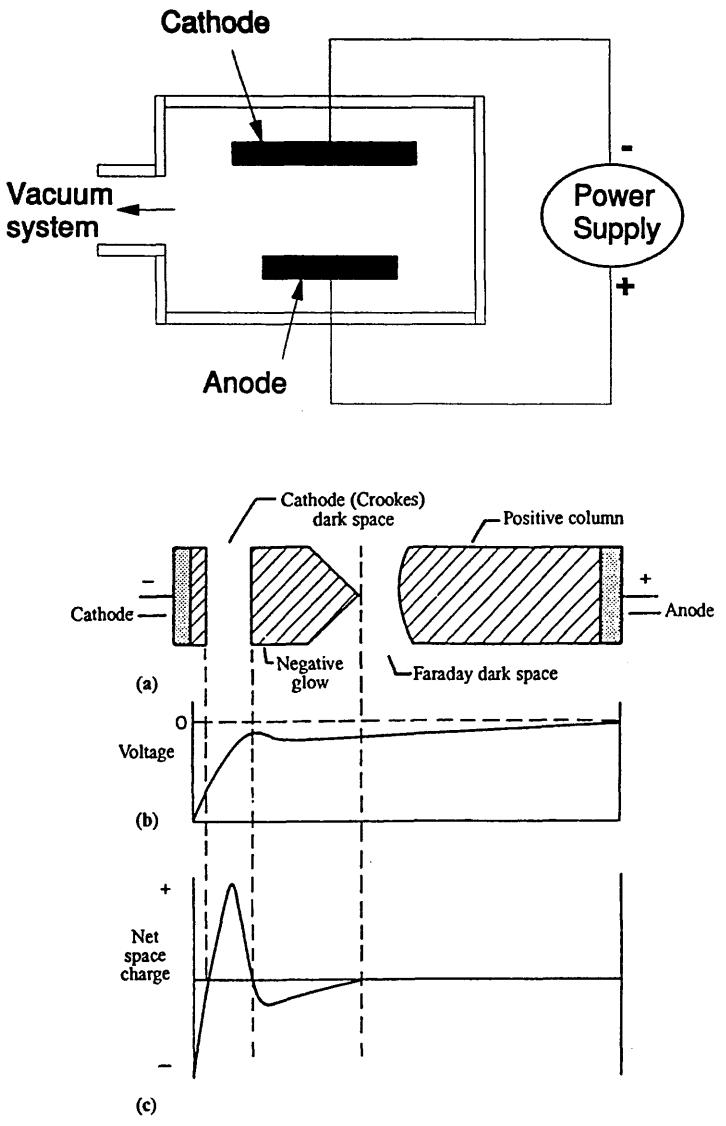

Figure 2 Schematic diagram of DC sputtering and plasma regions in the glow discharge

With low incident energies (< 50 eV) the ion impact causes very little effect. Only when the momentum of the impacting ions is large enough, exceeding the energy of the most weakly bound surface atoms, the collision cascade causes some atoms or clusters of atoms to leave the surface, i.e. sputtering occurs. The number of sputtered atoms and the energy of those emitted atoms depend on the target material, bombarding ion momentum and impact angle. The heavier the impacting atom, the

more atoms are released from the cathode surface. The quantity of atoms released per impacting atom is called the sputtering yield. This yield is a material property and relative figures of these for most bombarding atoms can be found from literature [12]. The impacting angle also influences the sputter yield. At certain angles the yield can increase by up to 3 times compared to the normal incidence angle [2].
At the ion impact there is also a chance that secondary electrons are released from the target, typically being a few percent of the quantity of sputtered atoms. These electrons are accelerated across the dark space toward the negative glow region where they ionise gas atoms sustaining the process. Further ion-target interactions are introduced as shown in Figure 3. The bombarding ions are generally from the inert gas (working gas), most commonly argon.

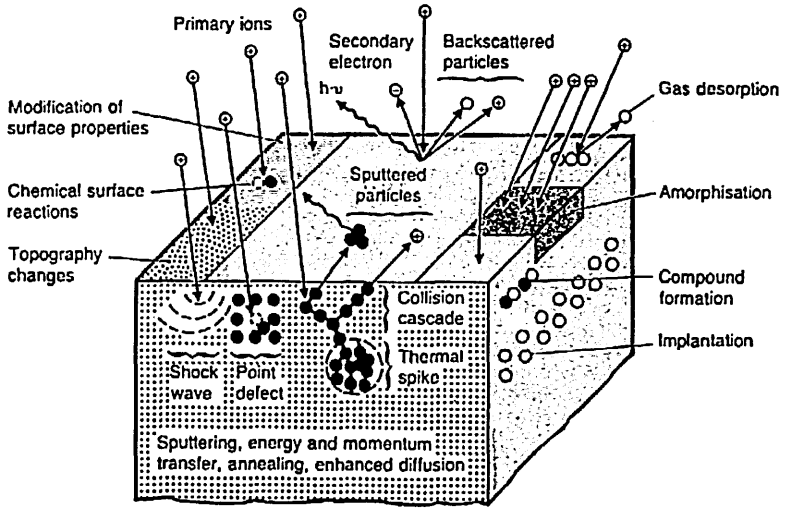

Figure 3 Schematic diagram of possible effects of ion bombardment

In conventional (diode, dc) sputtering the material removal is very slow due to low ionisation density. In magnetron sputtering a magnetic array is added behind the target so that the secondary electrons are not able to escape to the chamber walls, but are confined to a spiral path near the target surface ionising a far greater number of working gas atoms and generating an intense plasma in front of the target. This greatly improves the efficiency of the sputtering process. The use of the magnetic field is described in Figure 4. The downside of this process is uneven target consumption as the intensity of the plasma is highest where the magnetic field is parallel to the surface of the target.

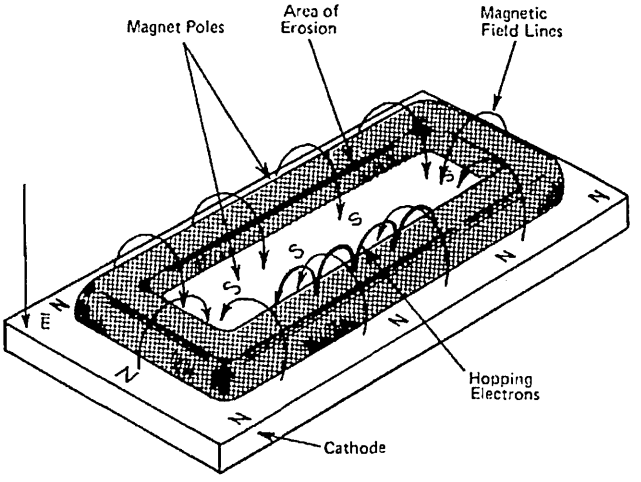

Figure 4 Schematic diagram of the magnetic confinement of the electrons in magnetron sputtering

A further development of the magnetic confinement of the secondary electrons was to unbalance the magnetic field so that part of the electrons can escape the magnetic confinement ionising the working gas near the substrate. The magnetrons with weak inner pole (type II) can provide up to 2:1 ratio of ions to deposited atoms at low substrate bias potentials [13]. Applying a negative potential to the substrate (bias) causes ion bombardment of the substrate that leads to changes in the coating described in detail in section 2.2. By arranging a number of unbalanced magnetrons that oppose one another, so that the magnetic field closes (closed field system, described in Figure 5) and confines the electrons in the centre of the coating chamber which further enhances the ionisation near the substrate [14].

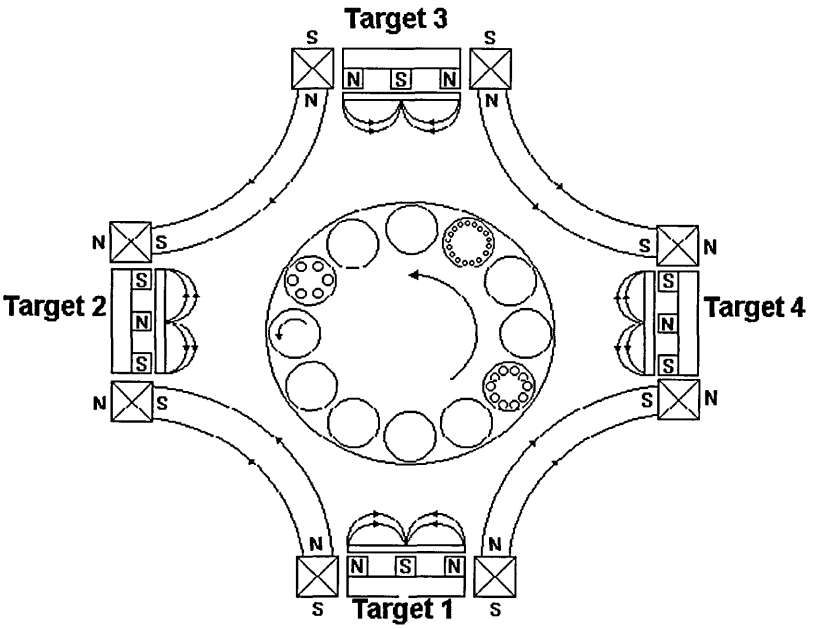

Figure 5 Schematic diagram of a closed field magnetron sputtering system

2.1.2 Cathodic Arc Evaporation

In cathodic arc evaporation an electrical arc (low voltage, high current) is generated between closely spaced electrodes. On the cathode (target material) a "cathode spot" with high current density (10^4-10^6 A/cm^2) is formed. This current density causes explosive local melting at temperatures ranging from 4000°C to 7000°C that vaporises the target material. A high percentage of the vaporised material is ionised in the arc and the ions are often multiply charged [15,16]. Since ions move slower than the electrons, positive space charge is generated in the plasma. In cathodic arc deposition adding a negative bias voltage to the substrate accelerates the ions towards the substrate, which leads to significantly higher ion energy of the arriving atoms (50-150 eV) than in sputtering (< 10 eV). This leads to higher adatom energy (mobility) and dense coatings.

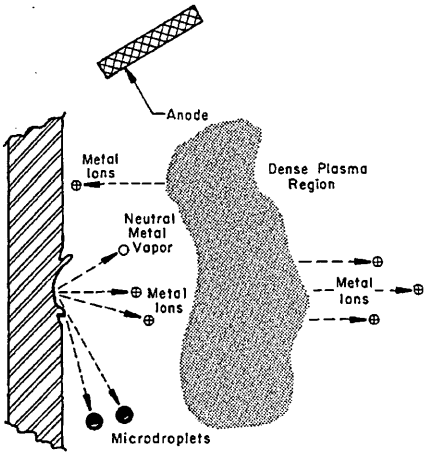

Figure 6 Schematic diagram of the vacuum arc evaporation process [2]

The current must be high enough to sustain and stabilise the arc. If the current is further increased the cathode spot may split into two or more spots. The cathode spot is not stationary and will move randomly if no external magnetic field is applied. The speed and the direction of the arc movement is affected by the gas composition and pressure, target material and magnetic fields. If an external magnetic field is used, the arc moves around the target in the region where the magnetic field is parallel to the surface (thus the name steered arc). Due to the increased cathode spot velocity the emission of macro-particles is lower with a steered arc [17,18].

The main downfall of the cathodic arc is "droplets" or "macros". These "droplets" are tiny solid or liquid particles that are generated at the arc spot when the target material is abruptly melted. As these droplets land on the substrate they generate local growth defects that are generally detrimental to the wear properties of the coating. Low melting point materials and slow (random) arc movement generate more and bigger droplets. The method commonly applied to eliminate droplets is a 90° arc ('duct') with a magnetic field steering the charged particles (ions) toward the substrates. The obvious drawback of this approach is that only the ions with the correct charge are used in the deposition reducing the deposition speed and efficiency. This method is called filtered arc deposition.

2.1.3 ABS Technology

Arc Bond Sputtering (ABS) is a hybrid of Unbalanced Magnetron Sputtering (UBM) and Steered Cathodic Arc (CA) combining the benefits of those technologies. A steered arc is used to generate a highly ionised metal plasma, which is utilised to etch the substrate before coating is deposited with UBM. This technology was developed by D. Münz et. al. at Hauser Techno Coating NV [19]. The magnetrons are arranged in closed field configuration in which the unbalancing can be adjusted using external electromagnets. The layout of the ABS machine is shown in Figure 4. In order to utilise CA and UBM using the same source the magnetic fields need to be modified between the two process steps. The outer poles of the magnetic array are retracted in arc mode as shown in Figure 7.

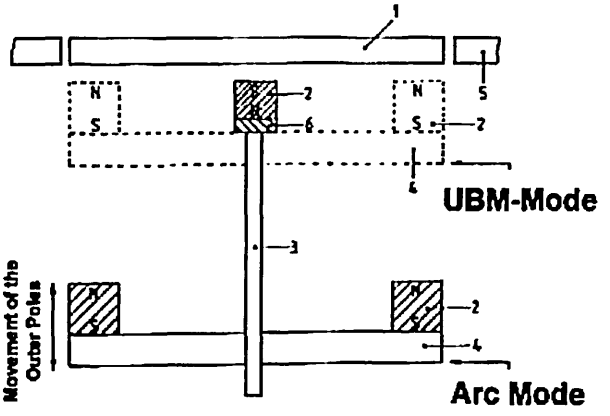

1 = target 3 = fixturing of center poles 5 = recipient

2 = permanent magnets 4 = magnetic yoke 6 = magnetic neutral spacer

Figure 7 Schematic diagram of the magnetic array in ABS system

In the steered arc mode metal vapour is highly ionised and thus can be accelerated towards substrate using a bias voltage. At low ion energies (bias voltage) the ion/atoms deposit on the surfaces. As the energy is increased the metal ion bombardment starts sputtering the substrate. Highly ionised ions will gain enough energy to implant several nanometres into the substrate. The metal ion etching with high bias voltages provides efficient cleaning of the substrate. The ion implantation has been shown to enhance the adhesion, thus the performance of the coating [20].

The downside in the use of cathodic arc is the increase of the growth defects caused by macro-particles inherent in the CA process [20-23].

Coating in the ABS process is generally carried out in magnetron sputtering mode as it provides flexibility in material choice and improved process control. The control over the unbalancing and bias voltage gives the ability to adjust the ion bombardment of the substrate.

2.2 Film Formation and Structure Zone Models

The structure evolution of thin films can be described by three processes [2]:

1. Nucleation
2. Growth of nuclei
3. Film growth

2.2.1 Nucleation

When the atoms arrive at a surface they can be:

1. Reflected immediately
2. Re-evaporate after a residence time
3. Condense permanently

If atoms do not immediately react with the surface they have a degree of surface mobility. The surface mobility depends on the energy of the arriving atom, together with the chemical composition and crystallographic planes of the surface. If the atom does not condense within a certain time it will re-evaporate. Residence time is a function of the bonding energy between atom and the surface, the substrate temperature and the number of mobile adatoms. The larger the free energy of the surface, the bigger probability there is for an atom to re-evaporate.

The adatoms condense on a surface by:

1. Making chemical bonds
2. Locating at preferential nucleation sites
3. Colliding or reacting with adsorbed surface species

Chemical bonds can be metallic (homopolar), electostatic (ionic) or electrostatic attraction (van der Waals). If the bonding force is strong the atom is said to be chemisorbed. On the other hand if the adatom-surface interaction is weak the atom is likely to adsorb at preferred nucleation sites. Such sites can be:

- Morphological discontinuities (steps, scratches)
- Lattice defects (dislocations or grain boundaries)
- Foreign atoms or change in chemistry

Mobile atoms can also nucleate by collisions with other mobile atoms. Thus the nucleation can depend on the arrival flux of the atoms. At high flux there are a large number of collisions and therefore a higher nucleation rate.

2.2.2 Growth of Nuclei

After the nucleation step, the grains will start to grow as more and more atoms arrive at the surface. Three different types of nuclei growth mechanisms have been determined [23a]:

1. van der Merwe (monolayer by monolayer growth)
2. Volmer-Weber (3D nucleation and growth)
3. Stranski-Krastanov (altered surface layer)

The nuclei grow as they collect atoms that diffuse over the surface. Initially isolated nuclei grow on the surface until they eventually form a continuous film. In van der Merwe mechanism the films forms one molecular layer at a time. This is not common for engineering coatings but can be utilised in silicon processing. The Volmer-Weber mechanism can be characterized by three dimensional growth and nucleation. The Stranski-Krastanov (S-K) growth is the most common for metal on metal deposition

and at low temperatures, where the adatom mobility is low. In the S-K mechanism an altered interfacial layer with pseudomorphic structure forms first, followed by nucleation of the grained structure on this layer. The initial grains then grow in size until they meet one another. It is important to realize that at low adatom energies the growth can result in voids at the interface if the nuclei growth is fast and nucleation is difficult as the growing grains meet before the surfaces are fully populated. Ideally an epitaxial growth, in which the growing film aligns itself to the underlying crystal structure, should be aimed for.

2.2.3 Film Growth

The details of the condensation processes that determine film morphology at low temperatures are not well understood, but the following factors have been identified as contributors:

- Angle of incidence of adatom flux
- Ratio of the deposition temperature to the melting temperature
- Energy released on condensation
- Adatom surface mobility
- Surface roughness
- Deposition rate
- Void coalescence
- Mass transport and grain growth during deposition
- Adsorption of inert and/or reactive gases
- Gas scattering of vaporised particles
- Bombardment by high energy particles

As can be seen the morphology of the films depends on multiple items. Some of them can be easily controlled, like the atmosphere and the adatom energy and flux, some are material properties, and some are determined by the limitations of the practical applications. Generally the surface roughness increases as the film thickness grows because some features and crystallographic planes grow faster than others. Strong ion bombardment of the substrates can be used to level the grains out.

Particulates on the surface induce local changes in the microstructure. These local features can grow at a higher rate than the rest of the coating as is shown schematically in Figure 8. They are also often poorly bonded to the film and the substrate and can easily come off leaving pinholes in the coating. Figure 9 shows an SEM image of such a defect on a Nb-CrN/NbN coating.

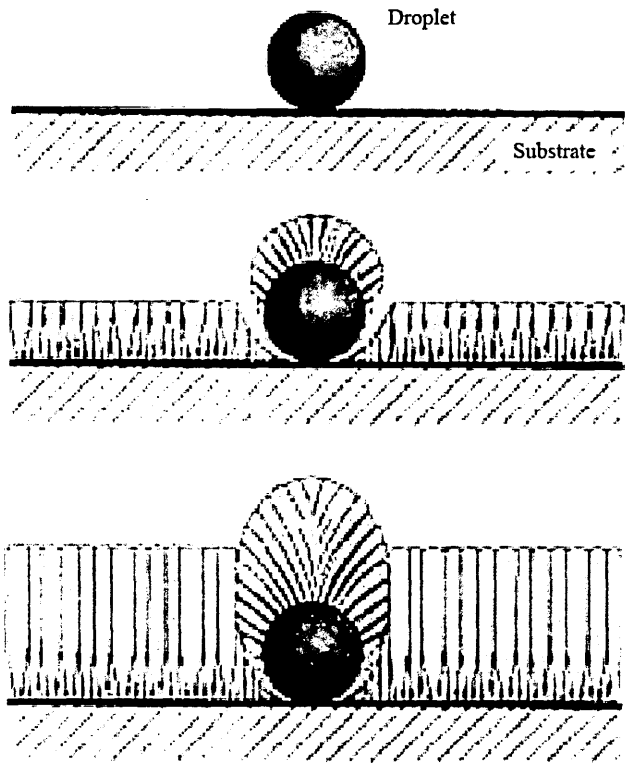

Figure 8 Schematic diagram on how a droplet on the surface affects local film growth

Figure 9 SEM cross-sectional image of a droplet and associated growth defect in Nb-CrN/NbN coating

Under conditions of high ion bombardment the growth defects can "heal". An investigation of the microstructure of arc deposited coatings showed dense columnar morphology even though the coatings were full of growth defects caused by droplets inherent to this process [23b]. Figure 10 shows a cross sectional micrograph of an arc deposited CrN/NbN coating with a droplet imbedded into the coating. The defect can be seen to self-repair within 100 nm of growth, thus a through coating defect is not formed under these deposition conditions. This behaviour shows that under the right conditions, normally involving high temperature and ion energies, the adverse growth around the defects can be prevented with the use of favourable deposition parameters leading to fully dense coatings.

Figure 10 Defect in arc deposited CrN/NbN that is closed under high ion bombardment

2.2.4 Structure-Zone Models

Typically the substrate material influences the film growth near the interface and it takes a substantial thickness before the film establishes its particular growth mode. The growth mode can be described by a Structure-Zone model.
The best known vacuum deposition stucture-zone models have been developed by Movchan and Demchishin (1969) [24], Thornton (1977) [25] and Meissier (1984) [26]. Figure 11 shows Thornton's structure zone model.

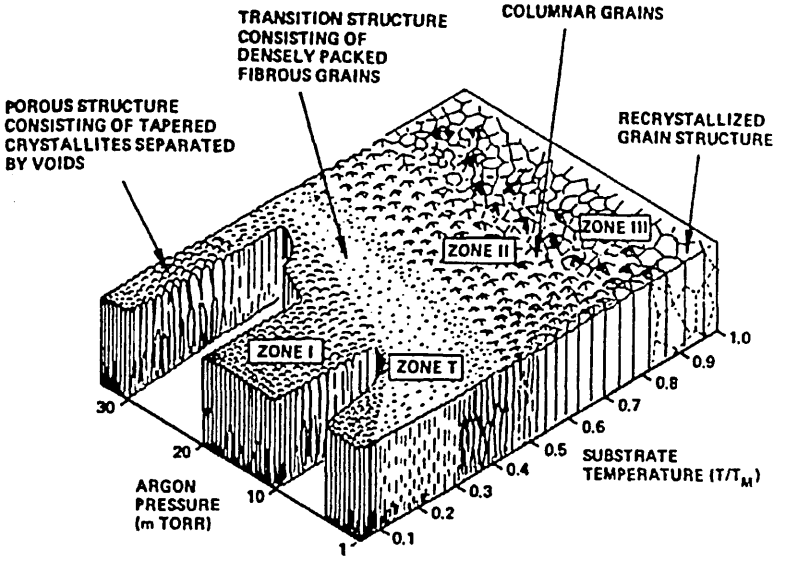

Figure 11 Thornton's structure zone model

Thornton et al. studied the effects of the relative substrate temperature (temperature divided by melting temperature of the coating, which relates to thermal energy, thus adatom energy on the surfaces) and argon pressure (relating to incoming ion energy, due to collisions with inert argon atoms) to the microstructure of the thin films. He observed 3 different zones that he named Zone 1, Zone T and Zone 2. He concluded that the roughness of the depositing film affects the structure since the peaks receive flux coming from all directions and if the mobility of the adatom is low the peaks grow faster than the valleys. In Zone 1 of the model the surface mobility of the adatom is not sufficient to generate sufficient flux of atoms to the valleys and thus the shadowing effects lead to columnar structure with open boundaries and voids between

the columns. High gas pressures extend this zone to higher temperatures due to the increased probability of collisions to the gas atoms that reduce the energy of the arriving atoms. The columns are generally not single grains and can be either large or small. If the angle of incidence is small the columnar growth is exacerbated as the valleys get even less flux.

In Zone T of the Thornton model the coating has fibrous morphology. This zone in often considered as a transition between Zones 1 and 2. The fibrous morphology is caused by bombardment with high energy atoms and ions that erode peaks and fill valleys.

In Zone 2 the adatom has enough energy to diffuse into the valleys. The resulting structure is still columnar but there are no voids at the grain boundaries. The grain size is also larger and the surface tends to be faceted.

In zone 3 the bulk diffusion is high and thus re-crystallisation and grain growth can occur. The resulting grains are large, though the structure can still be columnar.

Messier altered Thornton's model by replacing the pressure axis with an adatom energy axis, as shown in Figure 12. An increase in the bias voltage, for example, results in an increased average energy and enhanced the adatom mobility. The model illustrates that zone T microstructure can be achieved at lower temperatures as the energy of the adatom is increased.

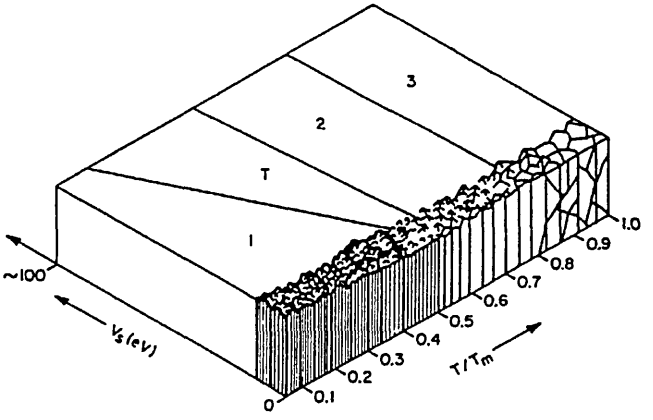

Figure 12 Messiers structure zone model

Kelly and Arnell developed the model further as higher ionisation rates became possible in closed field systems. This model describes the coating structures in terms of homologous temperature, bias voltage (or ion energy) and ion-to-atom ratio. They observed that the structure of the film can be altered by changing the incoming ion energy, the ion flux or by bombardment of the substrate with ions (mainly argon) by applying negative bias voltage to the substrate. Kelly's and Arnell's investigation revealed that the structures of coatings were either fully dense (Zone 3) or dense-columnar (Zone 2). Structures corresponding to zone 1 of Messier's model were not produced in their investigation, as shown in Figure 13.

The investigation shows that with the closed field sputtering systems "high temperature" structures can be achieved at relatively low temperatures while the formation of the "low temperature" zone 1 and zone T structures is suppressed. A high ion-to-atom ratio enables the production of dense high quality films even at low temperatures.

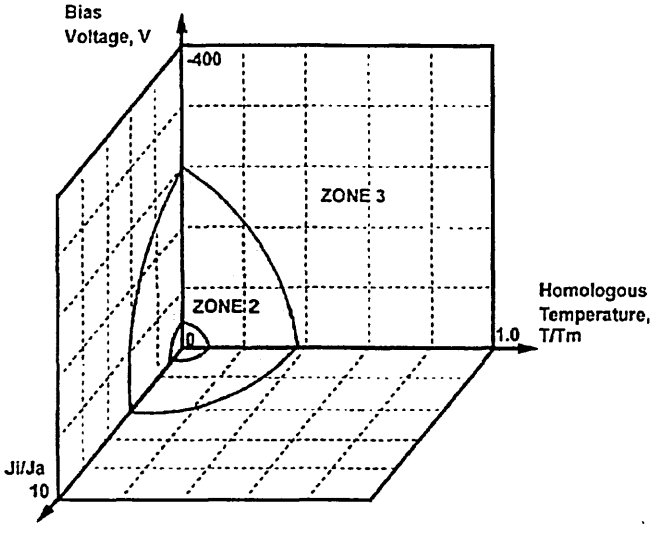

Figure 13 Kelly's and Arnell's structure zone model

2.2.5 Modification of the Microstructure and Morphology

The earlier studies, as described in the previous sections, have shown that the microstructure and the morphology of the coating can be affected by altering deposition conditions. The commonly used methods include [5]:

1. Bulk or surface heating
2. Changing angle of incidence
3. Changing deposition rate
4. Changing ion/neutral ratio in the flux
5. Changing gas pressure
6. Affecting bombardment by energetic particles by
    a. Changing potential of the substrate (bias voltage)
    b. Modifying magnetic fields in the deposition chamber (ionisation near the substrate)
7. Changing coating composition by
    a. Alloying target material (impurities, dopants)
    b. Changing power ratio between cathodes made from different materials (co-deposition)
    c. Changing gas composition (in reactive sputtering)
8. Post deposition heat treatment

The most effective way to alter the microstructure is through changing the energy of the adatoms via an increase/decrease of thermal or kinetic energy, thus increasing/reducing the mobility of the adatoms. Further, bombardment with energetic particles can also cause resputtering and/or point defects that may act as nucleation sites. A large flux of atoms is generally regarded as beneficial as it increases nucleation and the ratio of contamination versus arriving atoms is smaller. PVD coatings deposited at low temperatures generally exhibit large internal stresses that may be relieved with post deposition heat treatment.

2.2.6 Growth related film properties

Films deposited using PVD invariably have properties that differ from bulk materials [27]. Columnar morphology and residual film stress are influencing many properties of the deposited film.

The residual stress that is characteristic of atomically deposited films can be either tensile or compressive. It can also be very high approaching the yield strength of the material. Generally tensile stress is present in coatings deposited at high gas pressures. They tend to develop when the growth does not allow the deposited atoms to find thelowest energy positions (adatom energy is small). Compressive stress is common under high energy particle bombardment. The origin of the stress is poorly understood, though there are models suggesting mechanisms [28]. It has been shown also that mechanical properties of the deposited metal and incorporation of impurities play a large role in the residual stress. With films deposited at high temperature the thermal shrinkage stresses due to mismatch of thermal expansion coefficients of the coating and the substrate can put the film in tension. Film stress also tends to change with the film thickness. Commonly stress builds up as the film thickness increases, but changes from tensile to compressive have also been observed. Local stresses can also build up at discontinuities in the substrate, such as steps and edges. High isotropic compressive stresses can produce "worm track" patterns in the failure areas while tensile stress can produce micro-cracking. As a rule of thumb high-modulus materials such as chromium are difficult to deposit due to extreme tendency for residual stress.

The density of the deposited films is often less than the bulk material due to voids and pinholes in the coating. The porosity will affect films mechanical and barrier properties as well as the surface area of the coating.

Both of the afore-mentioned items, along with the crystallographic structure influence the electrical properties of the coatings.

The atomistic methods can also be used to deposit material which can not otherwise exist. These amorphous or metastable coatings can have unique material properties that are still waiting to be discovered.

2.3 *Multi-component and multi-layer, superlattice structured coatings*

The PVD process facilitates the use of a number of different materials in the coating. Sputtering is the most versatile process since it is possible to use a number of cathodes with different target materials simultaneously. In addition to that, alloy targets can be also used to deposit metallic or ceramic compound materials. Further, different coating parameters (i.e. atmosphere/reactive gases and bias voltage) greatly affect the structure and properties of the coating.

2.3.1 Reactive deposition

Reactive deposition is the formation of a film of a compound either by co-deposition and reaction of a deposited species or by the reaction of a deposited species with the ambient gaseous environment [6]. Generally, in low temperature deposition, one of the components is condensable and the other is gaseous. Most common reactively deposited coatings are nitrides, oxides or carbides [2, 3].

The chemical reactions occur on surfaces, where deposited adatoms (metal) react with gas atoms that impinge on the surfaces (N, O or alkanes, such as methane). The reaction occurs also on the cathode (target) surface. In the stable state the target remains metallic due to continuous sputtering of its surface. If the partial pressure of the reactive gas is increased beyond certain point a reactive film starts to form on the cathode. This is a critical control point in the process, since it starts an irreversible poisoning process. As the film forms on the cathode the sputtering rate of the target material drops as the compounds have lower sputtering speeds. Further, some compounds, i.e. most oxides, are insulators reducing the electrical field in the dark

space. A lower deposition rate means a lower consumption of the reactive gas and thus increased partial pressure of the reactive gas. If the reactive gas pressure is reduced the system does not convert back to normal mode at the same pressure, but at a significantly lower one [2-5].

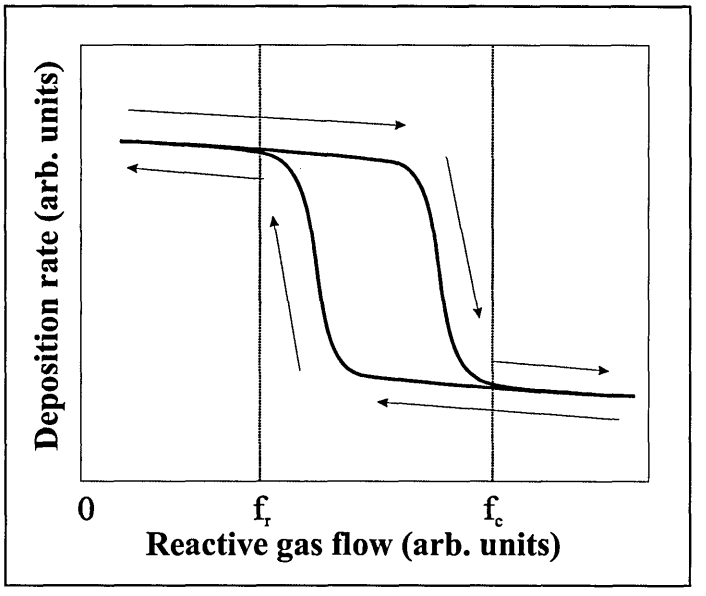

Figure 14 Deposition rate as a function of reactive gas pressure in reactive deposition (hysteresis effect)

This hysteresis effect (Figure 14) causes a control problem in reactive coating systems, since the "knee" in the curve is often the desired and most economical point in the coating process. There are several approaches to fixing this problem [2].

a) *Feedback loop of reactive gas flow* utilises optical emission measurements to control gas flow to keep the process in the desired position on the process curve.
b) *Increased pumping speed* reduces the size of the hysteresis loop as the vast majority of the gas goes to the pumping system instead of the deposited films.
c) *Dual cathode* setup where one of the pair is used as the anode for the half of the cycle and as the cathode for the other half provides stable operation in most difficult conditions as there is always an unoxidised anode surface.

d) *Gas/cathode separation* can function in a laboratory system where baffles and direct injection of the gas can be utilised to keep the reactive gas from the cathode

The Hauzer ABS coater at SHU relies on very high pumping speed and accurate pressure monitoring with a feedback loop to control the reactive deposition processes [19].

2.3.2 Multi-layer coatings

Most commercial coatings have a number of distinct layers. The most common reason for layer structure is to provide a gradient in hardness to reduce shear stresses at the interfaces of hard coatings. Layering can be used to enhance adhesion or to make more complicated diffusion paths. Layering can be also used to reduce intrinsic stress by using alternating layers of high and low stress.

In the CrN/NbN coatings this approach is exploited with the use of a CrN base layer. This layer is softer and has lower stress than the superlattice thus it provides a gradient into the interfacial stress. It has also very good adhesion to the substrate especially after Cr ion etching.

By adding an additional barrier layer between the CrN layer and the superlattice the corrosion properties of the coating on low alloy steels can be significantly enhanced. A niobium layer has been used due to its superior corrosion properties.

2.3.3 Nanoscale multilayer coatings

Nanoscale multilayer coatings are an extreme case of layered coatings. Nanoscale multilayer coatings (also often called superlattice coatings) refer to coatings, which have ultrafine (period, $\lambda < 10$ nm) layer structure of two distinct materials. The peak hardness is normally measured with the bi-layer thickness between 3-5 nm [29]. The period can be controlled by rotation rate of the turntable onto which the substrates are

fixed or by varying the target powers or by applying moving shutters in front of different targets [30]. A number of similar nanostructured coatings using a variety of material combinations are currently in commercial use.

The increase in hardness of the nanoscale multilayer structure was measured to be greater than expected from the "rule of mixtures" of the constituent materials [31, 31a]. More than thirty years ago, Koehler suggested that the fabrication of a layered structure of two materials with the same crystal structure results in a high strength material. He explained that the interfaces between the layers of materials with different shear moduli would act as barriers to the motion of dislocations [32]. A more detailed model about the dislocation movement in superlattices was developed by Xi Chu and Barnett [33, 34]. This model includes the fact that the interfaces are not usually abrupt and that interfaces wider than 1nm tend to reduce the effect of having alternate layers with different shear moduli. Their work revealed that for TiN/NbN coatings the hardness value has a maximum at an intermediate value of the superlattice period, λ. This was shown in practice by U. Helmersson et. al. for the TiN/VN superlattice coating (Figure 15) [29].

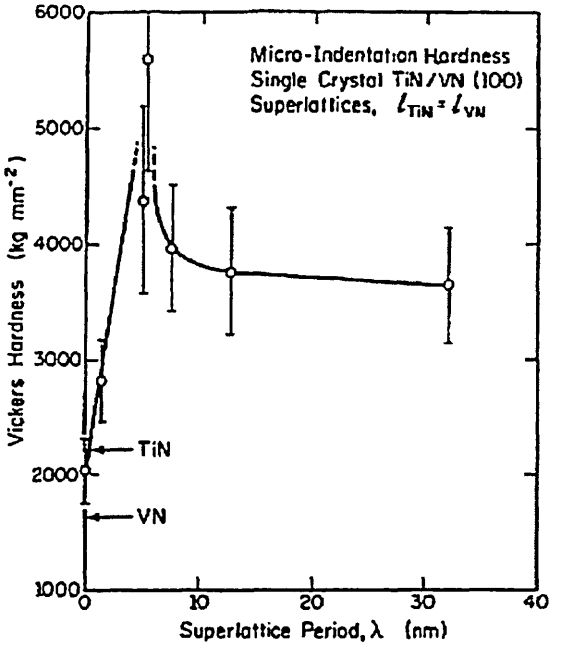

Figure 15 Hardness of the superlattice depends on the superlattice period

If λ is very small, the layers easily become too inter-diffused thus eliminating the shear modulus at the interfaces. Also if the interfaces are too close together the stress needed to move a dislocation is lowered due to the fact that interfaces can exert opposing forces on a dislocation at an interface. Although the nature of the enhanced hardness is still not fully understood, single crystal (TiN/NbN) and polycrystalline nitride (TiN/VN, TiAlN/CrN, TiAlN/ZrN, AlN/TiN) films have been successfully developed and brought into practice [35].

XTEM investigations of the wear mechanism of monolithical and nanoscale multilayer coatings revealed that the individual grains of columnar and monolithically grown coatings suffer severe plastic deformation when exposed to external shear forces. This deformation can be the source of mechanical failure. The depth of these failures is in the range 50 to 75 nm. Due to a chipping or a micro-delamination mechanism in the nanoscale multilayer coatings the failure depth was noted to be around 6-8 nm due to disruption of the crack propagation at the layer interfaces, as described in Figure 16 [36].

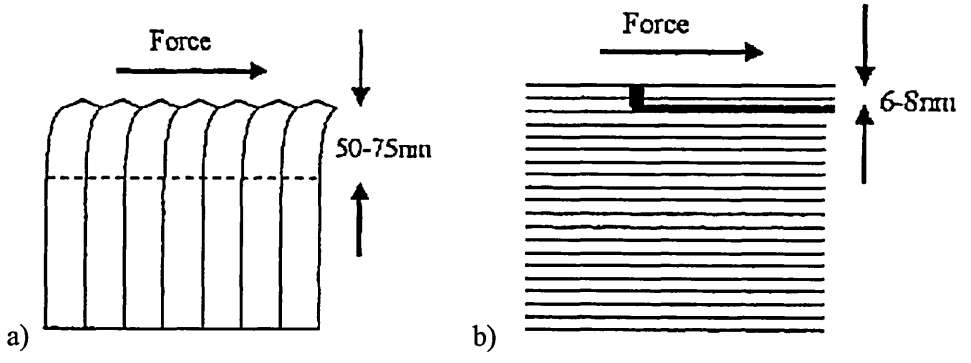

Figure 16 The wear mechanism of a) monolitical and b) nanoscale multilayer coatings

2.3.4 Duplex Coating

A combination of a conventional surface treatment, such as nitriding, and PVD coating is often referred to as a duplex coating. The surface treatment prior to PVD deposition will give enhanced surface properties to the substrate to a depth that far exceeds the thickness of the PVD coating. The effectiveness of the treatment varies largely depending on the substrate material. On highly alloyed steels, such as HSS, the aim has been to produce a thin, hard and well adherent layer as a gradient hardness layer, with the ultimate goal of improving adhesion and thus wear resistance of the tool. On low alloy steels the aim has generally been to improve the surface properties of these tough, impact resistant alloys as shown by Höck et al. in Figure 17 [37].

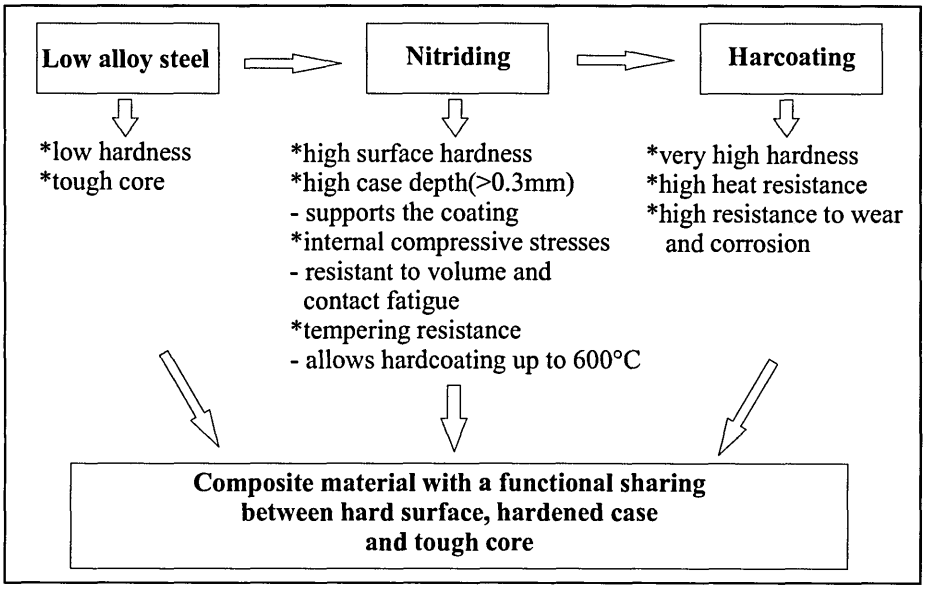

Figure 17 Combination of properties of duplex coating on low alloy steel

If the substrate cannot adequately support the forces it is subjected to, the coating will fail as shown by Zlatanovic, et al.. If the normal load that applied on the coated substrate is larger than the load bearing capacity of the substrate the substrate yields causing the hard coating to crack and fail as shown in Figure 18 [80].

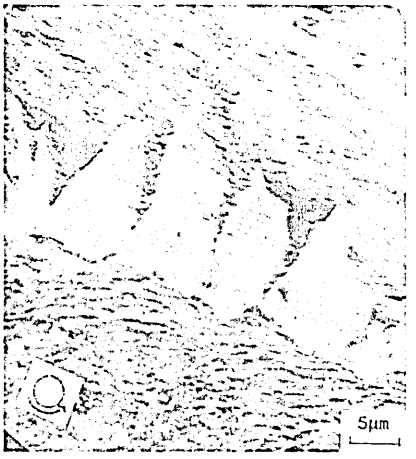

Figure 18 Coating failure due to insufficient support for the hard coating

Tribological coatings have been generally developed for very hard substrates such as high speed steel or cemented carbide. Such materials cannot always be used due to cost and manufacturing considerations.

The mechanical properties of the substrate near the interface affect the fatigue wear properties of the coated parts as the maximum shear stress occurs just beneath the surface (explained further in the section 2.5.3.). This stress can generate sub-surface cracks that propagate through the coating causing sudden failure of the coating as outlined in Figure 19. Duplex treatment of the near surface region can be used to improve both load bearing capacity and to reduce the crack formation.

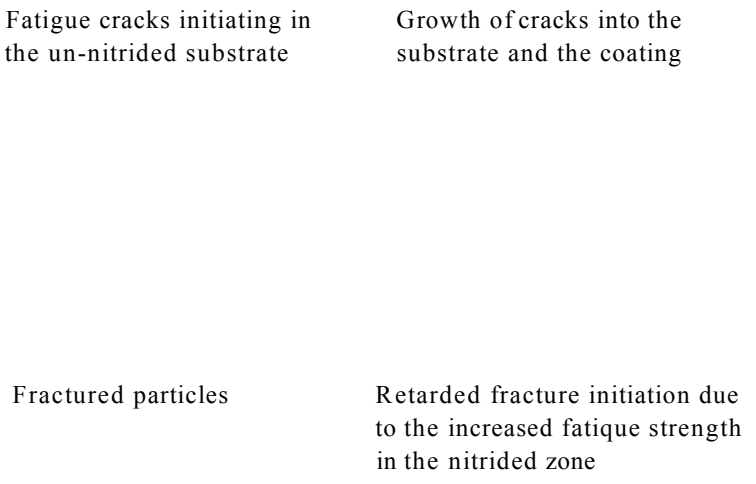

Figure 19 Schematic diagram of the way the crack propagation from the substrate to the coating can be prevented by surface treatment of the substrate. A load on the surface initiate cracks in the substrate (a) that will advance into the coating (b) causing fractures and fatigue failures of the coating (c) Increased load bearing ability and compressive stress in the nitrided zone prevents crack from forming and advancing in the substrate.

Most common surface hardening methods are nitriding, carburizing, carbonitriding and boriding. The basic principle in all these hardening methods is diffusion of a small gas atom into the metal lattice at an interstitial position in which it prevents the movement of dislocations which translates to higher hardness of the surface. There may also be a compound phase, such as Fe_4N, forming on the surface. The processes are normally done at high temperatures (up to 1000°C) in the presence of the reactive gas or liquid.

Recently nitriding has been used in combination with PVD coatings (duplex coatings) with good results [38-46]. The nitriding process can be performed prior to a PVD

process with any conventional method or in conjunction with the PVD process using low-pressure plasma nitriding [47]. Nitriding provides increased surface hardness (in excess of $H_V = 1000$), providing the support that is required by the coating. It also reduces the stress gradients at the interface caused by dissimilar properties with the PVD coating (over $H_V = 3500$). This is schematically presented in Figure 20.

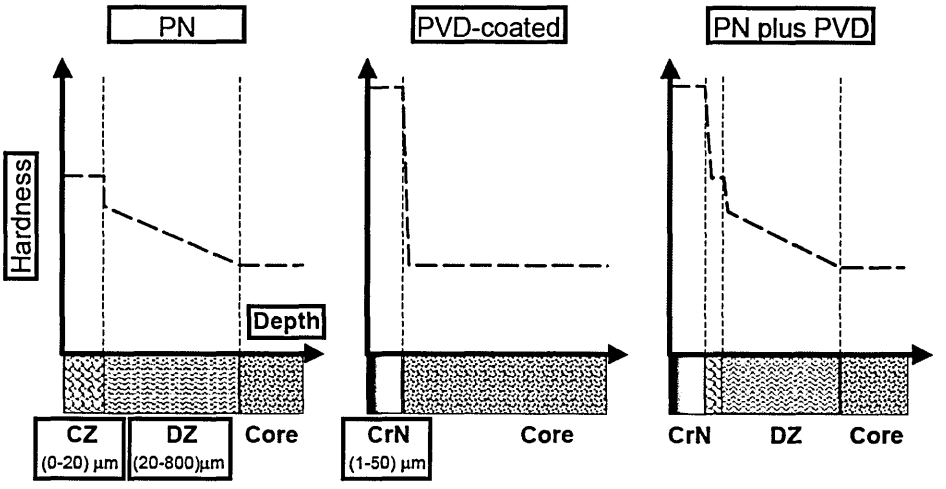

Figure 20 Schematic of the hardness profiles of duplex coatings, CZ refers to Compound Zone, DZ to Diffusion Zone and PN to Plasma Nitriding [48]

The compound layer (Fe_4N or Fe_3N) has often been regarded to be detrimental to adhesion and is thus often avoided or removed mechanically [39,43], yet it has been shown in some instances to improve wear resistance [38,40, 46]. The compound layer is generally thought to be problematic due to the porous top layer and instability at high temperatures (> 500°C). It can however be beneficial due to its high hardness and improved corrosion resistance. The work by Nayal et al. [46] demonstrated that metal ion etching prior to PVD coating may be required to achieve acceptable adhesion.

The biggest concern in the nitriding is the Fe_xN compound layer also called the "white layer". This Fe_xN layer may become unstable at elevated temperatures (ca. 500°C) converting back to soft α-Fe, also called the "black layer", causing a adhesive failure in any subsequent layer. A brittle or cohesive failure within the compound layer has been often identified as a cause of premature failure and many groups are determined to avoid it, even to the extent of removing it mechanically. It is also possible to avoid

the compound layer and perform the nitriding step in a PVD coating machine as demonstrated by Kammingaa et. al. [47].

Nitriding

Nitriding is a surface hardening process used to improve the wear, fatigue and corrosion properties of a wide variety of metals. Nitriding is generally done in partially dissociated ammonia at temperatures above 500°C. Nitrogen from ammonia diffuses into the metal yet it also forms compounds with the iron that make a very hard surface layer. The traditional nitriding process takes a very long time, 20-90 h which has led to the development of faster processes like plasma nitriding. In plasma nitriding a nitrogen plasma is formed in vacuum (100-1000 Pa) with a DC glow discharge. The treated surfaces are bombarded with positively charged nitrogen atoms that heat the surfaces to 400-600°C depending on the discharge power. Since the diffusion at low temperatures is very slow a higher power is used when a thicker case depth is needed. Plama nitriding is done in ammonia or nitrogen atmosphere with or without the presence of hydrogen or argon. Argon can be used to sputter the surfaces clean of impurities. The biggest advantages of plasma nitriding is reduced treatment time and energy usage as well as improved process control [3, 49].

The nitrogen initially forms FeN on the steel surface. Since this compound is not stable it decomposes into lower nitrides Fe_2N, Fe_3N and Fe_4N while the liberated nitrogen diffuses further into the steel lattice. An abundant supply of nitrogen creates a steep concentration gradient into the work-piece.

The characteristics of these compound layers, like phase composition and thickness, can be easily changed by varying the working parameters. For example, using low nitrogen concentration (15–30 vol.%) in the treatment atmosphere means that a compound layer consisting only of the Fe_4N (γ'-phase) will be produced, while increasing the nitrogen concentration, both iron nitrides are obtained. Further, a compound layer comprising only the Fe_3N (ε-phase) can be produced by adding a low amount of CH (usually 1–3 vol.%) in the treatment gas mixture. A γ'-phase layer is tougher and shows better wear and fatigue properties under severe loading conditions,

while an ε-phase layer increases anti-scuffing properties and is suitable for applications relatively free of shock loading or high localised stresses [50-53].

Carburizing

In carburising, steel is heated to 900°C in the presence of a carbon-containing gas such as methane or CO. Carbon then diffuses into the surface of the steel hardening it. The high temperature (as well as phase changes) used for this process often cause minute dimensional changes which limit the usability of this process for high accuracy components [3].

Carbonitriding

Carbonitriding is a hybrid of nitriding and carburizing. Ammonia is added to the carburizing gas, causing the formation of carbonitride film on the surfaces [3].

2.4 General Corrosion Theories

Corrosion is defined as "a chemical or electrochemical reaction between a material, usually a metal, and its environment that produces a deterioration of the material and its properties" [6]. Thus corrosion is closely related to the materials and the environment. Though corrosion can also occur in a gaseous environment corrosion experiments are mostly done in aqueous or aggressive humid environments.

Corrosion is driven by thermodynamics through a principle that reactions occur to achieve lowest possible energy. An investigation of the relevant thermodynamic equations will reveal which reactions can occur in a certain environment. However in practice the corrosion is normally limited by kinetics. Kinetics determine how fast corrosion reaction occur. For practical consideration, when the corrosion reactions happen at rates that are acceptable, corrosion is not occurring.

In respect to coatings the coating-substrate interactions should be taken into account since all coatings have/are susceptible to defects and the environment eventually penetrates the coating. Generally, good barrier properties can be provided only by a coating with a relatively pore-free structure and good adhesion.

2.4.1 Electrochemical reactions

Corrosion is an electrochemical reaction with four steps as described in Figure 21 [54, 55].

1. Anodic reaction (e.g. Metal dissolution: $Me \rightarrow M^{n+} + ne^-$)
2. Cathodic reaction (e.g. Hydrogen evolution: $2H_2O \rightarrow H_2 + 2OH^-$)
3. Ionic path between anodic and cathodic locations (electrolyte in aqueous environment)
4. Electronic path between anodic and cathodic locations (normally through metallic contact)

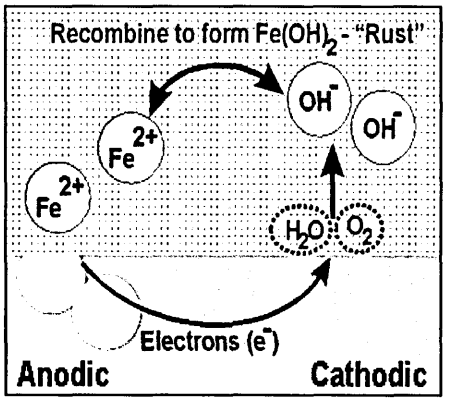

Figure 21 Schematic diagram of aqueous corrosion of steel

Since the reactions form a closed electrical circuit, all of the reactions have to be able to occur simultaneously, with the slowest of the reactions determining the rate of the reaction. Thus a common way to control corrosion is to limit the kinetics of one of the four components.

The driving force of any chemical reaction is a reduction in the free energy. Since corrosion products commonly have lower free energy than metals corrosion occurs. The change of the free energy consists of the sum of the potentials of the cathodic and anodic reactions. There are two ways to control corrosion through thermodynamics.

The first is to set the conditions so that the corrosion reactions cannot occur. The alternative to this is to offer a controlled reaction that is thermodynamically preferable to the detrimental corrosion reaction.

Many metals rely on passivation, i.e. formation of a stable oxide, for corrosion resistance. This works in an environment where the oxide can reform once broken. With such metals, like stainless steel, the predominant corrosion form is localised corrosion, i.e. pitting, where the corrosion is very fast in small active (anodic) areas, from where the passive film is broken, while the majority of the surface is passive (cathodic). Areas where the local conditions are dissimilar to the bulk can also cause localised corrosion. Such areas can form for example in crevices where limitations to material transfer cause differences in oxygen and metal ion concentrations. High temperatures and wear/flow conditions may also prevent a passive film from forming also resulting in localised corrosion [54-55].

2.4.2 Coating-Substrate System

In principle, the corrosion resistance is determined by the surface in contact with a corrosive medium. PVD coatings are generally chemically very stable and/or noble materials with very good corrosion resistance. Practically, however, the majority of these coatings, prepared by any PVD technique, behave to a less satisfactory extent with respect to their theoretical corrosion resistance. This is due to the presence of solution-path defects within these coatings, leading to galvanic and crevice corrosion between the coating and the substrate via the defects [56]. In these locations (and in locations where the coating has been damaged) the interaction depends on the chemical potential of the substrate with respect to the coating as shown in Figure 22.

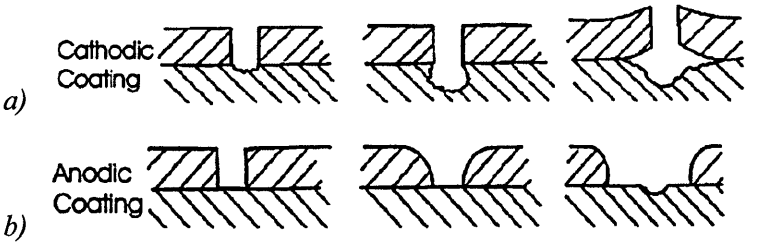

Figure 22 Corrosion of a) cathodic and b) anodic coating at defect location

If the chemical potential of the coating is higher than the substrate in a given environment (coating is more noble than the substrate, Figure 22 a) the coating becomes the cathode and the substrate the anode. This leads to the corrosion of the substrate, while the coating remains mostly intact. The ratio of the cathode/anode area is very high leading to situation where the anodic reaction or diffusion (ionic path) will determine the rate. This generally leads to rapid localised corrosion at the defect locations. The larger the potential difference between the coating and the substrate the higher the driving force thus leading to higher corrosion rate.

On the other hand if the coating is less noble than the substrate (Figure 22 b) the coating will be the anode and thus protect the substrate until the coating has corroded to an extent that separate anodic and cathodic regions can form on the substrate. If the coating is an insulator or there is an electrically insulating layer between the coating and the substrate such interactions will not occur.

The corrosion performance of PVD coatings is not very easily measured because the films are often very thin and electrochemically stable and/or noble. In such cases the coating porosity is a good measure of these defect densities and, if the porosity is sufficiently low, the sample will behave initially like the coating, i.e. it passivates or pits if the coating passivates or pits. If the porosity is high, a significant galvanic corrosion (with generally the substrate being the anode and the coating being the cathode) will make the coated sample behave like the substrate material, regardless of how noble the coating may be. In the ABS process the ion etching is done using a steered cathodic arc, which ejects micro droplets that generate growth defects like the

ones shown in Figure 9. These growth defects have been found to act as the location where the environment can easily penetrate the substrate and initiate localized corrosion. A schematic of the corrosion at the defect locations is shown in the Figure 23 [20-23,57-61].

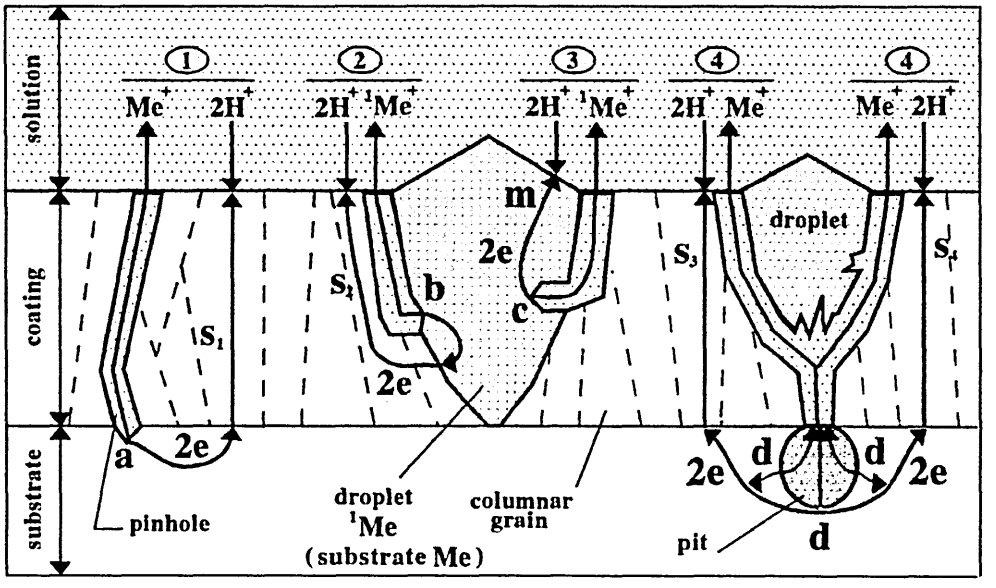

① *anodic:* $Me \rightarrow Me^+ + e$ (a) *cathodic:* $2H^+ + 2e \rightarrow H_2$ (S_1)

② *anodic:* $^1Me \rightarrow {}^1Me^+ + e$ (b) *cathodic:* $2H^+ + 2e \rightarrow H_2$ (S_2)

③ *anodic:* $^1Me \rightarrow {}^1Me^+ + e$ (c) *cathodic:* $2H^+ + 2e \rightarrow H_2$ (m)

④ *anodic:* $Me \rightarrow Me^+ + e$ (d) *cathodic:* $2H^+ + 2e \rightarrow H_2$ (S_3/S_4)

a: substrate at interface; b: droplet rim; c: droplet interior; d: pit substrate; S_i: adjacent coating grains; m: droplet top.

Figure 23 Schematic diagram detailing corrosion mechanisms at pinhole and growth defect locations [23].

Once the environment has reached the substrate a galvanic cell forms between the coating and the substrate. This generates an electrochemical reaction that causes rapid localised corrosion (pitting) at the defect locations. These pits eventually grow and the voluminous corrosion products form below the coating. If the adhesion of the coating is not good or the coating has strong intrinsic stress, the pressure at the interface may cause delamination of the coating, leading to total coating failure.

2.5 General Wear Theories

Wear happens when surfaces meet or move in respect to one another. The modelling of wear is very complicated, since there are many factors that determine the wear rate, as is shown in Figure 24 [62].

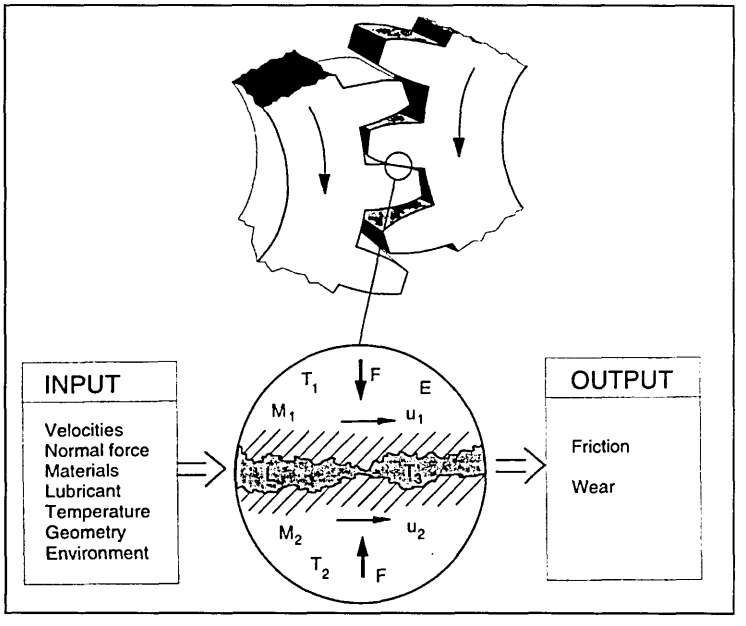

Figure 24 Key parameters that determine friction and wear in sliding contact

The general design appraisal of the tribological requirements on contact surfaces can be formulated. The following must not exceed design values:

1. Initial coefficient of friction
2. The wear of the coated surface
3. The wear of the counterpart
4. Fatigue during the designed lifetime

Thin film coatings have been successfully applied to number of tribological applications due to their extreme hardness, low friction and high oxidation resistance. Figure 25 lists the tribologically important properties of different zones in the coated surface [63].

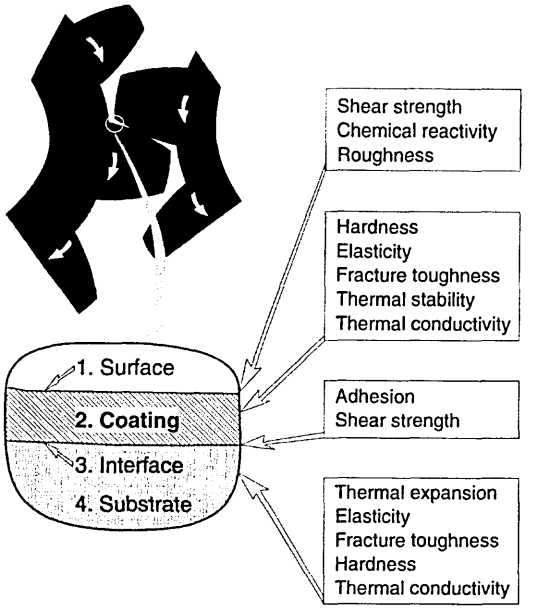

Figure 25 Different properties of surface affecting the wear rate

Basic mechanisms of wear can be categorised as

1. Adhesive wear
2. Abrasive wear
3. Fatigue wear
4. Chemical wear

The schematic presentation of wear modes can be seen in Figure 26 and are further discussed in the following sections [62].

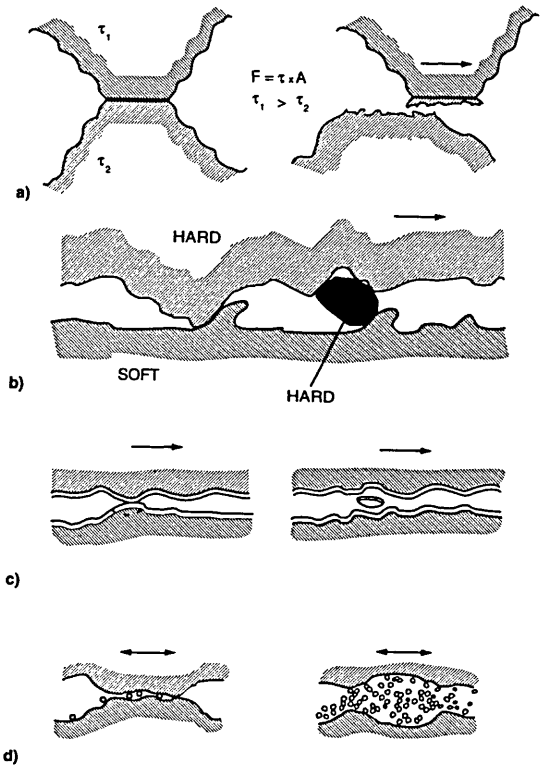

Figure 26 Basic wear mechanisms are a) adhesive, b) abrasive, c) fatigue and d) chemical wear

2.5.1 Adhesive wear

When asperities of one surface come into contact with asperities of counterpart they may adhere strongly together. Once the surfaces move in respect to one another the asperities will separate from the bulk resulting in material loss in one or both surface. It is suggested that adhesive wear is the dominating wear mechanism in un-lubricated sliding contacts.

2.5.2 Abrasive wear

Abrasive wear occurs in contacts where one of the surfaces is considerably harder than the other or where hard particles are introduced into the contact. The harder

surface asperities are pressed into softer surface. When the surfaces move against one another the softer material is removed resulting in wear scratches and grooves. The action of metal cutting has been described as abrasive wear on a large scale.

The effect of asperity deformation depends on the roughness and waviness of the contacting surfaces. It has been suggested that in the pin-on-disk wear tests the fractured coating asperities act as hard particles that result in abrasive wear.

2.5.3 Fatigue and delamination wear

Fatigue crack growth is a phenomenon resulting from cyclic loading and unloading at the stress level the material can sustain once but not if repeated number of times. In rolling, where the stress field moves repeatedly over a surface, fatigue of the near surface takes place, because the maximum shear stress occurs about one third of the contact length beneath the surface. The maximum stress moves towards the surface when the friction increases. For a friction coefficient exceeding 0.32 the maximum stress will be found at the surface. This fatigue forms subsurface voids or cracks that can easily propagate, thus liberating material.

Delamination wear occurs on a microscopic scale in contacts between asperities. Small cracks are nucleated below the surface. Further loading cycles can propagate the cracks that are parallel to the surface which eventually leads to delamination of the surface.

2.5.4 Chemical wear

In chemical wear the wear process is dominated by detrimental chemical reactions, initiated by the influence of the environment, in combination with contact mechanisms. A rubbing action can result in an environment that is favourable to chemical attack. Oxidation wear is the most common chemical wear process. The oxidation of material forms a thin, soft, oxide layer on the surface that is easily removed in sliding contact resulting in wear. In certain cases wear can be due to

chemical instability of the materials in the local environment during use. In cutting operations the local temperatures can exceed 700°C, which may lead to rapid oxidation wear of an unprotected tool.

2.6 CrN/NbN Nanoscale Multilayer Coatings

The chromium based hard coatings produced using PVD coatings, though highly successful, were found to have insufficient properties in situations where both corrosion and wear co-exist. Thus a nano-scale modulated structure was developed [64]. Niobium was selected in order to have a chemically stable combination with chromium as well as to enhance the corrosion resistance. An extensive research project, supported by the European Union funding (BRITE-EURAM project NEWCHROME no: BE-96-3305) was involved in developing a solution for replacing electrolytic hard chrome. This project focused on CrN/NbN coatings with the objective of finding the most appropriate coatings for numerous practical applications. The results have been published in numerous papers during and after the project [8, 23, 23a, 30, 36, 57, 59-61, 64-67]. In the following sections the results are organised according to sections corresponding to the following chapters presenting results of this research. This material provided the body of work on which the research in is thesis is built.

The process of preparing the CrN/NbN nanoscale multilayer coatings consists of multiple steps that are presented schematically in Figure 27. In the first stage metal ion etching is implemented to ensure the cleanliness of the surface and provide a good adhesion. Metal ions are generated using a steered arc discharge on one cathode and high bias voltage on the substrates, generating a strong electrical field which accelerates the metal ions towards the substrates. This metal ion bombardment can produce very intensive ion etching as well as ion implantation up to a depth of 10 nm. This is followed by depositing a base layer of CrN by magnetron sputtering that acts as a gradient hardness layer between the hard superlattice layer and the substrate.

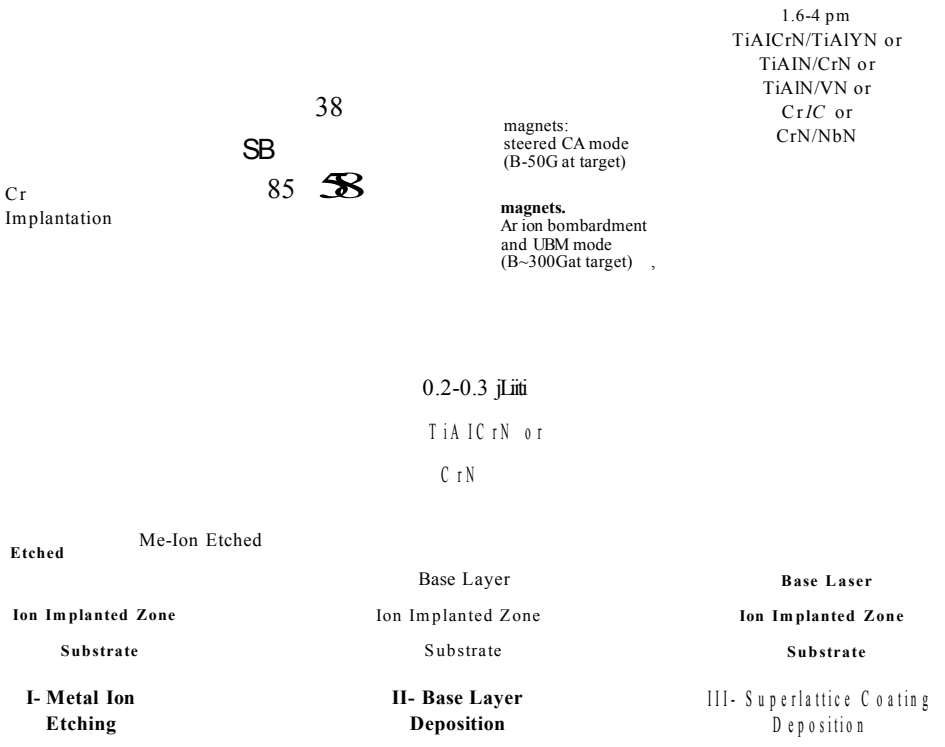

Figure 27 Summary of the ABS process including a schematic of the superlattice coatings [35]

2.6.1 Ion etching

The work by Schohnjahn et. al. showed that the ion etching and the parameters used during that step have a big impact to the tribological properties of the coating [20, 66, 83-86]. The work investigated the ion-induced changes to the microstructure and how that related to the functional properties of the coatings focusing mainly on coatings on cutting tools. The work showed the effects of etching time, Ar pressure, etching metal species and bias voltage. A brief summary of the main findings of the work is presented below.

Ion species

When substrates were treated using chromium cathodic arc etching the grain structure of the polycrystalline substrate could be easily observed. However with niobium and titanium etching such structure was however not found. This indicates either a lower

etching rate or the presence of an amorphised surface layer. Further, more droplets were found when a metal with a higher vapour pressure was used for etching.

While Cr was found to have fast etching rate, the Nb ions was found to deposit a nanocrystalline interface layer that should be beneficial to corrosion performance. Figure 28 shows the influence of the etching ion species on the corrosion performance of the Nb coated stainless steel. When Nb was used as the etching ion, virtually no corrosion damage was present after the test. The argon etched sample performed poorly showing notable corrosion damage.

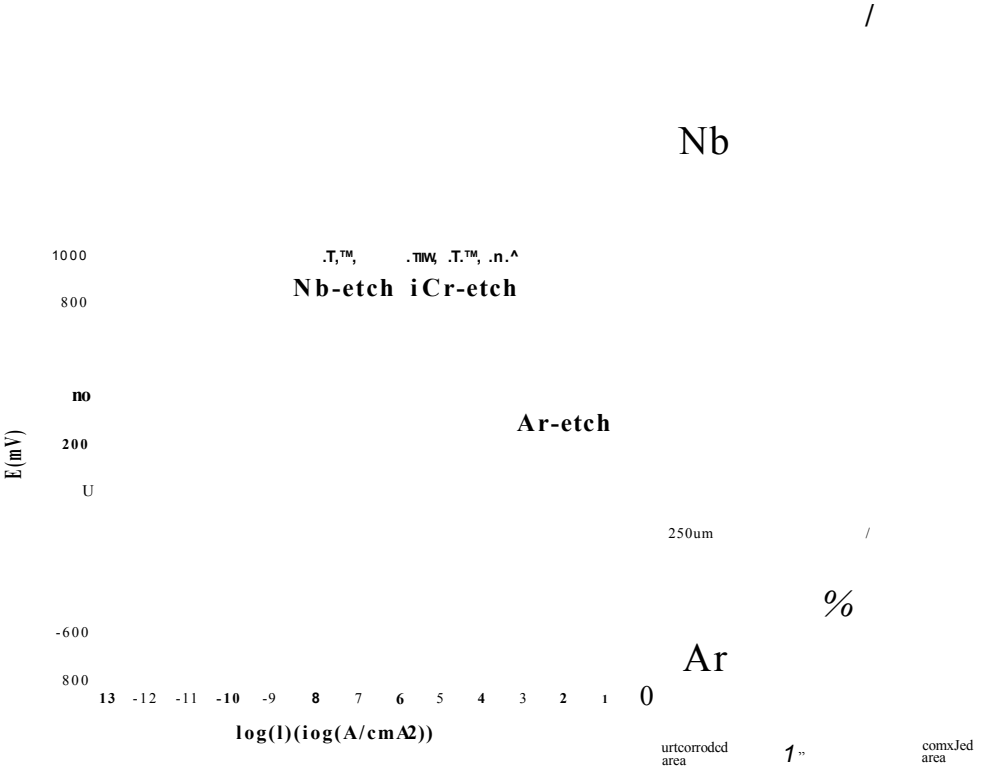

Figure 28 The influence of the etching ion on the corrosion properties in potentiodynamic polarisation test for stainless steel with a 1.3pm UBM deposited Nb coating [66]

Table 1 Correlation between etching ion species and adhesion, L_c[HSS] refers to a critical load in a pin-on-disk test with High Speed Steel substrate and L_c[cc] to critical load on cemented carbide. The appreciations e and c for microstructure stand for epitaxial and ccolumnar respectively [20]

Ion	U_s in V	Time in min	Pressure in Pa	L_c[HSS]	L_c[cc]	Microstr.
Ar	1200	20	0.06	27 ± 4	35 ± 2	c
Cr	1200	5	0.06	36 ± 4	67 ± 3	e+c
Cr	600	20	0.06	37 ± 3	58 ± 3	c+e
Cr	600	20	0.06	47 ± 5	68 ± 3	c+e
Nb	1200	20	0.06	50 ± 4	92 ± 4	c
V	1200	20	0.06	62 ± 3	113 ± 4	e
Cr	1200	20	0.06	59 ± 4	97 ± 5	e
Cr	1200	20	0.06	63 ± 3	141 ± 3	e
Cr	1200	8 + 2	$0.09+6x10^{-3}$	85 ± 3	–	e

The study also revealed a good correlation between the measured adhesion and tool life. On the other hand the etching step was found to have a great impact to the adhesion as is shown in Table 1. Two-step etching using Cr ion for the etching was found to be most suitable for TiAlN tool coatings leading to the best adhesion and the longest tool life.

Etching time

A short exposure time is desirable for various reasons. As plasma density varies with the substrate geometry, the areas that have the slowest etching rate determine the minimum duration that achieves uniformly clean surfaces. On the other hand at the positions of dense bombardment the damage can be excessive if the etching time is long. Also the number of droplets on the surfaces is related to the etching time; longer etching time resulting in more droplets, thus more localised defects to the coating. As

no significant microstructural differences between different samples (5-20 min etch time) was observed [20], the shortest etching time to a) remove the natural oxides at given oxygen partial pressure and b) achieve sufficient implantation on the etched metal, gives the best result.

Argon pressure

The etching rate was found to be almost linearly dependent on the Ar pressure in the pressure range used as can be seen in the Figure 29. A higher Ar pressure leads to more efficient etching. However, higher argon pressure has been shown to reduce the implantation of the ions as the gas collisions will reduce the average ionization state of the bombarding metal ions [87-88].

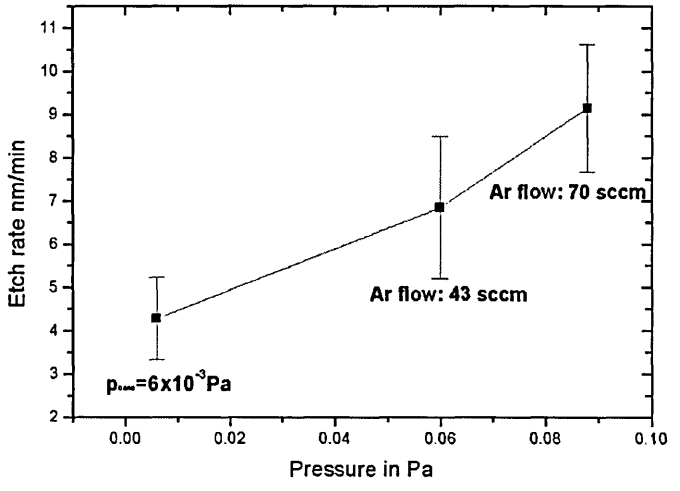

Figure 29 The influence of the argon pressure on the etching rate [20]

Bias Voltage

The etching rate was found to depend on bias voltage in accordance with Figure 30. As the bombarding energy dropped beyond a certain level no more etching was observed. For Cr that was around $U_b = -800$ V, depending on the geometry (edge effects). As the sputtering efficiency of Nb ions is lower this voltage can be assumed to be lower still.

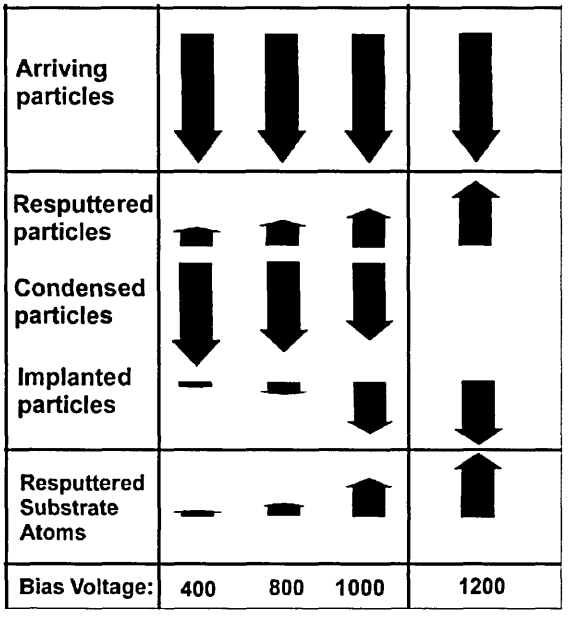

Figure 30 Schematic drawing of processes involved in Cr ion etching [20]

The conclusion from the aforementioned results was, that two-step etching; using first high argon pressure for a fast etching speed and the second part at low argon pressure to enhance implantation, would produce better results as the same result can be achieved in less time thus reducing the droplet induced growth defects. This was indeed shown to be true in the subsequent work [67].

2.6.2 Barrier layer

Barrier layer refers to a layer that is designed to prevent transport of ions or molecules from one side of the coating to another. In this work the barrier is generally preventing the electrolyte from reaching the substrate, and thus preventing corrosion. Niobium has been used in this application due to its electrochemical stability which arises from the formation of a stable Nb_2O_5 oxide layer [68]. Metallic niobium physical vapour deposited (PVD) coatings have been successfully deposited on various substrates and they have been shown to increase the corrosion resistance of stainless steels considerably [66, 69, 89-91]. Niobium has also been used successfully for the barrier layers in multilayered corrosion and wear-resistant CrN/NbN superlattice coatings. The properties of those coatings, when deposited on mild steel substrates, that are comparable or superior to that of 25 μm thick hard chrome

coatings. Metallic Nb coatings can be used as decorative coatings with a wide range of available colours through anodising [69,92] Figure 31 shows the effectiveness of this approach compared with the same coating without the barrier layer and electroplated hard chrome.

Figure 31 Surface of coated mild steel samples after salt spray test a)CrN/NbN, after 24 h b) Cr electroplated, after 200 h c)CrN/NbN with Niobium barrier layer, after 300 h [35]

2.6.3 CrN/NbN nanoscale multilayer

The superlattice coating has been investigated by several other groups besides the one at Sheffield Hallam University [113-115]. The coating has also been studied with coatings deposited using different coating technologies [112].

The NewChrome research concluded that the superlattice was found to perform best with a stoichiometric Metal-nitrogen composition, with around 3.5 nm superlattice spacing, which brings the hardness in the range of 50 GPa. This high hardness can be related to the high wear resistance of the coating (Kc = 2.1 x 1O l3m2N_l), which is one

order of magnitude better than that of hard chrome. The high bias voltage (U_b = -120 V) during the deposition of the nanoscale multilayer has been shown to be beneficial to the corrosion resistance of the coating [8, 35, 64, 71].

A thin CrN base layer was also found to be beneficial as and adhesion promoter/primer layer.. The CrN/NbN was initially deposited at high temperatures (450°C), but further work has also developed a low temperature version (250°C) of the coating [65].

3 EXPERIMENTAL

3.1 Sample Preparation Prior to Coating Deposition

The coatings were deposited on polished steel disks ca. 30 mm in diameter. Four steel grades were used: Corrosion resistant AISI 316 austenitic stainless steel, hardened M2 tool steel, low alloy mild steel and S154 high strength construction steel.
The sample disks were ground and then polished to $R_a = 5$ nm surface finish using 1μm diamond paste in the final stage. Prior to coating all samples were cleaned on an automated cleaning line comprising of a series of ultrasonically agitated cleaning and rinsing baths and a vacuum drier. Cleaning process consisted of nine immersions starting with degreaser, followed by alkaline and acidic cleaning solutions and series of rinses in de-ionized water.

3.1.1 Nitriding

The nitriding was done in a commercial low-pressure pulse plasma nitriding process by Eltro Ltd., UK using three different nitriding parameter sets. The atmosphere during the process was a 3:1 hydrogen/nitrogen gas mixture using three different processes described in Table 2 below. After nitriding the samples were mechanically polished to remove the porous surface layer and cleaned using the aforementioned cleaning process.

Table 2 Nitriding parameters

	Sample 1	Sample 2	Sample 3
Nitriding process	6h at 520°C	3h at 480°C +14h at 520°C	40h at 530°C
Case depth	170 μm	290 μm	400 μm

3.2 Coating Deposition Procedure

The coatings were deposited at 450 °C using an industrial sized multi-cathode HTC 1000-4 ABS combined cathodic arc/ unbalanced magnetron sputtering coating system, manufactured by Hauzer Techno Coatings BV. The height of the cathodes is approximately 0.6 meters and the distance between opposing cathodes is approximately 1.0 meter.

The processes followed the process diagram below (Figure 32). However, not all processes included all the process steps. The relevant processes are introduced at the beginning of each section.

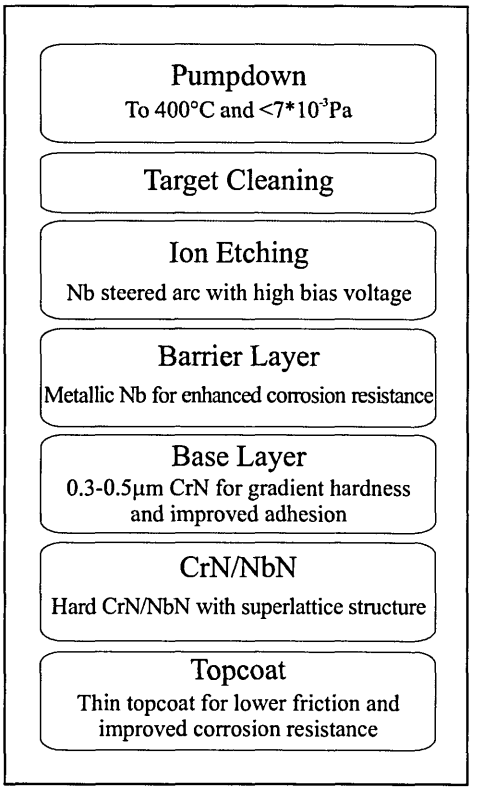

Figure 32 Generic process diagram for the coatings used in this work

All processes were performed using a configuration with two niobium and two chromium targets arranged as shown in Figure 33. The samples were subjected to 3 fold rotation in the X-Y plane during deposition, which ensures uniform coating thickness even for 3 dimensional parts. The speed of the primary rotation is controllable, but it was kept at 7.5 rpm for this work.

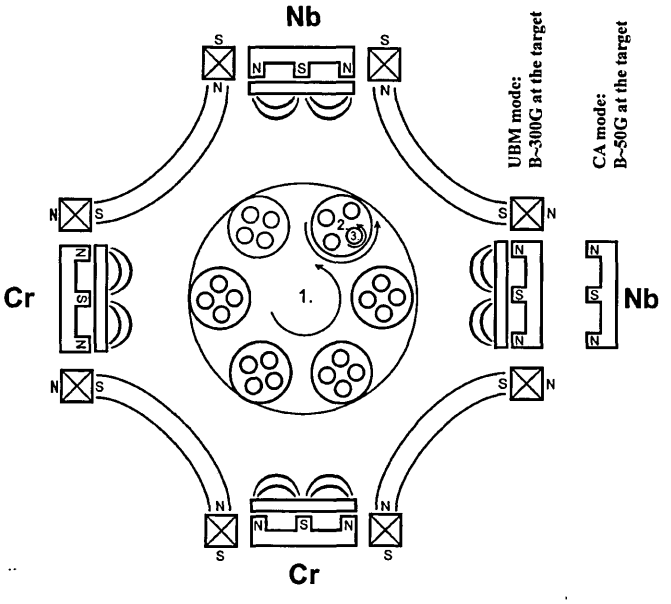

Figure 33 Schematic diagram of the process chamber (from above) of the Hauzer PVD coater showing the target arrangement, 3 fold rotation system and the adjustable (using electromagnetic coils) closed field magnetic arrangement.

3.2.1 Process parameters

This chapter provides a brief introduction to the most important process parameters and to the fundamental effects of those parameters.

Deposition temperature:

The deposition temperature strongly affects the film growth. At elevated temperatures the surface energy is higher, enabling the adatoms to move longer distances and find better (lower energy) nucleation sites leading to denser, better, films as shown in section 2.2.4. The higher temperature also reduces the intrinsic compressive stresses

that often cause adhesive and cohesive failures in the films. The high temperature (400-500°C) processes cannot be used on temperature sensitive materials that may have microstructural or dimensional changes at such temperatures. High deposition rates with high ion bombardment (bias voltage) often maintain the high temperature without the need for additional heating.

Cathode Power / Current

Each cathode has its own power supply that can be controlled by voltage, current or power. In UBM mode the set value was power. In steered arc mode the power supply is controlled by the current as the voltage (thus also the current) is not stable.

Gas flow

The control of the gases in the reactive process is critical to the deposition reactive processes as described in the section 2.3.1. In the Hauzer deposition system the gases can be controlled using flow and pressure data. The standard pressure controlled mode uses pressure measurement to drive a feedback loop on the mass flow controllers to maintain the desired pressure. In reactive processes the working gas (Ar) was set to a fixed flow rate while the reactive gas (N_2) was controlled using pressure feedback.

The working gas pressure affects two independent processes, ion bombardment and collision frequency (mean free path). Increasing the working gas pressure increases the ion bombardment on both the target (increasing the deposition rate at given voltage) and the substrate. On the other hand the added amount of gas molecules in the vacuum increases the probability of collisions between the atoms and gas molecules that will cause a reduction in both the kinetic energy and the ionisation state of the atoms/ions. These collisions also increase the amount of scattering of the depositing atoms.

The reactive gas partial pressure at a given deposition rate will affect the composition (stoichiometry) of the depositing film. Some processes/compounds are sensitive to the correct ratio of reactive gas to the metal on the surfaces, while some tend to form the preferred stoichiometry even with a notable excess of reactive gas. Such processes are easier to control and are thus preferable.

Bias Voltage

The ion bombardment of the substrates is controlled primarily by adjusting the bias voltage. The negative bias attracts ions that bombard the substrate thus increasing the energy of adatoms on the surface. The increased ion bombardment during the deposition also tends to smooth out the peaks/valleys of the growing columnar grains leading to smoother surfaces. The increased bombardment also causes re-sputtering of the adatoms thus causing thinner films. It should also be noted that the bombardment is not uniform over the surface of 3 dimensional parts such as sharp corners, edges and protrusions which face a higher electrical field and thus more intense bombardment. Excessive ion bombardment will lead to the working gas being buried into the coating.

Coil current / Unbalancing

The electromagnets surrounding each cathode can be used to adjust the balancing of the magnetrons. When the electromagnets are off, the magnetrons are balanced and the electrons are trapped close to the cathodes, thus very little ionisation occurs close to the substrate. Applying current to the coils causes the magnetron to become unbalanced and more electrons are released to ionise the working gas (Ar) close to the substrates. Therefore the coil current affects the ion bombardment of the samples together with the bias voltage.
In the steered arc mode the coil current can be used to adjust the position of the arc track as the arc has the highest probability of forming where the magnetic field is parallel to the target surface.

3.2.2 Pump-down and heating

The Hauzer PVD coating machines uses high speed pumping system consisting of a two-stage mechanical pump, a 1000 m^3/h roots blower and two 1600 m^3/h turbo pumps to quickly evacuate the chamber and to minimise the hysteris effect of reactive

deposition. The substrates were preheated to ca. 400°C in vacuum using radiation heaters. A vacuum of $7x10^{-3}$ Pa was attained before proceeding to the coating stages.

3.2.3 Target cleaning

The first stage of the coating process was target cleaning. The purpose of this step is to remove contamination from the target surfaces prior to coating, so that the contaminants will not be deposited into the interface region. The target cleaning is performed in balanced magnetron sputtering mode (argon atmosphere, p = 0.2 Pa) with mechanical shutters in front of the cathodes to prevent deposition onto the substrates.

3.2.4 Ion etching

The next stage of the process was ion etching. In this stage one target is operated in steered cathodic arc discharge mode with a high bias voltage applied to the substrates. The cathodic arc process provides a highly ionised metal plasma that is accelerated towards substrates with high bias voltage. Upon impact on the substrates, ions with high kinetic energy cause sputtering to occur, thus removing possible surface contamination. Further, these high energy ions can implant several nanometres into the substrate.

The bias voltage can be used to control the energy of the ions hitting the surface. The effect of ion energy and species on the etching has been described in detail in the work of Schönjahn [20]. The high bias voltage leads to efficient etching and some ion implantation yet causes significant heating of the substrates. An increase in argon pressure increases the number of Ar^+ ions hitting the substrate leading to faster etching. On the other hand it leads to more collisions between metal ions and Ar atoms leading to loss of ion energy and reduced ionisation conditions, ultimately leading to lower average energy of the metal ions hitting the substrates. Correct etching time is also important since too short an etching time will not remove all contaminants, yet too long an etching time increases the number of localised defects due to droplets generated in the cathodic arc discharge process. All coatings were

done using either Cr or Nb as target material, i.e. etching ion. The etching time used for this work was generally 15-20 minutes.

Cr etching has been the standard etching process for CrN/NbN coating thus it was used for coating tests where the standard coating was used as a reference. Cr etching generally provides better adhesion, thus leading to superior mechanical performance. The standard parameters for Cr^+ etching were:

- Step duration: 15 min
- Arc current: I = 100 A
- Bias Voltage: U_b = -1200 V
- Ar flow: 65 sccm,
- Coil current: I_c = 0.7 A

Nb etching was used to enhance corrosion performance via a thin nano-grained deposition layer that forms at the interface as described by Schönjahn et. al. [66]. The effects of the changes in the interface region and the effects on the performance of the coating was studied with an experiment using different bias voltages (U_b = -800 V → -1200 V) and different etching pressures (p = 0.004 Pa → 0.2 Pa). The work of Schönjahn et al. [66, 67] also showed a 2 step etching process in which the first step was etching with high bias voltage and high gas pressure and the second wasimplantation/surface modification with low pressure and lower bias voltage.

3.2.5 Barrier layer

A barrier layer of metallic niobium was deposited to improve the corrosion resistance of the coating. Niobium was used as it is one of the most corrosion resistant materials available due to its extremely stable oxide Nb_2O_5 [68]. The layer should protect the underlying material from corrosion if it was totally defect free.
The barrier layer was deposited in unbalanced magnetron sputtering mode using different bias voltages U_b = -75 V → -120 V. The low bias voltages should lead to thicker coatings exhibiting lower stress. The coating stress has been associated with corrosion behaviour with low stress leading to better performance [69]. On the other

hand a higher bias voltage should lead to higher ion bombardment, thus denser coating that should prevent voids at the crystal boundaries and at defect locations. It should also lead to smoother layers as the tops of the columnar grains should then become flat instead of dome-like. High ion bombardment has also been shown to facilitate the "healing" of the local defects as shown in the Figure 10 in the page 17 [112].

The deposition time was also altered from 1 hour to 3 hours, thus changing the layer thickness. For dense void-free films the layer thickness should not affect the corrosion behaviour. However it has been observed that as the layers grows, under high ion bombardment, some voids and point defects may be closed [118].

3.2.6 Base layer

A base layer of CrN was deposited in order to provide a layer of intermediate hardness between the relatively soft substrate and hard superlattice coating. This enhances the adhesion as the stresses at the interface are reduced [70]. The layer was deposited using two Cr targets operated in UBM mode with high power and the other two targets sputtered with low power to prevent target cross-contamination. The atmosphere was controlled by a pressure feedback loop where argon was flow controlled and nitrogen flow was controlled with an active feedback loop pressure controller. This argon/nitrogen control system has been shown to provide uniform results and with the correct parameters leads to a stoichiometric CrN coating.

The parameters used for the base layer were generally standard yet a higher bias voltage of $U_b = -100$ V was sometimes used. The standard parameters were:

- Step duration: 30 min
- Power: 2 chromium targets with 5 kW and 2 niobium targets with 0.5 kW
- Bias Voltage: $U_b = -75$ V
- Ar flow: 200 sccm, N_2 flow pressure controlled, $p = 3.6 \times 10^{-1}$ Pa
- Coil current, $I_c = 6A$

3.2.7 CrN/NbN nanoscale multilayer

The main part of the coating was the CrN/NbN nanoscale multilayer. The properties and parameters related to this layer have been extensively studied for the "New chrome" EU funded research project [8, 64, 71]. The deposition parameters were generally not altered from the ones that the previous work found to be the best. The standard parameters were:

- Step duration: 150 min
- Power: 2 chromium targets with 5 kW and 2 niobium targets with 10 kW
- Bias Voltage: U_b = -75 V or U_b = -120 V
- Ar flow: 200 sccm, N_2 flow pressure controlled, p = 3.8 x 10^{-1} Pa
- Coil current, I_c = 6 A

3.2.8 Top coat

A thin topcoat on a wear-resistant PVD coating can be beneficial to the tribological performance of the coating as it can alter the surface properties such as friction. Lembke et. al. demonstrated a reduced friction and improvement on the oxidation resistance of TiAlVN coating with the addition of an oxynitride topcoat [9].

The oxynitride topcoat used in this work was deposited in a mixture of dry air and argon. To establish the effect of ion bombardment on the coating structure and properties the bias voltage was varied from U_b = -75 V to U_b = -120 V while retaining the same total pressure during deposition (3.5 x 10^{-1} Pa). The effects of the changes in the total deposition pressure, P_T, were investigated keeping the bias voltage at U_b = -100 V and varying the total pressure from 3.5 x 10^{-1} Pa to 4.9 x 10^{-1} Pa. A reference coating without the topcoat was also prepared, keeping the total coating time the same as with the other samples, leading to a thicker CrN/NbN layer. The rest of the coating parameters remained the same:

- Step duration:

  CrN/NbN 90 min

  CrON/NbON 60 min

- Power: 2 chromium targets with 5 kW and 2 niobium targets with 10 kW
- Bias Voltage: U_b = -75 V during CrN/NbN and

  U_b = -75- -120 V during CrON/NbON
- Ar flow: 200 sccm, N_2 flow pressure controlled, $p = 3.8 \times 10^{-1}$ Pa
- Coil current, I_c = 6 A

3.3 Coating characterisation Techniques:

The coatings were studied using a number of characterisation techniques. The techniques can be divided into 4 categories

1. Microstructural investigation
2. Coating mechanical properties
3. Laboratory scale wear tests
4. Corrosion tests

3.3.1 Microstructural techniques

3.3.1.1 Transmission Electron Microscopy (TEM & XTEM)

In TEM the imaging, an electron transparent sample (thickness ca. 100nm) is illuminated with an electron beam that is perpendicular to the sample. The image forms below the sample by electrons that have passed through the sample. Figure 34 shows a schematic diagram of the CM30 TEM

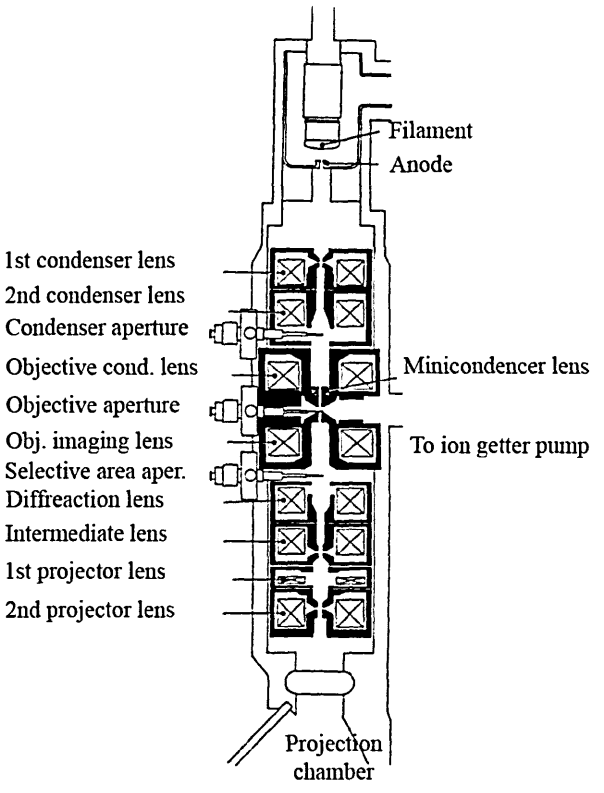

Figure 34 Schematic diagram of CM30 TEM

The image that forms when the electron beam that passes straight through the sample is focused on a projection screen is called the bright field image. The diffracted electrons are blocked with an aperture. It is the brightest, most accurate imaging mode.

On the other hand, also the electrons that have diffracted from the lattices according Bragg's law can also be used for imaging (dark field imaging). Image contrast is caused by number of parameters, such as differences in atomic number, phase or diffraction contrast. If a small selective area aperture is used to limit the area under investigation, the pattern of the diffracted electrons (SADP, Selected area diffraction pattern) can give further information, such as lattice parameter and crystal structure of the area under investigation.

Further analysis of the sample materials can be done analysing secondary emission from the illuminated sample area (XPS, X-ray photo electron spectroscopy or EDX, energy dispersive x-ray analysis).

In XTEM (cross sectional TEM) a thin, electron transparent cross-sectional sample is prepared and investigated with TEM.

A Philips CM20 TEM was used for the bulk of the TEM investigations. It used a tungsten filament to produce the electron beam that was accelerated to 200keV. The images were captured using electron sensitive film.
Some of the TEM work was performed with a Vacuum Generators HB 501 STEM/EDX FEG at the University of Illinois. This instrument was used mainly for the interface investigation and the elemental analysis of the interfaces. STEM (Scanning Transmission Electron Microscope) is similar to the TEM but it uses a highly focused electron beam to scan across the area of investigation. An additional benefit of this is the ability to focus the beam in one spot and measure the X-ray radiation which can be used for elemental analysis. By measuring at multiple locations across a line, an elemental line-scan can be made.
These techniques can be studied in detail in numerous publications. The author has found the book series by Williams and Carter valuable in leaning and understanding these methods [72].

3.3.1.2 X-ray diffraction (XRD)

In XRD the sample is bombarded by a beam of monochromatic x-rays at a well-defined angle, and measuring the intensity of the diffracted beam across different diffraction angles. The X-rays are diffracted in a crystalline specimen according to Bragg's law:

$$n\lambda = 2d\sin\theta$$

where λ is wavelength, d is inter-planar spacing and θ the angle between crystal plane and incident beam. This principle X-ray diffraction from the crystal lattice is shown in the Figure 35.

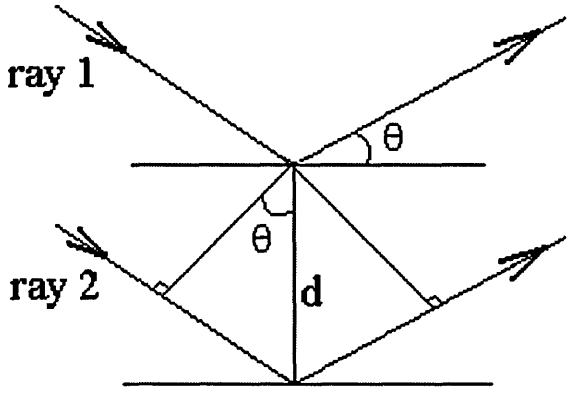

Figure 35 Principle of the X-ray diffraction from crystal planes

The phases can be identified by comparing the results of the measurement (the peak angles and the relative intensities) to the standards form JCPDS database that can be found on the instrument. For compounds, a computer aided fitting software can be used to separate overlapping peaks.

The texture was calculated using the inverse pole figure method. Inverse pole figures are represented in terms of "T*" values, which are a measure of the statistical change of any plane lying in the plane parallel to the surface. For a particular plane, (hkl), T* is:

$$T^*_{hkl} = \frac{I_{(hkl)} / R_{(hkl)}}{\frac{1}{n}\sum_0^n I_{(hkl)} / R_{(hkl)}}$$

Where $I_{(hkl)}$ is the intensity of the (hkl) reflection and $R_{(hkl)}$ is the intensity corresponding to a randomly oriented sample and n is the number of reflections considered. This method is described in more detail in reference [73].

The XRD measurements were performed using either a Philips PW 1710 or a Philips X'Pert MPD automated diffractometer using CuK_α radiation (λ = 1.54 Å). The scans were generally performed from 10° to 140° using either 1° glancing angle of Bragg-Brentano configurations. In glancing angle measurement the angle of the radiation source is kept constant to the surface of the sample and the measurement head is scanned across the selected range, while in Bragg – Brentano configuration the angles of both the source and measuring head angles are equal to the normal of the sample. The scan was done using 0.04° step with seven seconds measuring time for each step.

3.3.1.3 Scanning electron microscopy (SEM) and optical microscopy

In the scanning electron microscope a high energy (ca. 20 keV) electron beam is focused to a point on the sample and scanned across the area under investigation. When the primary electron beam hits the surface it effectively spreads and fills a teardrop-shaped volume, known as the interaction volume (shown in Figure 36), extending from less than 100 nm to around 5 μm into the surface. Interactions in this region lead to the subsequent emission of electrons and X-rays which are then detected. As the beam is scanned across the sample the instrument forms an image from the signal and the location of the electron probe.

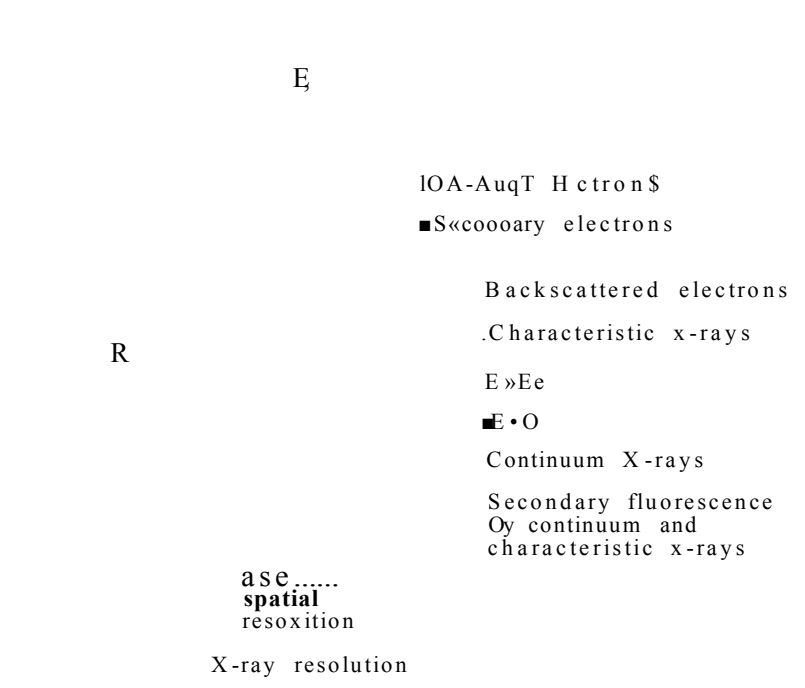

Figure 36 Interaction volume of an electron beam

The main detectors in the SEM are:

Secondary electron detector is the main imaging detector of the SEM. Secondary electrons are generated by an incident electron passing near enough to an atom to impart some of its energy to a lower energy electron (usually in the K-shell). This electron then leaves the atom with a very small kinetic energy (5 eV) and thus only secondaries that are very near the surface (< 10 nm) can exit the sample and be examined. Each incident electron can produce several secondary electrons. The production of secondary electrons is very topography related.

Backscattered electron detector can be used to detect differences in the atomic mass at the specimen. The electrons are generated when an incident electron collides with an atom in the specimen and “bounces” back. The production of backscattered electrons varies directly with the specimen's atomic number. This difference in backscatter rates causes higher atomic number elements to appear brighter than lower atomic number elements.

Energy dispersive X-ray (EDX) analysis can be used for semi-quantitative elemental analysis. The electron beam can cause atoms of the sample loose electrons from their inner electron orbits. As the void in the inner shell is filled from the outer shell the extra energy is released as radiation (x-rays). The frequency (energy) spectra of the radiation are characteristic for each element/atom, thus it can be used for elemental analysis. Comparing the collected spectra to a standard the relative amounts of each element can be calculated.

The instrument used in this work was Philips XL 40 SEM.

3.3.2 Coating mechanical properties

3.3.2.1 Pin on Disk

In pin on disk test a loaded pin is sliding on a disk as the disk rotates at given speed. A schematic of the test equipment can be seen in Figure 37.

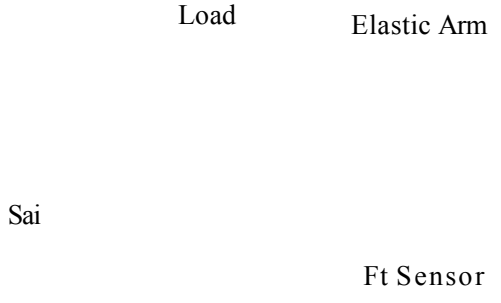

Figure 37 Schematic of the pin-on-disk machine

The friction force is measured with a force gauge in the elastic arm. This was recorded as a function of the sliding distance. From the curve any changes to the sliding or wear mechanism, i.e. wear of a layer in the coating, can be easily observed.

Wear of the disk can be measured after a pre-determined number of laps. The wear of the counterpart (pin or ball) can be measured after given distance. The frictional force can normally be measured also. The key parameters of the pin on disk tests are:

1. Materials and the geometry of the counterpart
2. Normal force applied to the pin
3. Sliding velocity

Generally no lubricants are used (dry sliding wear) and the wear debris is not removed from the wear track.

The pin on disk tests were performed using a CSEM Tribometer using a 6 mm ball as the counterpart. The material of the ball was either Al_2O_3 or 100Cr6 steel. The normal force applied was 5 N and the linear speed was 0.1 m/s. The tests were performed at room temperature in the absence of lubricants. The volume of the material loss from the wear track was analysed with TAYLOR-HOBSON FORM Talysurf_120L or Laser profilometer.

The basics of this method and the applicability of the results has been studied by numerous research groups and is adopted as a standard by ASTM and DIN [74-75].

3.3.2.2 Scratch test (adhesion)

The adhesion of the coating was measured using a CSEM REVETEST scratch tester. In this method a Rockwell C diamond tip is moved on the coating with linearly increasing normal load as shown in the Figure 38. The adhesion is expressed as critical load L_C that relates to the force at which consistent failure in coating integrity is observed. This method is covered by European Union standard EN 1071 -3.

Figure 38 Schematic drawing of the scratch test

3.3.2.3 Hardness measurements

The hardness was measured with three different methods. Hardness-depth profiles of the nitrided samples were generated from a polished cross-sections using Mitutoyo MVK-G1 hardness tester with Vickers diamond tip using 25 g normal loads. The hardness of the coatings was characterised using Knoop hardness measurement (Mitutoyo MVK-G1, 25 g normal load) and nano-indentation technique using Nanoinstruments XP nanoindenter (plastic hardness and Young's modulus, 500 nm indentation depth).

In all of these methods the principle is to use a hard tip of a defined shape to indent the surface and record the impression of the tip. The nano-indenter differs from the other methods by measuring the indentation depth during both the loading and unloading cycles. This gives the added benefit of being able to determine the Young's modulus of the surface. For thin films the conventional hardness measurements do not give reliable results for two reasons:

1. It has been shown that the indentation depth should not exceed 1/10th of the coating thickness in order of accurately describe the hardness of the coating (not the underlying substrate). The nano-indentation is the best method to determine hardness of the coating. The Knoop diamond tip is not symmetrical, and therefore not appropriate for the cross sections.

2. The hardness of the wear resistant coatings is very high (close to diamond hardness) and thus may distort the measurements obtained with diamond tip.

Two most comprehensive standards covering hardness methods are ISO 14577 and DIN ISI 4516 [76-77].

3.3.2.4 Impact testing

The purpose of the impact test is to determine the fatigue properties of the coating. Impact testing was performed using a CemeCon impact tester with 1 million impacts using 350 N impact load and **O** 6 mm cemented carbide ball. This method was developed in Aristotle University and CemeCon [78].

3.3.2.5 Coating thickness by ball-cratering measurement

The coating thickness was measured using the ball cratering method. A rotating ball of 30 mm diameter is used to mill a ball crater through the coating. A fine diamond slurry is applied to the contact to facilitate the milling and produce fine smooth surfaces. The diameter of the crater is measured using an optical microscope as shown in Figure 39.

Figure 39 Schematic diagram of ball cratering thickness measurement

The thickness of the coating can then be calculated using the simple geometric equation.

$$D = \frac{X \times Y}{\phi ball}$$

The dimensions X and Y were measured using an optical microscope image and fitting a circle to the wear track using measurement software.

3.3.2.6 Corrosion experiments

The corrosion performance of PVD coatings is fairly difficult to measure accurately and repeatedly because the films are often very thin and electrochemically stable and/or noble and they can often be considered to be porous. (see Appendix 2) Aqueous environments can normally penetrate the coating through the defects and pinholes inherent in PVD coatings [21-23, 57-61]. Once the environment has reached the substrate a galvanic cell forms between the coating and the substrate. This generates an electrochemical force that causes rapid localised corrosion (pitting) at the defect locations [21,23, 57]. The pits eventually grow and the voluminous corrosion products formed below the coating then cause interfacial delamination. This mechanism is difficult to evaluate electrochemically and therefore simple extended exposure tests such as salt spray are used in industry to evaluate the corrosion performance [79]. On the other hand salt spray tests are not ideal from a research standpoint when evaluating the corrosion resistance of PVD coatings since they require a number of test samples of reasonable size and long testing times to produce results which, when obtained, are not readily quantifiable. Also minor improvements in corrosion performance are difficult to detect in such tests.

3.3.2.6.1 Potentiodynamic polarisation

All electrochemical measurements were performed in 3% NaCl solution using a 3-electrode cell similar to the one described in Figure 40. During the potentiodynamic measurement the sample is polarised i.e. forced to a potential (vs. stable electrode i.e.

reference electrode, RE) using an external power source. The current is fed through auxiliary electrodes (AE).

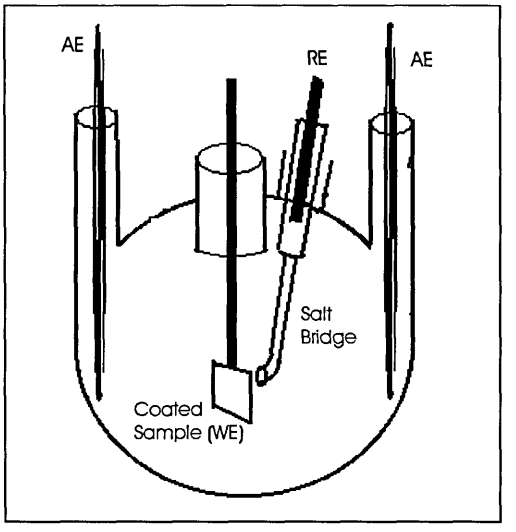

Figure 40 Schematic diagram of potentiodynamic polarisation test cell.

The current density *I* (current divided by exposed area) is recorded and plotted in a graph similar to the one in the Figure 41. Figure 41 also outlines the different regions that are commonly observed in the results [55]:

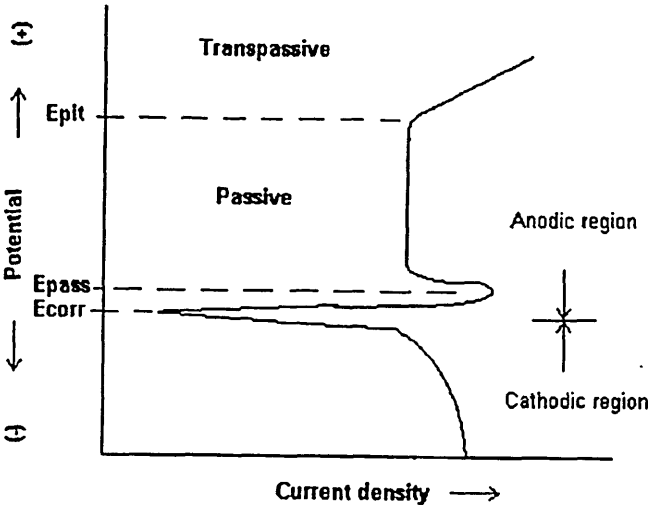

Figure 41 The different regions of the potentiodynamic polarisation curve of passivating material

Cathodic region:

Negative currents are measured in the portion of the graph which is called the cathodic region. The common practice is to plot the negative currents as their nominal value. There the working electrode (WE) behaves as a cathode and the counter electrode (CE) as an anode. The reactions, which take place at the WE in this region, are, for example, generation of oxygen gas by the oxidation of water or the generation of chlorine gas due to the chloride-containing electrolyte.

Free corrosion potential E_{corr}:

The value of potential where the changeover from negative to positive currents takes place is called the free corrosion potential E_{corr}.

Anodic region:

Positive currents are measured in the portion of the graph called the anodic region. The WE behaves as an anode.

Passive zone:

As the formation of a protective film on the WE takes place, a sudden drop in corrosion current density is observed. Then the current density is maintained at a low and steady level until a breakdown of the protective film begins at E_{pit}.

The polarisation measurements were performed with EG&G Model 263A potentiostat from -1000 mV to 1000 mV using scan rate of 0.5 mV/s with Saturated Calomel Electrode (SCE) reference electrode. Before the polarisation measurements samples, were cleaned cathodically at -1.5 V for 100 seconds and then allowed to equilibrate at Open Circuit Potential (OPC) for 40 minutes.

With PVD coating on low alloy steels pitting is the dominant form of corrosion also in the polarisation tests. If the coating has good barrier properties and is electrochemically stable (in the potential range under investigation) it exhibits "passive like" behaviour in the anodic region. In this region the corrosion is limited to the localised defects in the coating and the anodic current expresses the amount of active area.

3.3.2.6.2 Other corrosion measurements

Salt spray tests are the industry standard for anticorrosion coating. They were performed according to ASTM B117 standard for salt spray tests. The samples were subjected to a salt spray at 98% humidity with a solution consisting 50 g/l NaCl with pH = 6.5-7.2 at 35°C. The samples were placed at ca. 45° angle with only the coated surface exposed to the environment. The duration of the test was 230 hours and the samples were inspected at the end of the test and also after 72 and 162 hours. 5 samples of each coating were tested with about 4 cm^2 surface area each [79].

4 SUBSTRATE MODIFICATION USING DUPLEX PROCESS

As discussed in the section 2.3.4 the substrate properties can have a strong influence on the mechanical and tribological performance of the hard PVD coatings. In order to get the very high wear resistance normally achieved on PVD coated hard alloys on softer structural and low alloy steels, a duplex process may be needed. A duplex process commonly refers to the application of two individual surface/subsurface modification processes to produce a combination of mechanical, metallurgical and chemical properties that cannot be obtained by any individual process [81].

In the work reported in this chapter used a nitriding process to modify the substrate surface to work better together with PVD. The major part of the work focused on the microstructure of the compound layer and the effects it had on the overall performance of the duplex treated steel.

The S154 grade high strength steel (composition: C 0.35, Si 0.3, Mn 0.6, Cr 0.7, Mo 0.6, Ni 2.5) was selected as the substrate. With a tensile strength of over 850 MPa, this steel is tough, impact resistant, heat treatable and it can also be easily machined and welded. It can also be readily nitrided with a notable increase in surface hardness. High speed steel and non-nitrided S154 samples were also prepared to act as references.

Eltro Ltd., UK, carried out the nitriding processes using a commercial low-pressure pulse plasma nitriding process using three different nitriding parameter sets that can be seen in Table 3. All the nitrided samples were then coated with CrN/NbN coating consisting of 0.5 μm thick CrN base layer and 4μm thick nanostructured CrN/NbN multilayer.

Table 3 The coating parameters used in this study

Nitriding Process (3:1 hydrogen/nitrogen atmosphere)	Sample 1 (170 µm case depth) 6 hours @ 520 °C	Sample 2 (290 µm case depth) 3 hours @ 480 °C followed by 14 hours @ 520 °C	Sample 3 (400 µm case depth) 40 hours @ 530 °C
Polishing & cleaning	Mechanical polish to R_a < 1µm finish		
Pump-down and heating:	400 °C at a pressure < 7 x 10^{-5} mbar		
Cr^+ etching (20min)	Arc current: I = 100 A, Bias Voltage: U_b = -1200 V Pressure: p = 1x10^{-3} mbar		
CrN (30min)	Power: 2 Cr targets with 5 kW each Bias Voltage: U_b = -75 V Pressure: p = 3.8 x 10^{-3} mbar		
CrN/NbN (150min)	Power: 2 Cr targets with 5 kW each and 2 Nb targets with 10 kW each Bias Voltage: U_b= -120 V Pressure: p = 3.6 x10^{-3} mbar Cr: 2*5 kW, Nb: 2*10 kW		

4.1 Microstructure and hardness of the nitrided zone

The microstructure and the mechanical properties of the substrates were investigated to evaluate the effects of the nitriding processes. The micrographs of the polished and etched cross sections (Figure 42 and Figure 43) clearly illustrate the affected layers with altered microstructure near the surface of the samples. In Figure 42 the 5 µm thick PVD coating can be seen at the surface of the samples (left hand side of the image) followed by a compound layer that ranges from 5 µm to 15 µm depending on the nitriding parameters used. The sample was etched using 5% Nital acid to help reveal the nitrogen affected microstructure. In Figure 43 the nitrogen affected microstructure can be observed up to a depth of 400 µm.

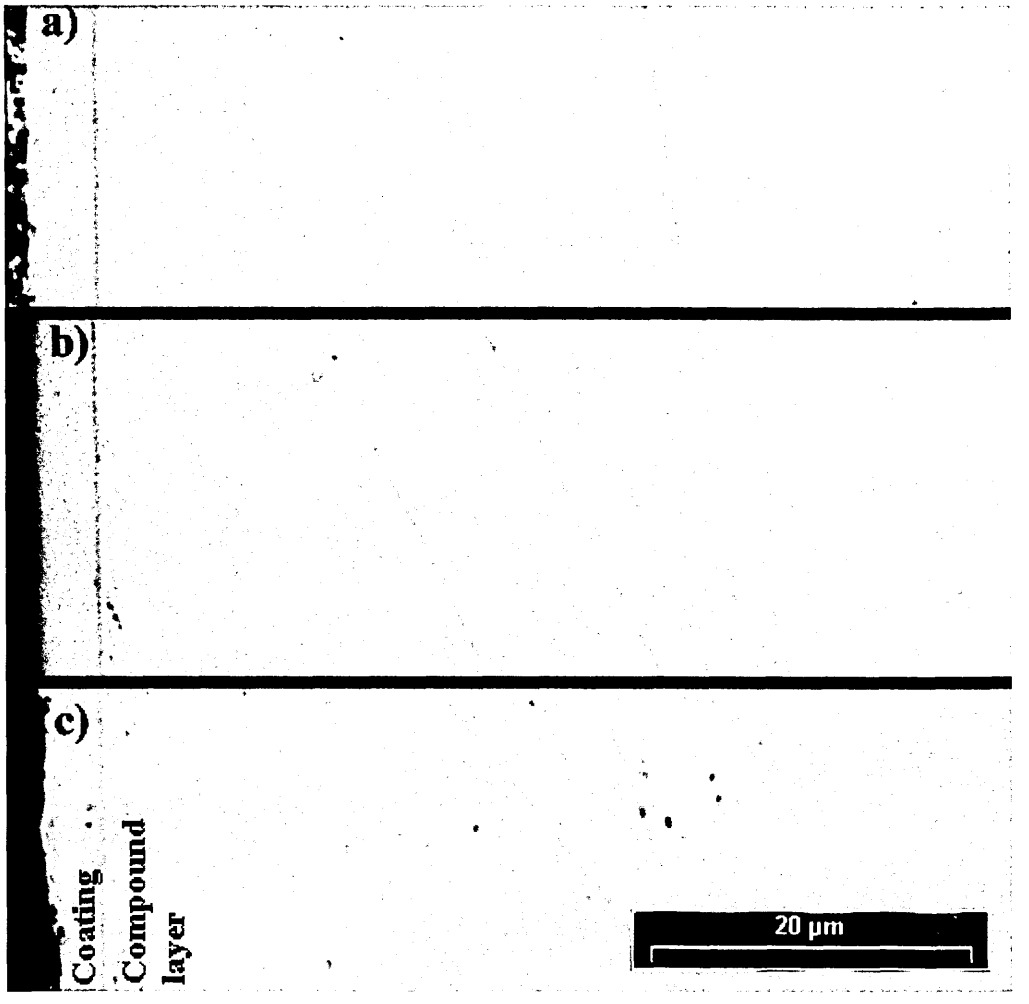

Figure 42 The coating and the compound layer are clearly visible in the polished cross-sections (optical micrograph) a) Sample 1 (170µm) b) Sample 2 (200µm) c) Sample 3 (400µm)

Figure 43 Etched cross-sections of duplex treated coatings a) sample 1 (170 µm case depth) (b) sample 2 (290 µm case depth) c) sample 3 (400 µm case depth). 0 indicates the top surface of the sample. The coating is visible on the left side of the image, followed by the compound layer.

The hardness-depth profiles ($H_{V,25g}$) of the nitrided zone (Figure 44) shows a significant increase in the surface hardness after nitriding. The surface hardness depends on the composition of the compound layer, as is shown later in this section reaching a value of almost 900 with sample 1 while being only 530 with sample 3. The longer nitriding processes for samples 2 and 3 give the nitrogen more time to diffuse deeper into the metal which can be seen as a larger case depth (the depth of the affected zone). The hardness of the PVD coating is still significantly grater than that of the compound layer and was measured to be 3200 ($H_{K,25g}$) on all coated samples.

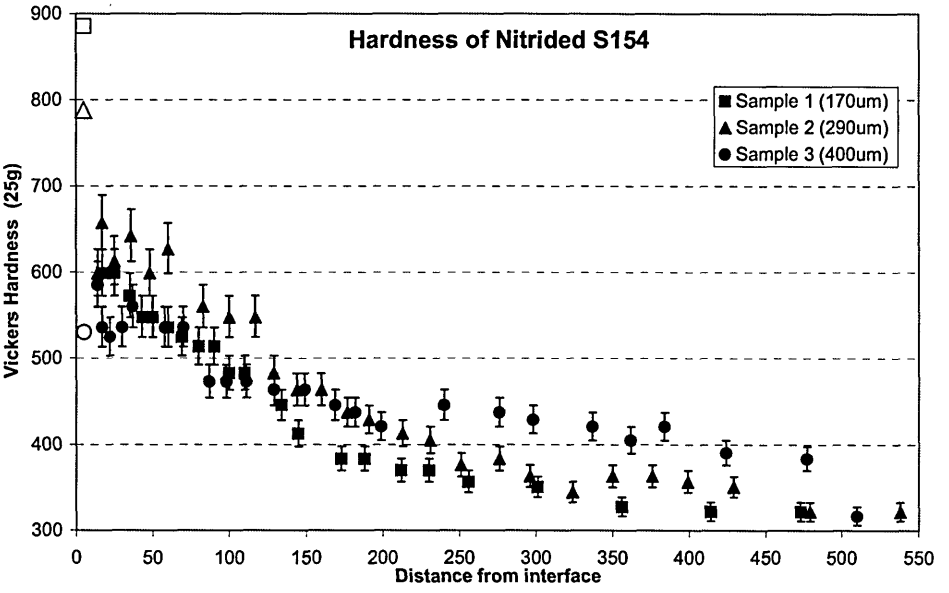

Figure 44 Hardness -depth profile of the nitrided S154 steel. The solid markers are measured from the polished cross-section, the open markers show the surface hardness.

The results of the hardness measurements show that, by changing the nitriding parameters, the hardness profile near the surfaces can be modified to suit the application. It is possible to design the nitriding process to achieve high surface hardness with relatively shallow hardening depth or low surface hardness and high case depth.

The XRD patterns from the 1° glancing angle measurements of the nitrided surfaces before coating can be seen in Figure 45. The two common ferrous nitride phases γ' (gamma prime, Fe_4N, FCC) and ε (Fe_3N, Hexagonal) were detected in the compound layer. Samples 1 and 2 have very similar patterns both showing ferrous nitride phases present, while sample 3 is virtually fully γ' phase.

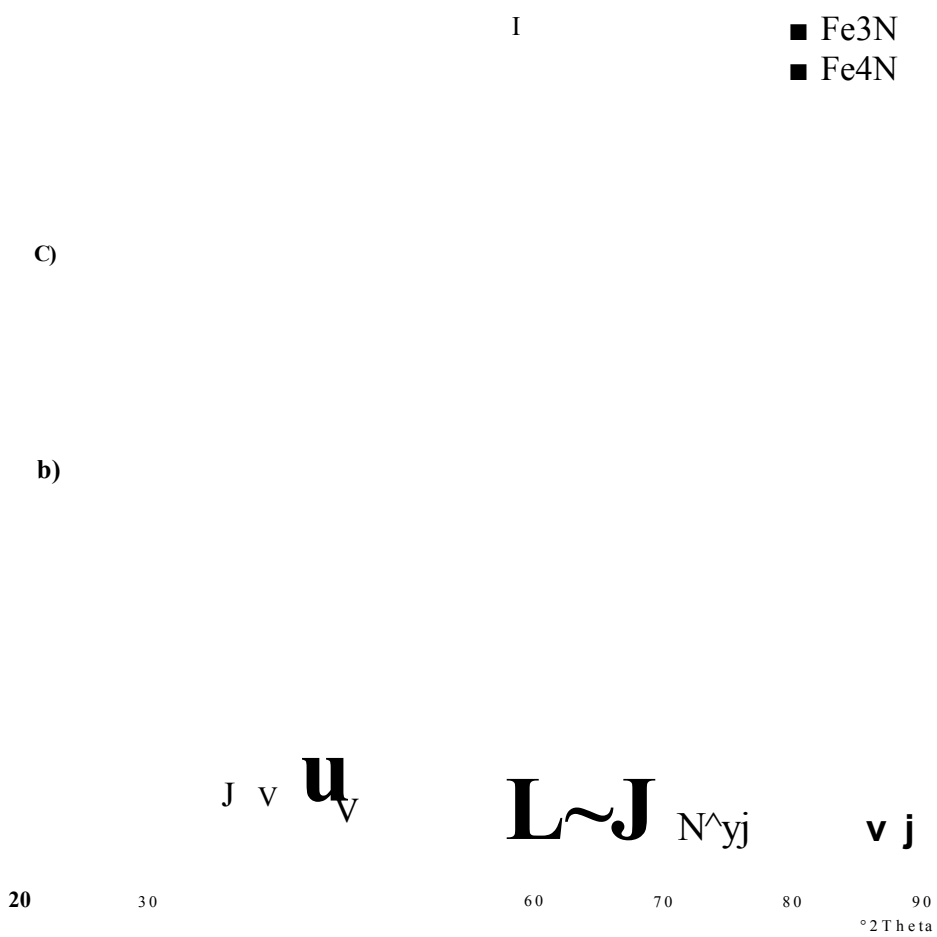

Figure 45 1° glancing angle XRD scans of the nitrided substrates prior coating a) sample 1 (170pm case depth) b) sample 2 (290pm case depth) c) sample 3 (400pm case depth).

The apparent phase compositions of the compound layers were calculated from the peak intensities using the formula presented in section 3.3.1.2. This shows that samples 1 and 2 have approximately 50% of the hard and corrosion resistant s phase (48% and 42%, respectively), while sample 3 is mostly the gamma prime phase (88% *y'* phase). The 1° glancing angle measurements show a higher proportion of the s phase with all samples than the Bragg-Bretano measurements (32%, 23% and 7%), indicating that there is more s phase at surface regions. This correlates well with the surface hardness measurements (Figure 44) as the e phase is known to be hard and brittle and the *y* phase softer and more ductile [50].

4.2 Wear and corrosion resistance of the nitrided and duplex treated samples

In wear tests the duplex treated samples were compared with samples treated with only one of the processes. PVD coated high speed steel (without nitriding) was also used as a reference. The wear test was performed using a standard pin-on-disk procedure (see section 3.3.2.1) and the corrosion tests by using potentiodynamic measurements (see section 3.3.2.6.1).

4.2.1 Wear behaviour

The results of the sliding wear tests (presented in Figure 46) show that sample 1 (170μm) clearly had the smallest sliding wear coefficient (2.6 x 10^{-15} m^2/N). Samples 2 (290μm) and 3 (400μm) had higher wear coefficient (6.7 and 10.7 x10^{-15} m^2/N, respectively). All the duplex treated samples clearly out-performed nitrided samples and the coated sample with no nitriding treatment. The wear rates of all duplex coatings are remarkably low as they are only 1/30th of the wear coefficient of the sample with the same coating or 1/100th of the nitrided but uncoated sample.

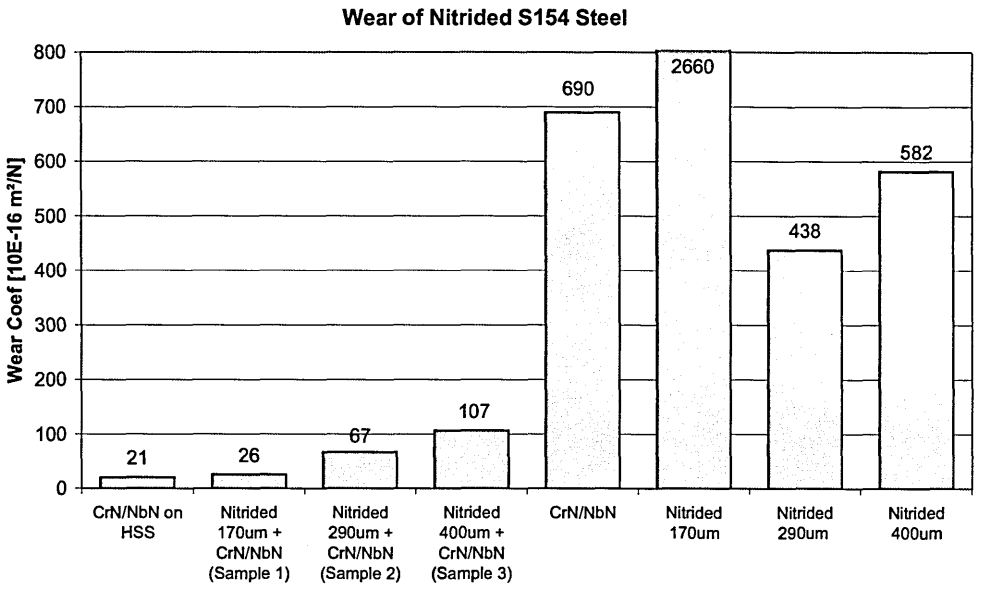

Figure 46 Sliding wear coefficients of S154 with different surface treatments

Further, the surface hardness seems to correlate well to the pin-on-disk wear behaviour. It should be noted that the wear rate of the Sample 1 (Duplex, PVD + 170μm) is approximately equal to the wear rate of the same coating on HSS with almost 3 times the bulk hardness of S154 steel ($H_V = 820$ vs. $H_V = 320$). The poor wear performance of the Nitrided 170μm sample was caused by the wear penetrating the hard compound layer that protects the substrate from excessive wear. This layer, even though hard, is relatively thin in comparison to the other nitrided samples, as shown on figure 43.

4.2.2 Fatigue behaviour

In the impact test the coatings were subjected to 1 million impacts by a ∅ 6 mm carbide ball at 350 N impact force and the impact areas were investigated using optical and SEM microscopes to analyze the fatigue behaviour of the system. There were considerable differences in the fatigue behaviour between the different samples. Though the sample 3 (400μm) did not perform very well in the wear test it exhibited excellent impact resistance. This can be seen from the micrographs of the impact craters after the impact test (Figure 47). The impact crater was the smallest in

diameter (d = 460 μm) and shows no sign of cracks or delamination. The diameter of the impact crater of sample 2 (290μm) was slightly larger, measured to be 475 μm, with some visible cracks around the edge of the crater. Sample 1 (170μm) had the largest impact crater with a diameter of 495 μm. Although the coating is fully intact there are a number of circular cracks clearly visible near the edge of the crater. The results can be explained by the previous results of microstructure and hardness measurements as the ductile γ' phase compound layer can deform under high pressure while the brittle ε phase fractures. The thicker compound layer and the case depth on the other hand provides better support for these high loads as indicated by the reduction of the impact crater size.

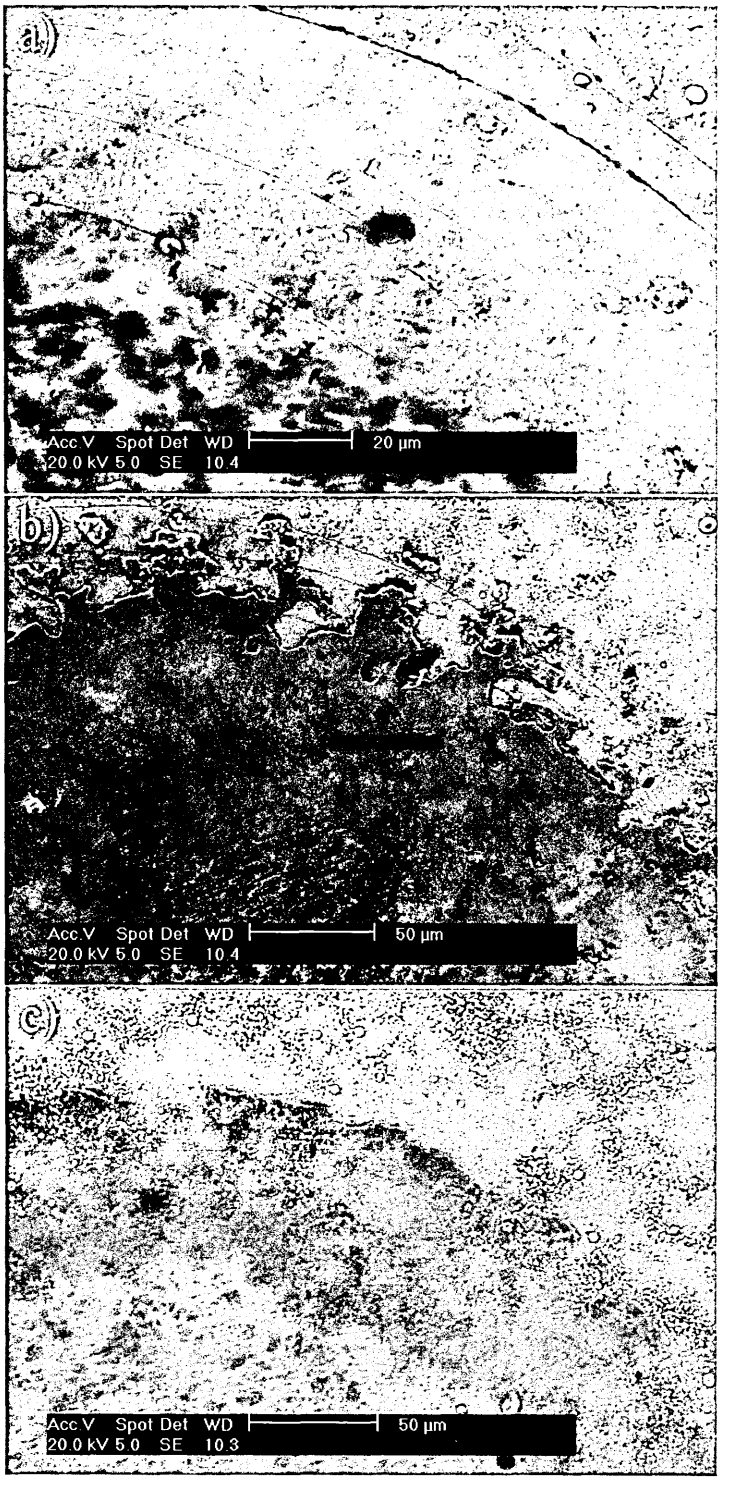

Figure 47 Impact craters of duplex treated samples a) sample 1 (170µm) (∅ = 495µm) b) sample 2 (290µm) (∅ = 475 µm) c) sample 3 (400µm) (∅ = 460 µm) after $1x10^6$ impacts at 350 N.

4.2.3 Adhesion test results

In the adhesion testing sample 3 (400μm) displayed the highest critical load in the scratch test exceeding that of the HSS by 15 N (60 N vs. 45 N). This high adhesion can be attributed to the gradual reduction in the hardness from the coating to the substrate. This gradient (figure 44) reduces the stresses at the interface zones when the coated surface is deformed. The stress due to the dissimilar material properties can lead to extreme shear stress along the interface and delaminate the coating. The improved adhesion may be also doe to the structure of the compound layer (γ phase, FCC) which is the same as that of the coating (FCC) and thus may introduce local epitaxial growth promoting adhesion. The critical loads of 45 N (sample 2, 290μm) and 35 N (sample 1, 170μm) were also high compared to the HSS sample (critical load of 45 N) and the un-nitrided S154 sample (critical load of 25 N). From the SEM investigation of the scratch of sample one (figure 43) it can be clearly seen that the failure is a brittle fracture taking place in the compound layer. The similar failures were detected on the other nitrided samples but the Sample 1, 170 μm this was quite clear. The better load support of the thicker nitriding layer as shown by the fatigue tests (4.2.2) will have influence to the scratch results as the diamond will penetrate to different depths depending on load bearing capability.

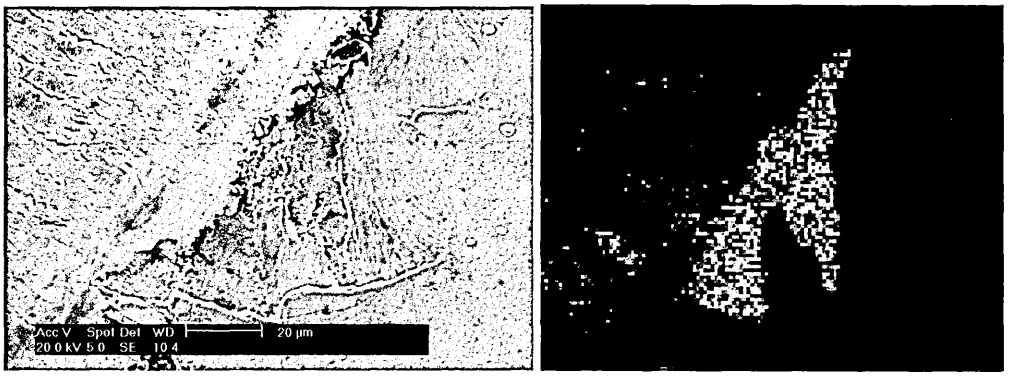

Figure 48 Scanning electron micrograph of coating adhesion failure on sample 1 (170μm) a) secondary electron image b) Energy dispersive X-ray distribution map (EDX map) of Fe kα

4.2.4 The corrosion test results

The results of the potentiodynamic polarisation tests in 3% NaCl solution are shown in Figure 49. In this environment the untreated S154 does not passivate at all. Whereas all the coated samples showed "passive like" anodic behaviour. There is clear improvement in the corrosion resistance of all PVD coated samples in comparison to the uncoated S154. All the duplex treated samples outperformed the coated sample. When different duplex treated samples are compared with one another, sample 1 (170μm case depth with compound layer consisting of manly the ε-phase) has the highest corrosion resistance followed by sample 2 (290μm) and sample 3 (400μm with the compound layer consisting of mainly the γ′-phase), respectively. If anodic current at +500mV vs. SCE is considered as the criterion, the best system (sample 1, 170μm) has almost 3 orders of magnitude lower corrosion current than the coated (not nitrided) sample. The corrosion damage on these samples is localised, with the size of the pits increasing in diameter and depth from sample 1 to sample 3. No delamination of the coating was observed near the pit locations in any of the samples. The results of the corrosion experiments show that the nitriding can significantly improve corrosion performance. Further, the increased amount of the corrosion-resistant ε-phase in the compound layer was found to be beneficial to corrosion resistance as the anodic corrosion currents decreased as the amounts of the ε-phase increased.

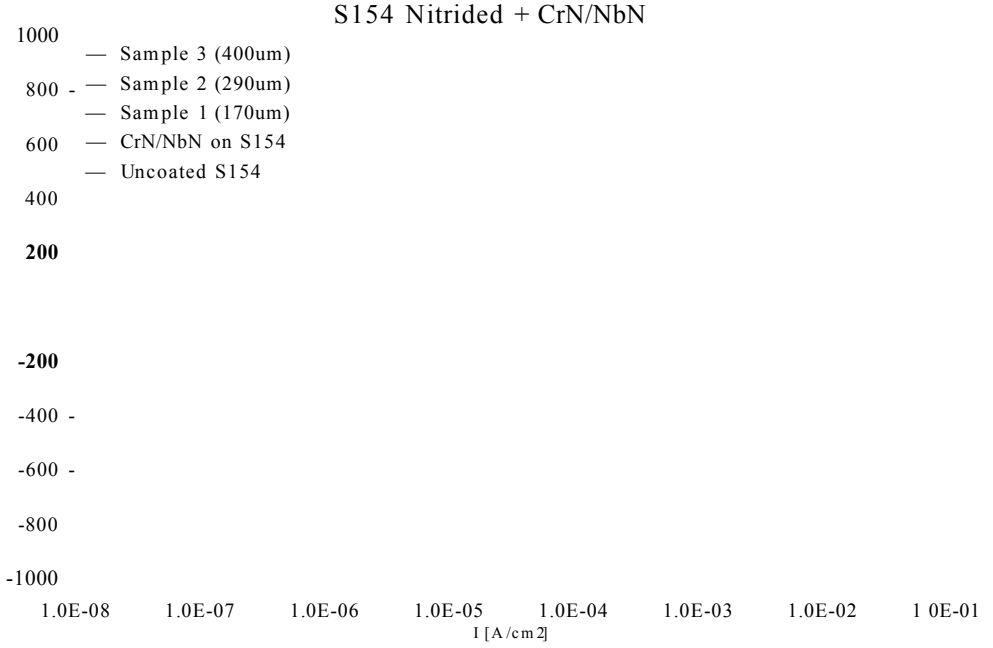

Figure 49 Results ofpotentiodynamic polarisation tests of duplex treated SI 54 in 3% NaCI solution. The corrosion performance deteriorates as the amount of the s-phase on the compound layer decreases from Sample 1 (48%) to Sample 3 (12%))

4.3 Discussion

As a result of this investigation it can be concluded that the substrate material critically affects all tribological aspects of the coating. The idea behind duplex treatments is to utilise the synergy of two different surface treatment methods in a way that maximises the benefits of both while minimising the weaknesses. In this case nitriding process was selected as the first treatment. With nitriding the case depth is sufficient to provide good support to the hard PVD coatings. The depth can exceed the economically viable PVD coating thickness by more than 10 times. The hard and corrosion resistant compound layer further improves the surface hardness and enhances the corrosion performance of the duplex system. From the results it can be seen that the microstructure of the affected area clearly have an effect on the mechanical and chemical properties of the duplex treated nitriding + CrN/NbN PVD coating. Using different nitriding process parameters the nitrided zone and consequently the duplex treated part can be optimised to suit the application at hand. The compound layer is generally thought to be problematic due to a porous top layer and instability at high temperatures (500°C). It can however be beneficial due to its high hardness and improved corrosion resistance. It has to be noted, however that sufficient adhesion and impact resistance has to be achieved for any industrial application. The results suggest that there may have to be a trade-off between wear and impact resistance, at least on low alloy steels such as S154.

The results of the measurements are summarised in Table 4. The micrographs and hardness measurements show that the microstructure of the compound layer changes with different nitriding process parameters. The two common phases γ' (Fe_4N, FCC) and ε (Fe_3N, Hexagonal) were identified in the compound layer. The γ' phase is generally considered to be softer, more ductile with better impact resistance than the harder and more brittle ε phase. In tribological applications ε phase is generally preferred [39]. One of the benefits of pulse plasma nitriding is that the process parameters can be easily and reliably adjusted to obtain a desired surface condition. All samples had a compound layer consisting of a mixture of both phases with the fraction of ε phase reducing from sample 1 (170μm) to sample 3 (400μm). Further, by

comparing the results from glancing angle (1°) and Bragg-Brentano measurements it is shown that the ε phase is present at higher concentration near to the surface of the sample. This is usual as the higher nitrides convert to lower ones (4 $Fe_3N \rightarrow 3\ Fe_4N$ + N) and the freed up nitrogen diffuses deeper into the substrate where it locates in interstitial positions of the lattice or at grain boundaries hindering dislocation movement, thus hardening the affected area. The temperature of the PVD coating process was within acceptable limits as the cross-section micrographs showed no instability of the compound layer during the coating process (i.e. the black layer). The microstructural analysis correlates well with the surface hardness measurements in which sample 1 (170μm) showed very high surface hardness of $H_{V,25g} = 890$, which can be associated to the hard ε phase and sample 3 (400μm) presented a relatively low surface hardness of $H_{V,25g} = 530$ relating to the softer γ phase.

Table 4 Summary of the properties of the duplex treated samples

	Sample 1	Sample 2	Sample 3
Nitriding process	6h 520°C	3h 480°C +14h 520°C	40h 530°C
Case depth	170μm	290μm	400μm
Compound layer 1° GA B-B	4μm , 48% ε phase 32% ε phase	7μm , 42% ε phase 23% ε phase	10μm , 12% ε phase 7% ε phase
Surface hardness	$H_{V,25g} = 890$	$H_{V,25g} = 790$	$H_{V,25g} = 530$
Sliding wear coefficient	$2.6x10^{-15}$ m²/N	$6.7x10^{-15}$ m²/N	$10.4x10^{-15}$ m²/N
Adhesion (L_c)	35 N	45 N	60 N
Impact resistance	Fair	Fair	Good
Impact crater diameter	495 μm	475 μm	460 μm
Anodic corrosion current density at +500mV vs. SCE	$5*10^{-6}$ A/cm²	$7*10^{-5}$ A/cm²	$3*10^{-4}$ A/cm²

The surface hardness of the nitrided substrate also correlates well with the pin-on-disk wear behaviour as can be seen from the Figure 50. The wear rate of the sample 1 (170μm) is approximately equal to the wear rate of the same coating on M2 HSS, the latter having almost 3 times the bulk hardness of S154 steel. The wear rates of all duplex coatings prepared are remarkably low.

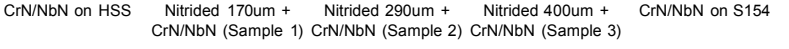

Figure 50 Comparison of the Pin-on-Disk wear results and surface hardness of the nitrided substrate of the duplex treated samples

On the other hand in the impact testing the results were the opposite. Sample 3 (400pm) with high case depth and of almost a pure y'-phase compound layer showed excellent impact resistance. The impact crater was the smallest and showed no cracking. It also exhibited the highest critical load in the scratch test exceeding that of the High Speed Steel sample by 15 N (60 N vs. 45 N). This high adhesion can be attributed to the gradual reduction in the hardness at interface regions as it reduces the shear stress, which may cause the adhesive failure, at the interface. The crystal structure of the compound layer (y'phase, FCC) is also same as that of the coating (FCC), which may introduce local epitaxial growth and hence improved adhesion [20,82].

Despite the excellent wear behaviour of sample 1 (170pm) the adhesion was not as good as with samples 2 (290pm) and 3 (400pm), though it was still notably better than the untreated sample. This probably resulted from brittle fracture initiating within the compound layer rather than simple delamination of the coating. Both the coatings which contained significant amounts of the s phase (samples 1 and 2) also showed cracks in the impact crater thus showing the brittle nature of the s phase in the compound layer. This was also evident from the SEM investigation of the scratch test failure sites.

The corrosion behaviour is also greatly affected by the nitriding process and microstructure. All the nitrided samples outperformed the non-nitrided coated sample, which, on the other hand, clearly outperformed the uncoated sample. At an anodic potential of +500mV vs. SCE sample 1 (170pm) has almost 3 orders of magnitude lower corrosion current density than the same coating without nitriding and 2 orders of magnitude lower than sample 3 (400pm). These results indicate that the compound layer plays a big role in the corrosion performance. The compound layer is very corrosion resistant, as can be seen from the etched cross sections where the etching acid has no impact on the compound layer. The results also show that the s phase is preferred when good corrosion resistance is required. Although sample 1 (170pm) had the thinnest compound layer its anodic current density was significantly lower than that of sample 3 with more than twice the compound layer thickness. The corrosion currents also decreased with increasing amount of s phase as can be seen in Figure 51.

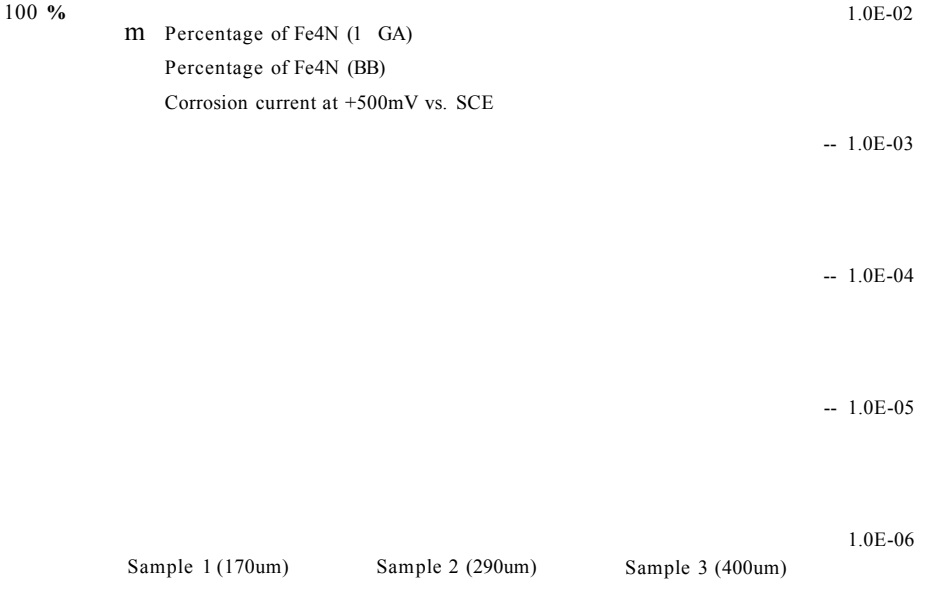

Figure 51 The relation between the phase composition of the compound layer and anodic corrosion current

In industrial applications the compound layer composition should be carefully considered as both phases have their distinct benefits. The hard ε phase gives high surface hardness and good corrosion performance yet can have limitations regarding adhesion and impact resistance due to brittle fractures in the compound layer. The more ductile γ'phase can promote very good adhesion and impact resistance. Large case depth means reduced deformations with high impact loads. All samples studied for this work had a compound layer with a mixture of both phases. The ratio of each phase should be carefully considered for the specific industrial application. In order to achieve the desired result, a nitriding process that allows the engineering and consisted reproduction of the desired compound layer microstructure should be used.

It has to be noted however that the duplex treated parts were not tested in a real life application. Also the slight polishing done after the nitriding step may not be a viable approach in mass production mainly due to poor consistency in more complex parts. Ideally nitriding should be carried out in a PVD chamber using a low pressure plasma nitriding process. The main reasons why this is not commonly done is the cost associated due to the long treatment times. Further study should be conducted using components from an industrial application, i.e. for wood cutting where corrosion, wear and impacts affect the lifetime of a cutting tool. Then it would be possible to engineer the duplex treatment to the specific application and benchmark the results to the existing technology. This would also enable a cost analysis to be performed, noting also that improving the lifetime of a tool can reduce downtime associated with tool change and thus improve the productivity of the work centre or process, therefore bringing benefits far exceeding the price of a tool.

5 INTERFACE MODIFICATION BY ION ETCHING

The interface structure and composition have been shown to influence adhesion whereas adhesion determines the wear and corrosion performance [19, 66]. The ABS (Arc Bond Sputtering) technology provides good opportunities for interface engineering via the possibility of metal ion bombardment in arc discharge evaporation mode by applying a high bias voltage at the substrate [19, 83]. By using proper parameters and selecting appropriate ion species for the bombardment, the interface can be modified to provide an optimal growth platform for the coating. Nb ion bombardment of the substrate coating interface has been shown to result in a deposition of a 10 nm thick layer with nanocrystalline structure. This layer has been shown to provide improved corrosion properties for the coating [83-86]. An etching process with two separate steps has been shown to yield good results. Generally the first step is used to provide a fast etching speed and to minimise the time required and the second step to enhance ion implantation. For corrosion-resistant applications using niobium ion etching the first step is still used for etching, while the second is used to deposit a corrosion resistant Nb implantation layer.

In this chapter the effect of the different parameters employed during the Nb metal ion surface pre-treatment step on the interface microstructure and the tribological and corrosion performance of a Nb/CrN/(CrN/NbN) multilayer PVD coating is reported. Table 5 summarises the parameters used for this work. The U_b = -1200 V and U_b = -800 V etching processes were used as a benchmark.

Table 5 Deposition parameters of the coatings in this section

	Ion Etch			Nb barrier layer	CrN	CrN/NbN
	Duration	U_b [V]	p [Pa]			
1200V	20 min	-1200	0.14	Duration:	Duration:	Duration:
800V	15 min	-800	0.10	180 min	30 min,	150 min,
2 step I	5 min followed 10 min	-1200 by: -800	0.20 0.14→ 0.03	Power: 2 x 8 kW U_b= -100 V p = 0.21 Pa	Power: 2 x 5 kW U_b = -120 V p = 0.38 Pa	Power: 2 x 10 kW (Nb) + 2 x 5 kW (Cr), U_b = -120 V, p = 0.36 Pa
2 step II	14 min followed 6 min	-1200 by: -800	0.14 0.10→ 0.03			

The TEM cross-section and the schematic diagram describing the coating can be seen in Figure 52.

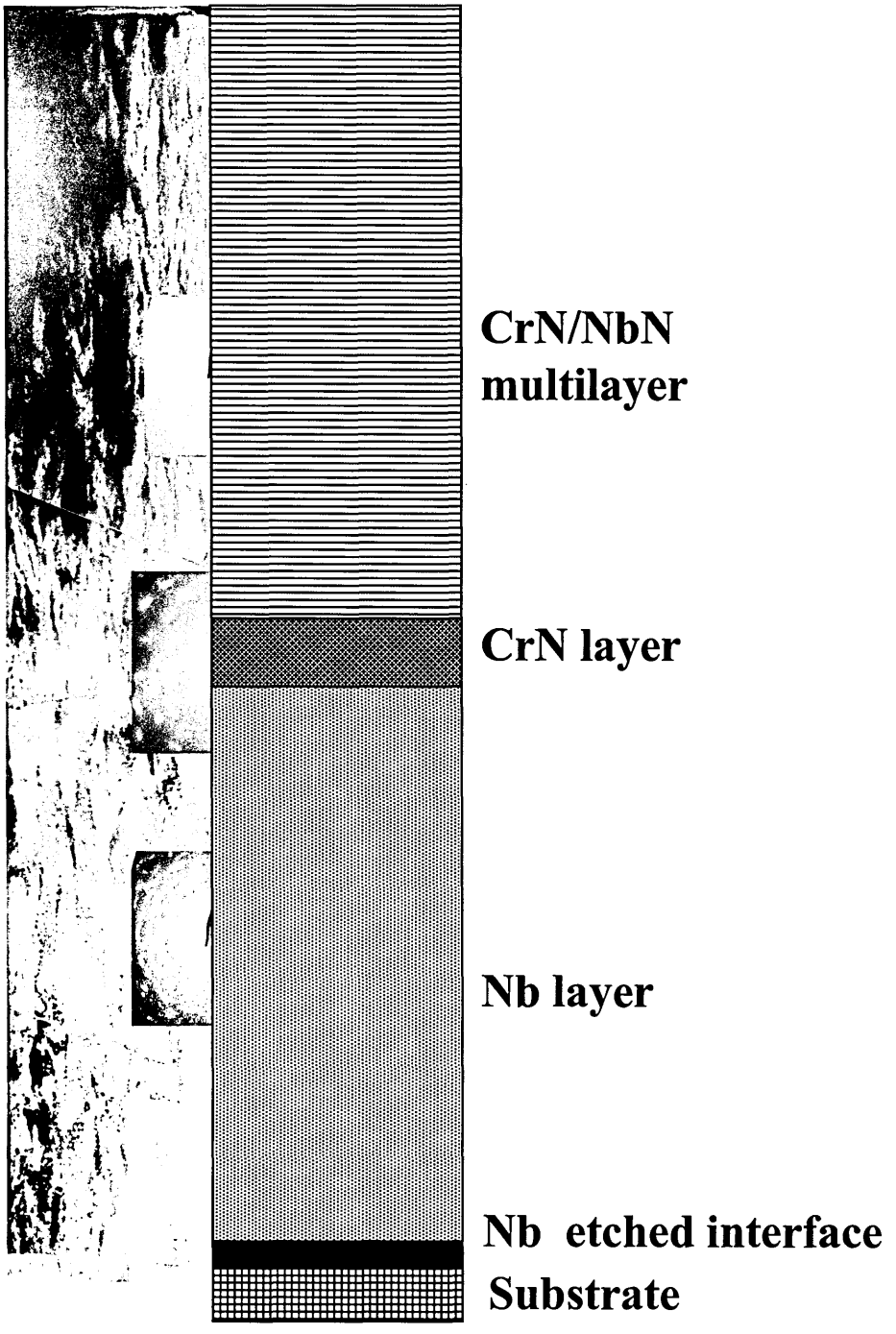

Figure 52 XTEM image and schematic of the coatings used in this section. The total coating thickness is up to 9μm consisting of the following layers: 5-10nm Nb interface layer, 4.5μm Nb barrier layer, 0.5μm CrN interface layer and 4μm CrN/NbN multilayer with bi-layer thickness of 3nm.

5.1 Microstructure at the interface

The XTEM/EDS investigation of the substrate-coating interfaces clearly shows the effect of the Nb-ion bombardment. An approximately lOnm thick deposition layer at the interface zone with a nanocrystalline microstructure (Figure 53). EDS linescans (Figure 54) over the interface showed that the nanocrystalline area consisted of gradient composition of Nb from 20% Nb to 80% Nb mixed with the base material. With high bias voltages the arriving metal ions can have sufficient energy to implant a short distance into the substrate. However, the majority of the atoms/ions arriving at the substrate do not have enough energy to implant and are thus deposited. Under these conditions (also argon ions bombard the surfaces) the atoms on the surface are intermixed with the atoms at the substrate forming a thin layer with a nanocrystalline structure.

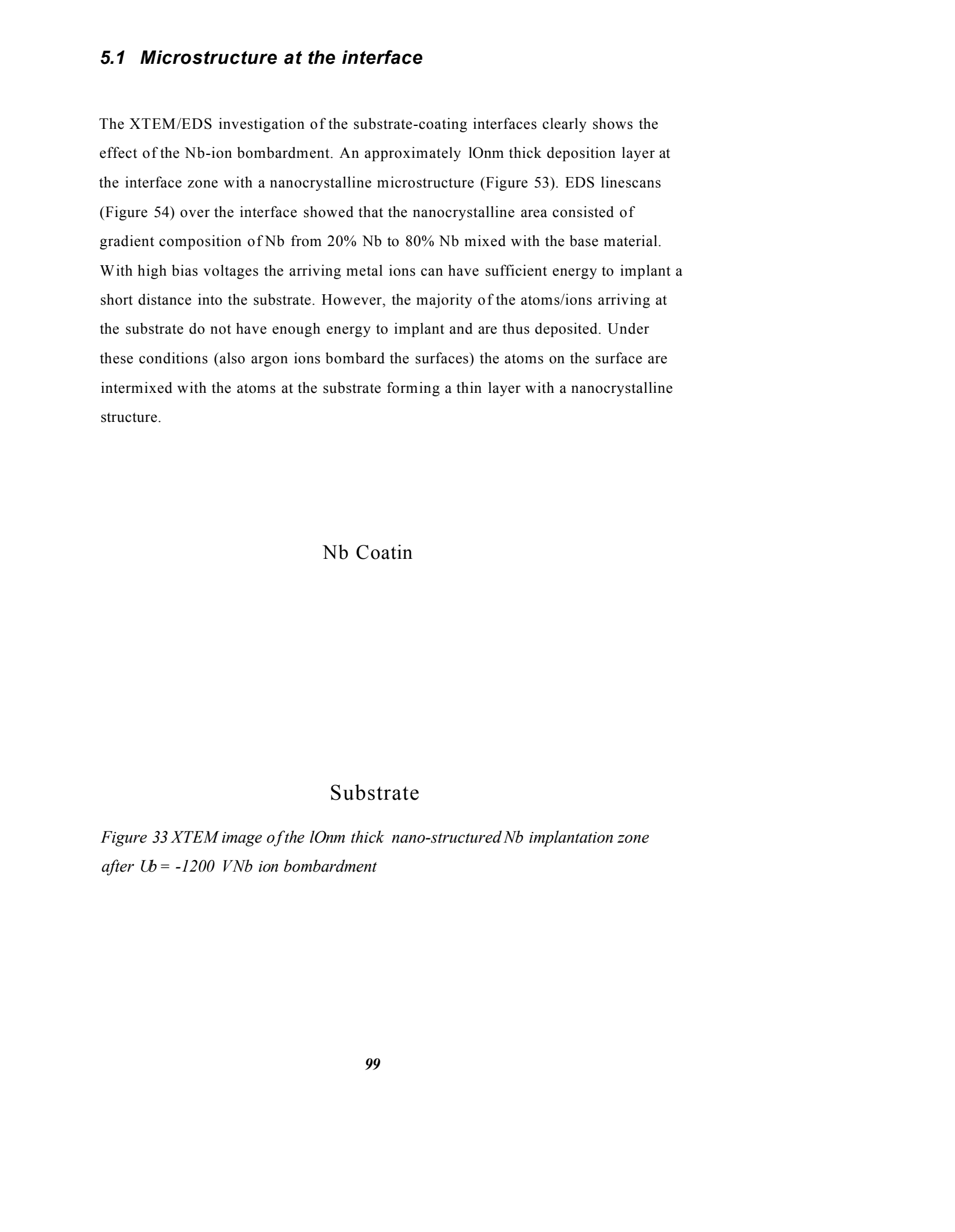

Figure 33 XTEM image of the lOnm thick nano-structured Nb implantation zone after Ub = -1200 VNb ion bombardment

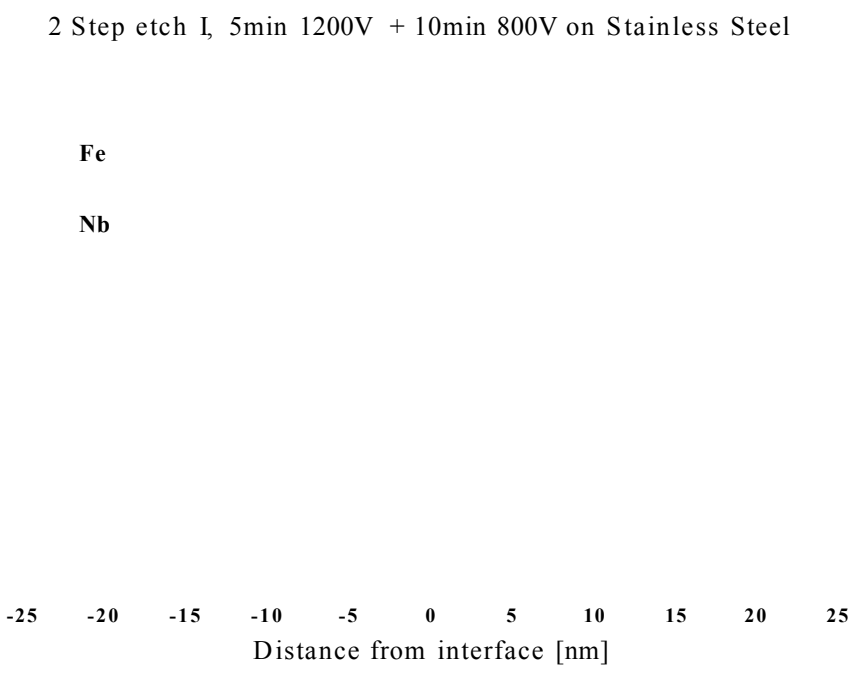

Figure 54 EDX linescan across the interface region after Nb ion bombardment

Etching at a lower bias voltage, Ub= -800V, was found not to be very effective. In this case two separate layers were found at the interface, one consisting of chromium and niobium and the other of niobium. The STEM image of the interface and the EDS trace can be seen in Figure 55 and Figure 56, respectively. This deposition layer of chromium and niobium was determined to be an artefact from the cathode cleaning process step as the same power was used on all the targets and the Nb sputtering rate is 50% slower resulting in a composition of approximately 30% Nb and 70% Cr. Therefore it can be determined that the shutters in front of the targets are not 100% effective in preventing deposition onto the samples. Further, it has been established that the increased amount of chromium at the interface can be used to indicate insufficient etching because the etching should be capable of removing such very thin impurities from the surface. Thus it can be concluded that at low bias voltages during the Nb etching step no etching actually occurs. On top of this thin artefact layer the nanostructured Nb deposition layer is still present.

Figure 55 The interface zone of the Ub = -800 V Nb etched sample showing a deposition layer of Cr and Nb followed by a layer of nanostuctured Nb deposition

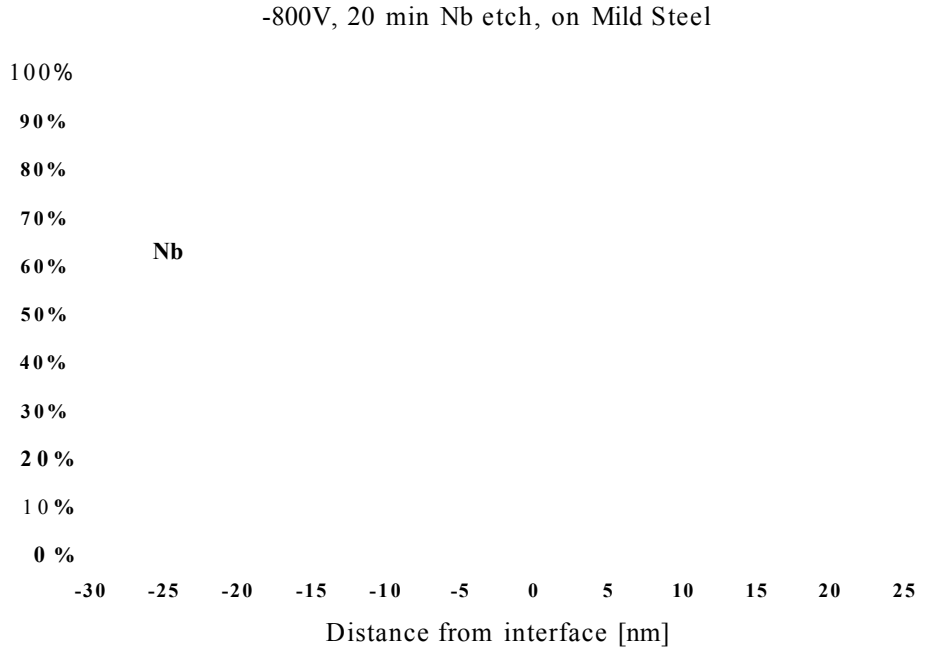

Figure 56 EDX linescan across the interface zone of the Ub = -800 V Nb etched sample showing a deposition layer of Cr and Nb at the interface

Furthermore, a two-step etching processes were tested, where the first half (step) was designed to etch the surface clean and the second was for the deposition of the thin nanocrystalline niobium layer to improve the corrosion resistance.
The two-step etched samples were also investigated with XTEM/EDS but no discemable difference between the microstructure of the different processes could be observed. The EDS line-scans of the samples in this section can be seen in Figure 57.

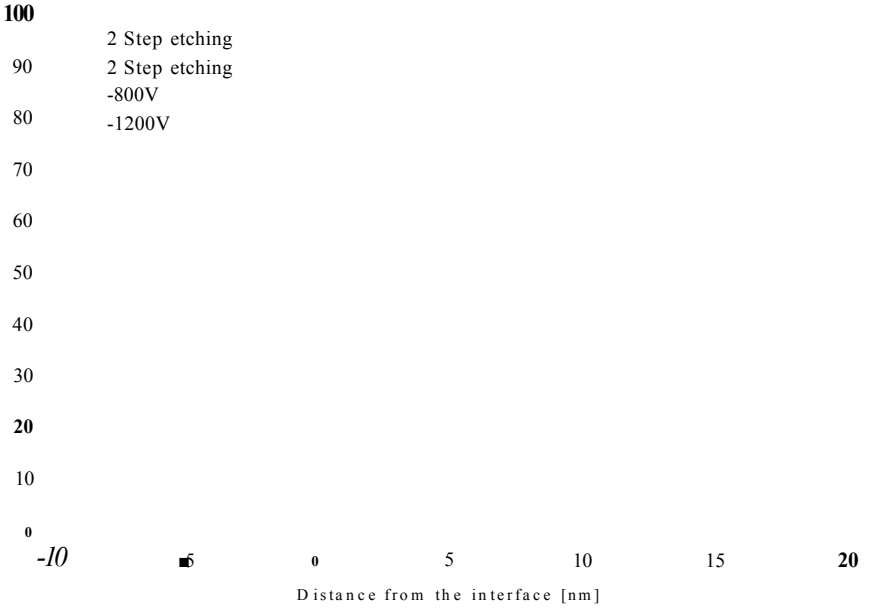

Figure 57 Niobium EDS line scans across the interface show similar interfacefor the 2 two step processes and the Ub - -1200 V one step process

The microstructural investigation shows that the etching speed of Nb metal ions is rather low even at high bias voltages of -1200 V. At -800 V there is virtually no sputtering but only deposition. The deposition under such bombardment yields the nanostructured layer that can be seen in Figure 53 and Figure 55. This deposition layer should be beneficial in improving the corrosion resistance. However, insufficient etching will not be able to remove any surface contaminations, consequently low adhesion may result in a corrosion failure as the stress resulting from the growth of voluminous corrosion products can delaminate the coating along the interface thus exposing uncoated surface to the environment. The two step

approach should eliminate this concern as the first step should effectively remove the contaminant from the surfaces.

5.2 Effect of etching parameters on tribological properties and corrosion resistance

The surface preparation etching step can be clearly seen to affect both the tribological and corrosion properties of the coating. The mechanical properties are summarised in Table 6 and the results of the potentiodynamic polarisation test results can be seen in Figure 58.

The adhesion measurement shows a noticeable difference between the coatings. Etching with low bias voltage (15 minutes, -800 V bias, $p_{Ar} = 0.1$ Pa) was noted to have insufficient effect resulting in rather low adhesion ($L_c = 21$ N). The best adhesion was achieved with the standard 20 min $U_b = -1200$ V etching. The results indicate that the lower bias voltage second step reduces the mechanical properties of the coating slightly. Still this minor negative effect was not totally unexpected, as the 2 step etch processes were designed primarily to improve the corrosion properties of the coating.

Table 6 Adhesion of the Nb-CrN/NbN coatings using different ion etching parameters on HSS

Coating	Adhesion (L_c)
-1200 V etch	49 N
-800 V etch	21 N
2 step etch I (5min -1200 V, 10min -800 V)	44 N
2 step etch II (14min -1200 V, 6min -800 V)	45 N

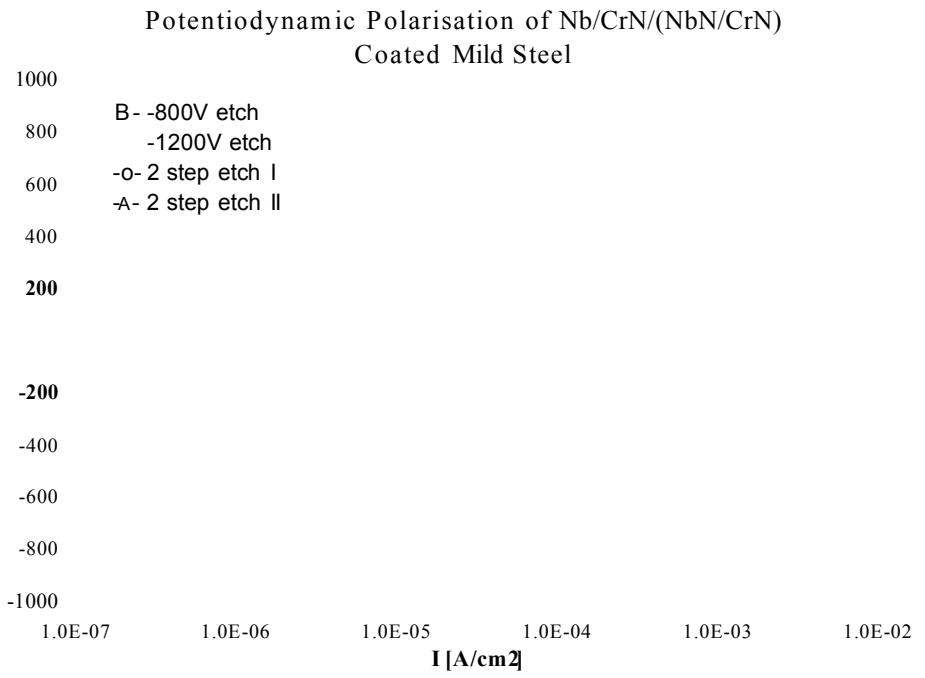

Figure 58 The results of the potentiodynamic polarisation tests for the CrN/NbN coatings with different etching processes

In 3% sodium chloride solution all coatings displayed “passive like” behaviour in the anodic region up to +1 V vs. SCE. However there were big differences in the anodic corrosion currents. The two-step etching processes indeed yielded some improvement in the corrosion resistance. The best coating, the latter of the two-step processes with longer etching step duration, had an anodic current density at +500 mV vs. SCE around 25% compared to the reference coating (1.5 x 10‘5A/cm2 vs. 5.4 x 10‘5A/cm2), The second two step etching process also showed a positive effect on the corrosion performance. Still, it was not expected that the 2 step etching II would outperform 2 step etching I as the longer etching time is supposedly causing more localised defects leading to more potential corrosion sites.

Unexpectedly the Ub = -800 V coating performed very poorly in the test. The poor performance can be attributed to adhesive failure, in which the corrosion deposits (rust) that form underneath the coating at defect locations will delaminate the coating exposing the untreated surface. On these untreated surfaces corrosion proceeds extremely rapidly (i.e. mild steel in sea water).

Figure 59 shows the corrosion damage on the surface of the sample prepared with U_b = -800 V Nb etching and in Figure 60 the damage on the sample prepared with U_b = -1200 V Nb etching. From these figures one can see the corrosion deposit delaminating the coating in worm patterns if the interface adhesion is poor. On the other hand with good adhesion the corrosion damage is limited to the area of the initial corrosion "pit". The coating defect from where the corrosion initiated can still be seen on top of the pit.

Figure 59 Corrosion damage on the U_b = -800 V prepared sample after polarisation test. The corrosion advances in "wormhole" patterns along the interface. The delamination of the coating due to the voluminous corrosion deposits and poor adhesion continuously exposes uncoated substrate to the corrosive environments leading to corrosion failure.

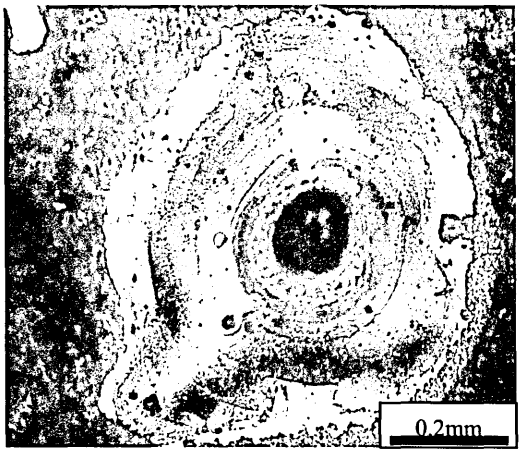

Figure 60 Corrosion damage on U_b = -1200 V etched sample. The corrosion damage is limited close to the original coating defect (visible in the centre of the pit). The good adhesion of the coating prevents the corrosion from advancing along the interface leading to dome-like corrosion "pit", where the rate of the corrosion is determined by the diffusion of the ions through the coating defect.

5.3 Discussion

The etching process parameters have been shown to affect both the mechanical and the corrosion properties. In the analysis of the microstructure of the coatings it was shown that the etching efficiency of the Nb ions is rather poor below -1000 V bias voltage. At bias voltages lower than this the Nb starts to form a nanostructured deposition layer that is expected to be beneficial to the corrosion performance. Such a layer was indeed observed at the interface region and it was also shown to have a positive effect on the corrosion performance, provided that the adhesion of the coating was good.

Further, it was observed that the two-step process outperformed the single-step process in the corrosion tests, indicating that the approach can be utilised in practice. However caution should be exercised as it was also shown that insufficient etching of the interface will lead to poor adhesion that may lead to a failure at the interface. In coatings like CrN/NbN the corrosion has been shown to be localised, and often starts at point defects in the coating. As the corrosion starts the voluminous corrosion products, that can expand to 10 times the volume of the metal, create a stress at the interface that may delaminate the coating if the adhesion is poor. This exposes uncoated substrate to the environment leading to catastrophic corrosion failure. On the other hand if the adhesion of the coating is good the corrosion products start blocking the diffusion of the oxygen to the substrate and thus start to slow down the corrosion. This is shown in the schematic drawing below (Figure 61)

Good adhesion Poor adhesion

Figure 61 Schematic illustration of the corrosion failure through adhesive failure

6 NIOBIUM BARRIER LAYER

Niobium is widely known to be a very stable material chemically and is therefore used in a wide range of applications requiring extreme corrosion resistance. The electrochemical stability of niobium is based on the formation of a Nb_2O_5 oxide layer on the surface which is stable even under the most hostile environments [68]. Metallic niobium PVD coatings have been successfully deposited on various substrates and they have been shown to increase corrosion resistance of stainless steels considerably [66, 69, 89-91]. They have also been used successfully as barrier layers in multilayered CrN/NbN coatings yielding corrosion resistant coatings that are comparable or superior to that of 25 μm thick hard chrome. Metallic Nb coatings can also be used as decorative coatings with a wide range of colours available through anodising [69,92].

This chapter describes how film thickness and bias voltage influence the crystal structure, the localised defect density and the mechanical and electrochemical properties of the ABS deposited Nb coatings. The Nb barrier layer is intended to be used together with a very hard and wear-resistant CrN/NbN superlattice coating to further improve the corrosion resistance of the coating. The Nb coatings were deposited using bias voltages varying from U_b = -75 V to U_b = -150 V in 25 V intervals. The investigation focused on barrier coatings of two thicknesses of approximately 1.5 μm (1 hour of deposition time, subsequently referred as 1Nb) and 4.5 μm (3 hours of deposition time, subsequently referred as 3Nb). The Nb films were studied alone and in combination with the CrN/NbN coating. The coating parameters are summarised in Table 7 and Table 8.

Table 7 The summary of the deposition parameters of the niobium barrier layer coatings

	Pressure [Pa]	Bias voltage	Power	Other
Heating	<0.007			
Target Cleaning (2min)	0.20		2 x 1 kW	
Nb ion etching (15min)	0.2-0.06	-1200 V	1.3 kW	Cathodic Arc
Coating: 1Nb 60min, 3Nb 180min	0.20	 -75 V, -100 V, -125 V, -150 V, -75 V, -100 V, -125 V, -150 V	2 x 8 kW	Sample label: 1Nb -75V 1Nb -100V 1Nb -125V 1Nb -150V 3Nb -75V 3Nb -100V 3Nb -125V 3Nb -150V

Table 8 The deposition parameters of the Nb-CrN/NbN coatings

	Pressure [Pa]	Bias voltage	Power	Other
Heating	<0.007			
Target Cleaning (2min)	0.20		2 x 1 kW	
Nb ion etching (15min)	0.2-0.06	-1200 V	1.3 kW	Cathodic Arc
Nb layer: 1Nb (60min) 3Nb (180min)	0.20	-100 V	2 x 8 kW	Sample label: 1Nb CrN/NbN 3Nb CrN/NbN
CrN layer (30min)	0.36	-75 V	2 x 5 kW	
CrN/NbN layer (150min)	0.38	-120 V	2 x 5 kW & 2 x 10 kW	

6.1 Microstructure

A detailed analysis of the microstructure of the Nb layer and tribological performance of the Nb coatings was performed. Analysing the structure of the coatings can indicate the underlying reasons for the different results of the functional tests. The findings can then be correlated to the coating parameters enabling further enhancement of the coating performance.

The macrodefects caused by surface impurities have been identified as a major cause of the localised corrosion of highly corrosion-resistant coatings such as Nb [21, 23, 57]. In order to correlate the surface topography and defect density to the corrosion

performance an investigation of the surface of the coating with SEM plan-view observation of the (HSS) samples was performed.

A cross-sectional TEM (XTEM) investigation of the microstructure of the coatings (Figure 62 and 63) showed columnar grain morphology with no apparent voids between the columns even in coatings deposited at lower bias voltages. All the coatings have a dense columnar structure, while the coatings deposited at low bias voltages showed a more distinct columnar microstructure. The columns become almost indistinguishable at U_b = -150 V. This is consistent with the theoretical structure models as the increased argon bombardment causes densification of the microstructure at the expense of the grain growth. Also, a reduction in the grain diameter and the thickness of the coating can be observed with increasing bias voltage. It can be also observed that, at the lower bias voltages, the tops of the grains have distinct dome features which disappear at -150 V bias.

Figure 62 XTEM images of the 1Nb coatings deposited using different bias voltages

Figure 63 XTEM images of the 3Nb coatings deposited with different bias voltages

The average grain size increases as the films grow thicker. The 10 nm thick nano-structured zone caused by the Nb ion etching can be observed at the interface. On top of this layer forms a very fine crystal structure with random orientation as the arriving atoms cannot organise according to the substrate microstructure but select a random orientation. This is followed by a rapid grain growth, where only preferred growth planes survive. (See the dark field XTEM of the interface region, Figure 64). This continues up to 0.2 μm from the coating/substrate interface (about 10 minutes of

deposition) after which the preferred growth directions <110> and <111> begin to dominate and clear columnar structure is observed. The interface region exhibits typical Stranski-Krastanov (S-K) growth as explained in chapter 2.2.

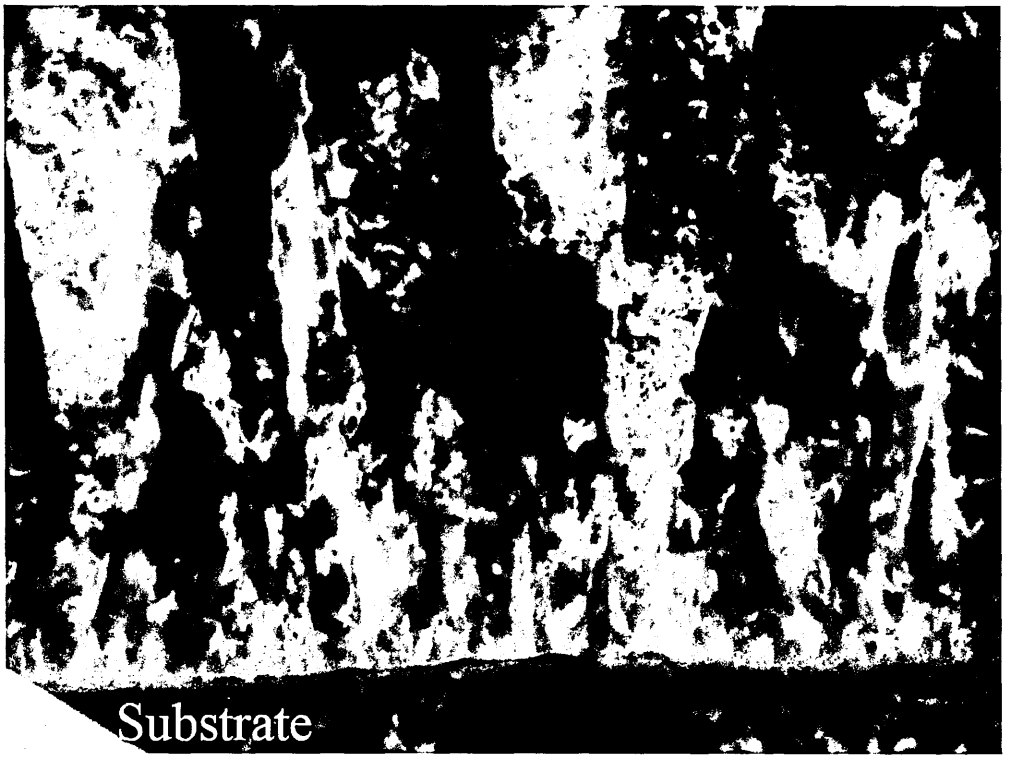

Figure 64 Dark field XTEM image of the interface region of the 1Nb -75V coating showing the nano-structured implantation zone and competitive grain growth

The average column diameter grows gradually with increasing thickness. It increases from approximately 110 nm at U_b = -75 V (70 nm at U_b = -150 V) at 1μm thickness to 230 nm (120 nm at U_b = -150 V) at 3 μm thickness. At U_b = -150 V individual grains are not always clearly defined due to numerous of lattice defects and columnar sub-grains in the microstructure that are formed under intense argon ion bombardment.

A TEM plan view investigation (see Figure 65) showed a fully dense microstructure with no voids even in coatings deposited at the lowest bias voltage used (U_b = –75 V). As the higher bias voltage reduces the voids between the grains, it is clear that the higher bias will not have an effect of closing such voids as they are not already apparent in this sample.

Figure 65 TEM plan view of the 1Nb -75V coating, showing fully dense structure

The coated samples were observed from the top with SEM to view the topography and the point defects in the coating. A comparison of the 1Nb samples can be seen in Figure 66 and the 3Nb samples in Figure 67. The number of defects was then analysed using image analysis software. The results can be seen in the Table 9.

From the results it can be concluded that the number of the defects was not notably reduced as the bias voltage was increased. However, a clear reduction to the number of the defects comes from coating thickness as the thicker 3Nb coatings clearly had fewer defects than the thin coatings. This is especially notable for smaller defects and voids. With a thick coating deposited at low bias voltage (U_b = -75 V) the number of large defects was significantly greater than with the coatings deposited at higher bias voltages. Overall the number of the defects is very high even with the best coating amounting to 90 defects per 1 mm^2.

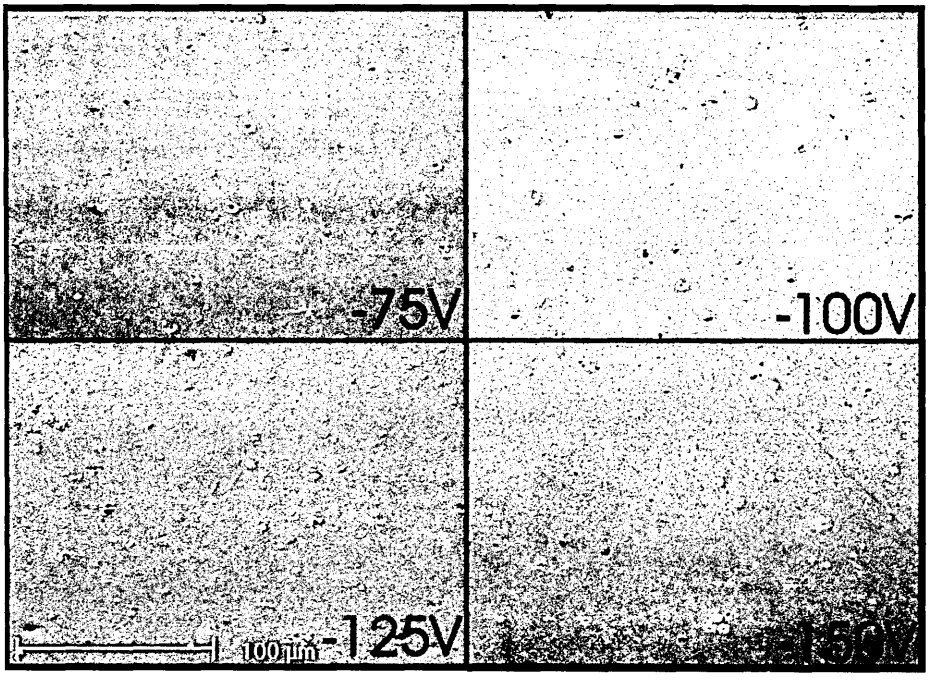

Figure 66 Plan view SEM observation of the 1Nb coatings reveal large number of growth defects in the coating

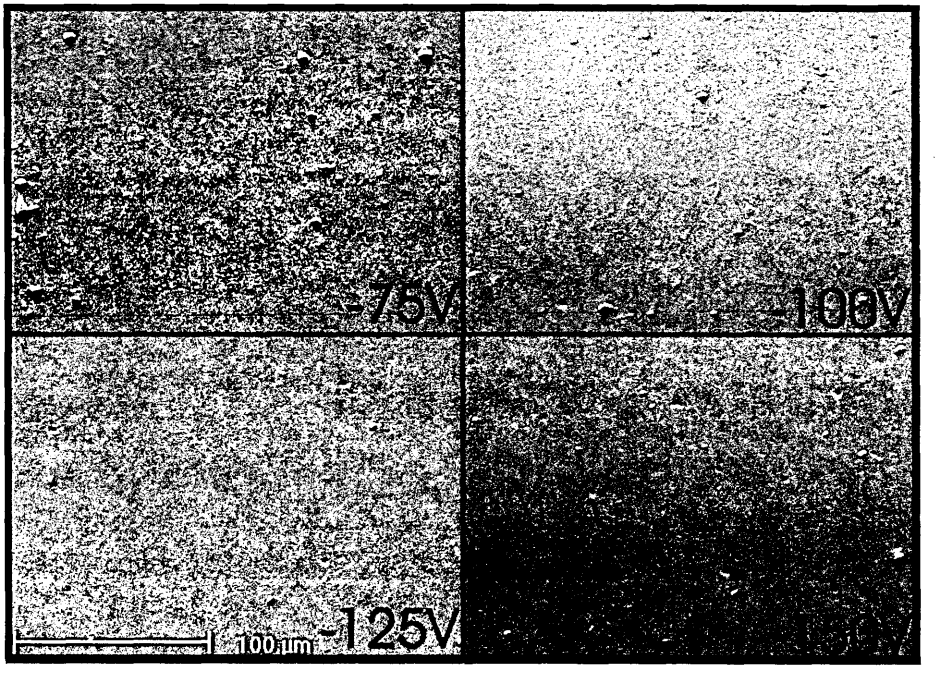

Figure 67 Plan view SEM observation of the 3Nb coatings reveal growth defects visible in the coating yet at significantly lower quantity than with the thinner coating

Table 9 The number of growth defects in 1mm² of Nb coating (Quantified from the SEM plan view images with image analysis software)

1Nb				
Defect size	-75V	-100V	-125V	-150V
>10μm²	204	256	421	266
<10μm²	3267	2432	4045	1806
3Nb				
Defect size	-75V	-100V	-125V	-150V
>10μm²	131	111	90	97
<10μm²	1862	936	950	967

With low bias voltages the defects can grow larger due to shadowing effects as the ion bombardment is not sufficient to smooth out the growth at the boundary region of the defect and the coating. Further, the boundary region around the defect becomes less dense and further increases the chances of the ejection of the defect in the corrosion environment. With the thinner coating, it was observed, that a number of substrate imperfections were still visible in the plan-view observation. This indicates that a certain coating thickness needs to be attained before surface imperfections are covered and thus good barrier properties achieved. The results of the corrosion testing can be seen to support these findings.

Further effects of the increased bombardment due to high bias voltage was noted in a semi-quantitative EDX analysis of the coatings, that showed an increase of the Ar content in the coatings as the bias is increased (Table 10, page 118). With voltages below $U_b = -100$ V there was virtually no argon incorporated in the coating. At $U_b = -125$ V the Ar content of the coating was 2.5 at% which at $U_b = -150$ V increased to 3.5 at %. in the thinner coating and 4.5% in the thicker coating. This incorporation of argon affects the mechanical properties and the intrinsic stress that may have a positive effect in "healing" growth defects as shown in section 2.2.3. On the other hand this lattice strain and the related internal stresses can result in high stress at the coating-substrate interface potentially causing loss of adhesion. Argon is thought to be implanted into the lattice in interstitial positions causing lattice strain and hardening since the movement of dislocations is hindered. As the bombarding energy is increased the argon atoms/ions have a higher probability of being trapped into the

coating. On the other hand if the ion energy is not high enough the smoothening of the coating cannot occur as seen in the plan-view observation.

The texture of the coating was also investigated using X-ray diffraction in both glancing angle and Bragg-Brentano configurations. The XRD (Figure 68 and Table 10) showed significant changes in the texture of the coatings. Coatings deposited at $U_b = -75$ V developed a strong {110} texture with inverse polar figures for {110} reflection of 5.1 and 5.6 for the 1Nb and the 3Nb coatings, respectively. As the bias voltage was increased the intensity of the {110} peak relative to the {222} peak decreases. This indicates a less strong texture or possible change in texture. Indeed, with increasing bias voltage there is noticeable change towards {111} texture. The thicker coatings deposited at bias voltages of $U_b = -100$ V or higher have a strong {111} texture with T* values higher than 4 (see table 4). However, the {111} texture is less strong in the thinner coatings with 1Nb –125 V and 1Nb -150 V showing mixed {111}/{110} texture (inverse pole figures for {110} reflection from 2.0 to 2.3). There is also a noticeable peak shift toward lower 2θ angles as the bias voltage is increased (see Figure 68, {222} reflection, JCPDS standard 107.6°). This peak shift can be associated with lattice strain indicating a residual stress in the plane parallel to the coating surface. Since the pattern was measured in θ/2θ geometry (which measures d spacing perpendicular to the surface) a compressive stress in the film plane parallel to the surface causes an expansion perpendicular to the surface due to the Poisson effect.

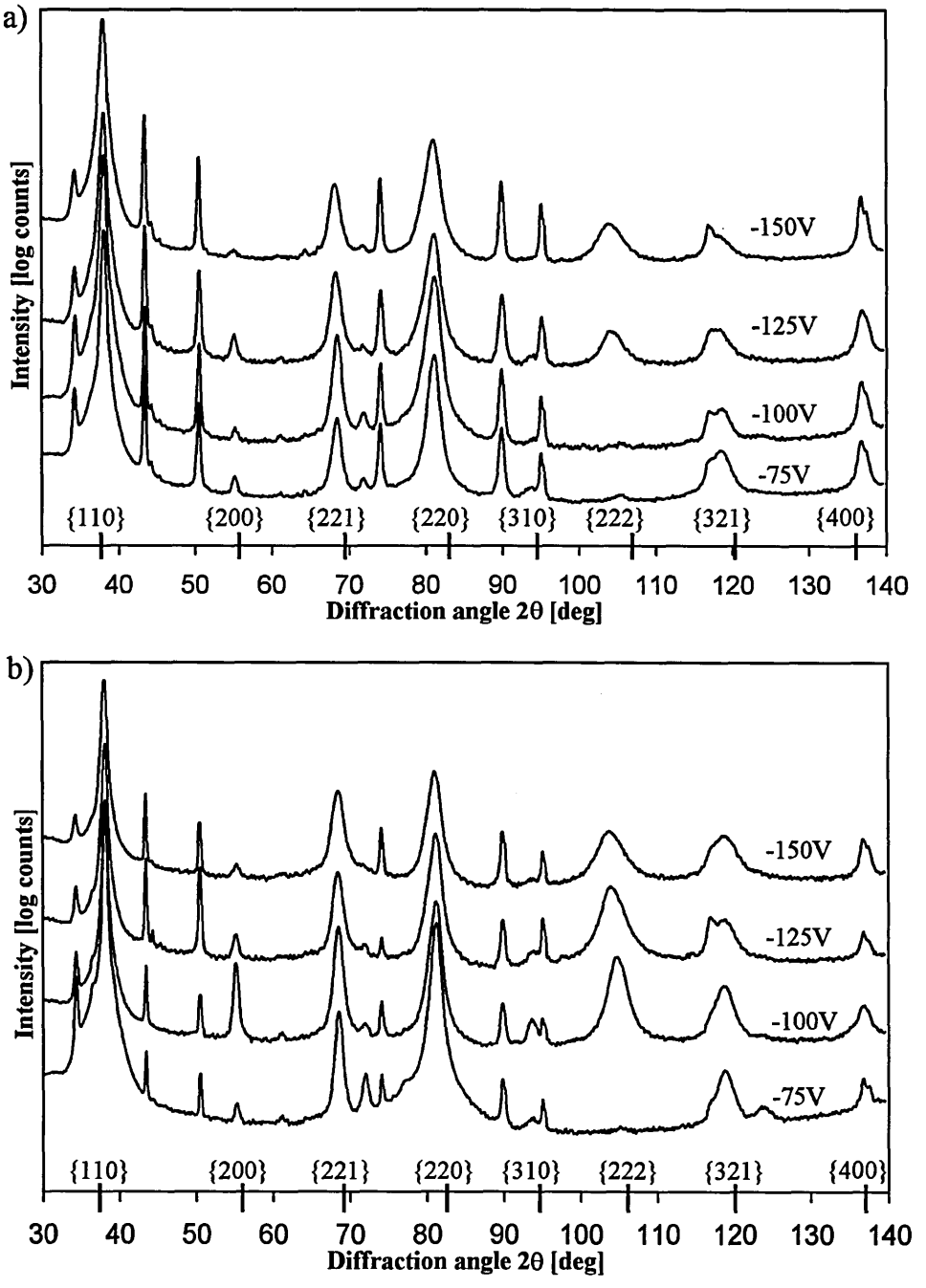

Figure 68 XRD traces for the Niobium a)1Nb and b)3Nb coatings showed significant changes in the crystal structure of the coating as the predominant growth direction shifts from <110> towards <111>

The microstructure of the UBM-deposited Nb coatings was shown to be a fully dense columnar structure. Even the coatings deposited using the lowest bias voltage (U_b = -75 V) were dense and feature a clearly defined columnar structure with {110} growth

direction as reported by Salagean et al. [69]. The microstructure of the coating is affected by the increased energy of the bombarding ions. It becomes less well defined and the growth direction was shifted towards the <111> orientation during further film growth. When high bias voltages were used both the thick and the thin coatings showed {111} texture with a 1 μm thick Nb film still showing mixed {110}/{111} structure. In texture evolution it is well established that, when the surface energy is dominant then the preferred orientation is dominated by the most closely-packed crystallographic plane [93,94]. In bcc metals such as Nb this is the {110} plane. Therefore it can be speculated that, during deposition at U_b = -75 V, the surface energy is dominant leading to the development of a {110} texture in both 1 μm and 3 μm thick films. With increasing bias voltage i.e. U_b = -125 V in the thinner films and U_b = -100 V in the thicker films a {111} texture starts to develop. One possible explanation for this is that the increased Ar^+ ion bombardment as the bias voltage is increased resulting in re-sputtering of the growing film. The close packed {110} plane has more atoms per unit area than the less densely packed {111} plane. Hence, the chance of re-sputtering an atom in a {110} plane is statistically higher than in a {111} plane. Therefore under conditions of high energy ion bombardment (U_B < -100 V) in competition for growth between {110} and {111} oriented grains, the {111} will grow at the expense of {110} oriented grains. The {111} texture in the thicker films (i.e. 3 μm) is stronger than for thinner films (1 μm) grown under the same conditions. This would lead one to the conclusion that the starting texture in all films was {110} and the {111} texture developed during growth under conditions of higher energy ion bombardment. Similar changes in texture as coating thickness increased was reported by Ward et al. [90].

6.2 Mechanical properties

Mechanically all the UBM deposited Nb coatings can be described as ductile with low to medium hardness. This combined with a Young's modulus similar to engineering steels gives a good basis for excellent adhesion as no stress due to dissimilar properties is generated at the interface when the surface is deformed.

The mechanical properties measured from the Nb coatings have been summarised in the Table 10.

Table 10 Summary of the properties of the coatings

Coating	Thickness [μm]	$H_{k,25g}$	H_p [GPa]	E [GPa]	Texture T*		at-% Ar
					(110)	(222)	
1Nb -75V	1.6				5.1	0.0	<0.3
1Nb -100V	1.4				5.0	0.0	<0.3
1Nb -125V	1.3				2.0	1.8	2.0
1Nb -150V	1.3				2.3	2.8	3.5
3Nb -75V	4.4	500	4.5	200	5.6	0.0	<0.3
3Nb -100V	4.0	490	5.2	190	0.9	4.5	<0.3
3Nb -125V	3.9	700	7.1	170	0.6	4.9	2.5
3Nb -150V	3.8	820	8.0	170	0.6	4.1	4.5

Increasing the bias voltage, thus increasing the energy of the bombarding ions, increases the hardness (up from $H_{K,25g}$ =490 or 4.5 GPa at U_b = -100 V to $H_{K,25g}$ = 820 or 8.0 GPa at U_b = -150 V) but has virtually no effect on the Young's modulus, E, which decreased slightly from 200 GPa measured at U_B= -75 V to 170 GPa at U_b = -150 V. All the coatings were measured to be harder than mild steel substrates ($H_{K,25g}$ = 350) yet softer than high-speed steel ($H_{K,25g}$ = 1050). The hardest coatings had hardness close to that of hard Cr ($H_{K,25g}$ = 900). Increase in the bias voltage from U_b = -100 V to U_b = -125 V causes a sharp increase in the hardness of the coating. This corresponds with the EDX results that indicate that a significant amount of Ar atoms have been trapped in the Nb lattice (up to 4.5 at-% Ar at U_b = -150 V) during coating

deposition. These trapped argon atoms may also cause lattice strain (expansion of the lattice parameter) as also indicated by XRD peak shifts towards smaller angles. The Ar would limit the movement of dislocations in the grains thus increasing the hardness of the coating. Earlier work by Paritong et. al. [91] showed that a similar increase in hardness can be also achieved by co-sputtering Nb with Cr. It should be also noted that as the increased bias voltage reduced the column diameter, d, significantly, the mechanical properties should change as described in the Hall-Petch relationship ($H = H_0 + k\, d^{-1/2}$) [31a] where H_0 and k are material dependent constants and d is grain diameter. The thickness of the coating is reduced by about 15% (from 1.6 μm and 4.4 μm at -75 V to 1.3 μm and 3.8 μm at U_b = -150 V) due to re-sputtering of the growing film as the bias voltage is increased from $U_b = -75$ V to $U_b = -150$ V. The adhesion of the Nb coatings was measured to be high with no adhesive failures in the scratch tests with up to 90N normal load (L_c > 90N).

6.3 Corrosion behaviour of Nb barrier layer

The results of the potentiodynamic polarisation measurements are shown in figures 67 a and b. The coated mild steel samples exhibited good corrosion resistance yet localised corrosion damage could be observed after the test. The shapes of the curves are approximately similar to those of bulk Nb, yet the current densities are 2-3 orders of magnitude higher in the anodic region. All coatings showed a "passive like" response in the anodic region indicating that the corrosion was occurring only at active corrosion sites i.e. defect locations. Thus the anodic currents can be suggested to correspond with the size of the active area.

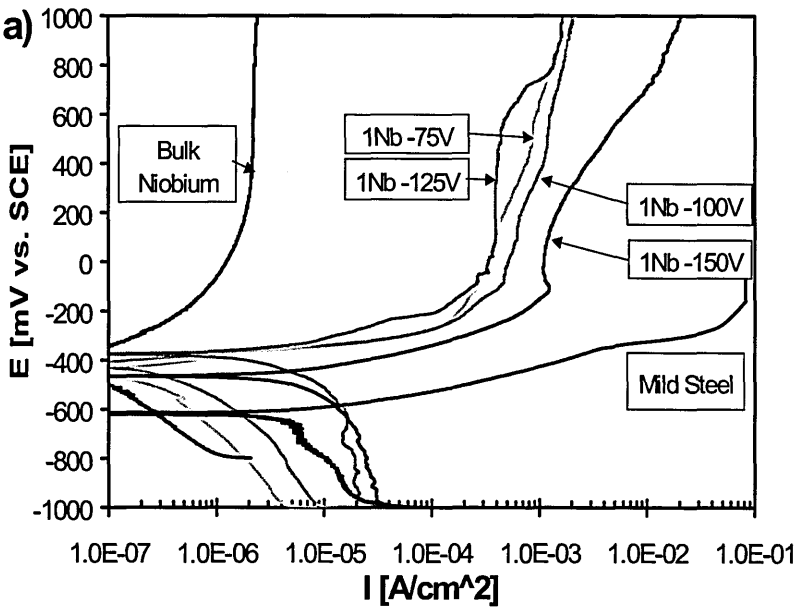

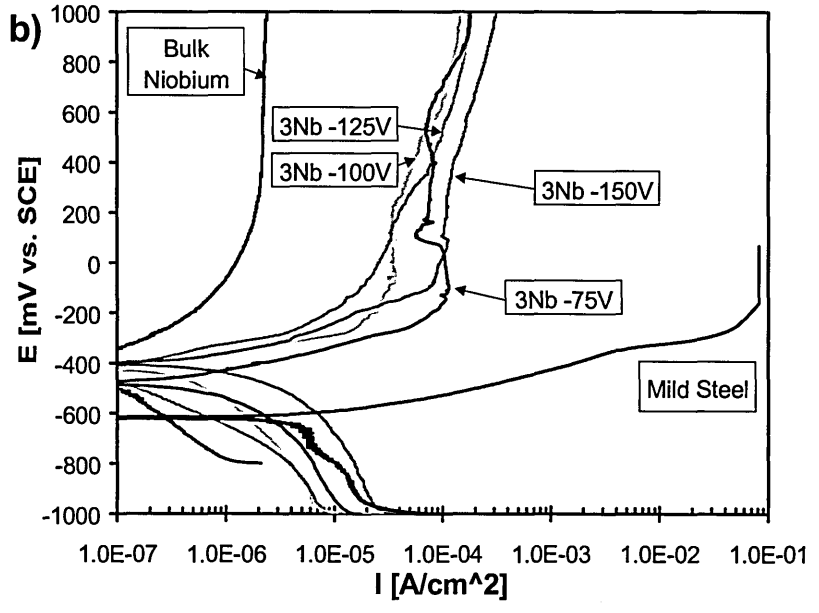

Figure 69 The potentiodynamic polarisation test results for a)1Nb and b) 3Nb coatings show a large improvement in corrosion performance compared with a mild steel substrate

The thickness of the Nb coating is clearly the most important factor in the corrosion performance of the coatings. The thicker coatings performed noticeably better than the thinner coatings with anodic current densities approximately one order of magnitude lower. This could also be observed visually as the corrosion damage to the

samples after the polarisation test was clearly smaller as shown in Figure 70 and Figure 71. The thinner coatings exhibited hundreds of corrosion locations while the thicker coatings had only tens. Coating delamination was observed for the INb -150V coating, which explains the high currents in the test. The effect of bias voltage on the corrosion performance was much smaller, yet the results indicate that the higher bias may be beneficial.

Figure 70 Optical micrographs of the INb sample surfaces, 8x magnification

Figure 71 Optical micrographs of the 3Nb sample surfaces, 8x magnification

The improvement in the corrosion resistance is too large to be explained only by an increased diffusion path length. Therefore a reduction of the defect locations as the film gets thicker has to play a part in the improved properties. It should also be noted that only a very small number of the defect locations observed in the SEM actually lead to a corrosion site as the area of the corrosion test was about 2000 times larger than the area shown in the SEM images in section 6.1 (figures 64 and 65).

The corrosion resistance of the coated mild steel samples is not significantly affected by the increased bias voltage. The samples deposited with Ub= -125 V showed the best corrosion resistance and the Ub = -150 V the worst. The poor corrosion resistance of the INb Ub= -150 V samples can be explained by local de-lamination of the coating during the tests. The reason for this delamination was thought to be excessive internal stresses within the coating and poor adhesion at the interface. The corrosion resistance of the thicker coatings was found to be clearly superior to the thin coatings. In the potentiodynamic polarisation test the anodic corrosion current densities were up to one order of magnitude lower than for the thinner coatings.

6.4 Performance of CrN/NbN nanoscale multilayer coatings with Nb barrier layer

Two types of the CrN/NbN coatings with Nb barrier layer were studied in this section. Both had a two-step Nb ion etching step and a metallic Nb layer deposited at U_b = -100V. "1Nb" coatings had a 1.5μm thick metallic Nb barrier layer (1 hour deposition time, thus labelled 1Nb) and "3Nb" coatings had 4.5μm thick barrier layer combined with the standard CrN/NbN coating.

The mechanical properties of the coatings are summarised in Table 11 showing both types of coatings to be very hard and wear resistant, although the thicker coating (3Nb) has a lower adhesion. However, the adhesion of both samples was still considerably better than that of an electroplated 25μm thick hard chrome coating. The thickness of the Nb film does not affect the hardness of the coating and both coatings attain approximately half of the plastic hardness of diamond. Sliding wear rate values of the 1Nb and 3Nb coatings were very low being, respectively, $1/20^{th}$ and $1/3^{rd}$ of the wear rate of hard Cr.

Table 11 Mechanical properties of the CrN/NbN coatings with Nb barrier layer

	Thickness [μm]	Adhesion, L_c on HSS [N]	Hardness, $H_{p,50mN}$ [GPa]	Sliding wear rate on MS [10^{-15} m²/N]
1Nb CrN/NbN	6	65	50	3
3Nb CrN/NbN	9	40	50	17
Hard Cr	25	15	18	58

The results of the potentiodynamic polarisation tests of Nb/CrN/NbN can be found in Figure 72. The figure shows the average of numerous potentiodynamic tests for the investigated coatings (the individual measurements were used in a study discussing the repeatability of these measurements, Appendix 2). The results show that all

coatings greatly improve the corrosion performance of the mild steel. Further, the 3Nb coatings provide clearly better corrosion resistance than the INb coatings, that displayed approximately equal corrosion resistance to the 25 pm thick hexavalent hard Cr.

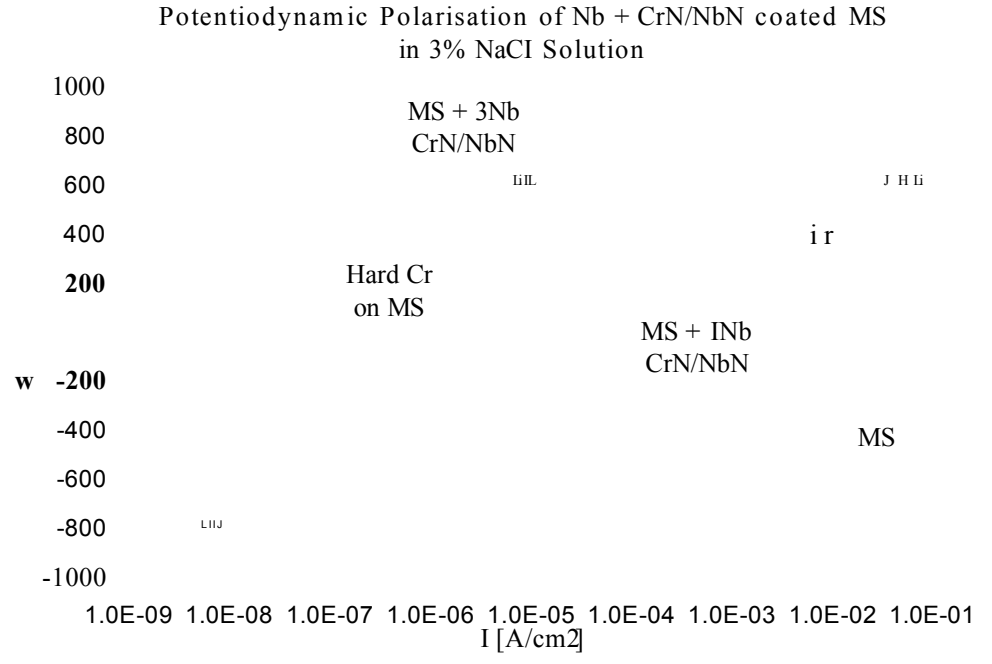

Figure 72 Potentiodynamic polarisation of mild steel coated with CrN/NbN with Nb barrier layers of different thicknesses

Salt spray tests were also performed to obtain comparison data for the electrochemical tests. Samples showed signs of corrosion after a few hours of exposure and after 72 hours all samples were clearly affected by corrosion. The samples with the thicker Nb coating had a number of small pinholes that were clearly visible due to rust surrounding the area near the actual pinhole (figure 73). The substrates with the thinner Nb coatings suffered greater corrosion as observed from the number of corrosion sites. After 166 hours of exposure the areas near pinholes were covered with thick layers of rust. Most of the surface area of the thicker coating samples was unaffected. There was little visible change between 166 h and 230 h of testing. During

the whole duration of the test the thicker Nb coating showed superior performance, due to the smaller number of corrosion sites.

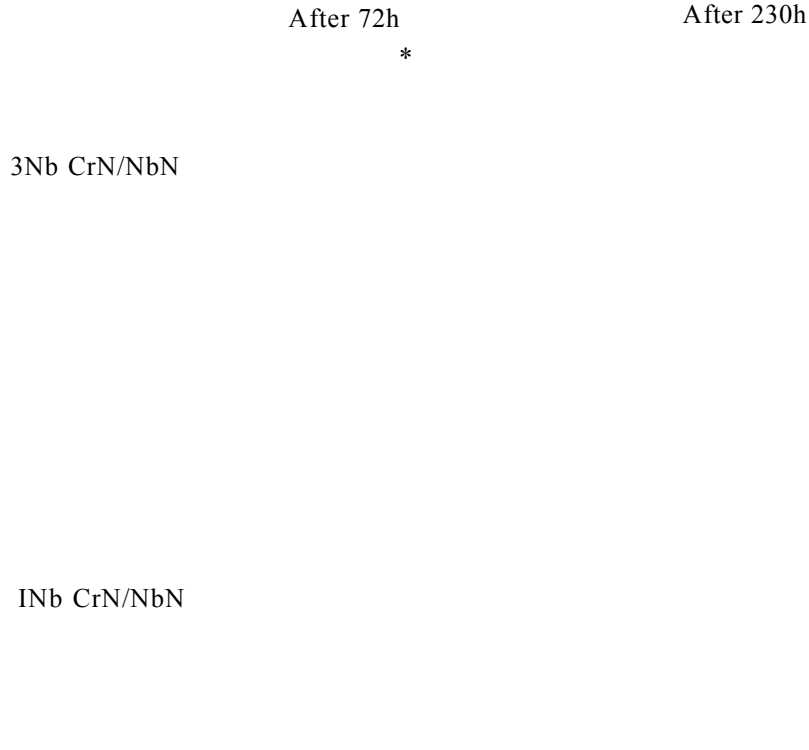

Figure 73 Corrosion on the samples after 72 h and 230 h of ASTM salt spray test

When the corrosion products were cleaned from the samples the coatings seemed to be intact and no delamination of the coating was observed. Optical micrographs of INb and 3Nb coated samples after cleaning can be seen in Figure 74 a and b, respectively. The higher number of corrosion sites on INb sample are also easily visible from these figures. The thicker coating (Figure 74b) has only 3 large (> 0.2 mm) corrosion sites in the pictured area of 13 x 10 mm, while the thinner Nb coating (Figure 74a) has approximately 40 similar or larger sites.

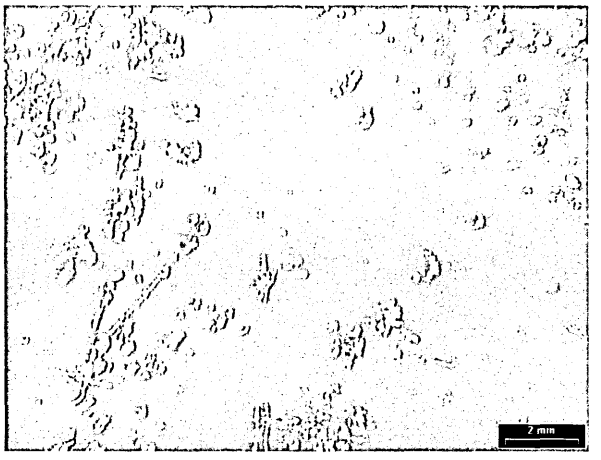

a)

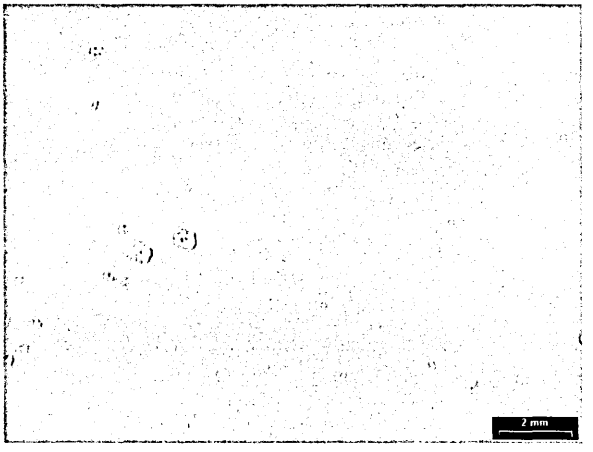

b)

Figure 74 Surface of the samples a) 1Nb CrN/NbN and b) 3Nb CrN/NbN after salt spray test after the removal of the corrosion products

Salt spray tests confirmed the results of the electrochemical measurements. The thicker coating performed better than the thin coating showing notably less corrosion within 72 hours of testing. The time to pit initiation was approximately similar to a 10 µm thick hard chrome coating on mild steel. Following salt spray testing the rust deposits were cleaned from the salt spray samples whereupon no delamination of the coating was observed. This indicates that the corrosion does not spread extensively along the interface between coating and substrate.

6.5 Discussion

As shown in the previous sections the thickness and the parameters of the niobium barrier layer greatly affect both the mechanical properties and the corrosion performance. The key finding is that the thickness of the layer seems to be the deciding factor.
The bias voltage was found to have only slight effect on the corrosion properties yet had a huge influence on the mechanical properties of the barrier layer.

The microstructure of the niobium layer changes as the film grows. It starts as Stranski-Krastanov growth in which numerous tiny randomly oriented grains on the nanocrystalline layer formed in the etching step. When the grains meet, the grains orientated in the preferential growth direction outgrow the others and after that (after about 10min of deposition time) the growth can be described as columnar with gradually increasing column size. With high bias voltages the column boundaries become blurred due to the large number of lattice defects and sub-grains. The structure was found to be fully dense even at low bias voltages with no low density areas between the columns. With increasing bias voltage there is noticeable change in the growth direction from the {110} towards the {111}. A similar shifts have been observed in previous studies of sputtered metal layers and these are generally due to preferential sputtering of the closely packed {110} oriented grains caused by increased argon bombardment [90].

The SEM investigation of the surface defects from above revealed that there is an enormous difference between the quantity and the type of defects that can be found on the thinner 1.5 μm thick coating compared to the thicker 4.5 μm thick coating. First, the number of defects on the thicker coating was about half of those found on the thinner one. More remarkably it seemed that the thicker coating was able to "close" or "heal" minor surface defects. This could explain the significantly improved corrosion resistance measured for the coatings with the thicker barrier layer.

The study of the mechanical properties revealed a significant increase of the hardness of the layer as the bias voltage was increased beyond U_b = -100 V. This can be

attributed to the argon that was found trapped into the lattice, preventing the dislocation movement. The increased hardness should improve the mechanical strength of the Nb- CrN/NbN coating. This hardening using bias voltage also makes it possible to deposit a gradually hardening layer from the soft substrate to the hard coating that would reduce the interfacial shear stress caused at the junction of dissimilar materials thus improving the adhesion and wear resistance. With Nb-CrN/NbN coatings the thicker Nb layer had a clearly detrimental effect on the mechanical performance of the coating. A higher bias than the U_b = -100V that was used in this work should improve the mechanical properties without affecting the corrosion performance, as long as the adhesion to the substrate can be secured.

The corrosion test results showed that the thicker coatings (about 4.5μm Nb layer) outperformed the thinner coatings (about 1.5μm Nb layer) by a significant margin in that the anodic current density was up to two orders of magnitude lower. The corrosion results of Nb barrier layer and CrN/NbN correlate well with the results for the barrier film alone.

7 TOPCOAT

Oxynitride top coatings have been studied due to their low electrical resistivity, biocompatibility, oxidation resistance as well as that use for solar devices. Most work focuses on TiNO coatings [95-97], though CrNO films have also been studied [98, 99]. TiAlN topcoats are in commercial use providing good oxidation resistance and low friction during dry high-speed cutting [100]. The structure of the oxynitride was reported to change from a crystalline (NaCl like structure, where O replaces N in the lattice) to an amorphous like structure as the oxygen content increases [97, 101]. Increasing oxygen content also increases the electrical resistivity considerably [95, 102]. An oxynitride coating can be deposited by sputtering in an argon and dry air atmosphere (ca. 70% N 27% O). Oxynitride topcoat was applied to the CrN/NbN superlattice coating with the aim of enhancing the tribological properties of the coatings.

The coatings studied in this chapter consisted of three layers. First, a 0.3 μm thick CrN base-layer, to provide improved adhesion through a gradient in hardness between the ultra-hard nanoscale multilayer and relatively soft metal substrate (High Speed Steel). This was followed by 2.5 μm CrN/NbN nanoscale multilayer with 3.5 nm superlattice period. The base layer and the CrN/NbN layer were deposited at a bias voltage, $U_B = -75V$ at total pressures $P_T = 3.8 \times 10^{-1}$ Pa and 3.6×10^{-1} Pa, respectively. The oxynitride process step was performed in a mixture of dry air and argon. To establish the effect of ion bombardment on the coating structure and properties, the bias voltage was varied from $U_b = -75$ V to $U_b = -120$ V while retaining the same total pressure during deposition (3.5×10^{-1} Pa). The effects of the changes in the total deposition pressure, P_T were investigated keeping the bias voltage $U_b = -100V$ and varying the total pressure from 3.5×10^{-1} Pa to 4.9×10^{-1} Pa. A reference coating was also prepared in which the CrN/NbN layer was made thicker while keeping the same total coating time. The deposition parameters are summarised in Table 12.

Table 12 Deposition parameters

Sample designation	Ion etching	CrN base layer	CrN/NbN	Oxynitride	
Reference	20 min Cr^+ etch 1×10^{-5} Pa U_b = -1200 V	30 min Cr: 2 x 5kW 3.8×10^{-5} Pa U_b = -75 V	150 min	N/A	
-75V			90 min Cr 2 x 5 kW + Nb 2 x 10 kW 3.6×10^{-5} Pa U_b = -75 V	U_b = -75 V, 3.5×10^{-5} Pa	60 min 2 x 5 kW + 2 x 10 kW
-100V				U_b = -100 V, 3.5×10^{-5} Pa	
-120V				U_b = -120V, 3.5×10^{-5} Pa	
-100V 4.1				U_b = -100 V, 4.1×10^{-5} Pa	
-100V 4.9				U_b = -100 V, 4.9×10^{-5} Pa	

7.1 Microstructure

The XTEM investigation shows that, at the lower deposition pressures, the oxynitride layer exhibits a dense columnar microstructure with a pronounced nanoscale multilayer architecture. The columnar structure of the underlying CrN/NbN layer is not interrupted at the interface region between CrN/NbN and the oxynitride layers yet the interface can be clearly identified as shown in Figure 75.

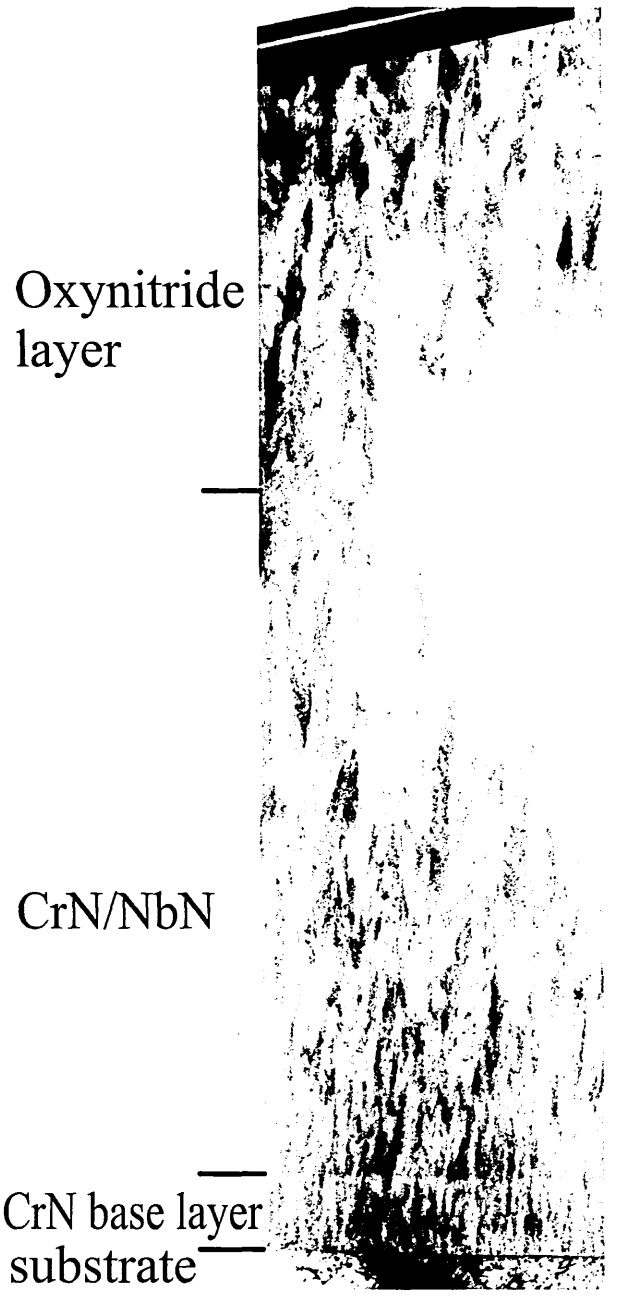

Figure 75 XTEM image of the CrN/NbN coating with oxynitride top layer

The superlattice layers are clearly visible in the oxynitride layer in the coatings deposited at 3.5×10^{-1} Pa (Figure 76). In the coating deposited at low bias voltage $U_b = -75$ V the columnar grains are well defined and have dome-like tops. The superlattice layers conform to the curvature of the grains and are therefore not parallel to the surface of the coating. Low density areas are also observed at column boundary regions. Increasing the bias voltage to $U_b = -120$ V (fig. 74b) gives a smooth and

continuous superlattice that is parallel to the coating surface as previously observed in conventional coatings deposited at U_b = -120 V [22] . At U_b = -120 V the structure is still columnar, yet individual grain boundaries are almost indistinguishable in the XTEM images. Furthermore no low density areas were found at the grain boundaries.

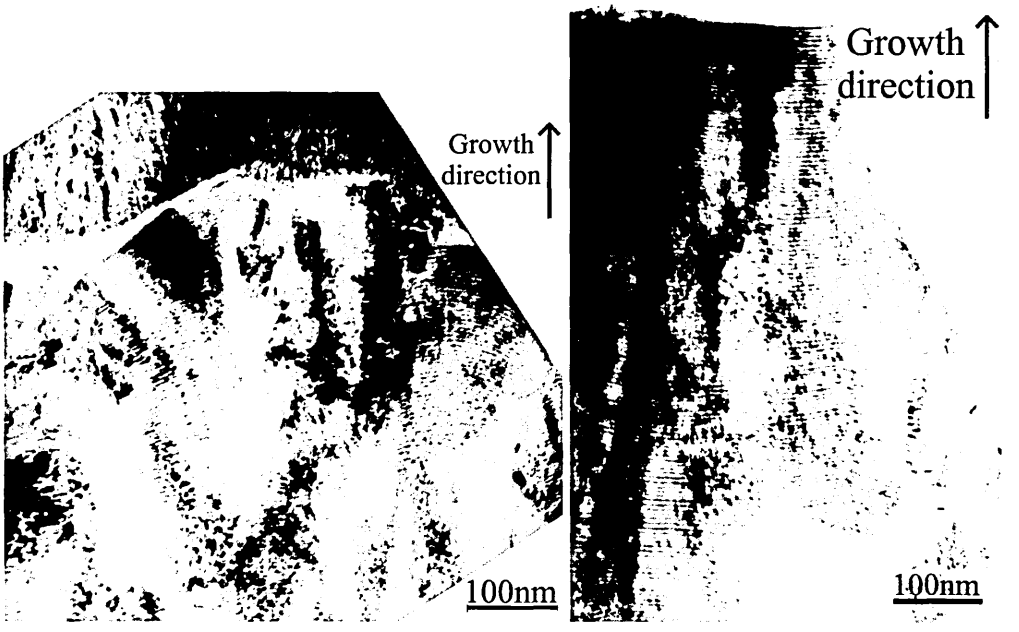

a) b)

Figure 76 Superlattice structure of the oxynitride layers conforms with the top of the grain, being a) "dome like" with low bias voltage (U_b = -75 V) and b) parallel to the coating surface at high voltages (U_b = -120 V)

The crystal structure of the coatings was analysed using XDR with Bragg-Brentano and glancing angle scans. The analysis showed the coatings to be crystalline in nature with a mixed texture of <111>, <100> and <110>. There were practically no differences between the results of the 2 different geometries so only the 1° glancing angle scans are shown in Figure 77.

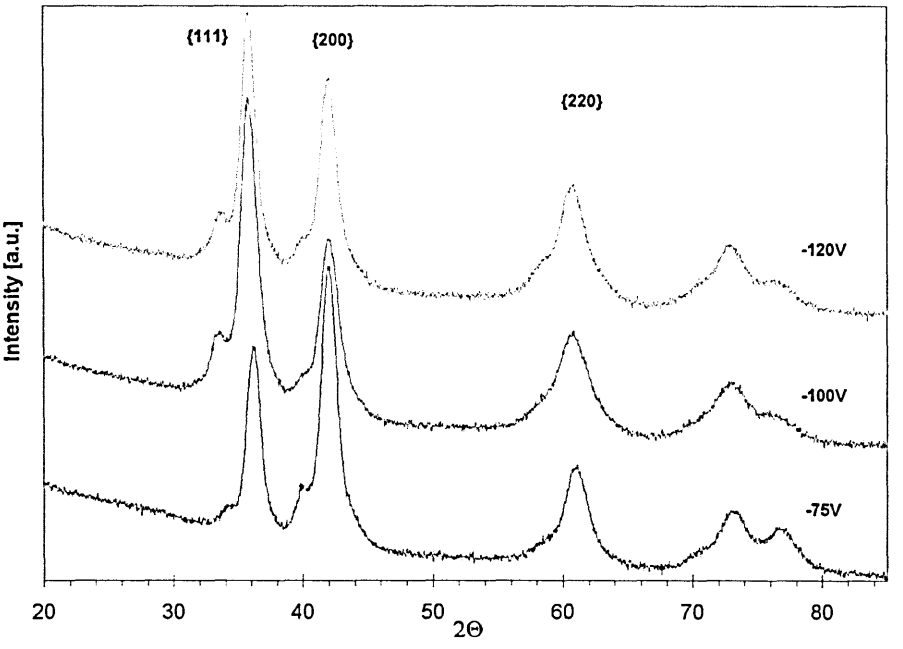

a)

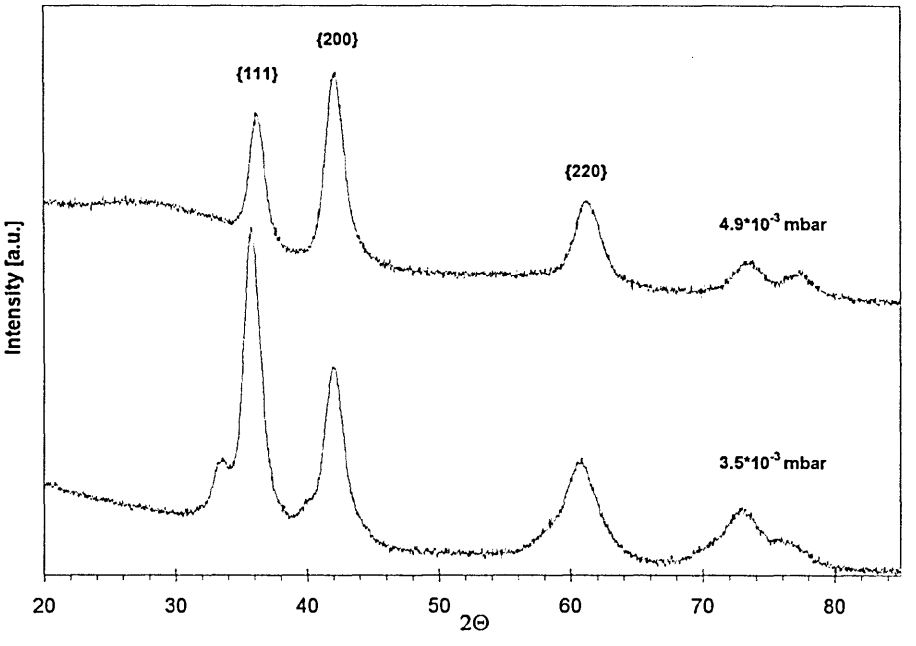

b)

Figure 77 XRD scans of the oxynitride topcoat at 1° glancing angle configuration ***a)*** *effect of bias voltage (p = 3.5 x 10^{-3} mbar) and* ***b)*** *effect of total coating pressure (U_b = -100V)*

The only phase identifiable in the scans was the fcc CrN/NbN. This indicates that oxygen is mainly absorbed in the lattice replacing the nitrogen at the octahedral site in the NaCl structure as presented by Wilhartitz et al. [98]. The increase in the bias voltage also caused a shift from {100} texture towards {111} texture (fig. 77 a). A change in texture from {100} to {111} has been observed previously [22,103,104] and follows the same trend as observed by Kadlec et al. [105]. The main reflections exhibit clear satellite peaks (ca. 2° smaller angle than the main peaks) that indicate the superlattice nature of the coating. This peak is clearly present for all other coatings except that deposited at $P_T = 4.9 \times 10^{-1}$ Pa). There is also a slight peak shift toward lower 2θ angles as the bias voltage is increased. This can be associated with lattice strain indicating a residual compressive stress in the plane parallel to the coating surface resulting from a more intense ion bombardment at high bias voltages. As the pressure during the oxynitride deposition stage was increased the crystal structure of the top layer became increasingly amorphous (Fig. 77b), as shown by diffuse peak at 2θ ca. 28° present in the coating deposited at a bias voltage $U_b = -100$ V using a total chamber pressure $P_T = 4.9 \times 10^{-1}$ Pa. Furthermore, the main Bragg reflections, {111} and {200}, did not exhibit satellite peaks indicating the loss of the superlattice architecture. Compared to the coating deposited at lower pressure the increased pressure caused a shift towards stronger {100} texture as well as a slight peak shift toward higher 2θ angles. This is because at the same bias voltage ($U_b = -100$ V) increasing the total gas pressure P_T from 3.5×10^{-1} Pa to 4.9×10^{-1} Pa decreases the energy of the bombarding ions and therefore has a similar influence on texture formation as reducing the bias voltage. Therefore the texture developed at $P_T = 4.9 \times 10^{-1}$ Pa at a bias voltage $U_b = -100$ V is similar to that developed at $U_b = -75$ V using a total pressure $P_T = 3.5 \times 10^{-1}$ Pa, that is, a {100} texture in both cases

7.2 Mechanical properties

The mechanical properties of the coatings are summarised in Table 13. The total thickness of the coatings varied from 4.8 μm for the reference coating to 5.3 μm for the $U_b = -75$ V, P = 3.5 x 10^{-1} Pa. The oxynitride coatings were generally thicker than the reference indicating the lower density of the oxynitride layer. As the bias voltage was increased the coating thickness decreases slightly. This is probably due to increased re-sputtering of the substrates and densification of the coating caused by increased ion bombardment. As the deposition pressure was increased the thickness of the oxynitride layer decreased from 2.2 μm at P_T = 3.5 x 10^{-1} Pa to 1.6 μm at P_T = 4.9 x 10^{-1}Pa.

Table 13 Properties of the coatings

Sample Designation	Coating thickness [μm]	Oxynitride thickness [μm]	Adhesion L_c on HSS [N]	Hardness (HK_{25g})	Al_2O_3 ball		100Cr6 Ball	
					Friction coef.	Wear rate [10^{-16} m^2/N]	Friction coef.	Wear rate of counter-body [10^{-17} m^2/N]
Reference	4.8		55	2900	0.69	23	0.57	16
-75V	5.3	2.3	53	3100	0.95	49	0.69	30
-100V	5.2	2.2	52	3200	0.72	30	0.49	7.5
-120V	5.2	2.2	56	3000	0.71	30	0.51	1.0
-100V 4.1	4.8	1.8	58	3000	0.75	30	0.56	4.4
-100V 4.9	4.6	1.6	54	2500	0.76	37	0.58	4.4

This may be due to the reduced sputtering rate and hence lower deposition rate resulting from increased target poisoning as the coating appeared to have low density (based on micro-structural analysis). The top surface of the oxynitride coatings deposited using low bias voltages or high pressures appeared rough and porous under an optical microscope. The surface roughness decreased with increasing bias voltage but increased with increasing deposition pressure. The coating deposited at a bias voltage of U_b = -120 V is especially very smooth when compared with the other coatings. This effect has been shown in earlier work to be the result of a reduction in

the number of growth defects with increasing bias voltage [103]. In addition increasing the deposition pressure from $P_T = 3.5 \times 10^{-1}$ Pa to $P_T = 4.9 * 10^{-1}$ Pa for a bias voltage U_b = -100V changes the colour of the coating from metallic grey towards black, thus reflecting a change from a mainly nitride phase to an oxynitride phase. The hardness values show that all of the coatings are very hard $H_{K, 25g}$ = 2500-3200. The hardness of the oxynitride coatings was generally slightly higher than that of the reference coating. The adhesion was ca. L_c = 55 N for all the coatings which is understandable given that they share the same pre-treatment and base layers.

The results of the pin-on-disk tribological tests can be seen in Figure 78 and Table 13. The friction coefficient against an alumina ball was approximately the same for all coatings (ca. 0.7), only the sample deposited at low bias voltage, U_b = –75 V, showed a higher value (0.95). As the sliding contact of the film against the counter body (Al_2O_3 ball) is oxide against oxide the higher friction is understandable. Higher friction also correlate with higher wear rates in these tests. When a 100Cr6 grade carbon steel ball was used as the counter body the friction coefficients for the oxynitride coatings were generally lower than that of the reference coating (0.57). The coating deposited at a bias voltage of U_b = –75 V exhibited a slightly higher friction (0.69) whereas the coating deposited at a bias voltage of U_b = –100 V exhibited the lowest friction coefficient (0.49).

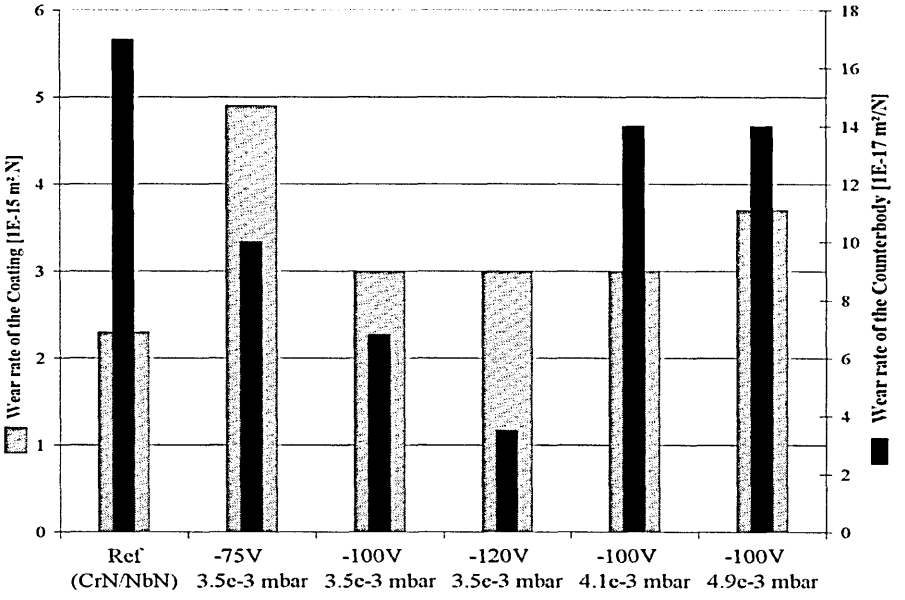

Figure 78 The results of pin on disk wear tests of oxynitride coatings

The wear rate of the oxynitride coating against alumina ball was always higher than that of the reference coating, as the sliding contact of the film against the counter body (Al_2O_3 ball) is oxide against oxide rather than nitride against oxide. The wear rate of an oxynitride coating deposited at a bias voltage of -75 V against alumina ball was almost double that of the reference coating with a wear rate of 37 x 10^{-16} m^2/N compared with 23 x 10^{-16} m^2/N. In contrast, however, the increase in wear rate for coatings deposited at bias voltages of -100V and -120V coating was only about 30%. For the samples produced at a constant bias voltage of -100 V the wear rate increased with increasing total pressure P_T. The higher wear rates at lower bias voltages and higher chamber pressure are probably due to the rough porous nature of the film deposited under these conditions where the intensity of the ion bombardment is less. The wear rate of the coating against 100Cr6 ball counter body could not be accurately measured due to material transfer to the wear track. The wear rate of the counter-body however reduces to one fifth (compared with the reference) when a topcoat deposited at U_b = -120 V has been applied. Also, the wear of the counterpart was reduced as the bias voltage was increased. The coatings deposited at high pressures showed increased counter-body wear due to rapid wear of the topcoat. Observation of the wear tracks of these coatings (Figure 79) showed that the wear mechanism of these three coatings is different. The coatings deposited at U_b = -120V exhibit wear track that is much narrower than the others and virtually no transferred material is

observed. The reference track is much wider as the coating has abraded the ball and there is also a significant amount of material from the ball on the track. The wear track of the coating deposited in high pressure ($P_T = 4.9 \times 10^{-1}$Pa) showed that the ball has eroded through the topcoat exposing the underlying superlattice coating and subsequently the wear resembles the reference sample.

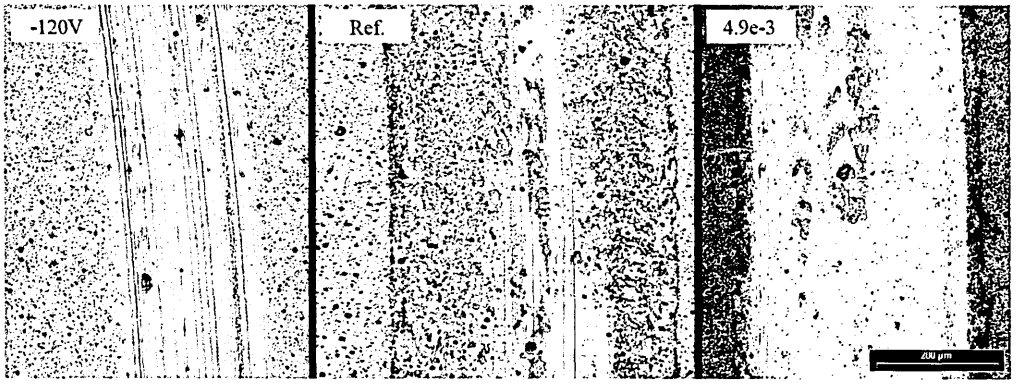

Figure 79 100x optical micrographs of selected wear tracks

Interestingly, the wear of the counterpart did not show a clear relation to the value of the friction coefficient. It is suggested, however, that the low wear rate combined with low counter-body wear was due to the superlattice nature of the topcoat. In the case of a superlattice that is parallel to the surface the wear can occur along the superlattice interfaces. This wear mechanism was presented by Luo et al. [36] after detailed wear analysis of superlattice coatings. The coatings deposited at high bias voltages have a strong, clear superlattice that is continuous, smooth and parallel to the surface as shown by the XTEM investigation. In this case the coating can break along the superlattice (period ca. 4.5nm) interfaces resulting in low abrasive wear of the counter-body. Thus the low counter-body wear rate can be related to the orientation of the superlattice relative to the specimen surface.

7.3 Corrosion results

The CrN/NbN coatings have excellent corrosion resistance, which enables the use of these coating in corrosive environments even in conjunction with low alloy substrate

materials. This can be seen from the results of potentiodymamic polarisation corrosion test in Figure 80. The best performing oxynitride coatings improved upon the already impressive corrosion performance of the reference coating. The coatings deposited at higher pressures performed considerably worse than the reference coating. The change in the bias voltage had a poor correlation to the corrosion results as the coating prepared at Ub= -75 V performed the best followed by the coating prepared at Ub= -120 V, while the Ub= -100 V coating exhibited the worst performance.

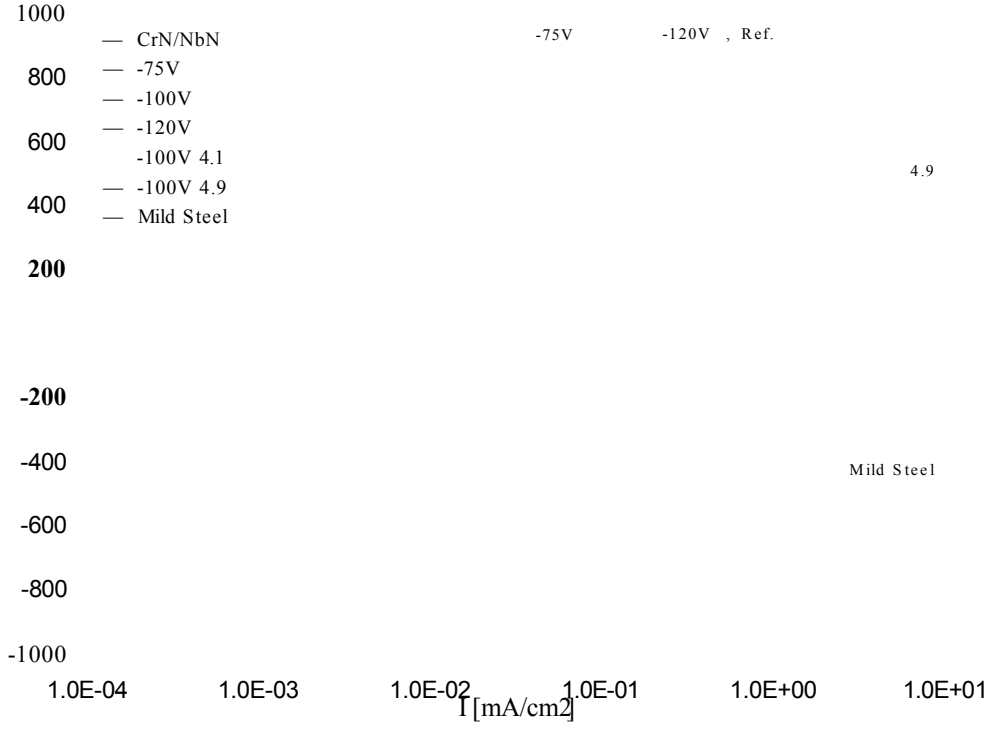

Figure 80 Potentiodynamic polarisation results of CrN/NbN coatings with Oxynitride topcoat

7.4 Discussion

The oxynitride deposition process was successfully performed in an industrial Hauzer PVD coating machine using a mixture of dry air and argon. The process did not require any major changes to the equipment and thus could be easily implemented as a commercial process.

The XRD investigation did not show a separate oxide phase indicating that the oxygen replaces nitrogen in the lattice. Also the microstructure of the coating remained very similar to the pure nitride at lower deposition pressures. At higher pressures the structure became more amorphous and loss of the superlattice was observed. These changes were detrimental to both the mechanical and corrosion properties of the coating. The increase in the bias voltage resulted in a shift towards the {100} growth direction as well as to a more pronounced superlattice. More notably, it was found that the tops of the grains produced at the lower voltages were not parallel to the surface. Thus the crack propagation leading to wear is not stopped at the superlattice boundary (as suggested by Luo et. al. [36]), leading to more wear.

The corrosion performance did not show notable improvement over the reference. The U_b = -75 V coating performed better than the reference, yet the coating deposited at U_b = -100 V was inferior in the corrosion tests. The coatings deposited at the higher pressures showed clearly inferior corrosion resistance when compared to the reference coating.

Overall the coatings deposited at higher pressures performed worse than the reference coating. The behaviour was similar to the reference coating. Only when the wear tests were performed using a hardened steel counter body (100Cr6 ball), a clear benefit of the topcoat was observed. The wear of the counter body was significantly reduced, in the case of the topcoat deposited at U_b = -120 V the wear was reduced by 80%. There was also virtually no material transfer to the wear track, which indicates that this coating might perform very well in a sliding contact against hardened steel counter body. This result indicates that the counter body may not have to be coated to prevent excessive wear. This is very important as the inside of the holes and cavities can be difficult to coat using a PVD process due to shadowing effects.

8 SUMMARY

8.1 Substrate enhancement

The work performed clearly shows the benefits of duplex treatments where two different surface treatment methods are used together to obtain a result that could otherwise be unobtainable. PVD coatings can be extremely hard and wear resistant, but are generally also very thin. These thin coatings require a very hard substrate to support them as the load bearing capability is provided by the substrate. In cutting tools very hard ceramics, for example carbides, can be used, but in tribological applications this is often not possible. In tribological applications the substrate often has to withstand impacts, for example in cutting tools and blades, as well as wear. Moreover, the economy and usability (can it be machined, welded, formed, etc.) of the material should not be neglected. Ideally the substrate should be like mild steel, that is cheap and easy to utilize. There are numerous duplex treatment possibilities and interesting engineering materials that would warrant studying, but for this work Plasma nitriding plus PVD and S154, a high strength engineering steel grade were selected. This steel has excellent strength combined with ductility. As an engineering grade it can also be welded and machined and heat treated.

The idea behind duplex coatings is to use two different types of processes that affect the surface in different ways. In nitriding the diffusion of nitrogen into the metal lattice causes hardening by preventing the movement of dislocations. The nitriding case depth here was measured to be up to 400 μm, exceeding the coating thickness by almost than 100 times.

Plasma nitriding and the PVD processes that were used for this work are commercial processes, yet since the samples were mechanically polished prior to PVD coating the process cannot be directly applied to commercial use without modification. There are many possible routes that can be used to commercialize this process. The plasma treatment can be done in the PVD coater using low pressure plasma nitriding, or the high pressure process can be tailored so that the surface is not contaminated. Further,

chemical or mechanical treatments can also be devised that clean the samples prior PVD deposition.

From the results of this investigation it can be concluded that the substrate material critically affects all the tribological aspects of the coating. All of the duplex treatments showed significant improvement over the reference coatings in all aspects. Further, no negative aspects for the duplex treated samples compared with the reference were observed. There were however significant differences between different treatments. The parameters used in the nitriding process gave different microstructures near the surface that were found to have a big effect on the tribological properties of the duplex treated samples. The biggest difference was found to be the composition of the 4-10 μm thick compound layer on the surface of the sample. The compound layer was found to contain two different, but common phases; γ' (Fe_4N, FCC) and ε (Fe_3N, Hexagonal). The γ' phase is generally considered to be softer, more ductile with better impact resistance than the harder and more brittle ε phase. From this information it can be projected that the ε phase will give better wear resistance while the γ' phase provides more impact resistance. The better corrosion resistance of the ε phase also leads to better corrosion performance. On the other hand the thicker case depth of samples with the γ' phase led to a better load bearing capability indicated by a smaller crater size in the impact test and the improved scratch test performance. (it should be noted that the higher critical load may be a result of the better load bearing capability i.e. less deflection at a certain nominal load or better adhesion or different failure mechanism or a combination of these facts.) This good behaviour in impact and scratch tests indicates that this type of pre-treatment would be superior in wear tests where the wear mechanism is fatigue or impact related.

The tests identified a correlation between the surface hardness and wear rate. Previously it has been observed that the good scratch test results (good adhesion) correlate well with the low wear results and the long tool life [85]. This time the coating with the worst scratch test result performed the best in the wear test. The result probably would be reversed as the nominal load on the pin is increased. It was however not possible to test this in the scope of this study.

Further, a correlation between the composition of the compound phase and the corrosion performance was found. The samples with more of the ε phase in the compound layer performed clearly better in the corrosion experiments. This is expected as the ε phase is generally considered more corrosion resistant than the γ' phase. It should be also noted that with the best duplex treated sample the anodic corrosion current was almost 3 orders of magnitude lower than for untreated S154 steel.

The wear properties of the same sample (highest amount of ε phase in the compound layer) were found to be excellent. The measured pin-on-disk wear rate was very close to the same coating on high speed steel. Compared with the hard chromium the wear rate is just 1% of the chrome (2.6×10^{-15} m²/N vs. 2.3×10^{-13} m²/N). It is also important to note that each of the surface treatments by themselves produced wear rates that were 30 and 120 times higher than the duplex treatment.

The results of these experiments were very encouraging inviting real life application testing. Possible applications for these duplex treated parts could be different blades or knives in, for example, the wood processing industry.

8.2 *Interface engineering*

The ABS process used in the PVD coaters that were used in this work enables efficient interface engineering using the steered arc discharge for metal ion bombardment/ion etching combined with sputtered coatings. Earlier work of Schönjahn et al. has shown that the parameters used for the etching step of the ABS process have a big impact on the properties of the coated part. The effects range from improved adhesion leading to longer tool lifetime in high speed milling to improved corrosion resistance. The previous work focused on the coating of cutting tools, so in this work the focus was on corrosion performance. In the earlier work niobium metal etching was found to create a thin nano-structured almost amorphous Nb layer at the interface. As this layer is very dense and has no grain boundaries it improves the corrosion resistance of the coating. On the other hand niobium ion etching was not as efficient at etching as chromium or argon ions, so great care is needed in order to

ensure the cleanliness of the surface. Otherwise the contamination on the surface may cause adhesive failure. This was indeed the case in some of the tests.

As the layers at the interface region are very thin, (only 10 nm) they are very difficult to investigate. Only the latest scanning transmission electron microscopes have the sufficient resolution to give accurate analysis of the interfaces. Still even with those the work is laborious and the areas investigated very small indeed.

The two-step etching approach using Cr as the etching ion, investigated by Schönjahn et. al. [67] was studied further in this work by applying it to Nb ion etching. The idea was that the first step provides faster etching at high argon pressures and the second step was for ion implantation at low pressure, as higher average ion energy is achieved in the absence of collision with gas atoms. The first part of the test was to identify the effects of the etching bias voltage on the interface and the properties of the coating. The etching efficiency of the Nb at U_b = -800 V was found to be minimal as only deposition had occurred at the interface (the very thin deposition layer from the target cleaning stage was still present after the etching). The rest of the investigated samples using one or two step etching showed similar interface structure. This may be due to the resolution of the instrumentation used or, alternatively, natural variations at different locations on the steel samples.
When the samples were subjected to tribological testing the sample prepared using U_b = -800 V etching was found to perform poorly. This was expected because of poor adhesion due to contamination at the interface. The adhesion of the other coatings were similar to one another, with the best being the one step etching at U_b = -1200V. Again, in the corrosion tests the sample prepared using U_b = -800 V etching preformed poorly, again due to adhesive failure. In corrosion tests the 2 step processes outperformed the 1 step processes by a comfortable margin.

8.3 Barrier layer

A niobium barrier layer was found to improve the corrosion properties of the CrN/NbN coatings significantly. A detailed study was carried out to determine how the deposition parameters and the related microstructural changes affected the functional properties of the coatings. The parameters that were studied were the bias voltage, which influences ion bombardment, and the coating time i.e. coating thickness.

The niobium films were found to have a dense columnar structure. At the low bias voltages the columnar structure was quite clear and the grain size was large. The tops of the grains had a clear dome-like shape that levelled out as the bias voltage was increased. Also the grain boundaries started to become indistinct at higher bias voltages. A shift in the preferred orientation towards <111> from <110> with increasing bias was also found to take place.
More importantly the inclusion of argon into the lattice of the niobium was observed. This led to a significant hardening of the Nb layer which in turn, should lead to better mechanical properties of a CrN/NbN coating with the Nb barrier layer. It should be noted however that the hardening can also be detrimental if the adhesion is insufficient as the internal stress in the coating will lead to higher stress at the interface that may lead to delamination of the coating. The values of hardness and Young's moduli of the coating correlate well with many engineering steels indicating a good match as a base layer. Ideally the coating should provide a gradient increase in hardness starting from the hardness of the substrate leading up to the hardness of the next layer. Based on the results in this study, such a gradient structure can be achieved by altering the bias voltage during the deposition of this base layer.

The corrosion measurements did not show a strong correlation between the bias voltage (or microstructure) and the corrosion behaviour. The coatings deposited at U_b = -125 V showed the best corrosion resistance in both sets of samples. However a significant difference in performance of the two coating thicknesses was observed. The thicker coating only exhibited a few large corrosion sites whereas the thinner coatings had thousands of such sites. This indicates that the growth of the coating

closes some of the smaller voids/defects. This "smoothening" of the surfaces was indeed visible on the plan view SEM observations in which only a fraction of the surface defects was visible.

The two coating thicknesses under investigation showed notable differences in the wear and corrosion tests. It was shown that the thicker, 4 μm thick, coatings give far superior corrosion resistance, yet the thinner 1.5 μm thick coatings gave far superior mechanical properties.

Similar hardening of the niobium layer was observed by Paritong et al. with a co-deposition of chromium and niobium [91]. This approach could be used to improve the mechanical properties further.

8.4 Top Coat

An oxynitride topcoat applied over the CrN/NbN superlattice coating was successfully deposited using the industrial sized Hauzer HTC 1000/4 UBM-ABS coating machine in argon/dry air atmosphere. The deposition rate was comparable to that of the CrN/NbN layer, but slower when as the deposition pressure was increased. The microstructure of the coating was similar to that of CrN/NbN coating and the oxygen is thought to replace the nitrogen in the lattice. At low bias voltages the microstructure was clearly columnar, while a high bias voltage densified the crystal structure and blurred the grain boundaries. The superlattice was clear and well defined in all cases. At low bias voltage the (111) growth direction was dominant leading to faceted grains with dome-like tops. Since the superlattice faces perpendicular to the direction of the growth locally, at the side of these columns the lattice is not parallel to the surface (superlattice waviness), which leads to very high wear as the superlattice is not parallel in the direction of the wear and the favourable wear mechanism of stopping of the crack propagation as was shown by Luo et al. can not take place [36].

At $U_b = -120$ V the dominant growth direction in the oxynitride was (100) and the superlattice was continuous, smooth and parallel to the surface leading to good wear resistance.

The oxynitride topcoat has been shown to be beneficial to the tribological properties of CrN/NbN superlattice wear and corrosion-resistant coatings. The topcoat provides a clear reduction in the friction coefficient against 100Cr6 steel. Yet more importantly the wear of the counter-sliding surface is reduced by 80%. This is significant since the coated parts are commonly used in combination with uncoated metal, when the wear of the counter-surface may be significant thus often requiring a coating on counter parts when it would not otherwise be necessary.

9 CONCLUSIONS

In this work a novel approach to the surface treatment was selected, in which multiple layers, each chosen for specific purpose, were optimised to combine the best properties of each. In this approach a careful consideration of macro- and microstructure of each layer is required in order to extract the good properties of each layer. It was shown in the work, that if such consideration is neglected a catastrophic failure may follow. In the case of the coatings the biggest problem is poor adhesion, that may cause a total failure of the coating, but also other critical considerations exist. As the number of layers and interfaces increase, the number of interactions between these increases exponentially. Thus it is not possible to test all possible combinations for each application. The only reasonable way to control the situation is through better understanding of the nature and the function of each layer and their relation to the other layers.

Throughout this work the intention was to take a very practical approach to the coating. The objective was to combine different approaches, such as nitriding to PVD, and investigate the specific interactions that are not otherwise apparent. It was discovered that in this case the parameters used in the nitriding can lead to different structures, each of which have specific properties beneficial for some applications. Similar tradeoffs were discovered in most sections of this work.

The CrN/NbN coating used in this work has been extensively studied in numerous studies and practical applications. Thus it was decided that the parameters and structure of that part of the coating would not to be concentrated on. Numerous practices and most test samples were kept constant with retain the compatibility to the earlier work. This together with the limited resources restricted the research group from using material and finishes that are used in the industry.

In this work four substrate materials were selected. As the structure and the mechanical properties of the substrate affect the end result profoundly the selection was not an easy one. The mild steel, M2 high speed steel and AISI 316 stainless steel

were selected as those were used in the earlier work and thus enabled comparison with the work found in the literature. S154 high strength steel was selected mainly due to good mechanical properties as well as ease of nitriding. The selection of the steel for a specific application and surface treatment is an important consideration as the real life tribological properties are largely dependent on it. The results of this work indicate that more detailed study on high strength engineering steels combined with duplex treatment and coating can result in superior result in practical tribological applications.

It has been shown that the optimisation of the coating parameters can have a huge effect on the properties of the coating. It is also very evident that the same coating will not give the best result in each application. Each application has its own failure mechanisms, which should be understood before the coatings can be engineered. The generic wear mechanisms, as presented in section 2.5, can be used as reference when analysing a new practical application.

For contact surfaces it is important to understand the forces and stresses at the contact points, as the forces above the fatigue and stress limits, considering all interfaces and intrinsic stress of the coating, will lead to quick failure. Each layer behaves differently under elastic deformation and may have its own fatigue limits. Modelling such a structure under real life conditions becomes next to impossible, so understanding mechanical properties (i.e. Young's modulus and hardness) of each layer is very valuable while designing a coating for a real application.

It is also important to regard the effects of the coated part to the counter body, since the wear resistant coatings can have a big effect to the parts/surfaces they come into contact with. This is common in sliding contacts where a coated surface can require a change (possibly a coating) to the counter surface as the wear of the counter body may be significantly increased by the coating. In cutting operations the counter body is normally the end product, thus it may have a direct effect on the quality of the product or even to the stability of the subsequent processes. In practical applications this effect can have a far greater economic impact than the effect on the tool life. This effect can not be generalised across a wide variety of applications, but it is important to understand that in the material/coating design that different low friction or anti-

stick top-coats can be used, provided that they are durable in the conditions under which they will be used.

Further, it is important to understand what happens to the coating-substrate pair in corrosive environments and how the selection of substrate material affects the performance of the coating. The highly corrosion resistant metals tend to be softer leading to poor mechanical properties. Also, for corrosion resistance they commonly rely on oxide layers that form on the surface, which may be easily worn off under mechanical wear conditions leading to erosion corrosion. A thin corrosion resistant coating may be sufficient to protect such a metal under light wear conditions. On the other hand the extra corrosion resistance of highly alloyed tool steels (i.e. martensitic or duplex stainless steels) may be needed in cutting operations in corrosive environments such as in the wood processing industry. The wear requirement becomes extreme as the coating needs to tolerate the high mechanical stress without delaminating or undergoing extensive wear. Duplex treatments show great promise in enabling the use of steel-coating combinations that would not otherwise produce the desired results.

The technologies used in this work were selected mainly due to availability to the research group, but also considering the global trends of reducing environmentally harmful processes and materials. PVD coating and plasma nitriding are being adopted in industry as a superior alternatives to the traditional surface treatment methods. Yet, as they are relatively new there are still numerous areas that are not commonly understood or are treated as trade secrets. The ABS technology, developed to improve interface enhancement options, has become a commercial success. It has recently seen competition from HIgh Power Impulse Magnetron Sputtering (HIPIMS) that is being developed by the same group utilising modern electronics and the innovative use of pulsed current. This new approach can give similar result in the ion etching stage without the micro-droplet induced growth defects that negatively influence the properties of the coating, especially corrosion performance.

The work carried out using the duplex treatment showed that duplex coatings using nitriding and PVD coating can have excellent wear and corrosion properties. With a properly implemented duplex treatment the S154 engineering steel can achieve

similar wear results to brittle high speed steel. The obvious advantages of using such an alloy are in the machining and manufacturing ease of any component. Compared to the non-nitrided coated samples or nitrided samples without coating the duplex samples out-performed the best non duplex treated samples with 4-20 times lower wear rates. The results also indicated significant (up to 3 orders of magnitude) improvement in the corrosion performance.

The composition of the compound layer was found to have a decisive effect on the properties of the system. The composition of this 5-10 μm layer seemed to make much more impact on the overall performance than the nitriding depth. The hard ε phase (Fe_3N) in the compound layer gives high surface hardness and excellent corrosion performance if the moderate impact resistance due to brittle fractures in the compound layer is agreeable. The more ductile γ' phase (Fe_4N) can promote very good adhesion and impact resistance. Large case depth means reduced deformations with high impact loads or high normal loads on rolling contacts. This shows that the plasma nitriding process, with which the compound layer can be accurately controlled, appears to be the way to produce the surface treatment with the desired compound layer composition.

As the relatively thin compound layer was shown to have a huge effect, the nitriding time (as diffusion is dependent on the time and the temperature) may be reduced to a level where it is feasible to combine the process directly within a PVD coating machine without greatly affecting the properties of the duplex coating. The duplex approach can also be applied on different steel grades to optimize the performance of the system in real applications. Also a further optimisation of the nitriding process based on these results may yield even better performance in the future.

The interface between the substrate and coating influences almost all aspects of the coating. The earlier work by Schöjahn et. al. showed that with the ABS process the interface can be modified with the metal ion etching to ensure optimal results [20, 66-67, 82]. The niobium ion etching was shown to produce good corrosion resistance, as well as good adhesion. A two stage etching process, designed to reduce the effects of the droplets, was also studied with positive results. This approach to etching was used also in this work. The etching efficiency of the niobium ion was found to be very small at voltages below $U_b = -1000$ V. This caused a very poor performance on the

samples that were not ion etched at higher voltages. The U_b = -800 V bias was shown to deposit a layer rather than etch. In the two-step etching process this layer was seen to improve the corrosion properties of the coating. Even though this layer was not clearly observed when the two step etching microstructure was investigated, the corrosion and adhesion results indicate that it improved corrosion resistance and reduced adhesion occured. On the other hand the adhesion of the coating was shown to have an effect on the corrosion performance. The good adhesion, combined with a low stress coating, prevents the corrosion from advancing along the interface and delaminating the coating, restricting corrosion to local "pits".

The niobium barrier layer has been shown to significantly improve the corrosion performance of CrN/NbN coated low alloy steels. The corrosion resistant niobium metal seems to be an ideal match with low alloy steels as the mechanical properties and the electrochemical potential, beneficial due to reduction of galvanic driving forces of corrosion, are very similar.

The effects of the deposition parameters as well as layer thickness were found to greatly influence the properties of the layer. The thicker layer was found to provide excellent corrosion properties, but this comes at the expense of reduced mechanical strength of the coating. The thinner coating has good mechanical properties but cannot match the thicker coating in corrosion performance. The difference between the corrosion performance of these coatings is about 1 order of magnitude. A notable difference was also observed in the quantity of defects visible on the coating surface. It should be however noted that the number of defects observed is still 2-3 orders of magnitude higher than the number of active corrosion sites observed after the corrosion test.

The increase of the bias voltage was found to increase the hardness of the Nb layers with only a minor effect on the corrosion performance. The increased hardness seems to correlate well with the argon content of the coatings. This leads to a conclusion that argon is trapped into the lattice preventing the movement of dislocations. The increase of mechanical strength of the Nb layer should result in the improvement of the wear properties of CrN/NbN coating with the Nb barrier layer and thus also the Nb-CrN/NbN coating. It should be however noted that increasing the internal stresses of the coating (as is the case with high bias voltages) may result in delamination of the

coating under wear conditions, as was observed with the thinner coating with -150V bias voltage.

The oxynitride topcoat was successfully deposited in the industrial Hauzer PVD coater using argon and dry air mixture. The idea of the oxynitride top-coat was two fold: 1st to act as low friction top-coat to reduce the wear of the counter body and 2nd to act as insulating layer to reduce the active surface of the cathodic coating. The friction was found to reduce slightly against 100Cr6 ball but increase with the oxide ball. The corrosion testing showed minor improvement.

The optimum coating parameters were found to be high bias voltage and low gas pressure producing a smooth superlattice that is parallel to the surface of the coating. In practice this leads to minor improvements in friction coefficient and corrosion performance. Still the biggest benefit of this top-coat appears to be a significant reduction of counter body wear. The reduction against the reference coating was found to be 80%. This can be very significant in a sliding contact against uncoated surface. Further, the sliding result also indicates a non-stick behaviour that is extremely desirable for cutting of "sticky" materials such as light alloys.

10 FUTURE WORK

Unfortunately it was not possible to include practical application trials to the scope of this work in order to demonstrate in practice how big improvements can be achieved with intelligent optimization. As the requirements for each application differ from one another and as the results of the study show there are no single "one-fits-all" solution. This creates a challenge to the future work on how to best utilise the existing body of knowledge for the problem at hand. Further work could involve an optimisation exercise for an application that includes numerous conflicting requirements like corrosion resistance, abrasion resistance and impact resistance. One of such applications identified during this work is mechanical wood peeling where the wear of the knife is critical to the quality of the product and the productivity of the machine [106, 107].

This work would have also benefited from more involved work with duplex processes as the results from that study show great promise for practical application. The nitriding parameters used for this study were selected without prior understanding of the effects of those on the properties of the duplex treatment. Further, a mechanical polishing step was performed prior the coating, which may be difficult to implement into an industrial process. Also an in situ plasma nitriding (in the PVD coater) would improve the logistics of the process and make it easier to industrialise.

This study was also mostly limited to standard metal samples, though an intelligent selection of the substrate will affect all aspects of the coating. High strength case hardening steels (with usage temperature up to the 500°C coating temperature) martensitic stainless steels and duplex steels would be at the top of the author's list. Mold and tool steels, such as AISI H13 and H11 have been already successfully duplex treated for hotworking and forming applications [108, 109]. Additional thought should be used to the evaluate the compound layers formed on these steels during the nitriding, as the composition of the compound layer will greatly affect the overall performance of the coating

Further research on different top-coat options would also increase the options available to the coating designer. There are great number of organic, ceramic and hybrid coatings with highly desirable properties, such as hydrophobic, anti-stick and low friction behaviour. These coatings are often very thin and can often only survive on top of a hard coating. Often it is not required that such a coating survives on the actual wear surface, yet it can prevent corrosion or improve sliding properties under conditions that are considerably less aggressive.

Further work has been already conducted in the area of interface preparation using high power impulse magnetron sputtering (HIPIMS), which gives the advantage of highly ionised metal plasma without the droplets inherent to the arc process [110-111]. This approach has shown significant improvement on both mechanical and corrosion properties of the coatings.

11 References

[1] D. Mattox, Foundations of Vacuum Technology, Noyes Publications, 2003, USA

[1a] W.R. Grove, On the Polarity of Gasses, Phil. Trans. Royal. Soc. (London), B142, 87, 1852

[1b] M. Faraday, Experimental Relations of Gold (and other metals) to Light, Phil. Trans., 147, 145, 1857

[1c] A. W. Wright, On the Production of Transparent Metallic Films by Electrical Discharge in Exhausted Tubes, Am. J. Sci. Arts, Vol. 13, pp. 49-55, 1877

[1d] R. Nahrwold, Ann. Physik, 31, 467, 1887

[1e] T.A. Edison, U.S. Patent 526,147, 1894

[1f] G. A. Veszi, J. Brit. Instn. Radio. Eng., 13, 183, 1953

[1g] D.M. Mattox, Sputter Deposition: Early effoerts, Plat. Surf. Finish., 88(9) 60, 2001

[2] D. M. Mattox, Handbook of Physical Vapour Deposition (PVD) Processes, Noyes Publications, 1998, p. 917

[3] D.M. Mattox. ASM Handbook vol. 5, ASM International, 1994 p.539-555

[4] K. Wasa, S. Hayakawa, Handbook of Sputter Deposition Technology, Noyes Publications, 1991

[5] H.K. Pulker, Coatings on Glass, 2nd revised ed., Elsevier Science, 1999

[6] ASM Materials Engineering Dictionary, ASM Handbook, ASM International, 1994

[6a] P. Hovsepian, W-D. Münz, Final report of BRITE-ERAM project NEWCHROME no: BE-96-3305

[7] C. Schönjahn, M. Bamford, L.A. Donahue, D.B. Lewis, S. Forder, W-D. Münz, Surf. & Coat. Technol. 125, 2000, p66-70

[8] P. Hovsepian, D.B. Lewis, W.-D. Münz, S.B. Lyon, M. Tomlinson, Surf. Coat. Technol.120-121 (1999) 535

[9] M. Lembke, PhD Thesis, Sheffield Hallam University, 2002

[10] S.L. Rohde, ASM Handbook vol. 5, ASM International, 1994 p 573-581

[11] K. Seshan, "Handbook of thin-film deposition processes and techniques", 2nd ed., Noyes Publications, USA, 2002

[12] J.L.Vossen, J.J. Cuomo "Glow discharge sputter deposition", Thin film Processes (ed. Vossen & Kern), Academic press, New York 1978

[13] B.Window, N. Savvids, J. Vac. Sci. Technol. A, Vol 4 (No. 2), 1986, p 196-202

[14] D. G. Teer, US Patent 5,556,519, 1996

[15] B. Jütter, V. F. Pucharev, E. Hantzsche, I. Beillis, Cathode Spots Handbook of Vacuum Arc Science and Technology, (eds. R.L. Boxman, P.J. Martin, D.M. Sanders), Ch 3, Noyes Publications 1996

[16] J.E. Daaler, Phys. Stat. Solid, 104:91 (1981)

[17] H. Randhawa, P.C. Johnson, Surf. Coat. Technol. 31 (1987) 303-318.

[18] J. Vyskocil, J. Musil, Surf. Coat. Technol. 43/44 (1990) 299-311

[19] W.-D. Münz, F. J. M. Hauser, D. Schulze, B. Buil, Surf. Coat. Technol., 49, 161, 1991

[20] C. Schönjahn, PhD thesis, Sheffield Hallam University, 2001, UK

[21] D.B. Lewis, S.J. Creasey, C. Wüstefeld b, A.P. Ehiasarian a, P.Eh. Hovsepian, Thin Solid Films 503 (2006) 143 – 148

[22] W.-D. Münz, D.B. Lewis, P. Eh. Hovsepian, C. Schönjahn, A. Ehiasarian, I.J. Smith, Surface Engineering 17 (2001) 15,

[23] H.W.Wang, M.M. Stack, S.B. Lyon, P. Hovsepian, W-D. Münz, Surf. Coat. Technol. 126 (2000) 279

[23a] J. A. Venables, G. D. T. Spiller, M. Hanbucker, Rep. Prog. Phys., Vol 47, 1984, p 399

[23b] P. Hovsepian, D.B. Lewis, Q. Luo, A. Farinotti, Thin Solid Films 488 (2005) 1-8

[24] B.A. Movchan, A.V. Demchishin, Phys. Met. Metallogr. (USSR), vol. 28, 1969, p83

[25] J.A. Thornton, Ann.Rev.Mat.Sci. vol. 7, 1977 p. 239

[26] R.Messier, A.P. Giri, R. A. Roy, J. Vac. Sci. Tech. A, Vol 2, 1984, p500

[27] M. Ohring, material science of thin films, Academic press, 1991

[28] H. Windischmann, Crit. Rev. solid state material Sci. vol 17 (no 6), 1992, p547

[29] U.Helmerson, S. Todorva, S. A. Barnett, J. -E. Sundgren, L. C. Markert, J. E. Greene, J. Appl. Phys., 1987, 62, 481

[30] W. –D. Munz, D. B. Lewis, P. Eh. Hovsepian, C. Schönjahn, A. Ehiasarian, I. J. Smith, Surf. Eng., 17 vol. 1, 2001, 15

[31] E.O. Hall, Proceedings of the Physical Society of London, B64, 747, (1951). 2.

[31a] N.J. Petch, , Journal of the Iron Steel Institute, 25, 174, (1953)

[32] Koehler JS. Phys Rev B 1970;2:547

[33] X.Chu, S.A. Barnett. J. Appl Phys. 77 (9), 1995, 4403-4411

[34] S.A. Barnett, A, Madan,"Superhard superlattices" Phys World, 11 (1) (1998

[35] P.Eh. Hovsepian, W.-D. Münz Vacuum 69 (2003) 27–36

[36] Q. Luo, W.M. Rainforth, W.-D. Münz, Wear 225-229 (1999) 74

[37] K. Höck, B. Larisch, H.-J. Spies, F. Vogt, "Investigations on hardcoating on pernitrided low allow steels" proceedings of PSE conference, 1993

[38] B. Podgornik, J, Vižintin, Vacuum, 68 (2003) 39

[39] J.M O'Brien, D. Goodman, ASM Metals Handbook Vol 4, (1991) p. 420

[40] B. Podgornik, J, Vižintin, O.Wänstrand, M. Larsson, S. Hogmark, H. Ronkainen, K Holmberg, Wear 249 (2001) 254

[41] A. Kagiyama, K. Terakado, R. Urao, Surf. Coat. Technol., 169-170 (2003) 397

[42] P. Panjan, I. Urankar, B. Navinšek, M. Terčeilj, R. Turk, M. Čekada, V. Leskovšek, Surf. Coat. Technol., 151-152 (2002) 505

[43] M. Pellizzari, A. Molinari, G. Straffelini, Surf. Coat. Technol., 142-144 (2001) 1109

[44] J.C.A. Batista, C. Godoy, G. Pintaúde. A. Sinatora, A. Matthews, Surface and Coatings Technology, 174-175, (2003), 891-898

[45] J.-D. Kamminga, R. Hoy, G. C. A. M. Jannsen, Surface and Coatings Technology, 200, 12-13, (2006), Pages 3856-3860

[46] G. Nayal, A.P. Ehiasarian, K. M. Macak, R.New, W.-D. Münz, I. J. Smith, E-MRS 2000 proceedings, (2000)

[47] J.-D. Kammingaa, R. Hoya, G.C.A.M. Janssenb, E. Lugscheiderc, M. Maesc, Surface and Coatings Technology 174 –175 (2003) 671–676

[48] J. Vetter, G. Barbezat, J. Crummenauer, J. Avissar, Surf. Coat. Tech., 200 (2005) 1962 – 1968

[49] A. Grill, "Cold plasma in materials fabrication, from fundamentals to application" IEEE Press, New York, 1994

[50] J.M. O'Brien, D. Goodman, in: ASM Handbook, vol. 4, ASM International, Materials Pard, OH, 1997, p. 420.

[51] C. Alves Jr., J.A. Rodrigues, A.E. Martinelli, Surf. Coat. Technol. 122 (1999) 112.

[52] M. Berg, C.V. Budtz-Jørgensen, H. Reitz, et al., Surf. Coat. Technol. 124 (2000) 25

[53] T. Bell, Y. Sun, A. Suhadi, Vacuum59 (2000) 14.

[54] W. Callister, "Materials Science and Engineering, an Introduction", 4th ed., John Wiley & Sons Inc., USA, 1997

[55] S.,D., Cramer, B., S., Covino, Jr., ASM Handbook vol. 13A, ASM International, 2003

[56] I. Milosev, B. Navinsek, H.H. Strehblow, Corrosion Properties of Hard PVD Nitride Coatings_with the Emphasis on TiN., Forschungsentrum, Julich, 1995

[57] M. Tomlinson, S.B. Lyon, P. Hovsepian, W-D Münz, Vacuum53 (1999) 117

[58] C. Robyr, P. Agarwal, P.Mettraux, D.Landolt, Thin Solid Films 310 (1997) 87

[59] C.Liu, A.Leyland, Q. Bi, A.Matthews, Surf. Coat. Technol. 141 (2001) 164

[60] C. Liu, Q. Bi and A. Matthews, Corros. Sci.43 (2001) 1953

[61] C.Liu, A.Leyland, S.Lyon, A.Matthews, Surf. Coat. Technol. 76/77 (1995) 626

[62] K. Holmberg, A. Matthews, "Coating Tribology, Properties, Techniques and Applications in Surface Engineering", Elsevier Science, Netherlands, 1994

[63] F.T. Hoffmann, P. Mayr, ASM handbook Vol. 18 Friction, Lubrication and Wear Technology, ASM International (1991), p 878

[64] P.Eh. Hovsepian, D.B. Lewis, W.-D. Münz, A. Rouzaud, P. Juliet, Surf. Coat. Technol., 116-119 (1999) 727

[65] D.B. Lewis, D. Reitz, C. Wüstefeld, R. Ohser-Wiedemann, H. Oettel ,A.P. Ehiasarian, P.Eh. Hovsepian, Thin Solid Films 503(2006) 133-142

[66] C.Schönjahn, H. Paritong, W.-D. Münz, R.D. Twesten, I. Petrov,. J.Vac. Tech. A19 (4) (2001) 1392

[67] C.Schönjahn, A. P. Ehiasarian, D. B. Lewis, R. New, W.-D. Münz, R.D. Twesten, I. Petrov,. J.Vac. Tech. A 19 (2001) p.1415

[68] G.L.Miller, Tantalum and Niobium, Butterworths Scientific, London, 1958

[69] E.E. Salagean, D.B. Lewis, J.S. Brooks, W.-D. Münz, I. Petrov, J.E. Greene, Surface & Coatings Technology 82 (1996) 57-64

[70] O. Bleeck, D. Münz, w. Schaller, Y. Y. Yang, Engineering Fracture Mechanics Vol. 60, No. 5-6, pp. 615-623, 1998

[71] P. Hovsepian, W-D. Münz, Final report of BRITE-ERAM project NEWCHROME no: BE-96-3305

[72] D.B. Willams, C. B. Carter, "Transmission Electron Microscopy: A Textbook for Materials Science 4 vol. set", Plennum Press, USA, 1996

[73] D.Rickerby, A.M. Jones, B.A. Bellamy, Surf. Coat. Technol. 37 (1989) 111

[74] standard ASTM G 99-95a

[75] standard DIN 50324

[76] standard ISO 14577- 1:2002

[77] standard DIN ISI 4516, 1988

[78] A.C. Sekkal, C. Langladel, A.B. Vannes, Tribology Letters, vol 15/3, p.265-274 (2004)

[79] American Society for Testing and Materials, ASTM Designation B 1 17-90: Standard Method of Salt Spray (Fog) Testing, 1991 Annual Book of ASTM Standards

[80] M.Zlatanovic, D. Kakas, Lj. Mazibrada, A. Kunosiéa and W.-D. Münz, Surf. Coat. Tech. 64 (1994) 173

[81] T. Bell, Ind. Lubr Tribol. 44 (1992) 3

[82] C.Schönjahn, L.A. Donohue, D.B. Lewis, W.-D. Münz, R.D. Twesten, I. Petrov, J.Vac. Sci. Technol. A 18(4) (2000) 1718

[83] W.-D. Münz, C. Schönjahn, H. Paritong, I.J. Smith, Le Vide, Science-Technique-Applicatious, Vol. 55. No. 297 (2000) 205

[84] H. Paritong, I. Wadsworth, L.A. Donohue, W.-D. Münz, Trans. Inst. Met. Finish. 76 (1998) 144.

[85] C. Schönjahn D.B. Lewis W-D Münz, I. Petrov, Surface Engineering, 16/2, April 2000, p.176-180(5)

[86] P.Eh. Hovsepian, W.-D. Münz, in: H. Dimingen (Ed.), Surface Engineering, EUROMAT, vol. 11, Wiley-VCH, Weinheim, 2000, p. 41.

[87] M. Kühn, R. Pintaske, F. Richter. IEEE Trans. Plas. Sci., 25(4):694-699, 1997

[88] P. J. Martin, D. R. McKenzie, R. P. Netterfield, P. Swift, S. W. Filipczuk, K. H. Müller, C. G. Pacey and B. James , Thin Solid Films, Volume 153, Issues 1-3, 1987, p. 91

[89] J.H. Hsieh, R. Lee, R.A. Erck and G. R. Fenske, Y. Y. Su, M. Marek and R. F. Hochman, Surf. Coat. Technol. 49 (1991) 52

[90] L.P. Ward, P.K. Datta, Thin Solid Films, 272 (1996) 52

[91] H.Paritong, M.Lembke, D.B.Lewis, W.-D. Münz, Surf. Coat. Technol. 116 119 (1999) 1145

[92] W-D. Münz, SVC, 36th Annual Technical Conference Proceedings (1993), 411

[93] G. Knuyt, C. Quaeyhaegens, J. D'Haen, L. Stals, Thin Solid Films, 258 (1995) 159

[94] J. Pelleg, L.Z. Zevin, S. Lungo, Thin Solid Films, 197 (1991) 117

[95] E. Alves, A.R. Ramos, N.P. Barradas, F. Vaz, P. Cerqueira, L. Rebouta, U. Kreissig, Surf. Coat. Technol. 180–181 (2004) 372.

[96] R.J. Koerner, L.A. Butterwoth, I.V. Mayer, R. Dasbach, H.J. Buucher, Biomaterials 23 (2002) 2835.

[97] J. Propst, U. Gbureck, R. Thull, Surf. Coat. Technol. 148 (2001) 226.

[98] P. Wilharititz, S. Dreer, P. Ramminger, Thin Solid Films 447 (2004) 289.

[99] St. Collard, H. Kupfer, G. Hecht, W. Hoyer, H. Mossaoui, Surf. Coat. Technol. 122 (1999) 181.

[100] M. Lembke, D.B. Lewis, W.-D. Münz, J.M. Titchmarch, Surf. Eng. (2001) 17.

[101] T. Suzuki, H. Saito, M. Hirai, H. Suematsu, W. Jiang, K. Yatsui, Thin Solid Films 407 (2002) 118.

[102] M. Fenker, H. Kappl , O. Banakh, N. Martin, J.F. Pierson, Surf. Coat. Tech. 201 (2006) 4152

[103] P.Eh. Hovsepian, D.B. Lewis, W.-D. Münz, Surf. Coat. Technol. 133–134 (2000) 166.

[104] D.B. Lewis, Q. Luo, P.Eh. Hovsepian, W.-D. Munz, Surf. Coat. Technol. 184 (2–3) (2004) 166.

[105] S. Kadlec, J. Musil, V. Valvoda, W.-D. Munz, H. Petersein, J. Schroeder, Vacuum 41 (1990) 2238

[106] P. Beer, M.A. Djouadi, R. Marchal, A. Sokolowska, M. Lambertin, S. Miklaszewski, Journal of Materials Processing Technology 92-93 (1999) 264-268

[107] C. Nouveau, M.A. Djouadi, C. Deces-Petit, P. Beer, M. Lambertin Surface and Coatings Technology 142-144, (2001) 94-101

[108] R. Rodriguez-Baracaldo, J.A. Benito, E.S. Puchi-Cabrera, M.H. Staia Wear 262 (2007) 380–389,

[109] M. Sokovic, P. Panjan, R. Kirn, Journal of Materials Processing Technology 157–158 (2004) 613–616

[110] M. Lattemann, A.P. Ehiasarian, J. Bohlmark, P.Å.O. Persson, U. Helmersson, Surface & Coatings Technology 200 (2006) 6495–6499

[111] C. Reinhard, A.P. Ehiasarian, P.Eh. Hovsepian, Thin Solid Films 515 (2007) 3685–3692

[113] D.C. Cameron, R. Aimo, Z.H. Wang, K.A. Pischow, Surface & Coatings Technology, 142-144 (2001), 567-572

[114] E. Bemporada, C. Pecchiob, S. De Rossib, F. Carassiti, Surface & Coatings Technology 188–189 (2004) 319– 330

[115] M. Fenker, M. Balzer, H. Kappl, Thin Solid Films 515 (2006) 27 – 32

Table of Figures

Available online at www.sciencedirect.com
SCIENCE DIRECT®
ELSEVIER
Thin Solid Films 460 (2004) 94–100
thin solid films
www.elsevier.com/locate/tsf

Influence of ion bombardment on the properties and microstructure of unbalanced magnetron deposited niobium coatings

T. Savisalo*, D.B. Lewis, P.Eh. Hovsepian, W.-D. Münz

Materials Research Institute, Sheffield Hallam University, Howard St., Sheffield S1 1WB, UK

Received 16 May 2003; received in revised form 21 November 2003; accepted 11 December 2003
Available Online 30 April 2004

Abstract

The effect of the ion bombardment to unbalanced magnetron deposited, approximately 1.5 and 4.5 μm thick, Nb coatings have been investigated as the bias voltage was varied from $U_B = -75$ to -150 V. Increasing bias voltage increased the hardness of the coating from 4.5 to 8.0 GPa. This was associated with residual stress and Ar incorporation into the Nb lattice. Strong {110} texture developed in the samples deposited at low bias voltages, while beyond $U_B = -100$ V a {111} texture became dominant. However, strong {111} texture was observed only with the thicker 3Nb coatings. Secondary electron microscopy investigation of the coating topography showed fewer defects in the thicker coatings. All coatings exhibited good corrosion resistance, with the thicker coatings clearly outperforming the thinner ones. Excessive bias voltages ($U_B = -150$ V) was found to lead to poor adhesion and loss of corrosion resistance.
© 2004 Elsevier B.V. All rights reserved.

Keywords: Niobium coatings; Bias voltage; Ion bombardment

1. Introduction

Niobium is widely known to be chemically very stable material and is therefore used in a wide range of applications requiring extreme corrosion resistance. The electrochemical stability based on formation of a Nb_2O_5 oxide layer on the surface, which is stable even under the most hostile environments [1]. Metallic niobium physical vapour deposited (PVD) coatings have been successfully deposited on various substrates and they have been shown to increase corrosion resistance of stainless steels considerably [1–6].

It has also been shown that using arc bond sputtering (ABS) technique [3] the corrosion performance can be further enhanced by Nb ion etching, utilising steered arc discharge, prior to the coating deposition, which was deposited using unbalanced magnetron sputtering (UBM) [7,8]. Metallic Nb coatings can be used as decorative coatings with a wide range of available colours through anodising [2,9]. They have also been used successfully as barrier layers in multilayered corrosion and wear resistant CrN/NbN superlattice coatings yielding coatings with properties, when deposited on mild steel substrates, that are comparable or superior to that of 25 μm thick hard chrome coatings [10,11].

Corrosion attack of PVD coated low alloy steel generally occurs at growth defects generated from droplets deposited during the metal ion stage [12]. The region adjacent to the growth defect is under-dense therefore the solution can find a path to penetrate the coating forming galvanic cell between the coating and the substrate [13]. The large area of cathodic coating surface when compared with the anodic substrate at the defect location creates accelerated pitting corrosion (small anode to large cathode effect). Furthermore, the corrosion products can cause the de-lamination of the coating near the initial pit resulting in complete failure. Thus the defect locations are dominating the corrosion protection ability of the coating.

The effect of intensified ion bombardment to the properties of Nb coatings has been studied by several

*Corresponding author. Tel.: +44-114-2213046; fax: +44-114-2213053.
E-mail address: t.savisalo@shu.ac.uk (T. Savisalo).

0040-6090/04/$ - see front matter © 2004 Elsevier B.V. All rights reserved.
doi:10.1016/j.tsf.2003.12.150

Table 1
Coating parameters

	Pressure (Pa)	Bias voltage	Power (kW)	Other
Heating	<0.007			
Target cleaning (2 min)	0.20		2.1	
Nb ion etching (15 min)	0.2–0.06	−1200 V	1.3	Cathodic Arc
Coating (60 min, 1Nb and 180 min, 3Nb)	0.20	−75 V, −100 V, −125V, −150 V	2.8	

research groups [2,4,5]. Their results are somewhat contradictory. They show, however, that the structure and the properties of the coatings depend on deposition conditions used. Increasing bias voltage increases the energy of the bombarding ions, which normally increases densification of the crystal structure of the coating. It also increases inherent (compressive) stress in the coating and creates additional lattice defects in the crystal structure. The internal compressive stress has been shown to reduce the number of growth defects, by for example, embedding them into the coating, thus improving barrier properties [14]. However, excessive internal stresses can lead to lower corrosion resistance mainly due to the loss of adhesion [10]. Increasing the thickness of the coating generally improves corrosion resistance. However, in many potential applications this approach is not possible due to economical considerations.

Nb PVD coatings have been shown to have potential use in number of decorative and anticorrosion applications [2,9–11]. However, it is necessary to have further understanding of the growth, microstructure and the properties of these coatings under different process parameters to obtain the full potential of these coatings.

2. Experimental details

2.1. Coating deposition

The metallic Nb PVD coatings were deposited on M2 high speed steel, mild steel and stainless steel substrates that were mechanically ground and polished with 1 μm diamond paste to a surface finish of R_a=0.05 μm. Prior the deposition the samples were cleaned using an automated cleaning line (by UCM) consisting of multistage ultrasonically agitated cleaning and rinsing process. The coatings were deposited at 450 °C using industrial sized multi-target HTC 1000-4 ABS combined cathodic arc/unbalanced magnetron sputtering coating system, manufactured by Hauzer Techno Coatings BV [7,8]. The deposition was performed in unbalanced magnetron sputtering mode using 2Nb targets. The substrates were subject to three-fold rotation to ensure uniform coating deposition. Steered arc Nb-ion etching [3] was used to improve the adhesion and corrosion resistant properties of the coating. The etching step used two different Ar pressures (0.2 and 0.06 Pa) to gain maximal benefits of ABS process namely etching (high Ar pressure) and implantation (low Ar pressure) as reported by Schönjahn et al. [15]. The Nb coatings were deposited using bias voltages varying from U_B=−75 to −150 V in 25 V intervals. Coatings were also deposited in two thickness of approximately 1.5 μm (1 h of deposition time, thus later referred as 1Nb) and 4.5 μm (3 h of deposition time, later 3Nb). A more detailed description of the parameters used in the coating processes can be seen in Table 1.

2.2. Coating characterisation

The hardness of the coatings were characterised using Knoop hardness measurement (Mitutoyo MVK-G1, 25 g normal load) and nano-indentation technique, (plastic hardness and Young's modulus, Nanoinstruments XP, 500 nm indentation depth). The CSM Revetest was used to perform scratch test. The electrochemical corrosion measurements were performed in 3% NaCl solution using 3-electrode cell with Saturated Calomel Electrode (SCE) reference electrode. The polarisation measurements were performed with EG&G Model 263A potentiostat from −1000 to +1000 mV using scan rate of 0.5 mV/s. Before the polarisation measurements the samples were cleaned cathodically at −1.5 V for 100 s and then allowed to equilibrate at open circuit potential (OPC) for 20 min.

The microstructure was investigated using Philips CM20 TEM for the cross-sectional transmission electron microscopy (XTEM) and Philips XL40 for secondary electron micrographs (SEM) and energy dispersive X-ray (EDX) analysis. Philips PW1820 was used for X-ray diffraction (XRD) measurements. The measurement was done using Bragg–Brentano and 1° glancing angle geometries. The texture was calculated using inverse pole figure method. Inverse pole figures are represented in terms of 'T^*' values, which are a measure of the statistical change of any plane lying in the plane parallel to the surface. For a particular plane, (hkl), T^* is:

$$T^*_{hkl} = \frac{I_{(hkl)}/R_{(hkl)}}{\frac{1}{n}\sum_{0}^{n} I_{(hkl)}/R_{(hkl)}} \quad (1)$$

Table 2
Summary of the properties of the coatings

Coating	Thickness (μm)	H_k 25 g	H_p (GPa)	E (GPa)	Texture T^* (110)	Texture T^* (222)	at.% Ar	Current density at 700 mV vs. SCE in potentiodynamic polarisation (A/cm^2)
1Nb −75 V	1.6				5.1	0.0	<0.3	1.0×10^{-3}
1Nb −100 V	1.4				5.0	0.0	<0.3	1.5×10^{-3}
1Nb −125 V	1.3				2.0	1.8	2.0	7×10^{-4}
1Nb −150 V	1.3				2.3	2.8	3.5	1.0×10^{-2}
3Nb −75 V	4.4	500	4.5	200	5.6	0.0	<0.3	1×10^{-4}
3Nb −100 V	4.0	490	5.2	190	0.9	4.5	<0.3	1×10^{-4}
3Nb −125 V	3.9	700	7.1	170	0.6	4.9	2.5	1×10^{-4}
3Nb −150 V	3.8	820	8.0	170	0.6	4.1	4.5	2×10^{-4}

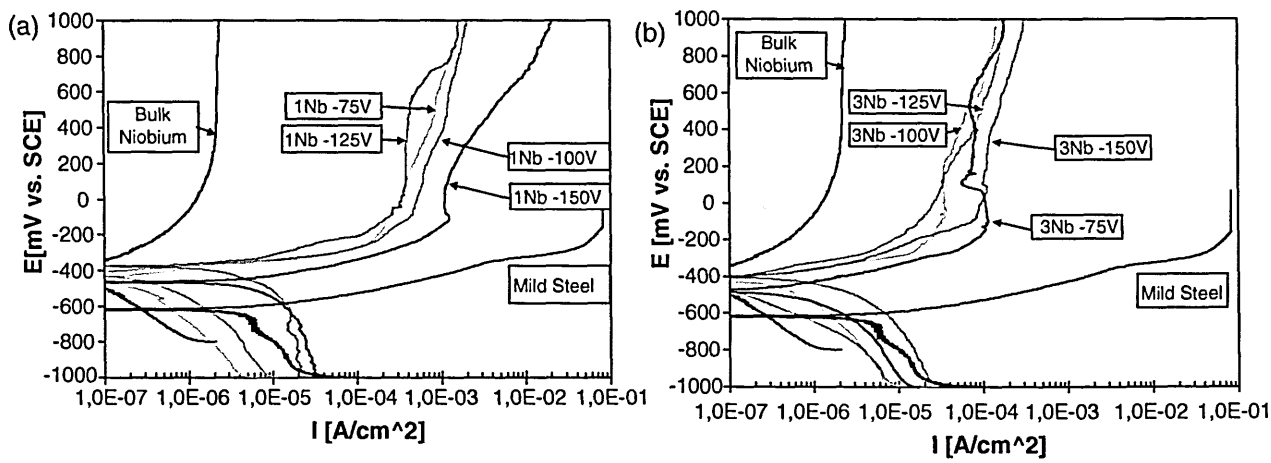

Fig. 1. Potentiodynamic polarisation of metallic Nb coatings in 3% NaCl solution (a) 1Nb coatings, (b) 3Nb coatings.

Table 3
The number of growth defects in 1 mm^2 of Nb coating (Quantified from the SEM plan view images with image analysis software)

1Nb				
Defect size	−75 V	−100 V	−125 V	−150 V
>10 μm^2	204	256	421	266
<10 μm^2	3267	2432	4045	1806
3Nb				
Defect size	−75 V	−100 V	−125 V	−150 V
>10 μm^2	131	111	90	97
<10 μm^2	1862	936	950	967

Where $I_{(hkl)}$ is the intensity of the (hkl) reflection and $R_{(hkl)}$ is the intensity corresponding to randomly oriented sample and n is the number of reflections considered (in this investigation $n=6$). This method is described in more detail in Ref. [16].

3. Results

The properties of the coating are summarised in Table 2. The hardness increased from 4.5 GPa at bias voltage of $U_B=-75$ V to 8.0 GPa at $U_B=-150$ V. A sharp increase in the hardness was observed between $U_B=-100$ V and -125 V as the hardness increased from 5.2 to 7.1 GPa. The Young's modulus decreased slightly with increasing bias voltage from 200 GPa measured at $U_B=-75$ V to 170 GPa at $U_B=-150$ V. The adhesion of the coatings was measured to be high with no adhesive failures in the scratch tests with up to 90 N normal load. The coating thickness decreased with increasing bias voltage from 1.6 μm (and 4.4 μm) at −75 V to 1.3 μm (and 3.8 μm) at −150 V due to re-sputtering of the growing film.

The results of the potentiodynamic polarisation measurements are shown in Fig. 1a,b. The coated mild steel samples exhibited good corrosion resistance yet localised corrosion damage could be observed after the test. The shapes of the curves are roughly similar to those of bulk Nb, yet the current densities are 2–3 orders of magnitude higher in the anodic region. The thicker coatings performed better than the thinner coatings with anodic current densities approximately one order of magnitude less. The $U_B=-125$ V coating exhibited the best corrosion resistance but the difference was only margin-

al. The 1Nb coating deposited at a bias voltage $U_B = -150$ V performed badly due to local delamination of the coating.

SEM plan view observation of the (HSS) samples showed differences in the coating topography. The number and size of growth defects were measured from the SEM images using an image analyser and the results are included in Table 3. The amount of defects was noted to generally reduce as the bias voltage was increased. The thicker 3Nb coatings had clearly fewer defects than the thin coatings.

Semi-quantitative EDX analysis of the coatings showed an increase of the Ar content in the coatings as the bias is increased (Table 1). With voltages below $U_B = -100$ V there was virtually no argon incorporated in the coating. At $U_B = -125$ V the Ar content of the coating was 2.5 at.% which at $U_B = -150$ V increased to 3.5 at.%. in the thinner coating and 4.5% in the thicker coating.

XTEM investigation of the microstructure (Fig. 2a,b) of the coatings showed columnar grain morphology with no apparent voids between the columns even in coatings deposited at lower bias voltages. The coatings deposited at low bias voltages showed a more distinct columnar microstructure, while the columns become almost indistinguishable at $U_B = -150$ V. A reduction in grain diameter can also be observed with increasing bias voltage. Near the coating/substrate interface the grain size is very fine. At 0.2 μm from the coating/substrate interface (approx. 10 min of deposition) larger grains can be observed. The average grain diameter also grows gradually with the increasing thickness. It increases from approximately 110 nm at $U_B = -75$ V (70 nm at $U_B = -150$ V) at 1 μm thickness to 230 nm (12 nm) at 3 μm thickness. At $U_B = -150$ V individual grains cannot

Fig. 3. Plan view TEM of 3Nb −75 V shows fully dense columnar structure.

Fig. 2. XTEM micrographs of the Nb coatings deposited with different bias voltages (a) 1Nb coatings, (b) 3Nb coatings.

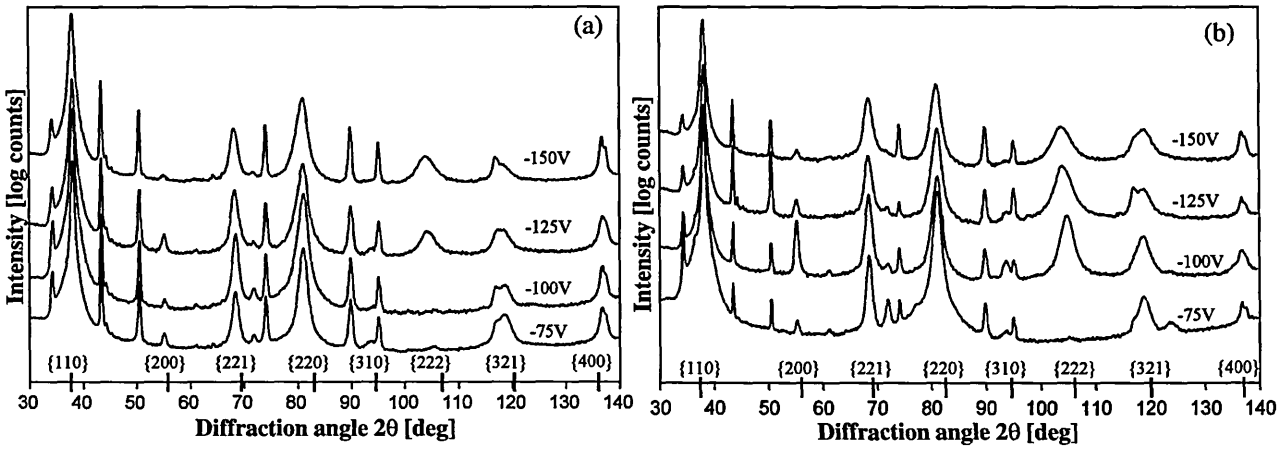

Fig. 4. Bragg–Brentano patterns of (a) 1Nb and (b) 3Nb coatings. (Intensity in logarithmic scale).

be followed through the coating due to large amount of lattice defects and columnar sub grains in the microstructure.

A TEM plan view investigation (see Fig. 3) showed fully dense microstructure with no voids in coatings deposited even at the lowest bias voltage used ($U_B = -75$ V).

The XRD (Fig. 4a,b and Table 4) showed significant changes in the texture of the coatings. Coatings deposited at $U_B = -75$ V developed a strong {110} texture with inverse polar figures for {110} reflection of 5.1 and 5.6. As the bias voltage was increased, the intensity of the {110} peak relative to {222} peak decreases. This indicates a less strong texture or possible change in texture and indeed with increasing bias voltage there is noticeable change towards {111} texture. The thicker coatings deposited at bias voltages of $U_B = -100$ V or higher have a strong {111} texture with T^* values higher than 4 (see Table 4). However, the {111} texture is less strong in the thinner coatings with 1Nb −125 V and 1Nb −150 V showing mixed {111}/{110} texture (inverse pole figures for {110} reflection from 2.0 to 2.3). There is also a noticeable peak shift toward lower 2θ angles as the bias voltage is increased (see Fig. 4, {222} reflection, JCPDS standard 107.6°). This can be associated with lattice strain indicating a residual stress in the plane parallel to the coating surface. Since the pattern was measured in $\theta/2\theta$ geometry (measures d spacing perpendicular to surface) a compressive stress in the film plane parallel to the surface cause expansion perpendicular to surface due to Poisson effect.

4. Discussion

This work film thickness and bias voltage was noted to greatly influence the crystal structure, the localised defect density and the mechanical and electrochemical properties of the ABS deposited Nb coatings.

Mechanically all coatings can be described as ductile with low to medium hardness. This combined with the Young's modulus similar to engineering steels explains good performance in scratch test even though some coatings were found to delaminate in corrosion tests. Increasing the bias voltage, thus increasing the energy of the bombarding ions, increases the hardness (up from $H_k = 490$, 4.5 GPa at $U_B = -100$ V to $H_k = 820$, 8.0 GPa at $U_B = -150$ V) but has virtually no affect to the Young's modulus. All coatings were measured to be harder than mild steel substrates ($H_k = 350$) yet softer than high-speed steel ($H_k = 1050$). The hardest coatings had hardness close to that of hard Cr ($H_k = 900$). Increase in the bias voltage from $U_B = -100$ to −125 V causes sharp increase in the hardness of the coating. This corresponds to the EDX results that indicate that significant amount of Ar atoms have been trapped in the Nb lattice (up to 4.5 at.% Ar at $U_B = -150$ V)

Table 4
Texture of the coatings (inverse pole figure method)

{hkl}	2θ	1Nb −75 V	1Nb −100 V	1Nb −125 V	1Nb −150 V	3Nb −75 V	3Nb −100 V	3Nb −125 V	3Nb −150 V
110	38.5	5.1	5.0	2.0	2.3	5.6	0.9	0.6	0.6
211	69.6	0.2	0.4	1.4	0.2	0.2	0.2	0.2	0.3
310	94.9	0.1	0.1	0.2	0.2	0.0	0.0	0.0	0.0
222	107.6	0.0	0.0	1.8	2.8	0.0	4.5	4.9	4.1
321	121.3	0.7	0.5	0.6	0.5	0.2	0.3	0.3	1.0

during coating deposition. These trapped argon may also cause lattice strain (expansion of the lattice parameter) as also indicated by XRD peak shifts towards smaller angles. The Ar would limit the dislocation movement in the grains thus increasing hardness of the coating.

The microstructure of the coatings was shown to be fully dense columnar structure. As the bias voltage was increased the columns became less pronounced so the columns could not be traced throughout the coating due to the large number of lattice defects and sub-grains. Increased bias voltage was also shown to reduce the grain diameter by up 50%, which should lead to improved mechanical properties. The thickness of the coating is reduced by approximately 15% due to re-sputtering of the growing film as the bias voltage is increased from $U_B = -75$ to -150 V.

Even the coatings deposited with lowest bias voltage ($U_B = -75$ V) were dense and feature clearly defined columnar structure with {110} growth direction as reported by Salagean et al. [2]. Increasing bias voltage to $U_B = -100$ V increases hardness only marginally. The microstructure of the coating is affected by the increased energy of the bombarded ions. It becomes less well defined and the growth direction was noticed to shift towards ⟨111⟩ orientation during film growth. When high bias voltages were used both thick and thin coatings showed {111} texture with a 1 μm thick Nb film still showing mixed {110}/{111} structure. In texture evolution it is well established that when the surface energy is dominant then the preferred orientation is dominated by the most closely packed crystallographic plane [17,18]. In bcc metals such as Nb this is the {110}. Therefore it can be speculated that during deposition at $U_B = -75$ V the surface energy is dominant leading to the development of a {110} texture in both 1 and 3 μm thick films. With increasing bias voltage, i.e. $U_B = -125$ V in the thinner films and $U_B = -100$ V in the thicker films a {111} texture starts to develop. One possible explanation for this is the increased Ar^+ ion bombardment as the bias voltage is increased resulting in re-sputtering of the growing film. The close packed {110} plane has more atoms per unit area than the less densely packed {111} plane. Hence, the chance of re-sputtering an atom in a {110} plane is statistically higher than in a {111} plane. Therefore under conditions of high energy ion bombardment ($U_B < -100$ V) in competition for growth between {110} and {111} oriented grains, the {111} will grow at the expense of {110} oriented grains. The {111} texture in the thicker films (i.e. 3 μm) is stronger the thinner films (1 μm) grown under the same conditions. This would lead one to the conclusion that the starting texture in all films was {110} and the {111} texture developed during growth under conditions of higher energy ion bombardment. Similar changes in texture as coating thickness increased was reported by Ward et al. [5].

The corrosion resistance of the coated mild steel samples is not significantly affected by the increased bias voltage. The samples deposited with $U_B = -125$ V showed the best corrosion resistance and the $U_B = -150$ V the worst. The poor corrosion resistance of the 1Nb $U_B = -150$ V samples can be explained by local de-lamination of the coating during the tests. The reason for this delamination was thought to be excessive internal stresses within the coating and poor adhesion at the interface. The corrosion resistance of the thicker coatings was found to be clearly superior to the thin coatings. In the potentiodynamic polarisation test, the anodic corrosion current densities were up to one order of magnitude lower than with thinner coatings.

The defect density was noted to generally reduce with the increasing bias voltage. However, the difference was not very conclusive. Yet, there was a clear reduction in the number of growth defects with increasing coating thickness. Consequently the {111} textured coatings was found to have fewer defects and therefore potentially an improved corrosion resistance.

5. Conclusions

Intensifying the ion bombardment by increasing the applied bias voltage was found to influence the properties and microstructure of the Nb coatings.

The hardness was increased from 4.5 to 8.0 GPa as the bias voltage was increased from -75 to -150 V. At higher bias voltages (> -100 V) Ar atoms were trapped in the Nb lattice during growth (up to 4.5% at $U_B = -150$ V). In parallel, there was a refinement in the diameter of the columnar grains by up to 50%.

Increased ion bombardment did not significantly influence the corrosion properties of the Nb coatings. The corrosion resistance is generally increased with the bias voltage, yet excessive bombardment ($U_B = -150$ V) was found to lead to poor adhesion and a lover corrosion resistance. The samples with the thicker coatings performed notably better in corrosion tests with anodic corrosion currents up to 1 order of magnitude lower than those of the thinner coatings.

The texture of the coating was found to change from strong {110} toward {111} with increasing Ar^+ ion bombardment. The thinner coatings deposited with high bias voltages showed mixed {110}/{111} texture, whereas in thicker coatings the {111} texture was already dominant at $U_B = -100$V. A reduction in coating thickness was also observed with increasing bias voltage.

References

[1] G.L. Miller, Tantalum and Niobium, Butterworths Scientific, London, 1958.
[2] E.E. Salagean, D.B. Lewis, J.S. Brooks, W.-D. Münz, I. Petrov, J.E. Greene, Surf. Coat. Technol. 82 (1996) 57.

[3] C. Schönjahn, H. Paritong, W.-D. Münz, R.D. Twesten, I. Petrov, J.Vac. Sci. Technol. A 19 (4) (2001) 1392.
[4] J.H. Hsieh, R. Lee, R.A. Erck, G.R. Fenske, Y. Y. Su, M. Marek, R.F. Hochman, Surf. Coat. Technol. 49 (1991) 52.
[5] L.P. Ward, P.K. Datta, Thin Solid Films 272 (1996) 52.
[6] H. Paritong, M. Lembke, D.B. Lewis, W.-D. Münz, Surf. Coat. Technol. 116–119 (1999) 1145.
[7] W.-D. Münz, D. Schulze, F.J.M. Hauzer, Surf. Coat. Technol. 50 (1992) 169.
[8] W.-D. Münz, C. Schönjahn, H. Paritong, I.J. Smith, Le Vide, Science-Technique-Applicatious, Vol. 55. No. 297 (2000) 205.
[9] W.-D. Münz, SVC, 36th Annual Technical Conference Proceedings (1993), 411.
[10] P. Hovsepian, D.B. Lewis, W.-D. Münz, S.B. Lyon, M. Tomlinson, Surf. Coat. Technol. 120–121 (1999) 535.
[11] W.-D. Münz, D.B. Lewis, P.Eh. Hovsepian, C. Schönjahn, A. Ehiasarian, I.J. Smith, Surf. Eng. 17 (2001) 15.
[12] W.-D. Münz, I.J. Smith, D.B. Lewis, S. Creasey, Vacuum 48 (5) (1997) 473.
[13] H.W. Wang, M.M. Stack, S.B. Lyon, P. Hovsepian, W.-D. Münz, Surf. Coat. Technol. 126 (2000) 279.
[14] P.Eh. Hovsepian, D.B. Lewis, W.-D. Münz, Surf. Coat. Technol. 133–134 (2000) 166.
[15] C. Schönjahn, A.P. Ehiasarian, D.B. Lewis, R. New, W.-D. Münz, R.D. Twesten, I. Petrov, J. Vac. Sci. Technol. A 19 (4) (2001) 1415.
[16] D. Rickerby, A.M. Jones, B.A. Bellamy, Surf. Coat. Technol. 37 (1989) 111.
[17] G. Knuyt, C. Quaeyhaegens, J. D'Haen, L. Stals, Thin Solid Films 258 (1995) 159.
[18] J. Pelleg, L.Z. Zevin, S. Lungo, Thin Solid Films 197 (1991) 117.

Available online at www.sciencedirect.com
SCIENCE DIRECT
ELSEVIER
Surface & Coatings Technology 200 (2006) 2731–2737
SURFACE & COATINGS TECHNOLOGY
www.elsevier.com/locate/surfcoat

Microstructure and properties of novel wear and corrosion resistant CrON/NbON nano-scale multilayer coatings

T. Savisalo, D.B. Lewis*, P.Eh. Hovsepian

Materials Research Institute, Sheffield Hallam University, Howard Street, Sheffield S1 1WB United Kingdom

Received 5 July 2004; accepted in revised form 25 January 2005
Available online 22 March 2005

Abstract

CrN/NbN nano-scale multilayer coatings have found use in a number of commercial applications where wear and corrosion resistance determine the service life of the components. To further improve their performance a novel CrON/NbON topcoat has been developed.

The coatings were deposited using an industrial Hauzer HTC 1000/4 UBM-ABS coating machine utilising the Arc Bond Sputtering method where cathodic arc metal ion etching is used to prepare the interface prior to coating deposition by unbalanced magnetron (UBM) sputtering. The oxynitride process was performed in mixture of dry air and argon at bias voltages varying from U_B=−75 V to −120 V at total pressures during deposition from $3.5*10^{-1}$ Pa to $4.9*10^{-1}$ Pa. The thickness of the oxynitride film varied between 1.6 and 2.3 μm, while the total coating thickness varied between 4.6 and 5.3 μm. The XTEM investigation revealed that the microstructure of the oxynitride layer was dense columnar with a pronounced nano-scale multilayer architecture. By X-ray diffraction (XRD), the coatings were identified as crystalline with mixed texture. As the pressure during the oxynitride deposition stage was increased the crystal structure of the top layer became increasingly amorphous/nano-crystalline. An increase in the bias voltage also caused a shift from {100} texture towards {111} texture.

The best performing oxynitride coatings had similar low sliding wear rates as the reference standard coating without affecting their corrosion resistance. However, the wear rate against a 100Cr6 counter body was reduced by a factor of 10 and the friction coefficient from 0.57 to 0.49. The wear rate of both the coating and the counter body was reduced as the bias voltage was increased, while increasing the deposition pressure had adverse effects on the tribological properties. The wear behaviour can be related to the special nano-scale multilayer structure of the oxynitride layer as coating with best tribological properties exhibits a pronounced nano-scale multilayer structure parallel to the coating surface.
© 2005 Elsevier B.V. All rights reserved.

Keywords: CrON/NbON nano-scale multilayer coatings; Corrosion and wear resistance; Unbalanced magnetron sputtering; Texture

1. Introduction

CrN/NbN nano-scale multilayer coatings have been developed to withstand wear and corrosion. These coatings show good corrosion and wear resistance even in very aggressive conditions [1,2]. Metal ion pretreatment in ABS (Arc Bond Sputtering) process has been shown to further enhance adhesion and corrosion resistance [3].

Oxynitride coatings have been studied due to their low electrical resistivity, biocompatibility, oxidation resistance as well as use in solar devices. Most work focuses on TiNO coatings [4–6], though CrNO films have also been studied [7,8]. TiAlN topcoats are in commercial use providing good oxidation resistance and low friction in dry high-speed cutting [9]. The structure of the oxynitride was reported to change from crystalline (NaCl like structure, where O replaces N in the lattice) to an amorphous/nanocrystalline like structure as the oxygen content increases [6,10]. Increasing oxygen content also increases electrical resistivity considerably [4]. Oxynitride coatings can be deposited by sputtering in argon–dry air atmosphere (ca. 70% N–27%O).

PVD coatings deposited on steel generally suffer from pitting corrosion at or near localised defects enhanced by

* Corresponding author.
E-mail address: drbrianlewis@aol.com (D.B. Lewis).

0257-8972/$ - see front matter © 2005 Elsevier B.V. All rights reserved.
doi:10.1016/j.surfcoat.2005.01.107

galvanic effects between cathodic coating and anodic substrate [11,12]. As the electrical conductivity of the oxynitride coatings is relatively low the galvanic effect is therefore reduced. An amorphous like structure is thought to be beneficial in terms of improved corrosion resistance as grain growth is disrupted, potentially reduces the effects of growth defects and the absence of grain boundaries reduces the pathways for corrosion. Koerner et al. reported high wetting angle for high oxygen content oxynitride coatings [5] that could reduce water penetration through pinholes. Also, Wierzchoñ et al. reported significant improvement of corrosion resistance with oxynitriding compared to nitriding of electrodeposited Cr coatings [13]. Excessive oxygen content may however lead to embrittlement of the coating [6].

An oxynitride topcoat was applied to the CrN/NbN nano-scale multilayer coatings in order to enhance the coatings tribological properties. The effects on the tribological properties and the structure of the topcoat were investigated with selected deposition parameters in order to gain understanding of the process, structure and growth development of these novel coatings.

2. Experimental details

2.1. Coating deposition

The coatings were deposited on M2 high speed steel in the fully hardened and tempered condition (HV~800), mild steel and stainless steel substrates that were mechanically ground and polished with 1 μm diamond paste to attain a surface finish of R_a=0.05 μm. Prior to deposition the samples were cleaned using an automated cleaning line (manufactured by UCM) consisting of a multistage ultrasonically agitated cleaning and rinsing process. Coatings were deposited using an industrial sized Hauzer HTC 1000/4 UBM-ABS coating machine utilising the Arc Bond Sputtering method where cathodic arc metal ion etching is used to prepare the interface prior to coating deposition by Unbalanced Magnetron Sputtering. For these coatings 4 targets (2 Cr and 2 Nb) were used, arranged in a closed field configuration. The substrates were subjected to 3-fold rotation to ensure uniform coating. Cr was used as etching ion for all coatings. The coatings consisted of three layers. First a 0.3 μm thick CrN base layer was deposited to provide improved adhesion through a gradient in hardness between the ultra-hard nano-scale multilayer coating and the relatively soft metal substrate. This was followed by a 2.5 μm CrN/NbN nano-scale multilayer layer with a 3.5 nm period. The base layer and the CrN/NbN nano-scale multilayer coatings were deposited at a bias voltage U_B=−75 V at total pressures P_T=3.8*10^{-1} Pa and 3.6*10^{-1} Pa, respectively. The oxynitride process step was performed in a mixture of dry air and argon. To establish the effect of ion bombardment on the coating structure and properties, the bias voltage was varied from U_B=−75 V to U_B=−120 V while retaining the same total pressure during deposition (3.5*10^{-1} Pa). The effects of the changes in the total deposition pressure, P_T was investigated keeping U_B=−100 V and varying the total pressure, P_T from 3.5*10^{-1} Pa to 4.9*10^{-1} Pa. A reference coating was also prepared in which the CrN/NbN layer was thicker while keeping the same total coating time. The deposition parameters are summarised in Table 1.

2.2. Coating characterisation

The hardness of the coatings were characterised using Knoop hardness measurement (Mitutoyo MVK-G1, 25 g normal load). The CSM Revetest was used to perform a scratch test. A CSM Tribotest Pin-On-Disk machine was used to determine the wear properties of coatings, which had been deposited on M2 high-speed steel substrates. Both Al_2O_3 and 100Cr6 balls were used with 10 cm/s linear speed and 5 N normal force. The wear rate of the coatings were measured after 12,000 laps with the100Cr6 ball counter body and 60,000 laps with the Al_2O_3 ball counter body, resulting in total distances travelled of 1.0 and 5.0 km, respectively. The thickness of the coatings was determined using a ball cratering method.

The electrochemical corrosion measurements were performed in 3% NaCl solution using a 3-electrode cell with a Saturated Calomel Electrode (SCE) reference electrode. The polarisation measurements were performed with an EG&G Model 263A potentiostat from −1000 mV to +1000 mV using a scan rate of 0.5 mV/s. Before the polarisation measurements the samples were cleaned cathodically at −1.5 V for 100 s and then allowed to equilibrate at an Open Circuit Potential (OPC) for 20 min.

The microstructure was investigated using a Philips CM20 TEM for the cross-sectional transmission electron

Table 1
Deposition parameters

	Ion etching	CrN base layer	CrN/NbN	Oxynitride	
Reference	20 min Cr^+ etch,	30 min, 2×5 kW,	150 min	N/A	
−75 V	1*10^{-5} Pa,	3.8*10^{-5} Pa,	90 min,	U_B=−75 V, 3.5*10^{-5} Pa	60 min, 2×5 kW+2×10 kW
−100 V	U_B=−1200 V	U_B=−75 V	3.6*10^{-5} Pa,	U_B=−100 V, 3.5*10^{-5} Pa	
−120 V			U_B=−75 V	U_B=−120 V, 3.5*10^{-5} Pa	
−100 V 4.1				U_B=−100 V, 4.1*10^{-5} Pa	
−100 V 4.9				U_B=−100 V, 4.9*10^{-5} Pa	

microscopy (XTEM). A Philips PW1820 was used for X-ray diffraction (XRD) measurements. The measurements were performed using both Bragg-Brentano and 1° glancing angle geometries.

3. Results and discussion

The mechanical properties of the coatings are summarised in Table 2. The total thickness of the coatings varied from 4.8 μm for the reference coating to 5.3 μm for the coating deposited at U_B=−75 V, P_T=3.5*10^{-1} Pa. The oxynitride coatings were generally thicker than the reference coating indicating a lower density in the oxynitride layer. As the bias voltage was increased the thickness decreased slightly. This was probably due to increased re-sputtering on the substrates and densification of the coating resulting from an increased ion bombardment. As the deposition pressure was increased the thickness of the oxynitride layer decreased from 2.2 μm at P_T=3.5*10^{-1} Pa to 1.6 μm at P_T=4.9*10^{-1} Pa. This may be due to the reduced sputtering rate and hence lower deposition rate resulting from increased target poisoning. The top surface of the oxynitride coatings deposited with low bias voltages or high pressures appeared rough and porous when examined by optical microscopy (Fig. 1). The surface roughness decreases with increasing bias voltage but increases with increasing deposition pressure. The coating deposited at a bias voltage U_B=−120 V coating is especially smooth when compared to the other coatings. This effect has been shown in earlier work to be as a result of a reduction in the number of growth defects with increasing bias voltage [15]. In addition increasing the pressure from P_T=3.5*10^{-1} Pa to P_T=4.9*10^{-1} Pa results in a change in colour from one of metallic grey towards black thus, reflecting a change from a mainly nitride phase to an oxynitride phase. The hardness values show that all of the coatings are very hard with H_k=2500–3200. The hardness of the oxynitride coatings was generally slightly higher than that of the reference coating. The adhesion was ca. L_c=55 N for all coatings which is understandable since they share the same pretreatment and base layers.

The cross-sectional transmission electron microscope (XTEM) investigation shows that at the lower deposition pressures the oxynitride layer exhibits a dense columnar microstructure with pronounced nano-scale multilayer architecture. The columnar structure of the underlying CrN/NbN nano-scale multilayer coating is not interrupted at the interface region between CrN/NbN and the oxynitride layers but the interface can be easily defined (Fig. 2). The nano-scale multilayer layers are clearly visible in the oxynitride layer in the coatings deposited at U_B=−75 V and U_B=−120 V using a total pressure P_T=3.5*10^{-1} Pa (Fig. 3a and b) and in the coating deposited at bias voltage U_B=−75 V (Fig. 3a) the columnar grains are well defined and have dome-like tops. The nano-scale multilayer layers conform to the curvature of the grains and are therefore not parallel to the surface of the coating. Low-density areas are also observed at column boundary regions. Increasing bias voltage to U_B=−120 V (Fig. 3b) gives a smooth and continuous nano-scale multilayer that is parallel to the coating surface. The structure is still columnar, yet individual grain boundaries are almost indistinguishable in the XTEM images.

X-ray diffraction analysis (XRD) (Fig. 4a and b) showed the coatings to be crystalline in nature with a mixed texture. The only phase identifiable in the Bragg-Brentano and glancing angle scans was fcc CrN/NbN. This indicates that oxygen is mainly absorbed in the lattice replacing the nitrogen at the octahedral site in the NaCl lattice as presented by Wilhartitz et al. [7]. An increase in the bias voltage also caused a shift from a {100} texture towards a {111} texture (Fig. 4a). This change from a {100} to a {111} texture has been observed previously [2,15,16] and follows the same trend as that observed by Kadlec et al. [17]. The main reflections exhibit clear satellite peaks (ca. 2° smaller angle than the main peaks) that indicates the nano-scale multilayer nature of the coating. This peak is clearly present for all other coatings except that deposited at P_T=4.9*10^{-1} Pa. There is also a slight peak shift toward lower 2θ angles as the bias voltage is increased. This can be associated with an increase in lattice strain indicating an increase in residual compressive stress in the plane parallel to the coating surface as a result of a more intense ion bombardment at higher bias voltages. As the pressure during the oxynitride deposition stage was increased the crystal structure of the top layer became increasingly amorphous/nano-crystalline (Fig. 4b),

Table 2
Properties of the coatings

	Coating thickness (μm)	Oxynitride thickness (μm)	Adhesion L_c on HSS (N)	Hardness (H_{k25g})	Al_2O_3 ball		100Cr6 ball	
					Friction coefficient	Wear rate (10^{-16} m^2/N)	Friction coefficient	Wear rate of counter body (10^{-17} m^2/N)
Reference	4.8		55	2900	0.69	23	0.57	16
−75 V	5.3	2.3	53	3100	0.95	49	0.69	30
−100 V	5.2	2.2	52	3200	0.72	30	0.49	7.5
−120 V	5.2	2.2	56	3000	0.71	30	0.51	1.0
−100 V 4.1	4.8	1.8	58	3000	0.75	30	0.56	4.4
−100 V 4.9	4.6	1.6	54	2500	0.76	37	0.58	4.4

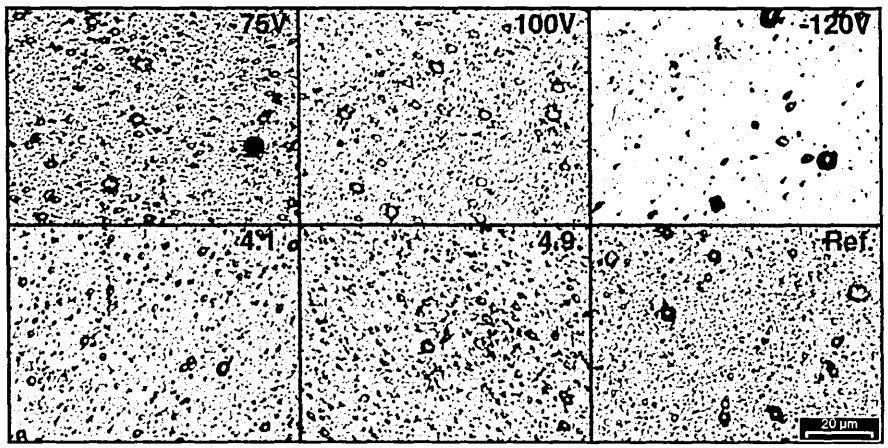

Fig. 1. The surface morphology of the oxynitride coatings.

as shown by diffuse peak at 2θ ca. 28° present in the coating deposited at a bias voltage U_B=−100 V using a total chamber pressure P_T=4.9*10^{-1} Pa. Furthermore, the main Bragg reflections {111} and {200} did not exhibit satellite peaks indicating some loss of the nano-scale multilayer architecture. At the same bias voltage of U_B=−100 V increasing the total pressure, P_T from 3.5*10^{-1} Pa to 4.9*10^{-1} Pa resulted in a change from a {111} to a {100} texture together with a slight peak shift toward higher 2θ angles. This is because at the same bias voltage (U_B=−100 V) increasing the total gas pressure P_T from 3.5*10^{-1} Pa to 4.9*10^{-1} Pa decreased the energy of the bombarding ions and therefore has a similar influence on residual stress and texture formation as reducing the bias voltage [16]. Therefore the texture developed at P_T=4.9*10^{-1} Pa at a bias voltage U_B=−100 V is similar to that developed at U_B=−75 V using a total pressure P_T=3.5*10^{-1} Pa, that is, a {100} texture in both cases.

The results of pin-on-disk tribological tests can be seen in Fig. 5 and Table 2. The friction coefficient against alumina ball was roughly the same with all coatings (ca. 0.7), only the coating deposited at U_B=−75 V showed higher value (0.95). In comparison the friction coefficients for the same coatings were with the exception of the coating deposited at U_B=−75

Fig. 2. Cross-section of the U_B=−75 V coating (XTEM, bright field) showing columnar structure throughout the coating.

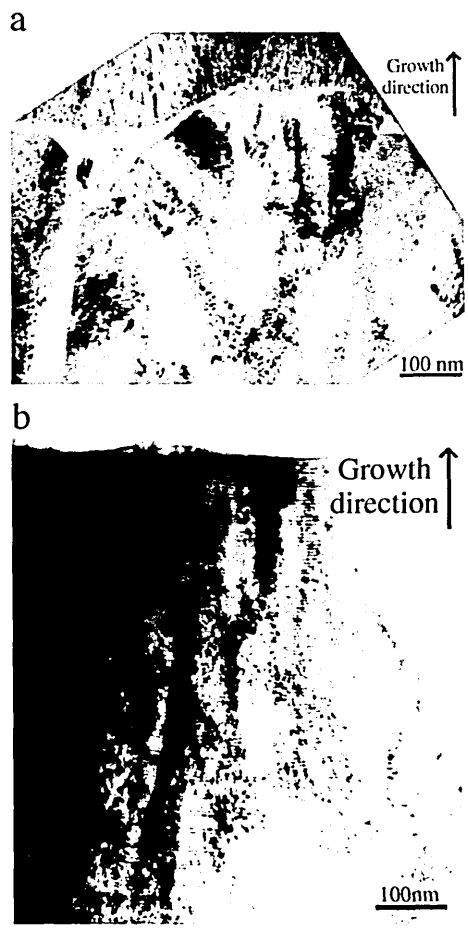

Fig. 3. Superlattice structure in oxynitride layer deposited at (a) U_B=−75 V and (b) U_B=−120 V (XTEM).

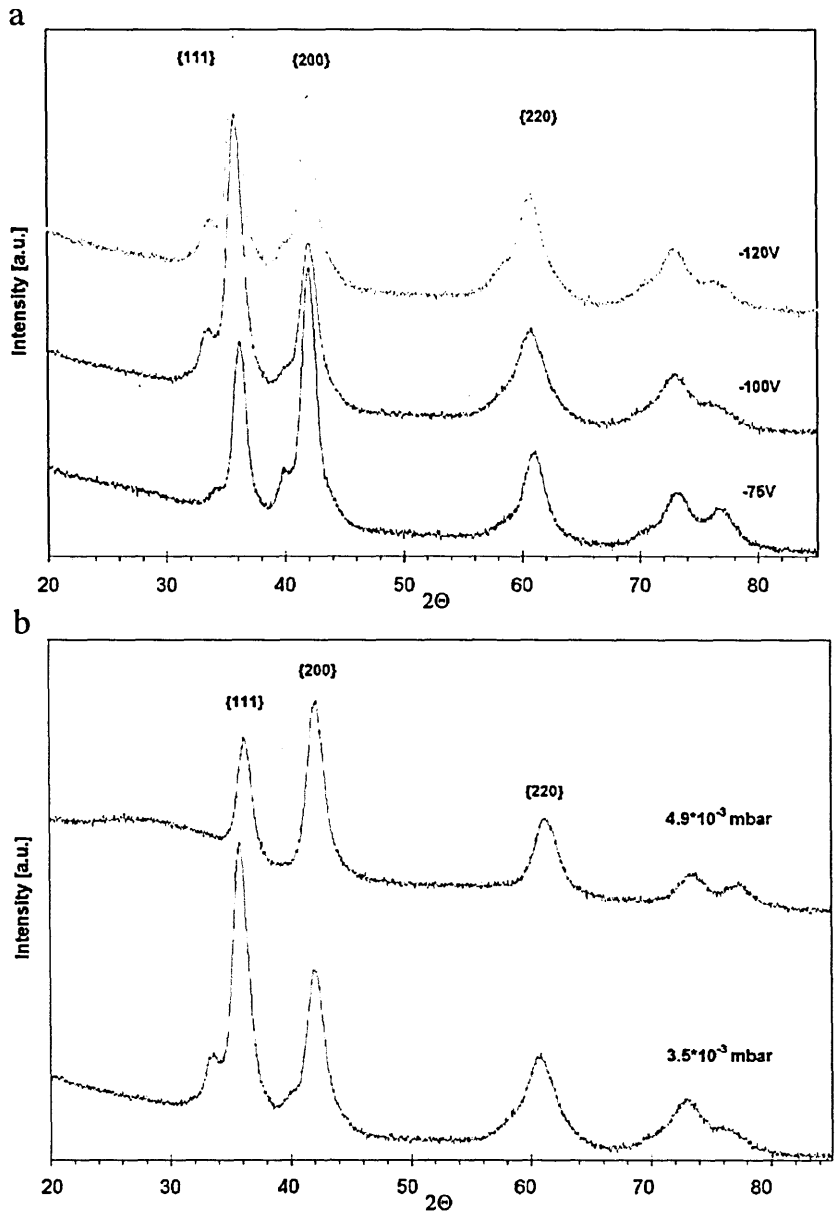

Fig. 4. XRD of the oxynitride topcoat at 1° glancing angle configuration. (a) Effect of bias voltage and (b) effect of total coating pressure.

V always systematically lower than that of the reference coating (0.57) when 100Cr6 ball was used as the counter body. As the sliding contact of the film against the counter body (Al_2O_3) is oxide against oxide higher friction coefficients than the same coating in sliding contact against a 100Cr6 ball is understandable because it is well known that similar materials e.g. oxides against oxides, metals against metals exhibit higher friction coefficients than do dissimilar materials e.g. oxides against metals. The coating deposited at a bias voltage of −75 V exhibited a slightly higher friction (0.69) whereas the coating deposited at a bias voltage of −100 V exhibited the lowest friction coefficient (0.49).

The wear rate of the oxynitride coating against alumina ball was always systematically higher than that of the reference coating against an alumina ball, as the sliding contact of the film against the counter body (Al_2O_3) is oxide against oxide. This is understandable because the friction coefficients of the oxynitride coating against an alumina ball are higher than that of the reference coating against an alumina ball and it is well known that increases in the friction coefficient in general result in increases in sliding wear rate. The wear rate of the oxynitride coating deposited at a bias voltage of −75 V against an alumina ball was double that of the reference coating with a wear rate of $37*10^{-16}$ m^2/N compared with $23*10^{-16}$ m^2/N. In contrast, however, the increase in wear rate in coatings deposited at U_B=−100 V and U_B=−120 V coating was only about 30%. At a constant bias voltage of −100 V the wear rate increased with increasing total pressure P_T. The higher wear rate at the lower bias voltages and higher chamber pressures are

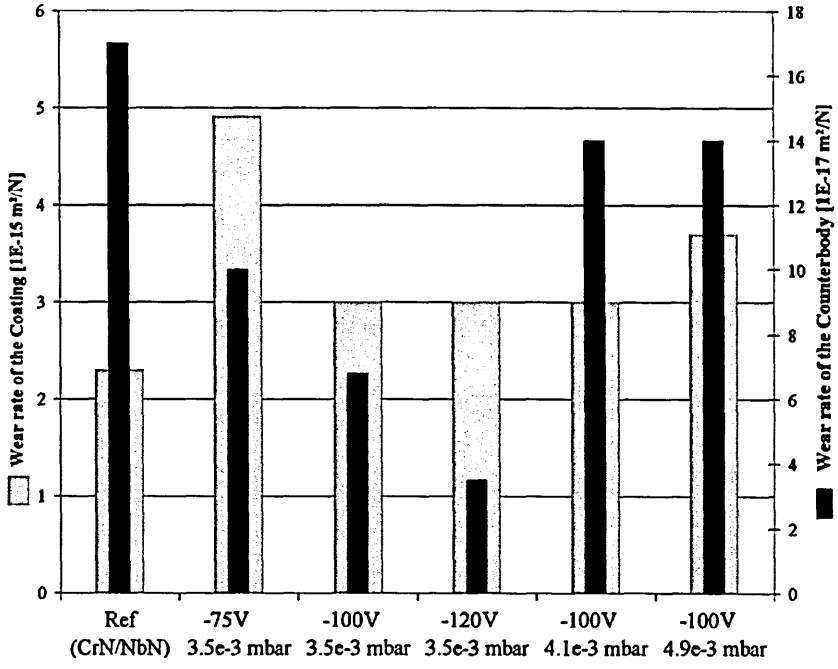

Fig. 5. Wear rates of the oxynitride coatings against alumina ball and wear rate of 100Cr6 counter body in Pin-on-Disk wear test.

probably due to the rough porous nature of the film deposited under these conditions where the intensity of the ion bombardment is less. The wear rate of the coating against 100Cr6 ball counter body could not be accurately measured due to material transfer to the wear track. The wear rate of the counter body however reduces to one fifth (compared with the reference coating) when topcoat with U_B=−120 V is applied. Furthermore, the wear of the counterpart was reduced as the bias voltage was increased. The high-pressure coatings, however, showed an increased counter body wear due to rapid wear of the topcoat. Interestingly, the wear of the counterpart did not show clear relationship to friction coefficient. It is suggested, however, that the low wear rate combined with low counter body wear is thought to be due to nano-scale multilayer nature of the topcoat of the coatings deposited at higher bias voltages where the nano-scale multilayer is parallel to the coating surface and wear can occur along the nano-scale multilayer interfaces. This method of wear was presented by Luo et al. [14] after detailed analysis of the wear mechanisms in nano-scale multilayer coatings. The coatings deposited at higher bias voltages have a strong clear nano-scale multilayer that is continuous, smooth and parallel to the surface as shown by the XTEM investigation. In this case the coating can break along the nano-scale multilayer (period ca. 4.5 nm) boundaries resulting in low abrasive wear of the counter

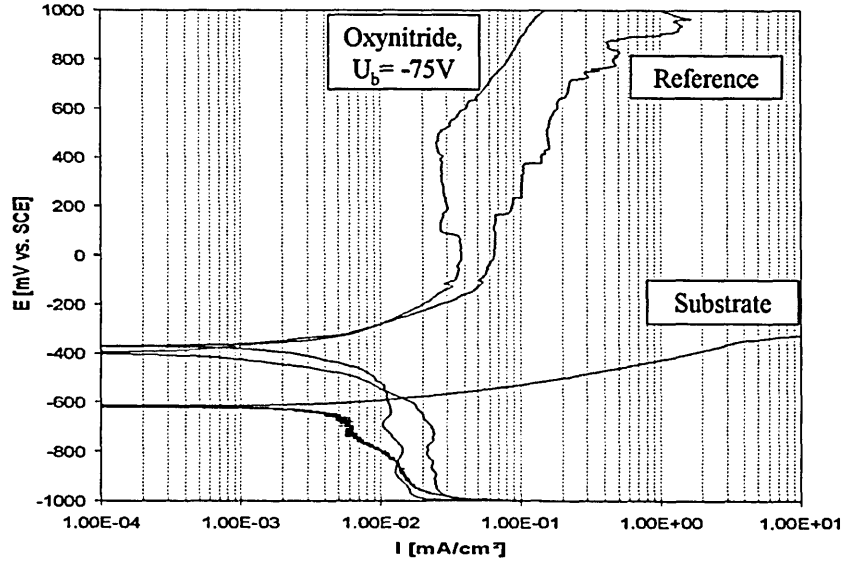

Fig. 6. The results of the potentiodynamic polarisation corrosion test (coated mild steel in 3% NaCl solution).

body. Thus, the low counter body wear rate can be related to the orientation of the nano-scale multilayer relative to the specimen surface.

The CrN/NbN coatings have excellent corrosion resistance, which enables the use of these coatings in corrosive environments even in conjunction with low alloy substrate materials. This can be seen from the results of the potentiodynamic polarisation corrosion tests in Fig. 6. The oxynitride coatings showed an improvement over the already impressive corrosion performance of the reference coating. In the anodic region the coating is passive to up to +600 mV and the corrosion current can be related to local corrosion at defect locations. The reference coating did not exhibit such 'passive' behaviour. After +600 mV the coating is attacked by preferential dissolution of Cr.

4. Conclusions

- An oxynitride topcoat for the CrN/NbN nano-scale multilayer coating was successfully deposited using an industrial sized Hauzer HTC 1000/4 UBM-ABS coating machine in an argon–dry air atmosphere.
- The deposition rate was comparable to that of the CrN/NbN nano-scale multilayer coating but decreased as the deposition pressure was increased.
- The microstructure of the coating was similar to the CrN/NbN and the oxygen is thought to mainly replace the nitrogen at the octahedral sites in the NaCl type lattice.
- At lower bias voltages the microstructure was clearly columnar, while at higher bias voltages the coatings densified and the column boundaries were less distinct. The nano-scale multilayer architecture was also retained.
- At the lower bias voltage ⟨100⟩ growth direction was dominant leading to faceted grains with dome-like tops. The nano-scale multilayer conformed to the curvature of the grains leading to nano-scale multilayer architecture that was not parallel to the surface. At U_B=−120 V the dominating growth direction in the oxynitride was ⟨111⟩ and the nano-scale multilayer architecture was continuous, smooth and parallel to the surface.
- The oxynitride topcoat has been shown to be beneficial to the tribological properties of CrN/NbN nano-scale multilayer wear and corrosion resistant coatings. The topcoat gives clear reduction in friction coefficient against 100Cr6 steel. Yet more importantly the wear of the counter-sliding surface is reduced by 80%. This is significant since the coated parts are commonly used in combination with uncoated metal, when the wear of the counter-surface may be significant, thus often requiring the coating on counter parts when it would not otherwise be necessary.
- A clear improvement in the corrosion resistance of the coatings was also observed.

References

[1] P. Hovsepian, D.B. Lewis, W.-D. Münz, S.B. Lyon, M. Tomlinson, Surf. Coat. Technol. 120–121 (1999) 535.
[2] W.-D. Münz, D.B. Lewis, P.Eh. Hovsepian, C. Schönjahn, A. Ehiasarian, I.J. Smith, Surf. Eng. 17 (2001) 15.
[3] C. Schönjahn, H. Paritong, W.-D. Münz, R.D. Twesten, I. Petrov, J. Vac. Sci. Technol., A 19 (4) (2001) 1392.
[4] E. Alves, A.R. Ramos, N.P. Barradas, F. Vaz, P. Cerqueira, L. Rebouta, U. Kreissig, Surf. Coat. Technol. 180–181 (2004) 372.
[5] R.J. Koerner, L.A. Butterwoth, I.V. Mayer, R. Dasbach, H.J. Buucher, Biomaterials 23 (2002) 2835.
[6] J. Propst, U. Gbureck, R. Thull, Surf. Coat. Technol. 148 (2001) 226.
[7] P. Wilharititz, S. Dreer, P. Ramminger, Thin Solid Films 447 (2004) 289.
[8] St. Collard, H. Kupfer, G. Hecht, W. Hoyer, H. Mossaoui, Surf. Coat. Technol. 122 (1999) 181.
[9] M. Lembke, D.B. Lewis, W.-D. Münz, J.M. Titchmarch, Surf. Eng. (2001) 17.
[10] T. Suzuki, H. Saito, M. Hirai, H. Suematsu, W. Jiang, K. Yatsui, Thin Solid Films 407 (2002) 118.
[11] W.-D. Münz, I.J. Smith, D.B. Lewis, S. Creasey, Vacuum 48 (5) (1997) 473.
[12] H.W. Wang, M.M. Stack, S.B. Lyon, P. Hovsepian, W.-D. Münz, Surf. Coat. Technol. 126 (2000) 279.
[13] T. Wierzchoń, I. Ulbin-Pokorska, K. Sikorski, Surf. Coat. Technol. 130 (2000) 274.
[14] Q. Luo, W.M. Rainforth, W.-D. Münz, Wear 225–229 (1999) 74.
[15] P.Eh. Hovsepian, D.B. Lewis, W.-D. Munz, Surf. Coat. Technol. 133–134 (2000) 166.
[16] D.B. Lewis, Q. Luo, P.Eh. Hovsepian, W.-D. Munz, Surf. Coat. Technol. 184 (2–3) (2004) 166.
[17] S. Kadlec, J. Musil, V. Valvoda, W.-D. Munz, H. Petersein, J. Schroeder, Vacuum 41 (1990) 2238.

Available online at www.sciencedirect.com
ScienceDirect
Surface & Coatings Technology 202 (2008) 1661 – 1667
SURFACE & COATINGS TECHNOLOGY
www.elsevier.com/locate/surfcoat

Structure of duplex CrN/NbN coatings and their performance against corrosion and wear

T. Savisalo [a,*], D.B. Lewis [a], Q. Luo [a], M. Bolton [b], P. Hovsepian [a]

[a] *Sheffield Hallam University, Materials Research Institute, Howard St, S1 1WB, Sheffield, United Kingdom*
[b] *Eltro (GB) Ltd. Unit B4 Armstrong Mall, Southwood Business Park, Farnborough, Hampshire, GU14 0NR, United Kingdom*

Received 29 March 2007; accepted in revised form 16 July 2007
Available online 27 July 2007

Abstract

In tribological applications the coating-substrate combination can be considered as a system, since both greatly influence the properties of that affect the tribological performance. Further, it is often desirable that both high wear resistance and corrosion resistance can be achieved even when low cost and easily machineable substrate materials are considered. Duplex surface treatment combining pulse plasma nitriding and PVD coating can provide solution for excellent wear and corrosion resistance for low alloy and constructional steels.

In this work three different pulse plasma nitriding processes were carried out prior to the CrN/NbN PVD coating to attain high surface hardness and enhanced load bearing behaviour for S154 high strength construction steel. The phase composition of the compound layer, formed in the nitriding process, was found to greatly affect the tribological properties of the duplex system. The compound layer with high amount of ε-phase contributed to superior corrosion and wear resistance, whereas the ductile γ'-phase compound layer provided better impact resistance and enhanced. The best duplex treated S154 samples had wear resistance comparable to that of similarly coated HSS. The corrosion resistance was also improved by duplex process. If anodic current at +500 mV vs. SCE is considered as criteria, the best system has almost 3 orders of magnitude lower corrosion current than with the PVD coating alone.
© 2007 Elsevier B.V. All rights reserved.

Keywords: Duplex; PVD; CrN/NbN; Nitriding; Corrosion; Wear

1. Introduction

PVD coatings have been shown to be very valuable in surface engineering providing a variety of desirable surface properties such as appearance, high wear resistance, low friction and good corrosion resistance [1,2]. In tribological applications coating-substrate combination should be considered as a composite since both greatly affect physical properties of the system. Very low wear rates have been reported with coated hard steels such as high speed steel [1,3,4] as these highly stressed hard coatings need strong support. If the load bearing capacity of the substrate is exceeded the wear is greatly increased [5,6]. Further, good corrosion resistance has been achieved with coated stainless steels [7–9]. In tribological applications both of these properties should be achieved simultaneously in combination with low price and easily machineable substrate material. Ductility of the substrate may also be required as components are commonly required to withstand impacts and deformation.

Nitriding is a commonly used surface treatment method to improve surface hardness and wear resistance of steels. The relatively inert white layer can also provide improved corrosion performance [10]. Lately nitriding has been used in combination with PVD coatings (duplex coatings) with promising results [5,10–16]. Nitriding process can be done prior to PVD process with any conventional method or in conjunction with PVD process with low pressure plasma nitriding. Nitriding provides increased surface hardness of HV=1000+ providing the support that is required by the coating as well as reducing the stress gradients at the interfaces with the PVD coating (HV=3500+). The compound layer (Fe_4N or Fe_3N) has been regarded to be detrimental to adhesion and thus avoided or removed mechanically [10,14], yet it has been shown in some instances to improve wear resistance [5,11,17].

* Corresponding author. Tel.: +358 40 521 6084.
E-mail address: tuukka.savisalo@savcor.com (T. Savisalo).

0257-8972/$ - see front matter © 2007 Elsevier B.V. All rights reserved.
doi:10.1016/j.surfcoat.2007.07.024

CrN/NbN superlattice coatings have been developed to withstand wear and corrosion. These coatings show good corrosion and wear resistance even in very aggressive conditions [1,4]. Metal ion pre-treatment in ABS (Arc Bond Sputtering) process has been shown to enhance adhesion and corrosion resistance further. Cr ion etching has been shown to provide optimal adhesion while Nb ions may be used for enhanced corrosion performance [3,4,8,18,19].

In this paper novel duplex nitriding-PVD CrN/NbN superlattice system is introduced and characterised. Microstuctural analysis are presented and their effects to mechanical and corrosion properties discussed.

2. Experimental

The coatings were deposited on ground and polished (R_a=0.05 μm) S154 steel and High Speed Steel (HSS) disks with 30 mm diameter. S154 is low alloy, high strength construction steel, with good machineability and weldability (composition: C 0.35, Si 0.3, Mn 0.6, Cr 0.7, Mo 0.6, Ni 2.5, similar to AISI 4340). The HSS samples were used as a reference and were not nitrided. The nitriding was done in a commercial low-pressure pulse plasma nitriding process by Eltro Ltd., UK. Three different nitriding parameter sets were used. The atmosphere during the process was 3:1 hydrogen/nitrogen gas mixture. Sample 1 was nitrided for 6 h in 520 °C (process 1), sample 2 for 3 h in 480 °C continuing further with 14 h in 520 °C (process 2), and sample 3 for 40 h in 530 °C (process 3). The main advantage of pulsed plasma process vs. plasma nitriding is improved process control through minimised arcing and more uniform heat distribution. Prior to coating a porous surface layer was removed with light mechanical polishing after which the samples were cleaned on an automated cleaning line comprised of a series of ten ultrasonically agitated cleaning and rinsing baths and a vacuum drier.

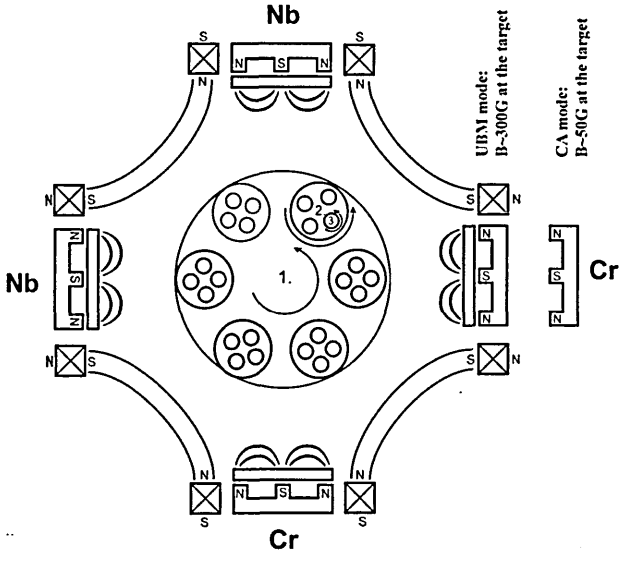

Fig. 1. Schematic diagram of the PVD coating machine setup.

Table 1
Coating deposition parameters

Nitriding process (3:1 hydrogen/ nitrogen atmosphere)	Sample 1 (170 μm case depth)6 h @ 520 °C	Sample 2(290 μm case depth)3 h @ 480 °C followed by 14 h @ 520 °C	Sample 3(400 μm case depth)40 h @ 530 °C
Polishing & cleaning			
Pump-down and heating:	400 °C with pressure $<7*10^{-5}$ mbar		
Cr^+ etching(20 min)	Arc current: I=100A, Bias voltage: U_b=−1200 V Pressure: $p=1*10^{-3}$ mbar		
CrN(30 min)	Power: 2 Cr targets with 5 kW Bias voltage: U_b=−75 V Pressure: $p=3.8*10^{-3}$ mbar		
CrN/NbN(150 min)	Power: 2 Cr targets with 5 kW and 2 Nb targets with 10 kW Bias voltage: U_b=−120 V Pressure: $p=3.6*10^{-3}$ mbar Cr: 2*5 kW, Nb: 2*10 kW		

The coatings were deposited at 450 °C using industrial sized multi-target HTC 1000-4 ABS combined cathodic arc/unbalanced magnetron sputtering (UBM) coating system, manufactured by Hauzer Techno Coatings BV. The coater is a four cathode drum type batch coating machine with the cathodes arranged in a closed field configuration. The coatings were done using configuration with two niobium and two chromium targets arranged as shown in Fig. 1. The samples were subjected to 3 fold rotation in X–Y plane during deposition, which ensures uniform coating thickness even for three dimensional parts. The process consisted of the following steps: heating and target cleaning, cathodic arc Cr ion etching using high bias voltage, UBM deposited CrN base layer and UBM deposited CrN/NbN nanostructured layer with lattice period of about 3 nm. The parameters used during the coating deposition are presented in more detail in Table 1. The properties and the structure of the coating have been studied in detail by Hovsepian et al. [8,20].

2.1. Coating characterisation

The mechanical properties of the samples were characterised using a series of analytical techniques. CSEM Revetest was used to measure adhesion (critical load, L_c), Mitutoyo MVK-G1 for the hardness measurements of the coating (H_k,25 g normal load) and CSEM pin-on-disk tribometer for measuring the sliding wear rate. For the sliding wear test Al_2O_3 ball was used at 5 N load and 10 cm/s linear speed. The wear was measured after 60 k laps. Impact tests were performed using a CemeCon impact tester using 350 N load with Ø6 mm 100Cr6 ball. Hardness-depth profiles of the nitrided samples were generated from a polished cross-sections using Mitutoyo MVK-G1 hardness tester with Vickers diamond tip (H_v,25 g normal load).

Potentiodynamic polarisation measurements were performed in 3% NaCl solution using a 3-electrode cell with a Saturated

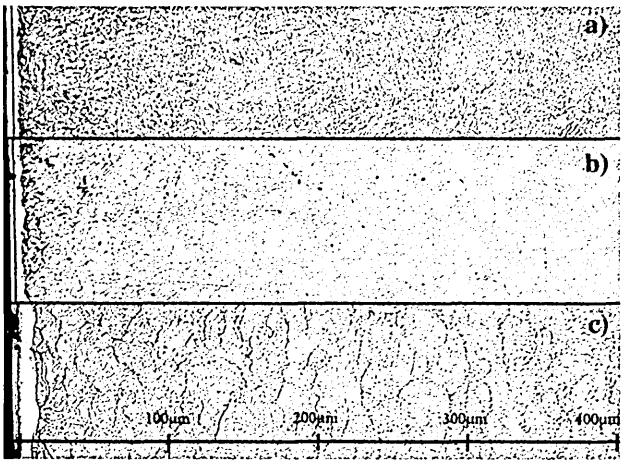

Fig. 2. a–c Etched cross-sections of duplex treated coatings a) sample 1 (b) sample 2 c) sample 3.

Calomel Reference Electrode (SCE) using on ACM Gill AC potentiostat over a potential range of ±1000 mV vs. SCE at scan rate of 0.5 mV/s. Prior to polarisation measurements samples were cleaned cathodically at −1.5 V for 100 s and then allowed to equilibrate at Open Circuit Potential (OPC) for 40 min.

Microstructure was analysed using XRD (Philips PW1820). Glancing angle (1°) and Bragg-Brentano scans were performed prior coating deposition to characterise the top layer of nitrided substrates. Cross sections and the impact craters were investigated using optical microscope and Philips XL40 SEM.

3. Results

The polished and etched cross sections of the coatings can be seen in the Fig. 2. The nitriding case depths were determined to be 170 µm, 290 µm and 400 µm with samples 1, 2 and 3 respectively The coating thickness was about 4 µm consisting of ~0.5 µm CrN base layer and about 3.5 µm CrN/NbN superlattice. The hardness of the coating was roughly constant with all samples, HK_{25g}=3000. The compound layer is also visible in the images with thickness varying from ~5 µm with sample 1 (170 µm) to ~15 µm with sample 3 (400 µm). The nitriding effect can be seen up to a depth of 500 µm with sample 3. The cross section micrographs showed no instability of the compound layer during the coating process (ie. black layer).

Hardness-depth profile (Hv_{25g}) of the nitrided zone can be seen in Fig. 3. The open markers indicate the measurements done from the surface, while the others are from the cross section. The highest surface hardness was measured with sample 1 (HV_{25g}=890), samples 2 and 3 being somewhat softer at HV_{25g}=790 and HV_{25g}=530, respectively. All of these are notably higher that bulk hardness of HV=320. After the compound layer (10 µm) up to the depth of about 200 µm the highest hardness was measured from sample 2. The hardness 100 µm bellow the surface was measured to be from 480 (Sample 3) to 540 (Sample 2) Sample 3 has the hardness of HV_{25g}=400+ up to the depth of 400 µm while the samples 1 and 2 retain the same hardness to the depths of 160 µm and 240 µm respectively.

The micrographs of the impact craters after 1 million impacts can be seen in Fig. 4. Sample 1 has the largest impact crater with diameter of 495 µm. The coating is fully intact yet there are number of circular cracks clearly visible near the edge of the crater. The diameter of the impact crater of sample 2 was measured to be 475 µm. It also has some visible cracks around the edge of the crater yet not to the same extent as sample 1. The sample 3 showed excellent impact resistance with the smallest impact crater (d=460 µm) and shows no sign of cracks or delamination. The results can be explained by the previous results of microstructure and hardness measurements as the ductile γ' phase compound layer can deform under high

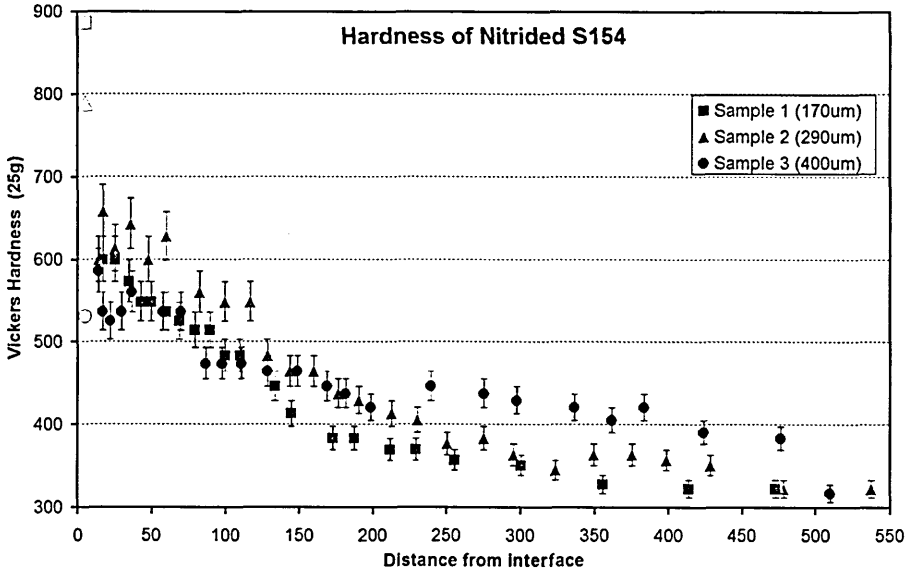

Fig. 3. Hardness-depth profile of the nitrided S154 steel samples.

Fig. 4. a-c Impact craters of duplex treated samples a) sample 1 (0=495 pm) b) sample 2 (0=475 pm) c) sample 3 (0=460 pm) after 1* 106 impacts at 350 N.

pressure while the brittle £ phase fractures. The higher case depth on the other hand provides better support for these high loads as indicated by the crater size.

Sample 3 also had the highest critical load values in scratch test (Lc=60 N). Sample 2 had critical load of 45 N and sample 1 had 35 N. The coated HSS sample had critical load of 45 N, while the coating on the un-nitrided S154 showed failures at a normal load of mere 20 N. The Fig. 5 shows SEM image and EDS map of a typical failure on the samples 1 and 2 with brittle type fracture going through compound layer and the coating.

The calculated sliding wear coefficients of the coated samples, along with nitrided S154 steel without the PVD coating and HSS (not nitrided) with the same PVD coating can be seen in Fig. 6. Sample 1 has clearly the smallest sliding wear rate (2.6* lCT 15 irr/N), which is similar to the HSS sample with significantly higher hardness (//v= 820). Samples 2 and 3 had slightly higher wear rates (6.7 and 10.7* 10 15 nr/N respectively). All the duplex treated samples had significantly lower wear than the reference samples of each individual process. The high wear rate of the CrN/NbN coated sample (6.9 * 10 1 nr/N) shows how poorly the hard, wear resistant coatings perform when the load bearing capacity of the substrate is exceeded. The wear rate was two orders of magnitude higher than the duplex treated samples and one order of magnitude higher than electrodeposited hard chrome (5.8 * 1 0 14 m2/N) [20]. The wear of the nitrided samples (without the CrN/NbN PVD coating) was high ranging from 4.4 *10 13 nr/N (Sample 2) to 2.7* 10~12 m2/N (Sample 1).

The results of the potentiodynamic polarisation tests can be found in Fig. 7. Comparing the duplex treated samples to the reference samples shows that significant improvement is achieved with duplex approach. The untreated substrate performed the worst with no passivation in the 3% NaCl solution. The PVD coated S154 sample (no nitriding) exhibited some "passive like" behaviour with anodic current densities around 3 orders of magnitude less that the untreated reference. All duplex treated coating outperformed the PVD coated reference. Comparing different duplex treated samples, the sample 1 has the highest corrosion resistance followed by sample 2 and 3 respectively. If anodic current at +500 mV vs. SCE is considered as criteria, the best system (sample 1) has almost 3 orders of magnitude lower corrosion current than un-nitrided sample. The corrosion damage on these samples is localised, with size of the pits increasing in diameter and depth from sample 1 to sample 3 (see Fig. 8). No delamination of the coating was observed near the pit locations.

The XRD patterns of the samples before coating can be seen in Fig. 9. Samples 1 and 2 have very similar spectra showing two ferrous nitride phases, y' (gamma prime, Fe4 N) and £

Fig. 5. SEM image of coating adhesion failure on sample 1 with EDS map of Fe.

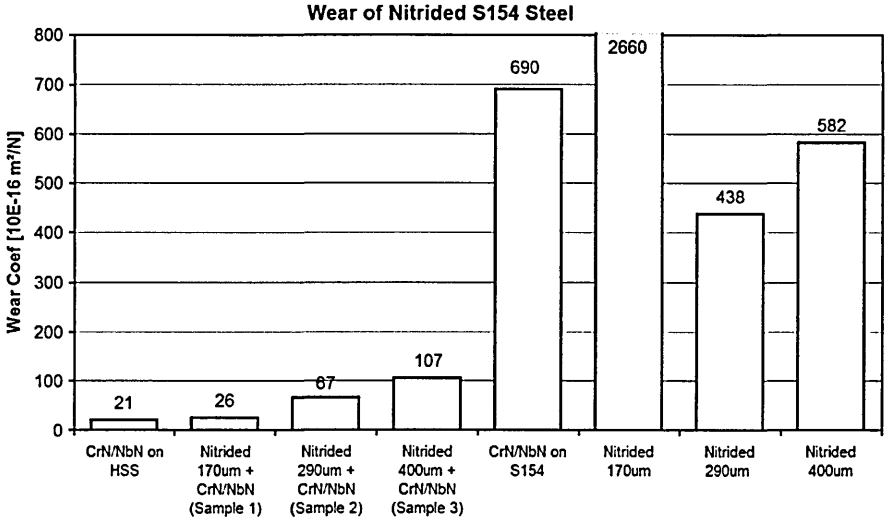

Fig. 6. Sliding wear coefficients of S154 with different surface treatments.

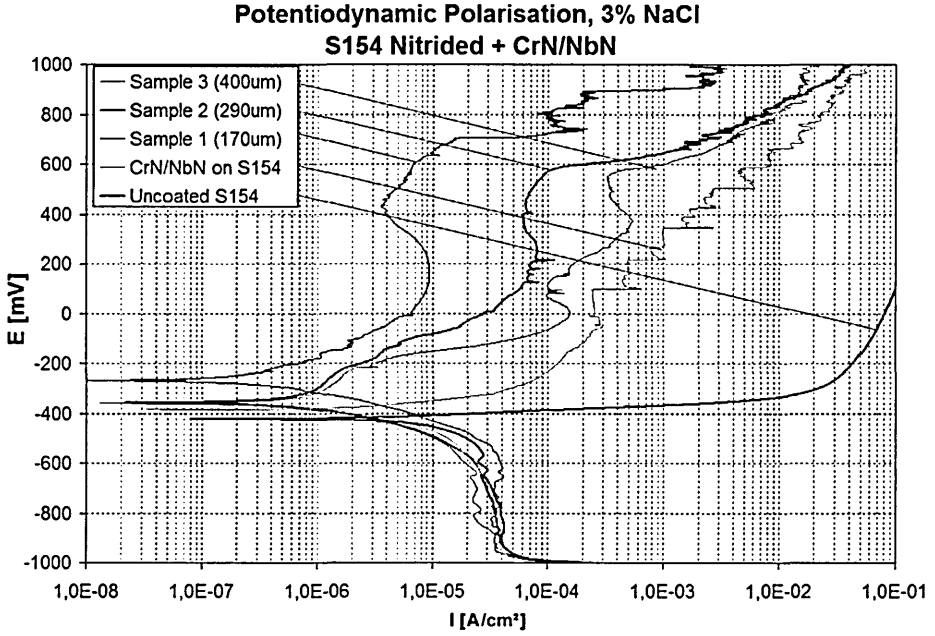

Fig. 7. Results of potentiodynamic polarisation tests of treated and untreated S154 steel in 3% NaCl solution.

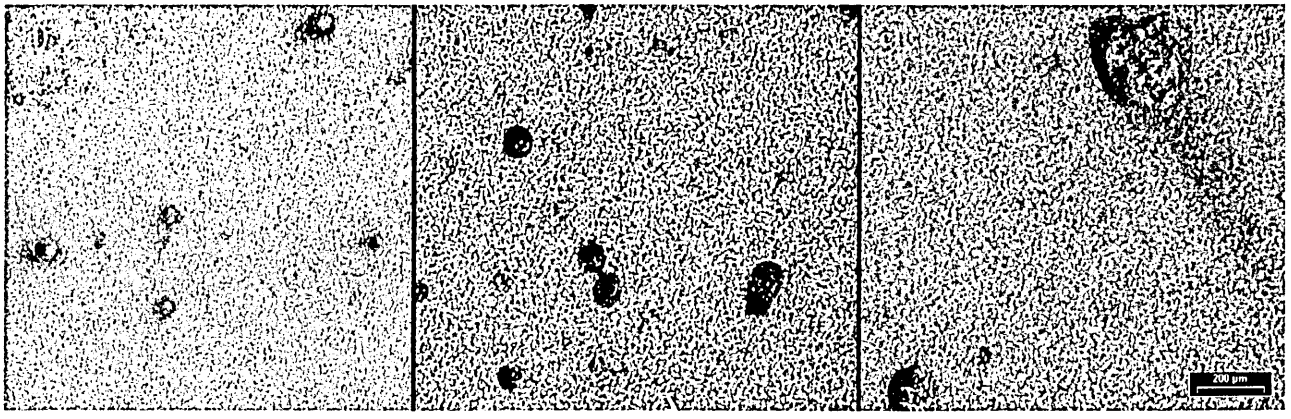

Fig. 8. Corrosion damage after the potentiodynamic polarisation test.

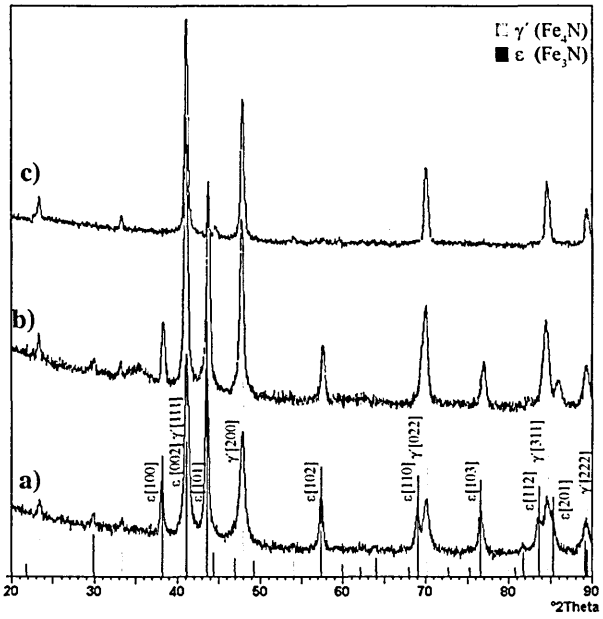

Fig. 9. 1° glancing angle XRD scans of the nitrided substrates prior PVD coating.

(Fe_3N) while sample 3 is virtually fully γ' phase. The glancing angle measurement show higher proportion of ε phase with all samples than the Bragg–Bretano measurements, indicating that there is more ε phase at surface regions. The apparent phase composition can be seen in Table 2 along with the summary of the mechanical properties of the samples.

4. Discussion

The nitriding process and the compound layer microstructure can be seen to greatly affect the mechanical and chemical properties of the duplex treated (nitriding+PVD coating) S154 steel. The compound layer is generally thought to lead to adhesion failure of the PVD coating due to porous top layer and instability at high temperatures (500 °C). It can however be beneficial due to its high hardness and improved corrosion resistance [21]. G. Nayal et al. demonstrated that metal ion etching prior to PVD coating may be required to achieve acceptable adhesion on the compound layer [17]. The duplex treated S154 investigated in this work exhibited excellent adhesion and tribological performance.

The micrographs and the hardness measurements show that the microstructure of the compound layer changes with nitriding process. The two common phases γ' (Fe_4N, FCC) and ε (Fe_3N, Hexagonal) were detected in the compound layer. The γ' phase is generally regarded as softer, more impact resistant phase and ε phase as hard and brittle. In tribological applications ε phase is generally preferred. [10] The apparent phase composition of the compound layers showed that samples 1 and 2 have roughly 50% of the hard and corrosion resistant ε phase (48% and 42%, respectively), while sample 3 is mostly gamma prime phase (88% γ' phase). The 1° glancing angle measurement show higher proportion of ε phase with all samples than the Bragg-Bretano measurements (32%, 23% and 7%), indicating that there is more ε phase at surface regions. This correlates well with the surface hardness measurements as ε phase is known to be hard and brittle and γ' phase softer and more ductile.

The surface hardness of the nitrided substrate correlates well with the pin-on-disk wear behaviour. The wear rate of the sample 1 (170 μm) is roughly equal to the wear rate of the same coating on M2 High Speed Steel, the latter having almost 3 times the bulk hardness of S154 steel. The wear rates of all duplex coatings prepared are remarkably low. All duplex treated samples clearly out-performed nitrided samples and the PVD coated S154 with no nitriding treatment. The poor performance of the PVD coating on untreated S154 steel is thought to be caused by insufficient support to the coating under the 5 N normal load subjected to the alumina ball leading to crack propagation through the coating causing accelerated wear.

There were considerable differences in the fatigue and wear behaviour between the different samples. Though the Sample 3 did not perform very well in the wear test it exhibited excellent impact resistance. The longer nitriding process used for Sample 3 yielded largest case depth and the thickest compound layer (~15 μm). This combination gives good support to the coating as shown by the impact crater with the smallest in diameter and absolutely no sign of cracks or delamination. Sample 3 also had the highest critical load in the scratch test exceeding the HSS by 15 N (60 N vs. 45 N). The excellent adhesion is attributed partially to the ductile nature of the γ' rich compound layer and the gradual reduction of the hardness that reduces the stress

Table 2
Summary of properties

	CrN/NbN on S154	Duplex treated S154 sample 1 (170 μm)	Duplex treated S154 sample 2 (290 μm)	Duplex treated S154 sample 3 (400 μm)
Compound layer	N/A	4 μm,	7 μm,	10 μm,
1° GA		48% ε phase	42% ε phase	12% ε phase
B–B		32% ε phase	23% ε phase	7% ε phase
Surface hardness	HV_{25g}=320	HV_{25g}=890	HV_{25g}=790	HV_{25g}=530
Sliding wear rate	$6.9*10^{-14}$ m^2/N	$2.6*10^{-15}$ m^2/N	$6.7*10^{-15}$ m^2/N	$1.1*10^{-14}$ m^2/N
Adhesion (L_c)	25 N	35 N	45 N	60 N
Impact resistance		Fair	Fair	Good
Impact crater		495 μm	475 μm	460 μm
Anodic corrosion current density at +500 mV vs. SCE	$2.6*10^{-3}$A/cm^2	$5.0*10^{-6}$A/cm^2	$7.3*10^{-5}$A/cm^2	$3.5*10^{-4}$A/cm^2

concentration at the interface as the diamond tip of the scratch tester deforms the surface. The crystal structure of the compound layer (γ' phase, FCC) is also same as with the coating (FCC), which may introduce local epitaxial growth enhancing the adhesion.

Despite the excellent wear behaviour sample 1 failed at relatively low critical load value in the adhesion test. We expect that to be caused by a brittle fracture initiating within the compound layer rather than simple delamination of the coating. Both of the coatings with the ε phase (samples 1 and 2) also showed cracks in the impact crater further showing the brittle nature of the ε phase compound layer. Brittle behaviour was confirmed by SEM observation of the scratch scar (Fig. 5).

The duplex treatment has significant positive impact to the corrosion resistance of the S154.

All coated samples showed "passive like" anodic behaviour. Since the corrosion is localised at the defect locations and the coating remain passive the anodic current density can be related to the active substrate area. At an anodic potential of +500 mV vs. SCE sample 1 has almost 3 orders of magnitude smaller corrosion current density than the same coating without nitriding and 2 orders of magnitude lower than sample 3. This indicates that the ε phase is beneficial to corrosion resistance as the anodic corrosion currents decreased with increasing amount of ε phase.

5. Conclusion

The mechanical and corrosion properties of the duplex treated S154 (nitrided- CrN/NbN nano-scale multilayer PVD coating) was found to be excellent. Low-pressure pulse plasma nitriding process was used to produce pre-treatments for a PVD coating and the ABS process with Cr ion etching made it possible to establish a very good adhesion on all samples despite the compound layer at the surface of the samples. The composition of the compound layer was found to greatly affect the properties of the duplex treated samples.

Based on the results of this study, a nitriding process that creates a hard surface layer would give the best wear properties for the duplex treated relatively soft and ductile steel such as S154. The hard PVD coating alone can not protect the soft steels against wear as the insufficient load bearing capacity will case quick failure of the coating as shown by the high wear coefficient of the CrN/NbN on untreated S154 steel. The good results can be achieved with a nitriding process where a hard compound layer is allowed to form on the surfaces. The composition of the compound layer can be tailored to the specific application by carefully controlling the nitriding process. In this study two phases γ' (Fe_4N) and ε (Fe_3N) were detected in the compound layer. Samples with ε phase rich compound layer were noted to have higher substrate surface hardness resulting in excellent sliding wear resistance in combination the CrN/NbN coating. For the best performing sample (Sample 1, 48% ε phase) the wear of the duplex treated S154 was similar to CrN/NbN coated M2 HSS despite having only less than half of the substrate hardness. The duplex treatment also gave significant improvement to the corrosion resistance. The anodic corrosion currents of the duplex treated samples were up to 3 orders of magnitude lower than with samples with the same PVD coating. The samples with ε phase rich compound layer had the highest the corrosion resistance. The ε phase hard phase is however subject to brittle fracture when subjected to deformation or impacts as demonstrated by scratch and impact test results. The sample with the compound layer consisting mainly of the softer γ' phase could not match the wear and corrosion performance of the other samples, yet it had excellent adhesion and impact resistance. Also the thicker case depth and the compound layer can provide better support at high loads as demonstrated by the smallest impact crater.

References

[1] W.-D. Münz, D.B. Lewis, P.Eh. Hovsepian, C. Schönjahn, A. Ehiasarian, I.J. Smith, Surf. Eng. 17 (2001) 15.
[2] B. Navinšek, P. Pajan, I. Milošev, Surf. Coat. Technol. 116-119 (1999) 476.
[3] C. Schönjahn, L.A. Donohue, D.B. Lewis, W.-D. Münz, R.D. Twesten, I. Petrov, J. Vac. Sci. Technol., A 18 (4) (2000) 1718.
[4] P.Eh. Hovsepian, D.B. Lewis, W.-D. Münz, Surf. Coat. Technol. 133-134 (2000) 166.
[5] B. Podgornik, J. Vižintin, Vacuum 68 (2003) 39.
[6] M. Zlatanović, D. Kakas, Lj. Maribrada, A. Kunosić, W.-D. Münz, Surf. Coat. Technol. 64 (1994) 173.
[7] M. Fenker, M. Balzer, R.V. Büchi, H.A. Jehn, H. Kappl, J.-J. Lee, Surf. Coat. Technol. 163-164 (2003) 169.
[8] P.Eh. Hovsepian, D.B. Lewis, W.-D. Münz, S.B. Lyon, M. Tomlinson, Surf. Coat. Technol. 120-121 (1999) 535.
[9] M. Tomlinson, S.B. Lyon, P. Hovsepian, W.-D. Münz, Vacuum 53 (1999) 117.
[10] J.M. O'Brien, D. Goodman, ASM Metals Handbook, vol 4, 1991, p. 420.
[11] B. Podgornik, J. Vižintin, O. Wänstrand, M. Larsson, S. Hogmark, H. Ronkainen, K. Holmberg, Wear 249 (2001) 254.
[12] A. Kagiyama, K. Terakado, R. Urao, Surf. Coat. Technol. 169-170 (2003) 397.
[13] P. Panjan, I. Urankar, B. Navinšek, M. Terčeilj, R. Turk, M. Čekada, V. Leskovšek, Surf. Coat. Technol. 151-152 (2002) 505.
[14] M. Pellizzari, A. Molinari, G. Straffelini, Surf. Coat. Technol. 142-144 (2001) 1109.
[15] J.C.A. Batista, C. Godoy, G. Pintaúde. A. Sinatora, A. Matthews, Surf. Coat. Technol., Article (in press).
[16] J.-D. Kamminga, R. Hoy, G.C.A.M. Jannsen, E. Lugscheider, M. Maes, Surf. Coat. Technol., Article (in press).
[17] G. Nayal, A.P. Ehiasarian, K.M. Macak, R. New, W.-D. Münz, I.J. Smith, E-MRS 2000 proceedings, 2000.
[18] P.Eh. Hovsepian, W.-D. Münz, Society of Vacuum Coaters, 45th Annual Technical Conference Proceedings, 2002.
[19] C. Schönjahn, H. Paritong, W.-D. Münz, R.D. Twesten, I. Petrov, J. Vac. Technol., A 19 (4) (2001) 1392.
[20] P.Eh. Hovsepian, D.B. Lewis, W.-D. Münz, A. Rouzaud, P. Juliet, Surf. Coat. Technol. 116-119 (1999) 727.
[21] F.T. Hoffmann, P. Mayr, ASM handbook Vol. 18 Friction, Lubrication and Wear Technology, ASM International, 1991, p. 878.

13 APPENDIX 2: Initial results using alternate electrochemical corrosion measurements

13.1 Experimental

The Linear Polarisation Resistance (LPR) and Electrochemical Impedance Spectroscopy (EIS) measurements were performed with EG&G Instruments Basic Electrochemistry System.

In LPR measurements the sample (WE) was polarised ±20mV vs. open potential. The corrosion response is linear in this region. The slope of I/U plot (R_p, polarisation resistance) is inversely related to the corrosion current i.e. corrosion rate. As a scan rate of 2mV/s was used the measurement takes only 20 seconds and since polarisation is relatively low the measurement does not affect the condition of the sample. Thus it is possible to measure R_p as a function of time.

For EIS measurements a ±10mV sine wave was used across the frequency range 100kHz to 0.1Hz with 50 measuring points in total. The data was then fitted into different models using EQUIVCRT Equivalent Circuit fitting software by B. Boukamp [18]. The nominal surface area of the samples in LRP and EIS measurements was approximately 2cm².

13.2 Linear Polarisation Resistance and Open Circuit Potential

The results from the LPR measurements along with their corresponding free potentials can be seen in Figure 1. Initially most samples show high polarisation resistance of more than 60kΩ cm². The measurement was not always successful immediately after immersion due to rapidly decreasing potentials. The polarisation resistance (which is inversely related to corrosion current) of the sample with the thicker Nb layer decreases rapidly within a few hours to around 25kΩcm² while the LPR values of the thinner coating the keeps dropping to just few kΩcm².

After ten hours of immersion in the NaCl solution all 3Nb samples have Rp values above 22 kΩcm² while 1Nb samples are less than 8 kΩcm². The behaviour of one 3Nb sample was completely different. It remained passive for the whole duration of the test with potentials of +220mV vs. SCE in the beginning and +125mV vs. SCE after 12 hours of immersion. The polarisation resistance was also extremely high registering values of over 1MΩcm². The exact R_p could not be calculated due to sensitivity of the system and noise in the measurements. No sign of corrosion was visible either.

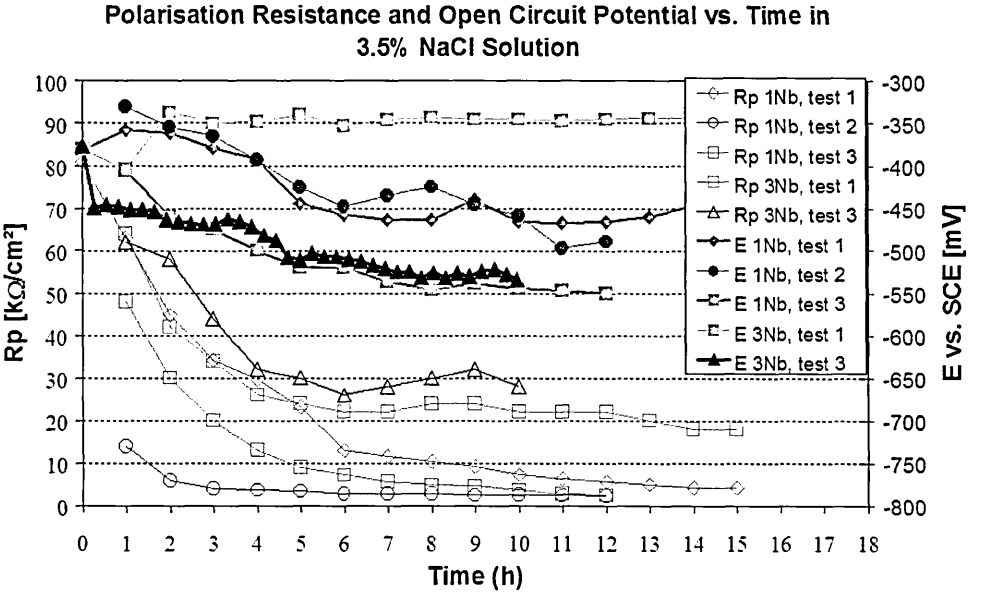

Figure 1 The results of the Linear Polarisating Resistance and Open Circuit Potential tests

13.3 Electrochemical Impedance Spectroscopy

The measured impedance and corresponding phase angles are shown in Figure 2 for 1Nb sample and in Figure 3 for 3Nb sample. These preliminary measurements were done with only one sample of each coating. The high frequencies of the impedance data usually represent the responses of the coating. The response in the high frequencies was similar in all measurements yet the impedance was up to one magnitude higher with the thicker coating at the frequencies between 1Hz to 10Khz. The response in the high frequencies was similar in all measurements yet the impedance was somewhat higher for the thicker coating at frequencies between 1kHz to 100kHz. In low frequencies the difference in impedance was notably higher being up to 1 magnitudes higher with the 3Nb coating. Also the low frequency response is notably affected by the immersion time. The extrapolation of the impedance in Nyquist plots, as shown in figure 4, after 10 hours of immersion gave R_p values of 300kΩcm² for the thicker and 40 kΩcm² for the thinner coating. Further analysis using equivalent circuit modelling is needed to understand the results fully.

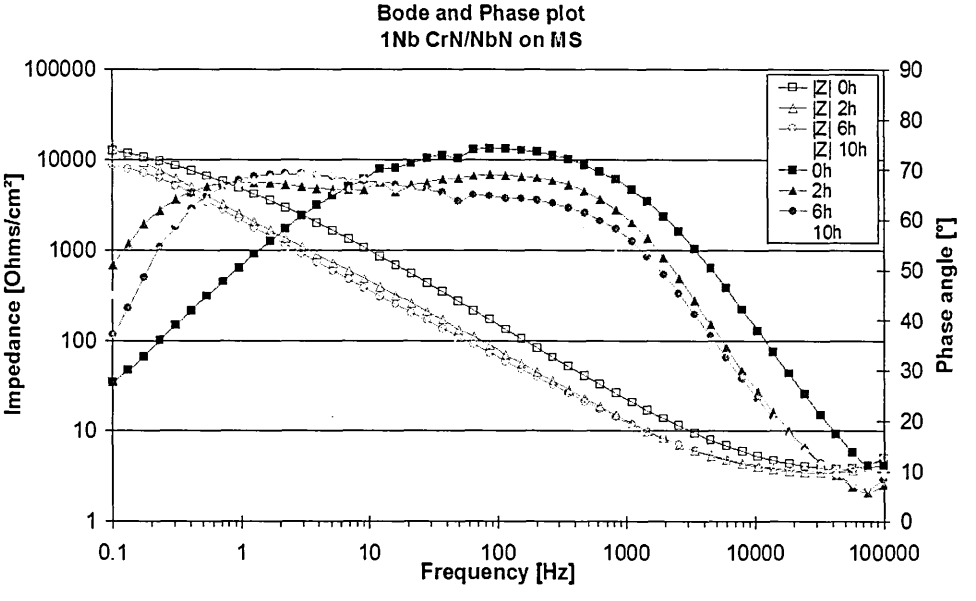

Figure 2 Bode and phase plots of selected EIS measurements of 1Nb CrN/NbN coated mild steel in 3% NaCl solution

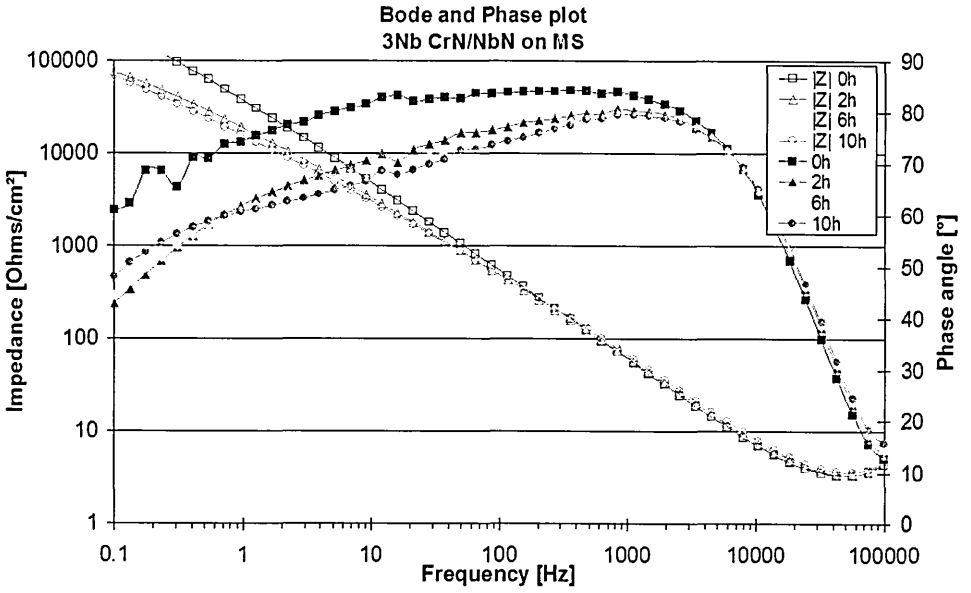

Figure 3 Bode and phase plots of selected EIS measurements of 3Nb CrN/NbN coated mild steel in 3% NaCl solution

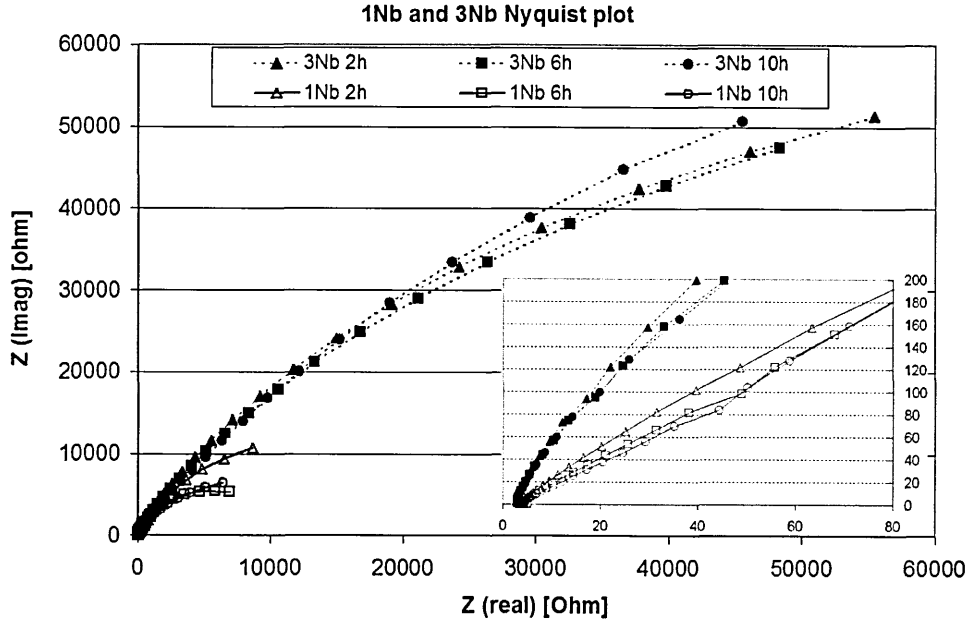

Figure 4 Nyquist plots of 1Nb and 3Nb coatings on MS after 2h, 6h and 10h in 3% NaCl solution

13.4 Repeatability and scatter in the potentiodynamic polarisation experiments

The Figure 5a-d consists of repeat tests of a same sample (in a different location) or a similar sample from the same coating run providing insight into repeatability and scatter of the results. The measurements also tested the effect of the size of exposed area to the polarisation result by using 1cm² and 4cm² areas.

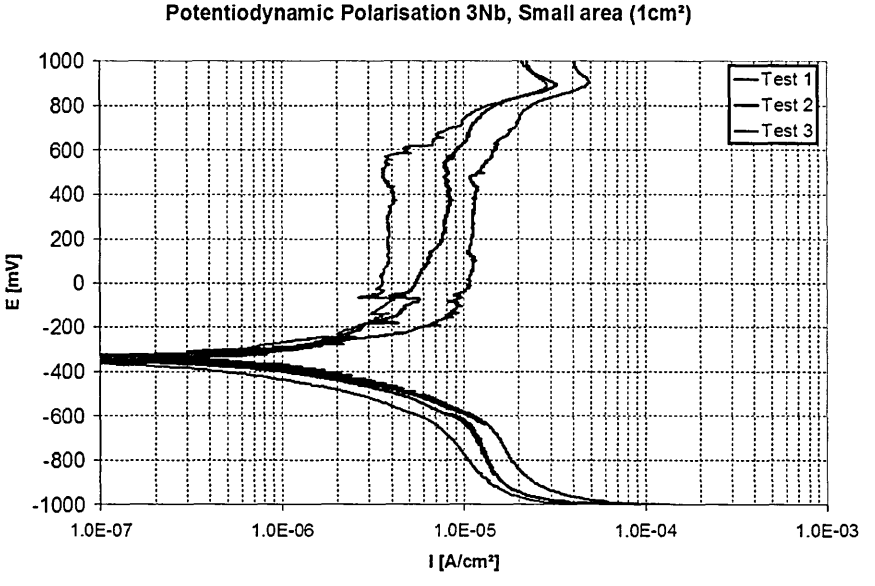

a)

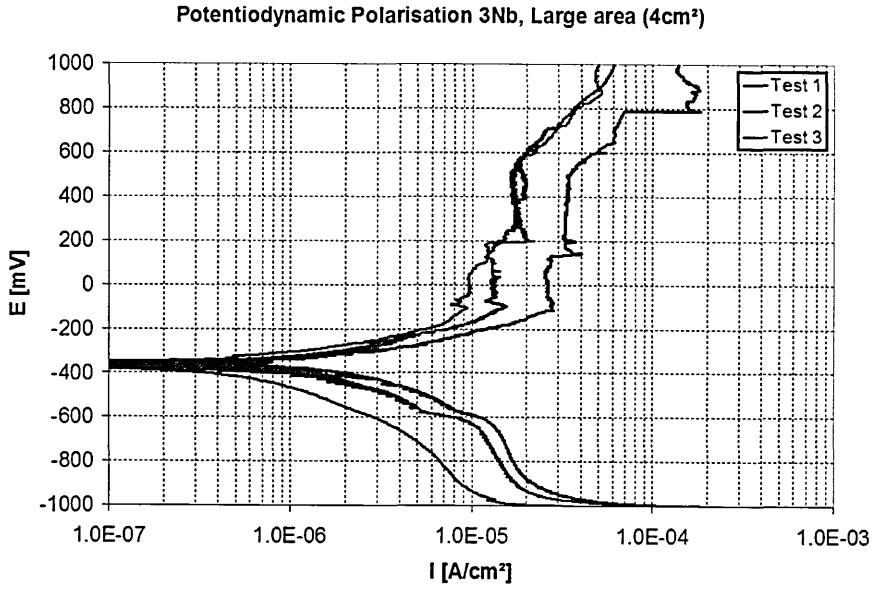
Potentiodynamic Polarisation 3Nb, Large area (4cm²)
1000
800
600
400
200
0
-200
-400
-600
-800
-1000
E [mV]
1.0E-07
1.0E-06
1.0E-05
1.0E-04
1.0E-03
I [A/cm²]
Test 1
Test 2
Test 3

b)

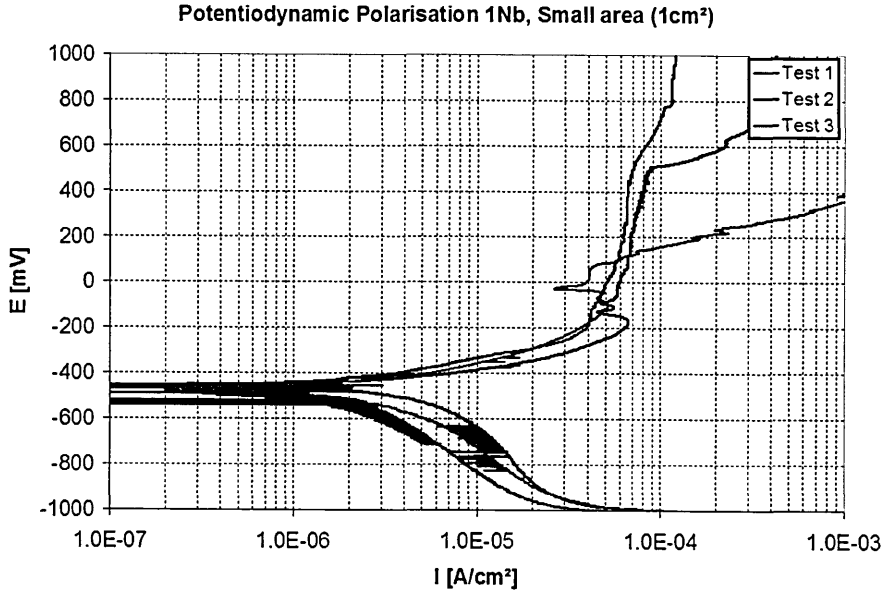
Potentiodynamic Polarisation 1Nb, Small area (1cm²)
1000
800
600
400
200
0
-200
-400
-600
-800
-1000
E [mV]
1.0E-07
1.0E-06
1.0E-05
1.0E-04
1.0E-03
I [A/cm²]
Test 1
Test 2
Test 3

c)

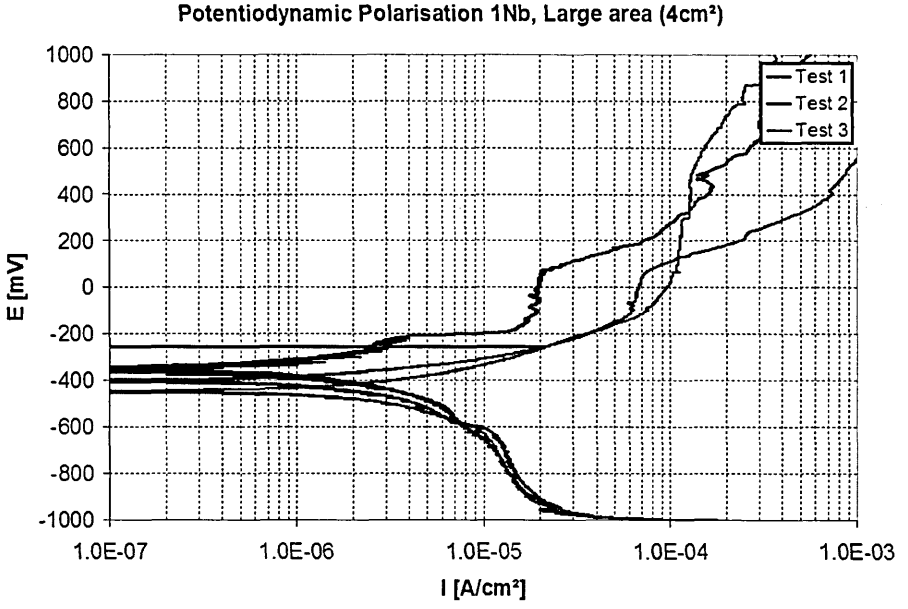

d)

Figure 5 Potentiodynamic polarisation of MS coated with CrN/NbN with a) 4.5μm Nb barrier layer, 1cm² sample area b) 4.5μm Nb barrier layer 4cm² sample area c) 1.5μm Nb barrier layer, 1cm² sample area d) 1.5μm Nb barrier layer 4cm² sample area in 3% NaCl solution

From the test results can be seen that there can be notable scatter between repeat potentiodynamic tests. In case of the thinner Nb coating (Figures 4 c and d) the differences between measurements were rather large. The deviation of E_{corr} in the six 1Nb measurements was over 100mV with lowest at –468mV and highest at –343mV vs. SCE. The average value was –430mV vs. SCE with larger samples showing more noble potentials (average –400mV vs. -460mV) and bigger deviations from average. The results also show rather different behaviour in the anodic region. Some coatings show passive type behaviour up to +1000mV while for some measurements the corrosion current rises continually with increase in potential. The larger surface area samples also appear to give more inconsistent results. If the "passive" current is examined, the difference between best and worst measurements is observed to be about 5 fold. The results from the smaller surface area samples show higher corrosion resistance than larger surface area samples. Visual inspection of the samples after the test showed varying degrees of localised corrosion that was clearly visible as rust coloured spots.

In case of the coating with the thicker Nb layer (Figures 1 a and b) the deviation in the polarisation test seems to be notably less. The deviation in the E_{corr} in the six 3Nb measurements was only 23mV with an average value of –355mV. The large samples showed slightly more negative values. The shapes of the curves are approximately similar with "passive like" current densities ranging from $3.9*10^{-6}A/cm^2$ to $3.2*10^{-5}A/cm^2$, the larger surface area samples showing higher currents

Evaluation of the corrosion performance of a coating with good barrier properties and a random distribution of defects was found to be non-trivial. The standard potentiodynamic polarisation method gives results that provide a reasonable estimate of the corrosion performance as well as giving some insight into the corrosion mechanisms occurring on the sample e.g. breakdown of local passive film. However the scatter observed from repeat measurements with these samples show the effect of the inherent metallurgical coating defects on the reproducibility of the results. Notably more scatter was observed with the 1Nb coating than with the 3Nb coating. This indicates different defect distributions in different coatings. The corrosion performance of the samples with a large surface area were measured to be inferior to samples with smaller surface area. Since the coating composition and the substrate material was similar this difference indicates that the sampled area of $4cm^2$ may not be large enough to provide uniform distribution of defects. We propose that the inferior results for the larger surface area samples are caused by a greater probability of including single (or few) large defect(s) that dominate the corrosion response.
The potentiodynamic polarisation measurements showed that the thickness of the Nb layer considerably influences the corrosion performance of the coating-substrate system. The 1Nb coated mild steel samples showed 5 to10 times higher current densities in the anodic region than the 3Nb coatings.

13.5 Summary

The defects inherent to PVD coatings can cause the interpretation of common electrochemical corrosion measurements to be non-trivial. The scatter was found to depend on coating substrate system as notably higher scatter was observed with 1Nb coating than 3Nb coating. The scatter was not found to be reduced by quadrupling the surface area used in the tests ($4cm^2$ vs. $1cm^2$). The results from samples having a larger surface area were also found to exhibit lower corrosion resistance. This could not be explained but is thought to be caused by large defects that have higher probability of existing in larger sample. This shows also that the area of $4cm^2$ is still not large enough to provide uniform distribution of defects.

All the measuring techniques (Potentiodynamic polarisation, LPR, EIS, OCP and salt spray test) gave similar results although the least amount of scatter was observed with the LPR method. OCP was seen to be somewhat unreliable with some samples contradicting findings of other test methods. EIS measurements of 3Nb coatings showed over one order of magnitude higher impedance values at low frequencies than 1 Nb coatings indicating significantly smaller amount of defects in the thicker coatings.